Graduate Student Theses, Dissertations, & Professional Papers

Graduate School

2008

Exploring the interaction between asymmetric phosphonates and acetylcholinesterase. Probing the gorge and P-site via customized covalent modification

Lilu Guo
The University of Montana

EXPLORING THE INTERACTION BETWEEN ASYMMETRIC PHOSPHONATES

AND ACETYLCHOLINESTERASE. PROBING THE GORGE AND P-SITE VIA

CUSTOMIZED COVALENT MODIFICATION.

By

Lilu Guo

B.S., Peking University, Beijing, P.R.China, 2000

Dissertation

presented in partial fulfillment of the requirements
for the degree of

Doctor of Philosophy
in Chemistry

The University of Montana
Missoula, MT

Summer 2008

Approved by:

Dr. Perry Brown, Associate Provost
Graduate School

Dr. Charles M. Thompson, Chair
Department of Biomedical & Pharmaceutical Sciences

Dr. Mark Cracolice
Department of Chemistry

Dr. C. Sean Esslinger
Department of Biomedical & Pharmaceutical Sciences

Dr. J.B. Alexander (Sandy) Ross
Department of Chemistry

Dr. Holly Thompson
Department of Chemistry

Guo, Lilu, PhD., Summer 2008 Chemistry

Exploring the interaction between asymmetric phosphonates and acetylcholinesterase. Probing the gorge and P-site via customized covalent modification.

Chairperson: Charles M. Thompson

Organophosphates (OPs) react with acetylcholinesterases (AChEs) to form a covalent bond at a specific serine residue in the active gorge, thereby providing a highly precise modification of this enzyme and an opportunity to explore protein structure, function and mechanism. The goal of this study is: 1) to show how covalent modification of AChEs by chromophore-linked OPs can be used to probe the active and peripheral sites of the protein and its local environment; 2) to differentiate AChE stereoselectivity with asymmetric phosphonothiolates.

Click chemistry was used as a key transformation method to prepare an array of chromophores linked to a reactive fluorophosphonate (FP) head group. Chromophore-linked FPs varying in length and chromophore were synthesized and computer-modeled to visualize and calculate positioning of the chromophore-FP-AChE relative to the protein active gorge. The inhibition rates of chromophore-FPs against recombinant mouse AChE (rMAChE) and electric eel AChE (EEAChE) were determined via colorimetric assay and the dansyl containing FPs were demonstrated to be the most potent. In addition, the binding effects of the chromophore and FP moiety to protein were evaluated and results demonstrated that the size and structure of chromophore and the length of the ligands mutually affect the inhibition potency. Dansyl, dabsyl and pyrene were the best chromophores with least interaction with AChEs.

To examine the interactions of asymmetric analogs of the OP compounds within the steric confines of AChEs, the synthesis of phosphonothiolate enantiomers as anti-AChEs was conducted using a chiral auxiliary for separation. X-ray analysis and ^{31}P NMR were used to show an exclusively separation of the two diastereomers. The kinetic parameters k_i and K_D for the inhibition of recombinant human AChE (rHuAChE) were determined. A 4-fold difference in anti-AChE potency was observed between S_p ($k_i = 1.7$ x 10^3 M^{-1}min^{-1}) and R_p ($k_i = 9.0$ x 10^3 M^{-1}min^{-1}). These enantiomers link to the chromophores via click reaction to form chromophore-linked asymmetric phosphonothiolates (CLAPs), which can be used to study AChE stereospecificity.

ACKNOWLEDGEMENTS

TABLE OF CONTENTS

LIST OF ABBREVIATIONS

ACN	acetonitrile
Abs	absorbance
ACh	acetylcholine
AChE	acetylcholinesterase
AD	Alzheimer's disease
C	concentration
d	doublet
dd	doublet of doublets
DMF	dimethylformamide
dt	doublet of triplet
DTNB	5,5'-dithiobis(2-nitrobenzoic acid)
EEAChE	electric eel acetylcholinesterase
eq	equivalents
g	gram
h	hour
Hz	hertz
J	NMR coupling constant (in Hz)
m	multiplet
m	meta
M	molar (molarity)
MHz	megahertz

min	minute
mmHg	millimeters of mercury
mmol	millimole
mL	milliliter
NMR	nuclear magnetic resonance
o	ortho
p	para
2-PAM	2-pyridinium aldoxime methiodide
ppm	parts per million
rHuAChE	recombinant human acetylcholinesterase
rMAChE	recombinant mouse acetylcholinesterase
rt	room temperature
s	singlet
sec	second
t	triplet
TEA	triethylamine
TLC	thin layer chromatography
μL	microliter

LIST OF FIGURES

LIST OF SCHEMES

LIST OF TABLES

CHAPTER 1

INTRODUCTION

This research attempts to study how covalent modification of acetylcholinesterases (AChEs) by organophosphonates (OPs) can be used to probe structure and differentiate between enzymes and their mechanisms. Specifically, the objectives include: 1) syntheses of a panel of customized, racemic OP probes of AChE bearing reactive moieties and reporter groups, 2) covalent inactivation of AChEs by custom OP probes to seat a tethered chromophore at a predictable depth within the protein to determine the interaction between the ligand and the enzyme; 3) syntheses and anti-AChEs analysis of asymmetric OP custom probes to elucidate the stereospecificity of AChEs.

The broader impact of this study is that AChEs are essential to neuromuscular and brain function through the breakdown of neurotransmitter (NT) and other esters. OP compounds impose a majority of their toxic action through biochemical interactions with AChEs. Health concerns originating from the high toxicity of OP nerve gases, and more importantly the use of OP insecticides make the understanding of mechanism of OP-AChE interaction an imminent task.

Acetylcholinesterases (AChEs) are ideal enzymes for mechanistic studies and method development due to a rich database about their structure, catalytic mechanism,

and functional knowledge of their active sites (Taylor, 1994; 1995). Chapter 2 of this thesis discusses the AChE background in greater details, explicating the two interaction sites on the protein: the catalytic active site and the peripheral active site. The catalytic active site (A-site) responsible for hydrolysis of acetylcholine (ACh) is comprised of a catalytic triad (His-Glu-Ser) located halfway through the protein at the bottom of a 20Å gorge that connects to the protein surface. The peripheral site (P-site) located on the entrance of the gorge attracts cation substrates that transiently bind prior to gorge entry and eventually arrive at the A-site. AChE activity can be suppressed by introducing interacting molecules at the A-site, at the P-site, or both.

Typically, OP compounds block the A-site at the catalytic serine of AChE by a covalent modification. Certain cation ligands like propidium inhibit AChE via P-site binding in a process termed 'steric blockage' (Johnson, 2003; Roseberry, 1999; Mallender, 1999). The most potent inhibitor was recently manufactured by taking the advantage of dual binding to both the A- and P-sites while using the gorge to connect the two inhibitor pieces (Lewis, 2002). To investigate the P-site mechanism spectroscopically, and optimize the dual binding opportunity, various types of chromophores are envisioned as potential P-site inhibitors. Their-linked OP moieties are designed to covalently modify the A-site to place the chromophore at the P-site to probe the interaction with the enzyme. Chapter 4 centers on the design and synthesis of a panel of chromophore-linked fluorophosphonates (FPs) that vary in the ligand length and chromophore structure to optimize this dual binding effect.

The inhibition rate (k_i) is a general measurement of the anti-AChE potency of OP and therefore, FP compounds. In Chapter 5, a comparison between chromophore-FPs

and a control containing only FP moiety in the inhibition potency is discussed and demonstrates that the size and structure of chromophore and the length of the ligands mutually affect the inhibition potency. To visualize and calculate positioning of the chromophore-FP-AChE relative to the protein active site/gorge/peripheral site, molecular modeling of the chromophore-FP:AChE complex are also presented in Chapter 5. The docking results further explained the steric blockage effect of the big chromophores.

Although the A-site of AChE has been the principle target for researchers to investigate and known for its highly conserved and sterically constrained structure, the stereoselectivity of OP-AChE interaction in phosphorylation and dephosphorylation processes remains unclear and recently emerged as a hot topic. Previous studies have shown that phosphorus stereochemistry dictates the extent and the rate of inhibition and reactivation of AChE (Doorn, 2000, 2001; Ryu, 1991; Berkman, 1993). To address the stereospecificity of AChEs and other OP-reactive proteins in a greater detail, more available and generally applicable asymmetric phosphorus compounds are desired.

Different methods to synthesize asymmetric phosphonothiolates are discussed in this study and a reliable and flexible synthetic route for preparation of asymmetric phosphonothiolates is proposed (details in Chapter 4). The phosphonothiolates enantiomers are prepared with an attached propylazo group as the building blocks for the 'click' reaction, providing our study in the immediate future a specific opportunity to construct the chromophore-linked asymmetric phosphonothiolates (CLAPs) via click reaction and observe this stereospecificity spectrally and quantitatively.

The phosphonothiolate enantiomers undergo reactions with AChE with ejection of a thiol group to generate stereoselectively-modified AChE that can be examined by

3

various means.   In Chapter 5, the kinetic parameters k_i (inhibition rate constant) and K_D (dissociation constant) of the phosphonothiolate enantiomers for the inhibition of recombinant human AChE (rHuAChE) were examined to demonstrate differences in anti-AChE potency between S_p and R_p - isomers.

CHAPTER 2

BACKGROUND

2.1 ACh, AChE and the Cholinergic System

Acetylcholine (ACh) is one of the oldest and best understood neurotransmitters in the mammalian central nervous system (CNS). ACh is synthesized in and released from cholinergic neurons, which are localized in various parts of the CNS. Cholinergic neurons projecting from basal forebrain nuclei play important roles in cognitive processes such as learning and memory. Cholinergic neurons in striatum are involved in movements and motor functions. Degeneration and dysfunction of cholinergic neurons are related to several neurodegenerative diseases such as Alzheimer's disease (Evans, 1989; Kihara, 2004) and Huntington's disease (Pisani, 2001; Growdon, 1977).

In presynaptic cholinergic neurons, ACh is synthesized from choline and acetyl CoA through the action of choline O-acetyltransferase (ChAT) (Parsons, 1993) (Scheme 2.1).
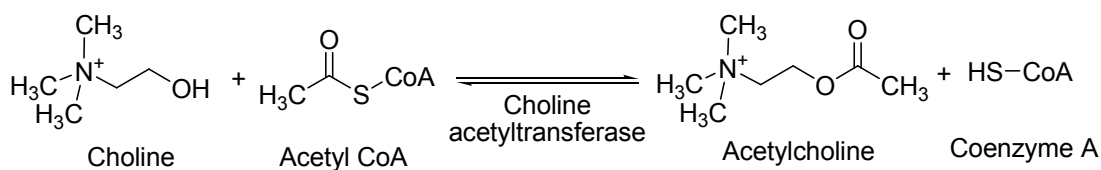
Scheme 2.1. Synthesis of acetylcholine.

Dietary choline and phosphatidylcholine serve as the sources of free choline for

ACh synthesis. Acetyl CoA is derived during the metabolism of glucose. Newly

synthesized ACh is translocated into synaptic vesicles by the vesicular ACh transporter

(VAChT). When the nerve impulse reaches the synapse, triggered by calcium gradient,

synaptic vesicles containing ACh fuse with presynaptic membrane (exocytosis) and

release ACh into the synaptic cleft (Fig 2.1).
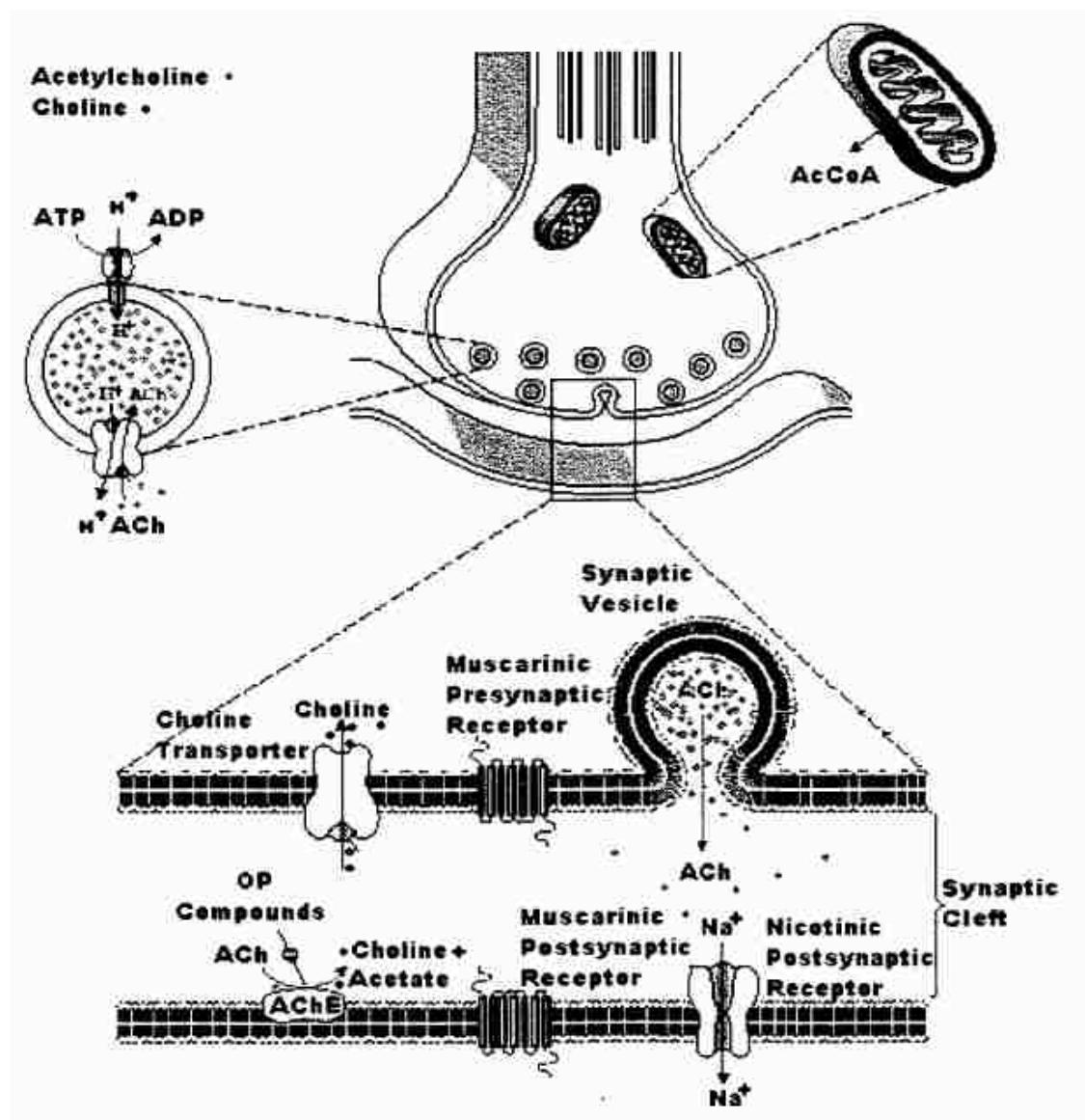
Figure 2.1. Cholinergic synapse (adapted from Feldman 1984).

A single motor-nerve terminal contains 300,000 or more vesicles (Katz, 1965) and single synaptic vesicles are estimated to contain from 1,000 to over 5,000 ACh molecules each. When released into synaptic cleft, ACh activates cholinergic receptors on membranes of postsynaptic neuron and proximal glia (Aschner, 2000). There are two major types of cholinergic receptors: nicotinic receptor and muscarinic receptor. The nicotinic receptor is a ligand-gated channel composed of five subunits. The activation of nicotinic receptor results in a rapid membrane depolarization caused by the influx of Na^+ and Ca^{2+} and excitation. Nicotinic receptors are primarily responsible for the peripheral effects of ACh at the autonomic ganglia and the neuromuscular junction (Itier, 2001). Muscarinic receptors belong to a big family of G-protein coupled receptors (GPCRs). The activation of muscarinic receptor involves the binding of GTP to the receptor and initiation of second messenger systems, which lead to a cascade of intercellular pathways. Muscarinic responses are slower, compared with nicotinic receptor, and may produce excitation or inhibition (Eglen, 2006).

Following the repolarization of postsynaptic neurons, ACh left in the synaptic cleft must be removed immediately to avoid hyperpolarization. This is achieved by enzyme-catalyzed hydrolysis of ACh. The enzyme involved in this process is called acetylcholinesterase (AChE).

2.2 Structural and Mechanistic Features of AChE

Acetylcholinesterase (AChE) is a 60 KDa protein belonging to the alpha/beta hydrolase family. Depending on the functions, AChE exists in several forms and is localized both intracellularly and extracellularly. Cytosolic AChE is responsible for breaking down excess intracellular ACh and AChE in the synaptic cleft or the neuromuscular junction clears extracellular ACh.

Structurally, the *Torpedo California* AChE (*Tc*AChE) is similar to most alpha/beta hydrolases, with 12 beta sheets surrounded by 14 alpha helices (Sussman, 1991). The x-ray crystal structure of *Tc*AChE demonstrated the presence of a long and narrow gorge, approximately 20 Å deep leading to the active site. The gorge is lined with conserved aromatic residues and only approximately 5 Å wide defined by Tyr121 and Phe330 residues. Because the diameter of the quaternary portion of ACh is 6.4 Å, substantial conformational change of the gorge must be involved in the translocation of the substrate molecules (Colletier, 2006).

The kinetic models for AChE (Marcel, 1998; Johnson, 2003) suggest that there are at least two substrate-binding sites, the active site, at the bottom of the active-gorge, and the peripheral anionic site (PAS), near the entrance of the gorge (Figure 2.2).
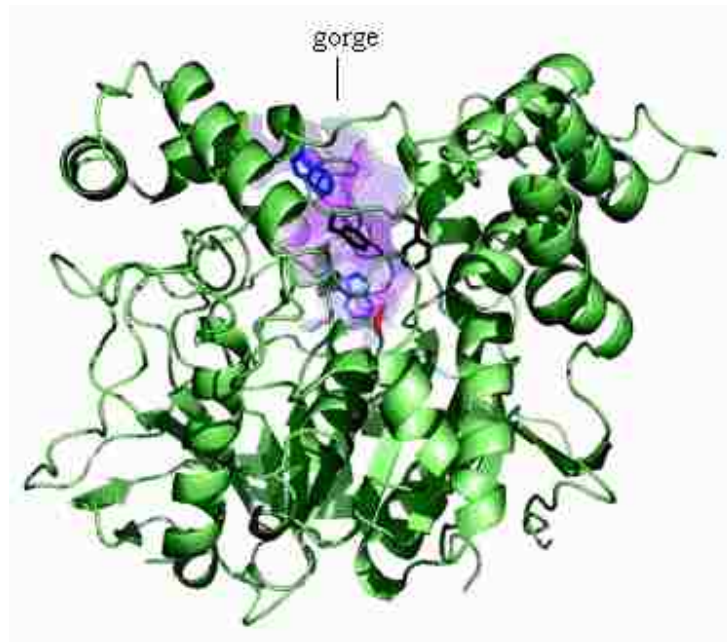
Figure 2.2. Structure of Torpedo AChE with the surface of the gorge outlined as a purple surface (Adapted from Silman, 2005).

The active site is composed of two subsites: the esteratic subsite and the catalytic anionic subsite (CAS). The esteratic subsite in AChE (Figure 2.3) contains a typical serine-hydrolase catalytic triad, Ser200-His440-Glu327 in *Tc*AChE (in mammalian AChE, Ser203-His447-Glu334) (Harel, 1993; Sussman, 1991). A few important structure components with contribution to ACh binding in the active site have been identified over the years, including the oxyanion hole formed by residues Gly118, Gly119 and Ala201, the acyl-pocket formed by Trp233, Phe288, Phe290 and Phe331 (Harel, 1996). The CAS contains no negative charged residues, but the indole ring of Trp84, and Glu199 and Phe330, which makes a cation-π interaction with the quaternary group of ACh (Sussman, 1991).

The active site inhibitors inactivate AChE and prevent the substrate molecule from binding, either by interacting with the active site with high affinity and occupying the site (such as tacrine, Wlodek, 1996) or by reacting irreversibly with the active site (such as organophosphates and carbamates, Bartolucci, 1999).
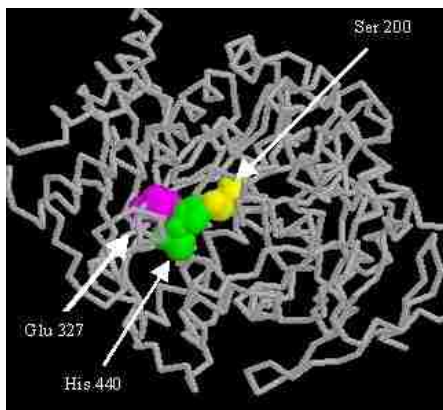
Figure 2.3. Important residues in the esteratic subsite (Harel, 1993; Sussman, 1991).
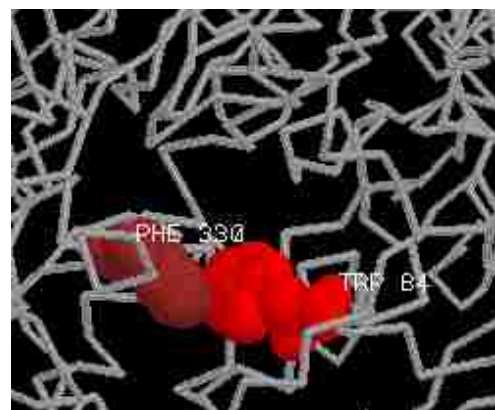
Figure 2.4. The catalytic anionic subsite (Harel, 1993; Sussman, 1991).

Site-directed mutagenesis studies and binding studies of inhibitors such as propidium, BW284C51, d-tubocurarine (Fig 2.6), the mamba venom toxin, and fasciculin (Radić, 1991, 1994; Barak, 1994), revealed that three essential amino acids, Trp279, Tyr70 and Asp72 (Figure 2.5), form the peripheral anionic site (PAS) (Johnson, 2006). The solution of the 3D structures of above AChE-inhibitor complexes further supported the hypothesis (Harel, 1993; Bourne, 1999; 2003).
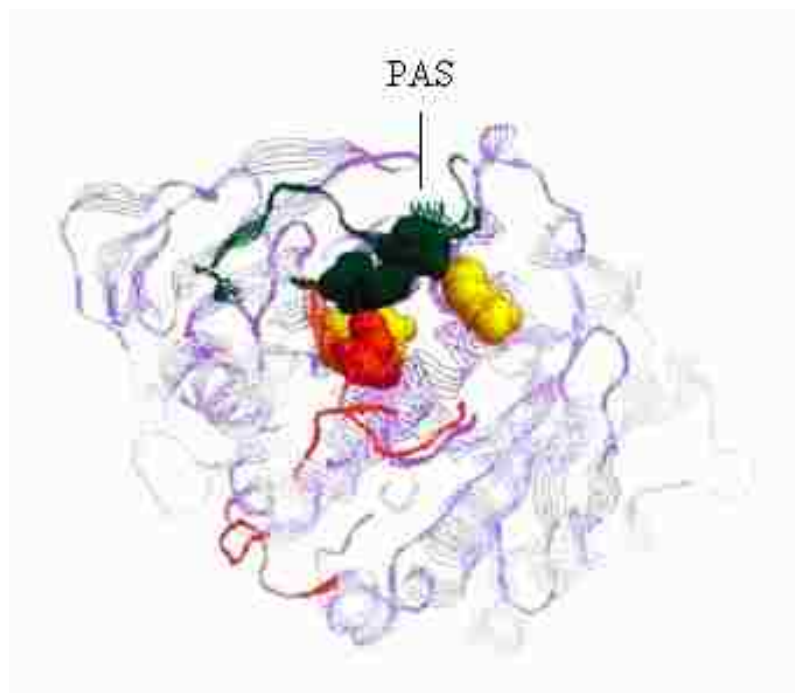
Figure 2.5. Structure of Torpedo AChE showing the PAS-associated residues (shown in space filling mode): Tyr 70, Asp 72, Trp 279, Tyr 121 and Tyr 334 (Adapted from Johnson, 2006).

BW284c51

propidium iodide
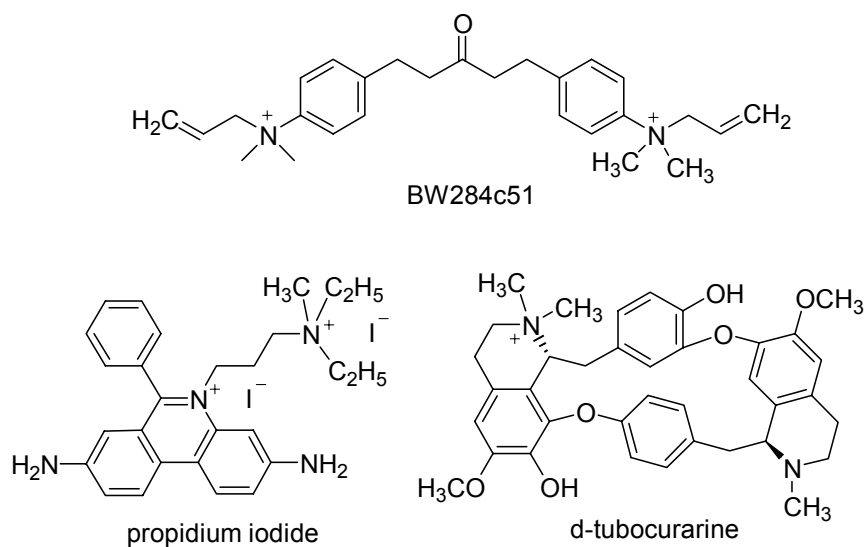
d-tubocurarine

Figure 2.6. Structures of propidium, BW284C51 and d-tubocurarine.

The PAS has been demonstrated to be involved in catching and guiding substrate molecules into the active site, and likely gives rise to allosteric modulation of the enzymes activity (Zhou, 1998). Inhibition of the PAS can inactivate the enzyme activity because of the resulting conformational changes. It has also been proposed that the substrate binding to the PAS prevents the hydrolyzed choline from leaving the active site (Rosenberry, 1999; Johnson, 2003, Stojan, 2004).

Bis-quaternary cation inhibitors such as decamethonium, simultaneously bind to the active and peripheral sites, thus occupying the entire catalytic gorge, which is known as 'dual-site binding' (Harel, 1993).

2.3 AChE Hydrolysis of ACh

AChE is a serine hydrolase that belongs to the esterase family within higher

eukaryotes. This family acts on different types of carboxylic esters. The primary

biological role of AChE is the rapid termination of the neuronal impulse that occurs when

ACh is released into the synaptic cleft. Following the production of an end-plate

potential at the motor end plates of skeletal muscle or the polarization of the postsynaptic

neurons, AChE removes ACh from the synaptic cleft by catalyzing its hydrolysis to

acetate and choline (Scheme 2.2, Schumacher, 1986).
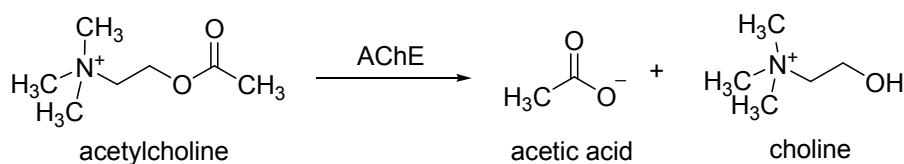
Scheme 2.2. Hydrolysis of acetylcholine by acetylcholinesterase.

AChE hydrolysis of ACh demonstrates the hallmark elements of an acid-base

catalyzed reaction, including both acetylation and deacetylation processes. Acetylation

of the serine hydroxyl (Ser 200) within the esteric subsite is catalyzed by the basic

imidazole moiety in His440 and the acidic moiety in Glu327. Free AChE is regenerated

by a deacetylation step assisted by water. A simplistic representation of the AChE active

site for the hydrolysis of ACh is outlined in Scheme 2.3. In addition to the regions shown

in the scheme, it has also been proposed that the PAS facilitates initial association and

alignment of ACh (Zhou, 1998) and the quaternary trimethylammonium choline moiety

of ACh is stabilized principally via a cation-π interaction with Trp84, Glu199 and Phe330

in the CAS (Sussman, 1991). It is emphasized that AChE is a highly complex and

dynamic protein, and consequently, there are a number of hydrophobic/hydrophilic

regions in the active gorge that may be involved in allosteric modulation of the hydrolysis

activity.
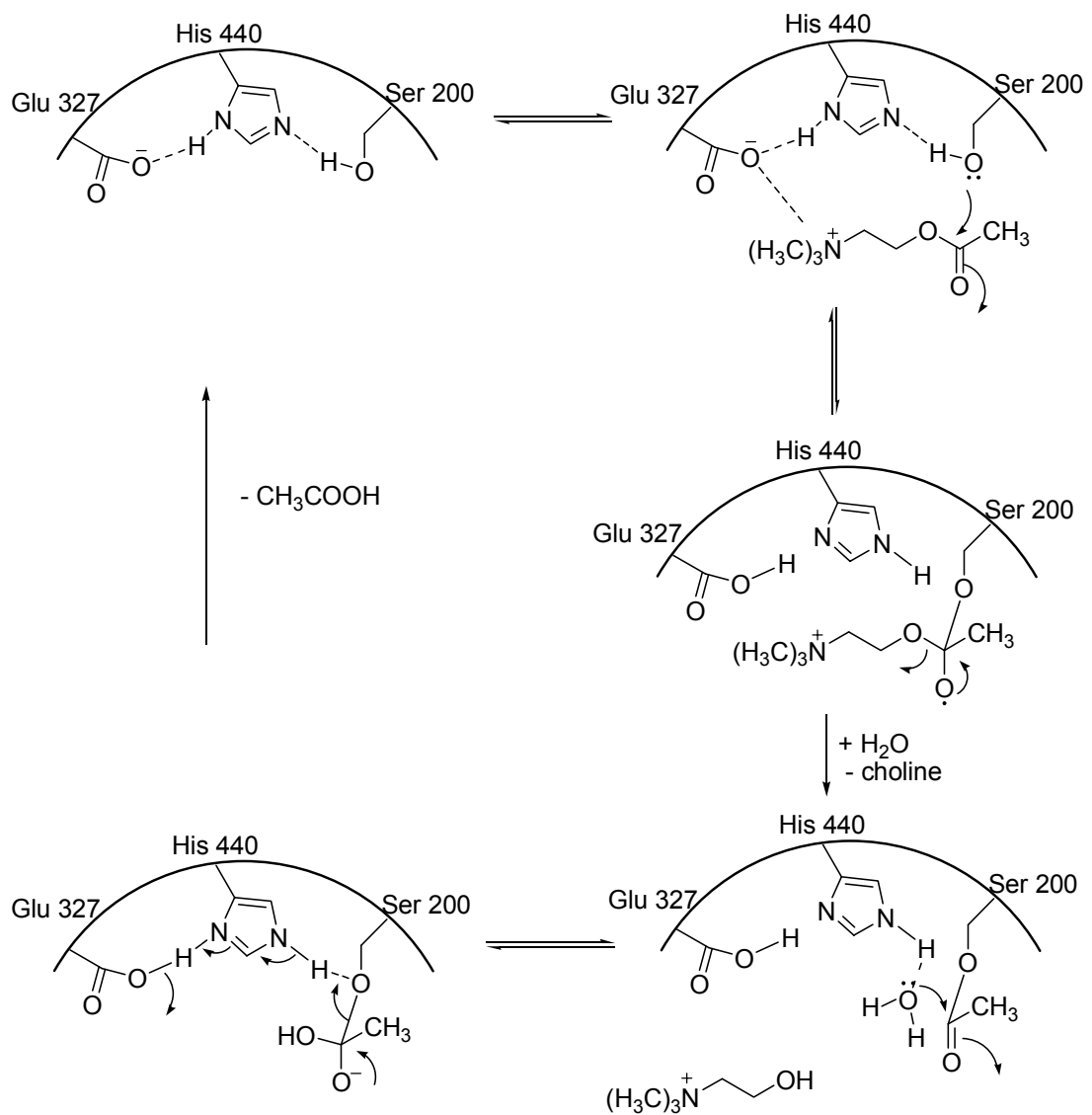
Scheme 2.3. Mechanism of ACh hydrolysis by AChE.

2.4 Organophosphorus Compounds (OPs)

Organophosphorus (OP) compounds are derived from phosphoric, phosphonic or phosphinic acids and the phosphorus-linked oxygens are substituted by sulfur or nitrogen atoms. General structures of several OP compound types are shown in Figure 2.7.
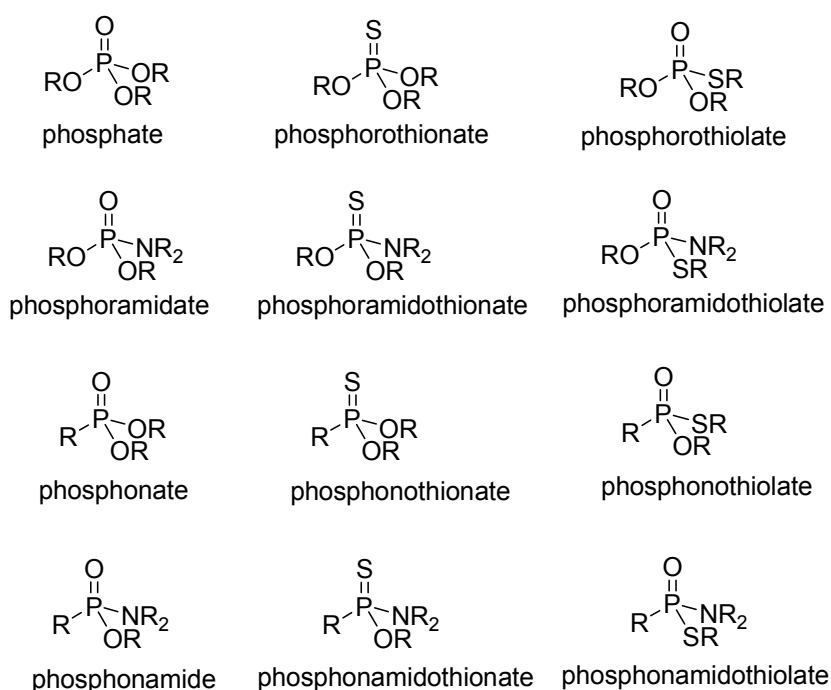
Figure 2.7. Nomenclature of OP compounds.

Organophosphorus compounds are used primarily as pesticides, drugs and nerve agents imposing their toxicity through the inhibition of AChE. It is a requirement for anti-AChE activity that one of the ligands attached to the phosphorus atom must be a good leaving group. Fluoro(-F), thiol (-SR), phenoxy (-OPhNO$_2$) and cyano (-CN) groups are some among the common but better leaving groups. A few well-known OP

insecticides and chemical warfare agents are listed in Figure 2.8. The majority of

organophosphorus insecticides are phosphorothioates; nerve agents are phosphonates or

phosphonothioates whereas industrial chemicals are typically organophosphates.

insecticides and their oxon metabolites

X = O: paraoxon
X = S: parathion

X = O: chlorpyrifos oxon
X = S: chlorpyrifos

X = O: diazoxon
X = S: diazinon

insecicides

dichlorovos

metrifonate

profenofos

nerve agents

Sarin

Soman

VX

Tabun

others

DFP

mipafox
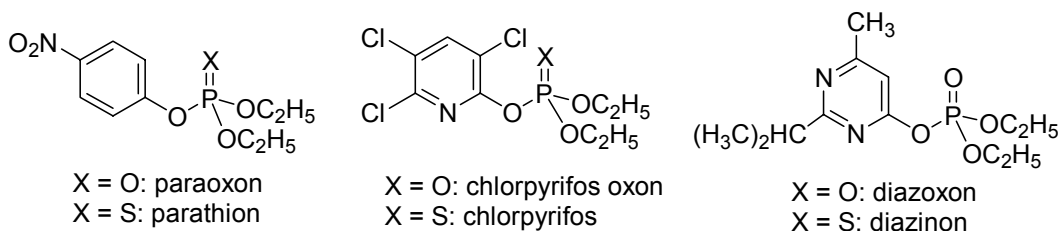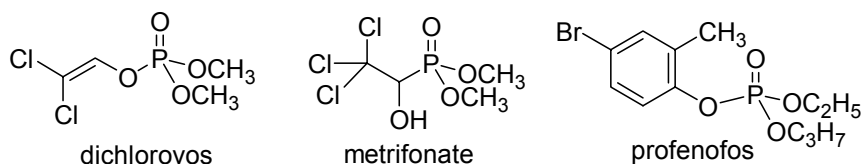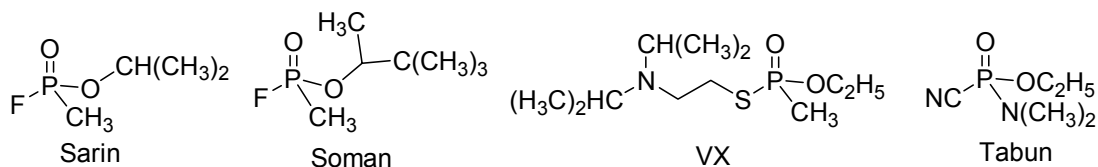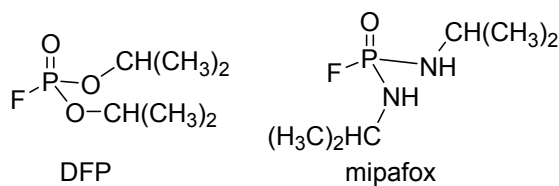
Figure 2.8. OP insecticides and their metabolites, chemical warfare agents, and designed
compounds for potency or selectivity.

Most fluorophosphonates, especially those with short branched-chain alkyl groups,

have shown a powerful inhibitory action on acetylcholinesterase (Saltmarsh, 2000;

Steinberg, 1989). Fluorophosphonates (FPs) bearing a chromophore have been used as

probes for the active site of AChE (Saltmarsh, 2000; Steinberg, 1989; Amitai, 1982;

Berman, 1978). This aspect of OP reactivity will be discussed in greater detail in the

following sections.

A thiol (-SR) leaving group is preferred in many studies towards AChE

stereospecificity. A phosphonothionate compound is prone to undergo thiono-thiolo

rearrangements to offer a phosphonothiolate, which is an OP compound with a thiolate

ester leaving group (Scheme 2.4). This isomerization process can be induced by thermal

and chemical means (Eto, 1974; Metcalf, 1953).
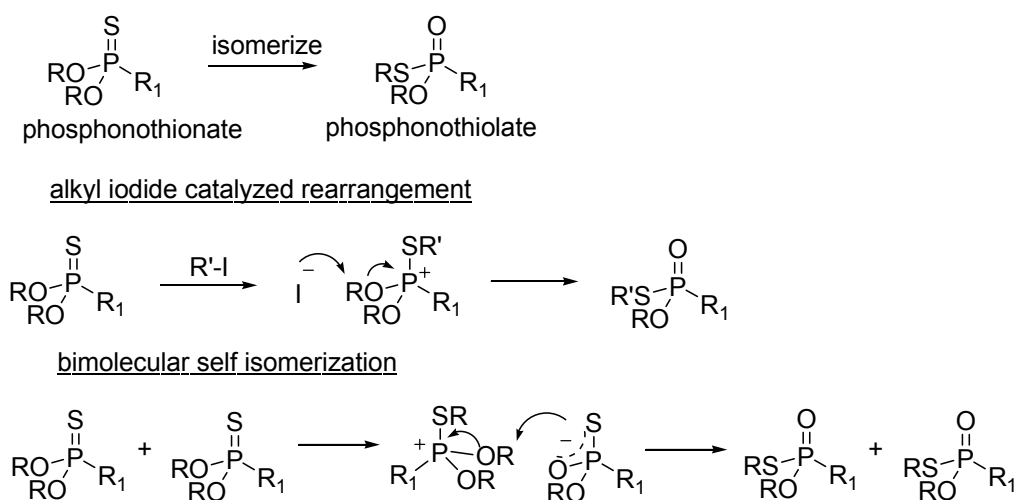
Scheme 2.4. Thiono-thiolo rearrangement.

The thiono-thiolo rearrangement can be triggered by reaction of a

phosphonothionate with an alkyl iodide to form S-alkyl isomer by alkylating the thionate,

following with dealkylation. Intermolecular or self-isomerization occurs primarily at

elevated temperatures when one phosphonothionate is dealkylated to produce an ambient

17

ion pair that realkylates at the more nucleophilic sulfur atom (Scheme 2.4). The

rearrangement of OP compounds with thiolate esters as leaving groups is studied in more

detail in Chapter 4.

2.5 Mechanism and Kinetics of AChE Inactivation by OPs

The inhibition of AChE can be categorized into two classes based on their inhibition mechanisms. The first class of inhibitors acts to competitively impede hydrolysis without reacting with the enzyme (discussed in Section 2.8). Others inhibit AChE by interacting with the serine in the active site and the resulting inhibitor-AChE adduct is more stable than acetate and resistant to hydrolysis.

Organophosphorus compounds inactivate AChE by phosphorylating the active site serine hydroxyl where one ligand of phosphorus is displaced as the leaving group (Scheme 2.5). This produces a covalently modified AChE which is catalytically inactive. The first step in the inactivation of AChE involves the reversible formation of an enzyme-inhibitor complex and is represented by the equilibrium constant, K_D (the quotient of dissociation rate constant: association rate constant) (Main, 1964). K_D is generally considered as a measure of an OP's affinity for the enzyme active site (Fukuto, 1990). The second step of inhibition leads to the irreversible phosphorylation of AChE by forming a covalent bond. The chemical covalent modification of the serine hydroxyl is responsible for the ultimate loss in the enzyme activity of hydrolyzing ACh. The phosphorylation rate constant k_p is a measure of the reactivity of the enzyme-inhibitor complex (Main, 1964; Fukuto, 1990). The overall rate of inhibition is presented as the bimolecular reaction (or rate) constant, k_i. This parameter is a function of both K_D and k_p ($k_i = k_p/K_D$) and is a measure of the inhibition potency of an OP inhibitor.
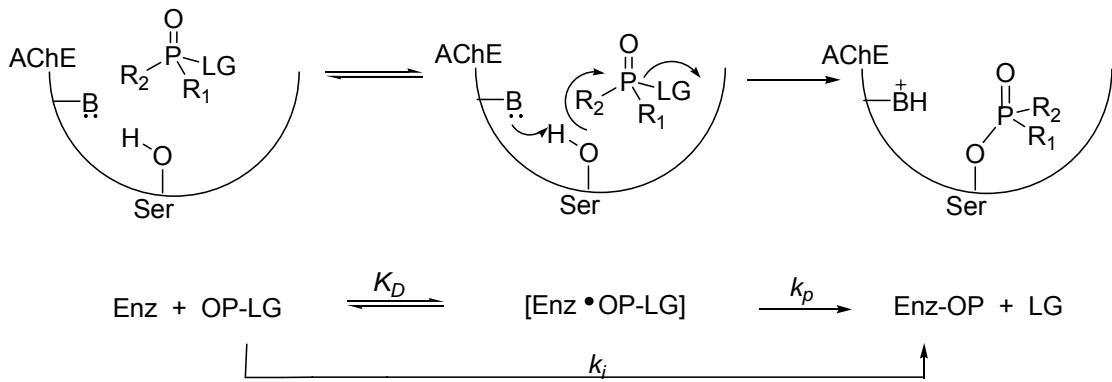
LG: leaving group
K_D: dissociation constant
k_p: phosphorylation rate constant
k_i: inhibition rate constant

Scheme 2.5. Mechanistic and kinetic description of AChE inactivation by an OP.

The bimolecular reaction constant k_i, dissociation constant K_D, and phosphorylation constant k_p can be determined by a concentration-dependent method, using Equations 2.1 and 2.2 as defined by Main (Main, 1964):

$$\frac{1}{[i]} = \left(\frac{\Delta t}{\Delta \ln v} \right) k_i - \frac{1}{K_D} \qquad (2.1)$$

where:

$[i]$ is the concentration of inhibitor;

Δt is the time of incubation;

$$\Delta \ln v = \ln v_0 - \ln v = \ln \frac{v_0}{v} \qquad (2.2)$$

in which:

v_0 is the control rate of enzyme;

v is the rate for sample with inhibitor;

Typically, $1/[i]$ is plotted against $\Delta t/\Delta \ln v$ and the slope of the resulting straight line is k_i and the inverse of the intercept is K_D. The phosphorylation rate constant k_p is deduced from the equation: $k_p = k_i \times K_D$.

When the dissociation constant (K_D) is much greater than the inhibitor concentration and the reversible step of inhibition can be disregarded, inhibitory potencies (k_i) can also be determined experimentally by a time-dependent manner (Equations 2.3 and 2.4):

$$\frac{1}{[i]} = \left(\frac{\Delta t}{\Delta \ln v} \right) k_i \qquad (2.3)$$

$$\Delta \ln v = k_i [i] \Delta t \qquad (2.4)$$

where the time dependent loss of enzyme activity is monitored in the presence of a specific concentration of OP inhibitor (Aldridge 1950). This equation is more convenient to work with as it requires a single concentration of the inhibitor. However, it is most applicable when $1/K_D$ is insignificant. The comparison of inhibitory potencies with this method may require using same inhibitor concentration.

The inhibition potency, k_i, can also be expressed in terms of IC_{50} value. IC_{50} is a parameter that represents the molar concentration of inhibitor that causes a 50% reduction of enzyme activity during a discrete period of incubation with the inhibitor. Consequently, the IC_{50} value of an OP inhibitor against AChE can be determined by Equation 2.5 (Eto, 1974).

$$\frac{1}{IC_{50}} = \left(\frac{\Delta t}{\ln v_0 - \ln 0.5v_0}\right)k_i$$

$$\frac{1}{IC_{50}} = \left(\frac{\Delta t}{\ln 2}\right)k_i$$

$$IC_{50} = \frac{0.695}{\Delta t \times k_i} \qquad\qquad (2.5)$$

2.6 Post-inhibition Phase of AChE Inhibited by OPs

Upon phosphorylation, there are three post-inhibition routes that an AChE can possibly undertake: (a) reactivation, in which the phosphoester-serine bond is broken either spontaneously (water) or mediated by oxime antidotes, (b) "aging", in which a phosphate oxyanion is produced by the cleavage of a phosphoester bond other than the phosphoserine, or (c) non-reactivation, in which the enzyme is unable to recover its activity by mechanisms other than aging (Eto 1974, Westheimer 1987).

These post-inhibition fates are discussed in detail in the following sections.

2.6.1   Spontaneous Reactivation

Phosphorylated AChE can spontaneously recover its enzymatic activity if the serine-phosphate bond is cleaved via hydrolysis to regenerate an active serine residue (Scheme 2.6). The mechanism of spontaneous reactivation is similar to the second step of the AChE-catalyzed hydrolysis of ACh (in Scheme 2.3). However, the rate of spontaneous reactivation (k_0) of AChE inactivated by an OP is far slower than the turnover rate for the natural substrate, ACh (Eto 1974).
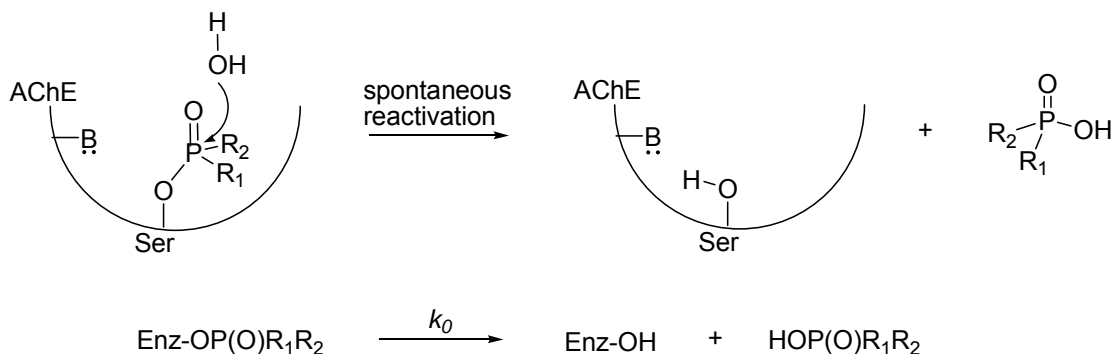
Scheme 2.6. Spontaneous reactivation of AChE inhibited by an OP.

The spontaneous reactivation of inactivated AChE by an OP inhibitor is dependent upon a number of factors including the enzyme source, pH, ionic strength, and temperature (Lieske 1980, 1990; Lanks 1981; Fisher 2000). In addition, the rate at which AChE recovers from OP inhibition is also dependent upon the nature and reactivity of the appended phosphoryl groups. The rate of spontaneous reactivation is greatest when less bulky ligands (R_1 and R_2) are used in OP diester compounds because of less steric hindrance (Lotti, 1991).

2.6.2 Oxime-Mediated Reactivation

The observation that phosphorylated AChE can be reactivated by the nucleophilic attack of a weak nucleophile, water, has led to exploration of the possibility of AChE reactivation promoted by use of stronger nucleophiles such as oximes (Wilson 1955, 1958). It has since been found that reactivation process of AChE is affected by several factors including the relative strength of the nucleophile, the orientation of the nucleophile with respect to the OP-AChE conjugate, and the prevention of aging. These considerations have led to the development of various oximes as potential antidotes to

AChE poisoning (Froede, 1971; Wilson 1992). The structures of generally used oximes are illustrated in Figure 2.9.
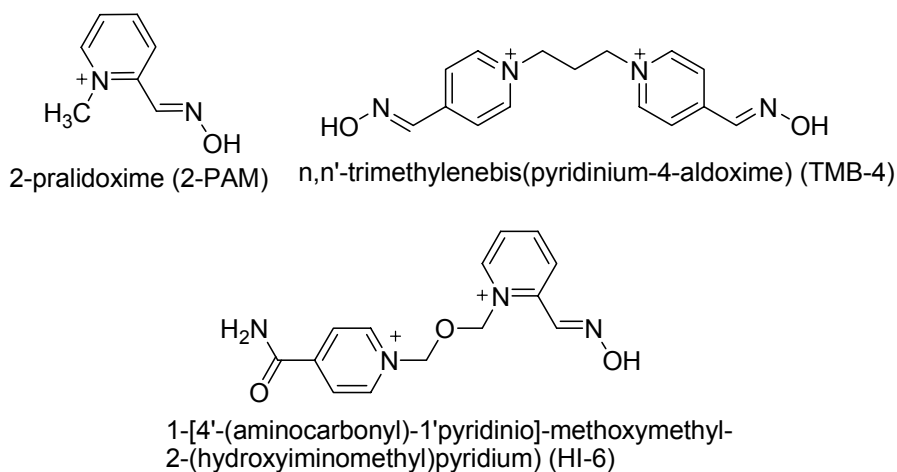
Figure 2.9. Oxime reactivation agents.

Oxime-mediated nucleophilic reactivation of OP inhibited AChE was proposed to proceed via the similar mechanism as scheme 2.6 (Scheme 2.7) (Aldridge 1975; Luo 1999).
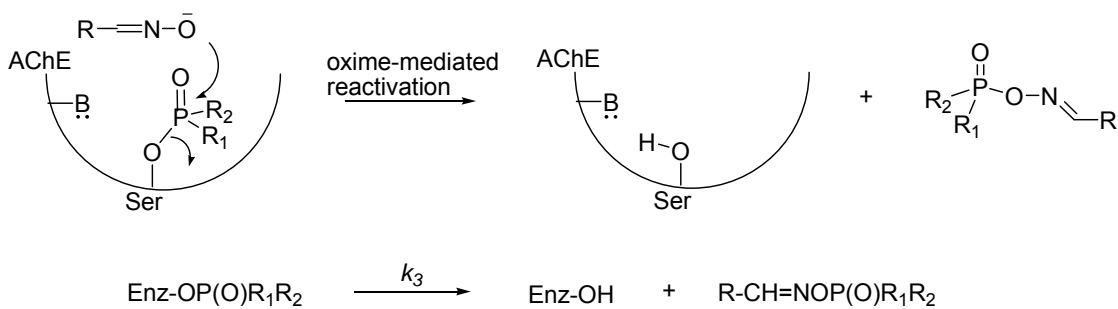
Scheme 2.7. Oxime-mediated reactivation of AChE inhibited by an OP.

There are a lot of similarities between this mechanism and that of spontaneous reactivation. The displacement of the OP moiety is dependent on the nature of the ligands linked to the phosphorus atom in both reactivation processes (Lotti, 1991), and smaller ligands are displaced with greater efficacy than compounds with bulkier groups. It has been suggested that this trend is due in part to the dimensional constraints imposed by the gorge structure obstructing oxime access (Wong, 2000), and competing aging mechanisms that are favored by bulkier groups.

2.6.3 Aging and Non-reactivation

Some OP-enzyme adducts undergo post-inhibitory reactions such as secondary dealkylation of the conjugated OP to produce an anionic phosphylated conjugate that is particularly resistant to all forms of reactivation, a process known as 'aging' (Scheme 2.8).

$$\text{Enz-OP(O)R}_1\text{(OR}_2\text{)} \quad + \quad \text{H}_2\text{O} \quad \xrightarrow{\; k_{AG} \;} \quad \text{Enz-O-P(O)(O}^-\text{)R}_1 \quad + \quad \text{R}_2\text{OH}$$
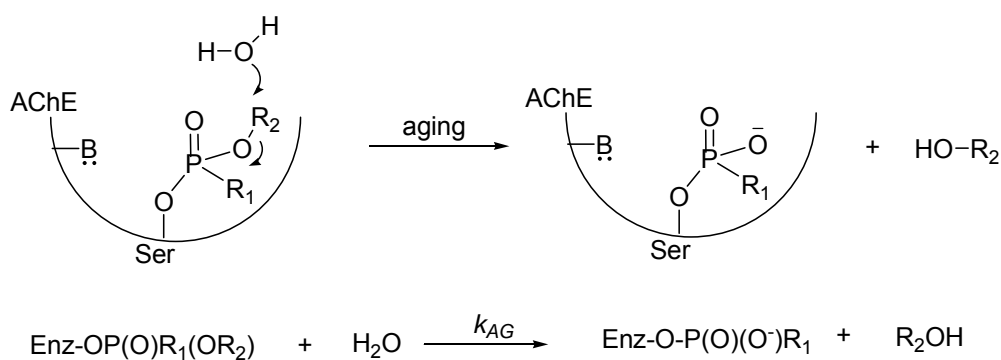
Scheme 2.8. Aging of AChE inhibited by an OP.

The negative charge introduced by the loss of an alkyl group during the aging process causes a significant charge repulsion barrier to dephosphylation because the inherent anionic phosphoester is resistant to nucleophilic attack (Westheimer 1987).

Aging is not the only phenomenon that results in non-reactivable AChEs. Non-reactivation can also be caused by a number of factors, including possible modification of the enzymes' tertiary structure resulting in loss of normal enzyme function (Morel, 1999; Sentjurc, 1999), steric occlusion of the phosphorylated active site that restricts the access of reactivating nucleophiles (Wong, 2000), and covalent modification of a residue other than serine in the active site (Mullner, 1980). These post-inhibitory processes also result in a time-dependent loss of the enzyme's ability to reactivate but do not involve a secondary dealkylation of the OP-AChE adduct, which is unique in aging.

2.7 Stereochemical Aspects of Organophosphorus Compounds

One of the most important structural features about OP compounds is their stereochemistry. The sp^3-tetracoordinated phosphorus atom becomes an asymmetric center when four ligands attached are non-identical. Chiral nonracemic phosphorus compounds are ubiquitous in asymmetric synthesis, both as ligands in metal-based processes and more importantly, as designed asymmetric inhibitors against AChE. Although P-stereogenic ligands have proven to be effective stereoselective inhibitors (Berkman, 1993), only a few have been made because of the difficulties in their synthesis. Synthesis is mostly based on resolution and the generation of a mixture of diastereomers (Valentine, 1984; Berkman, 1993; Wu, 1994; Reddy, 2002), which is discussed in greater details in Chapter 4.

Because the phosphorus atom is directly involved in the covalent modification to the active site of AChE, the chirality of an OP compound presumably affects mostly the inhibitory and post-inhibitory processes. The mechanism of stereoselective inhibition of AChE by OP-inhibitors has been suggested to be steric limitations within binding domains of the active site (Jarv, 1984). A 4,200-fold difference in inhibitory potency has been observed for the enantiomers of sarin (Figure 2.8).

Previous studies have suggested the classification of three binding domains (D1, D2 and D3 in Scheme 2.9) that precisely complement the three groups on phosphorus after the oxygen's position is fixed by the H-bond with the acidic residue (Jarv, 1984). Structural studies indicate that domain D3 (pointing to the gorge entrance) probably accommodates the leaving group, while domains D1 and D2 are responsible for

recognizing the ligands that remain attached to phosphorus after phosphorylation
(Scheme 2.9) (Jarv, 1984).

LG: leaving group
D1, D2 and D3: binding domains in the active site of AChE
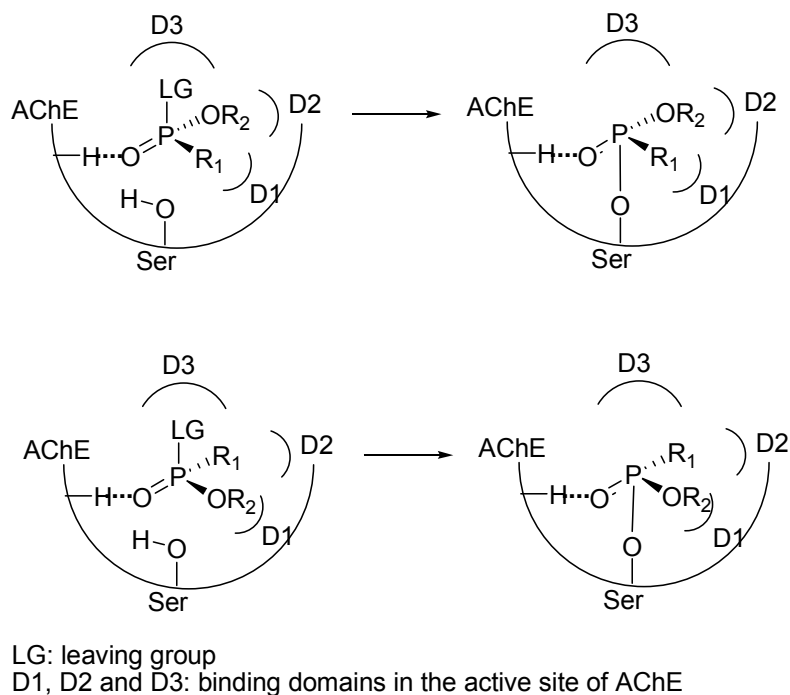
Scheme 2.9. Stereoisomeric forms of AChE inhibited by an asymmetric OP.

If the positions of the leaving group and the phosphoryl oxygen are held by D3
and acidic residue respectively, the molecular recognition between the binding pocket
and the remaining two ligands (R_1 and OR_2) is highly dependent on the absolute
configurations of the chiral center. Therefore, enantiomeric OPs have different inhibition
rates.

Additionally, chiral preferences have also been observed in post-inhibition
(reactivation or aging) kinetics experiments. The reactivation rates of stereoisomeric

phosphorylated AChE (OP-AChE conjugate) are so different that one OP-AChE is irreversibly inhibited (Wong, 2000; Doorn, 2000).

Phosphorothiolates are one general type of AChE-reactive molecules that have been shown to react with AChE in high stereoselectivity manner with ejection of thiol group (Ryu, 1991; Berkman, 1993; Thompson, 1996; Doorn, 2000). They become acknowledged mostly because of the success of their synthesis strategies and flexibility in design.

Phosphonothiolates bearing an asymmetric phosphorus atom have similar inhibition mechanism and activity as phosphorothiolate. However, few stereospecificity studies have been reported for phosphonothiolates mostly due to the limitation in their synthesis. In this study, asymmetric phosphonothiolates are successfully synthesized (Chapter 4) in an attempt to explore the stereoselectivity of the binding process.

2.8 <u>Mechanism and Kinetics of AChE Inactivation by Reversible Inhibitors</u>

In contrast to the irreversible organophosphorus inhibitors, reversible inhibitors can only transiently bind to AChE without covalent modifications. Weak interactions such as hydrogen bonds, hydrophobic interactions and ionic bonds involved in binding to AChE, can be easily removed. Various types of compounds have been discovered as reversible inhibitors against AChE (Fig 2.10).
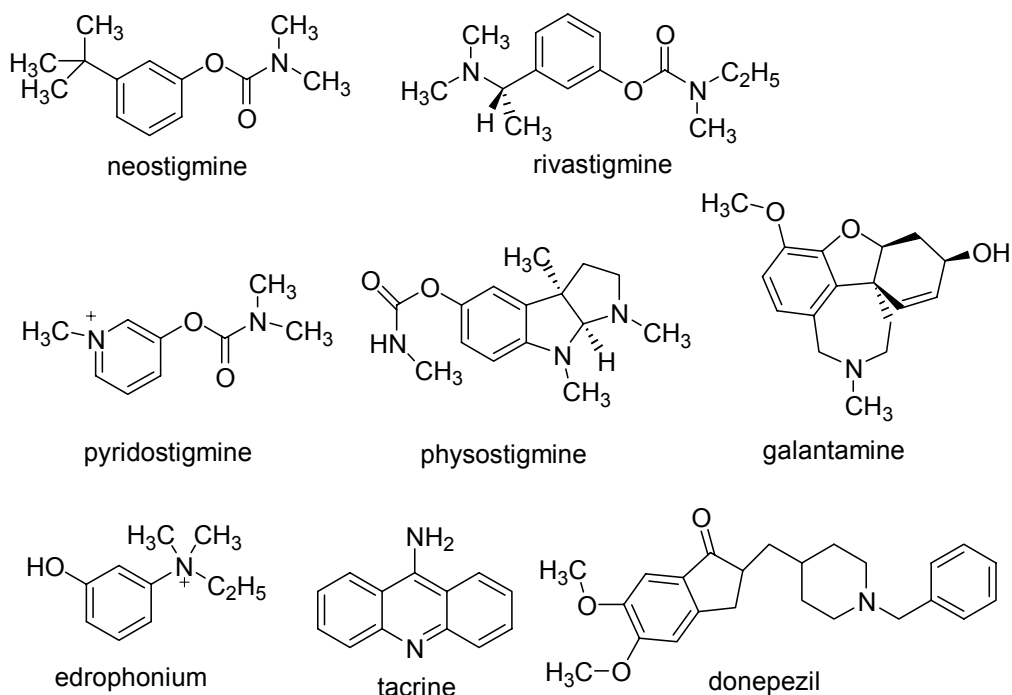
Figure 2.10. Examples of reversible acetylcholinesterase inhibitors.

Generally, reversible inhibitors are classified into competitive, noncompetitive and mixed-type inhibitors according to the changes of inhibition efficiency while varying the concentration of the substrate (Berg, 2002). Competitive inhibitors and the substrate

have affinity to the same active site of the enzyme therefore cannot bind simultaneously. Non-competitive inhibitors reduce enzyme's activity but do not interfere with substrate's binding to the active site, resulting in the inhibition depends only on the concentration of the inhibitor. In mixed-type inhibition, the inhibitor and the enzyme's substrate bind to the enzyme at the same time, however, the two binding processes affect each other.

The binding of reversible inhibitors to the enzyme can be quantitatively described as Figure 2.11. The enzyme-substrate complex ES is formed reversibly through the bimolecular reaction between enzyme E and substrate S. After catalysis, enzyme E and product P are released and free enzyme is regenerated. Dissociation constants K_i or K_i' describe the binding of inhibitor (I) to E and ES.

$$E + S \rightleftharpoons ES \rightleftharpoons E + P$$

with

$$E + S \quad + \quad ES$$

$$I \qquad\qquad I$$

$$\Big\updownarrow K_i \qquad\qquad \Big\updownarrow K_i'$$

$$EI \qquad\qquad ESI$$
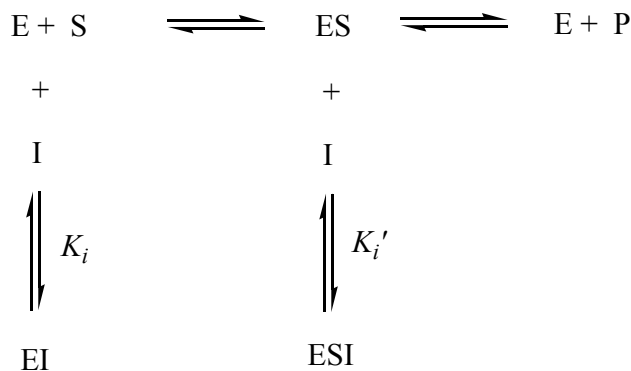
E: enzyme
S: substrate
I: reversible inhibitor
P: product from substrate and enzyme

Figure 2.11. Kinetic description of reversible enzyme inhibitors.

The three types of inhibitors have different affinities to free enzyme E and enzyme-substrate complex ES. Competitive inhibitors only bind to free enzyme (E) but

not to ES; non-competitive inhibitors bind to both E and ES with same affinity ($K_i = K_i'$); and mixed-type inhibitors bind to both E and ES, but with different affinities.

The dissociation constants (K_i and K_i') of a reversible inhibitor can be determined by fitting the kinetic data to a Lineweaver-Burk plot (Burk, 1934) according to a modified Michaelis–Menten kinetic equation (equation 2.6) based on the quasi steady state approximation (Briggs, 1925):

$$V = \frac{V_{max}[S]}{\alpha K_m + \alpha'[S]} = \frac{(1/\alpha')V_{max}[S]}{(\alpha/\alpha')K_m + [S]}$$

$$\frac{1}{V} = \frac{\alpha K_m}{V_{max}} \times \frac{1}{[S]} + \frac{\alpha'}{V_{max}} \qquad (2.6)$$

where the modifying factors α and α' are defined by the concentration of an inhibitor and its two dissociation constants:

$$\alpha = 1 + \frac{[I]}{K_i} \qquad (2.7)$$

$$\alpha' = 1 + \frac{[I]}{K_i'} \qquad (2.8)$$

V is the reaction velocity (the reaction rate),

K_m is the Michaelis-Menten constant,

V_{max} is the maximum reaction velocity, and [S] is the substrate concentration.

The Lineweaver-Burk plot of $1/V$ versus $1/[S]$ is used to determine the types of inhibitors based on the slopes and intercepts. When the Lineweaver-Burk plots of different [I] have the same y-intercept as uninhibited enzyme but different slopes and x-

intercepts (α' is a constant), the inhibitor is a competitive inhibitor since V_{max} is unaffected by competitive inhibitors. Noncompetitive inhibition generates plots with the same *x*-intercept (K_m is a constant) but different slopes and *y*-intercepts (α is unchanged). Mixed inhibition causes different intercepts on both the *y*- and *x*-axes and different slopes (Fig 2.12).
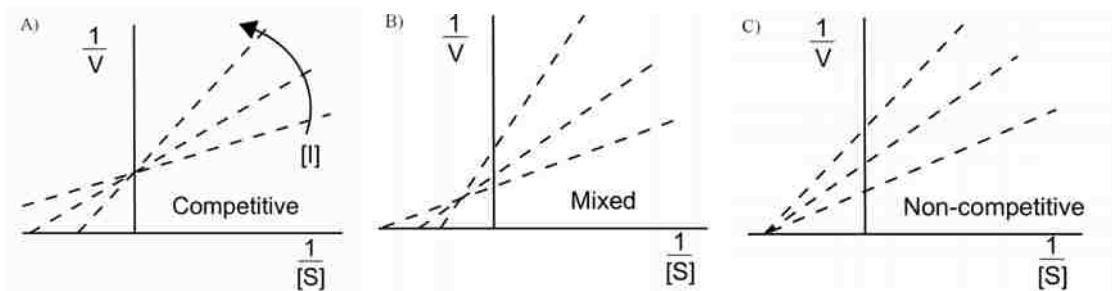
Figure 2.12. Lineweaver-Burk plots of different types of reversible enzyme inhibitors (http://en.wikipedia.org/wiki/Image:Inhibition_diagrams.png).

Based on equation 2.9, the competitive inhibition constant K_i is obtained by secondary plot of the slope versus the inhibitor concentration and the resulting *x*-axis intercept represents -K_i of the inhibitor. The noncompetitive inhibition constant K_i' is obtained by secondary plot of the *y*-intercept versus the inhibitor concentration and the resulting *x*-axis intercept represents -K_i'.

$$\frac{1}{v} = \left(\frac{K_m}{V_{max}} + \frac{K_m[I]}{V_{max}K_i} \right) \times \frac{1}{[S]} + \left(\frac{1}{V_{max}} + \frac{[I]}{V_{max}K_i'} \right) \qquad (2.9)$$

2.9 OP-Tethered Reporter Groups

We and other groups have shown that OP inhibitors of AChE bearing a reporter

group (chromophore) can be used to probe the enzyme activity (Liu, 1999; Cravatt, 2000;

Saltmarsh, 2000). This strategy is to seat a reporter group (chromophore probe) into the

gorge of AChE, to elucidate the environment at a given depth within the protein. The

general architecture of a molecular probe is illustrated in Figure 2.13.
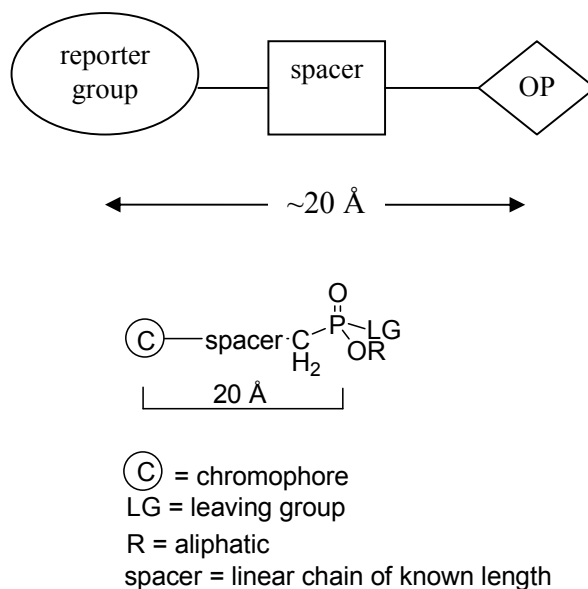
Figure 2.13. General design of the OP probes**.**

An organophosphate (OP) group is selected to covalently modify the active site of

AChE, thereby placing the probe in the gorge region but removed from the immediate

vicinity of the catalytic serine. Spacer groups were used to position the reactive

phosphorus atom 16~20 Å from the further edge of the chromophore moiety. This length

is to assure that the reporter group is placed at the entrance of the gorge when the phosphorus group binds to the active site.

Numerous applications in protein chemistry are rapidly shifting towards the use of fluorescent-based detection methods. The most important reasons for this shift are the availability of numerous spectrally distinct fluorescent labels and their wide variety of uses to replace the radioactive compounds. Consequently, reporter groups in this study are also chosen from different types of chromophores.

The major factors affecting chromophore performance are considered to make intelligent choice in chromophore selection:

(1) Molar extinction coefficient (ε).

Defined by $A = \varepsilon$ x b x C, in which A is the amount of light absorbed by a chromophore, ε is molar extinction coefficient in $M^{-1}cm^{-1}$, b is light path in centimeters, and C is the molar concentration of the chromophore. The molar extinction coefficient ε is a direct measure of a chromophore's ability to absorb light (Singer, 1996). This capability is essential to determine the amount of light that a molecule can generate via fluorescence emission. Most chromophores in common use have molar extinction coefficients at their wavelength of maximal absorption ranging between 5000 and 200,000 $M^{-1}cm^{-1}$ (Haugland, 1996). A larger ε value provides more convenience in UV-Vis and fluorescence emission spectrum analyses. However, determination of the inhibition rate of chromophore-linked OPs against AChE by Ellman method (Ellman, 1961) has to be conducted at 412 nm by observing the absorbance changes; thus, a chromophore with a large ε (strong color) may block the readings of spectrophotometer, especially when the absorbance of the chromophore is close to 412 nm.

(2) Absorption wavelength (*Abs*).

The longest wavelength absorption maximum in nanometers is expressed as *Abs*. In order to distinguish different chromophore-linked OPs in the future, chromophores with different *Abs* are desired. However, it is worth noting that a chromophore with a broad *Abs* is out of favor because of the potential overlapped spectrum. Also as mentioned earlier, chromophores with λ_{max} of approximately 412 nm absorbance should be avoided.

(3) Structure.

Different types of chromophores are available commercially. Considering the features of the peripheral anionic site of AChE, positively charged chromophores may bind to the peripheral anionic site on the gorge, while uncharged chromophores may not. Large chromophores can possibly block the entrance to the gorge, and small ones may slip into the gorge easily. Chromophores with a lot of aromatic rings may bind with aromatic residues in AChE, but attention needs to be paid in preparation because of the poor solubility of large, uncharged groups.
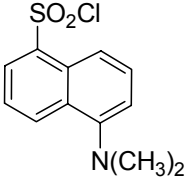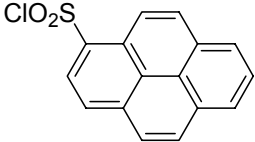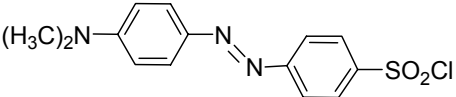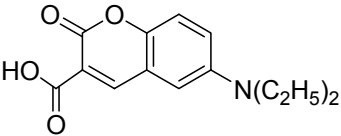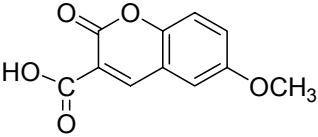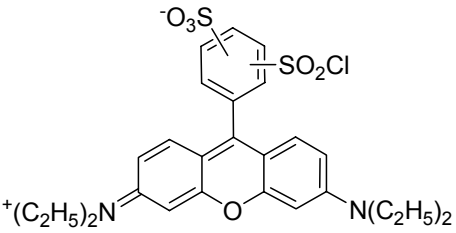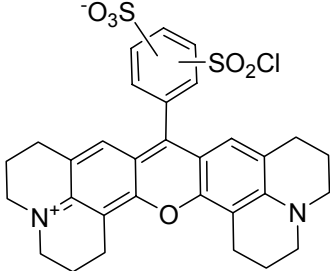
(4) Availability and price.

Some chromophores are too expensive therefore seldomly used by researchers and only available in the mixture of isomers, while some are inexpensive, commonly-used and well-characterized. Amine-reactive probes are widely used to probe proteins mostly because of the stability of the resulting chemical bond in biophysiological conditions. They are selected in this study to facilitate the linkage between the chromophore and OP moiety in the synthesis scheme in the future. Amine-reactive chromophores are mostly acylating reagents that from carboxyamides, sulfonamides,

ureas, and thioureas upon reaction with amines. Sulfonyl chlorides, including the dansyl, pyrene, Lissamine rhodamine B and Texas Red derivatives, are highly reactive and the resulting sulfonamides are extremely stable. Succinimidyl esters and carboxylic acids are also excellent reagents for amine modifications because of both stability and availability.

Considering all the factors above, the following chromophores are chosen (Table 2.1) based on molecule size, functionality, structure, absorbance (*Abs*), emission maximum spectrum (*EM*) and molar extinction coefficient (ε).

Table 2.1: Structure and properties of chromophores.

Structure	Name	*Abs*	ε: M⁻¹cm⁻¹	*EM*
	5-dimethylamino naphthalene-1-sulfonyl chloride (**dansyl chloride**)	372	3900	none
	1-pyrenesulfonyl chloride	350	28,000	380
	4-dimethylamino azobenzene-4'-sulfonyl chloride (**dabsyl chloride**)	466	33,000	none
	7-diethylamino coumarin-3-carboxylic acid	409	33,000	473
	7-methoxyl coumarin-3-carboxylic acid	336	20,000	402
	Lissamine™ (rhodamine B sulfonyl chloride)	568	88,000	583
	Texas Red sulfonyl chloride	588	84,000	601

The chemical properties of the selected chromophores are obtained from Molecular Probes Handbook (Haugland, 1996) and all of them are amine-reactive chromophores.

Dansyl chloride is one of the most commonly used amine-reactive chromophores, however, it is nonfluorescent until reacting with amines. The resulting dansyl amides are environmentally sensitive, indicating that their fluorescence quantum yields and emission spectral respond with changes of their local surroundings. The absorptivity of dansyl derivatives is weak compared with that of the more strongly UV light-absorbing chromophores such as pyrenesulfonyl chloride. Pyrenesulfonyl chloride derivatives have extremely long fluorescence lifetime (>100 ns), which is widely used in fluorescence anisotropy measurements. Dabsyl chloride derivatives have broad and intense visible absorption but no fluorescent signal, making them useful as acceptors in fluorescence resonance energy transfer (FRET) applications to study the interactions between two chromophores.

Coumarin derivatives are shorter wavelength reactive dyes for preparing the brighter fluorescent chromophores. The carboxylic acid groups in coumarins make them amine-reactive. Derivatives of 7-aminocoumarins have been widely applied in protein chemistry as labeling reagents and the methoxycoumarins have been used to achieve stable signal in solutions because they are pH-insensitive.

Lissamine rhodamine B and Texas Red sulfonyl chlorides have larger size than other chromophores and both are positively charged. They are long-wavelength light-emitting dyes and only available as mixtures of isomeric sulfonyl chlorides. Lissamine rhodamine B sulfonyl chloride is much less expensive and emits a shorter wavelength

than Texas Red sulfonyl chloride. Among all the rhodamines, the Texas Red

chromophores exhibit very little spectral overlap with other chromophores since it has the

longest emission spectrum. Moreover, the fluorescence quantum yield of Texas Red is

usually higher than that of Lissamine rhodamine B sulfonyl chloride. It is worth noting

that Texas Red sulfonyl chloride is highly unstable in water, however, the corresponding

sulfonamides are extremely stable (Haugland, 1996).

2.10 Click Chemistry

With the growth of drug discovery and combinatorial synthesis in the past two decades, the generation of lead compounds, and consequently, the reliability of the individual reaction to link the building blocks is required for high-throughput screening. Click chemistry is one of these approaches to the synthesis of drug-like molecules constructed by reactive building blocks to accelerate the drug discovery.

Sharpless and his coworkers defined click chemistry as a "modular, wide in scope, stereospecific" chemistry reaction, which gives "very high yield in simple reaction conditions, and generates only inoffensive byproducts" (Kolb, 2001). Of these reactions, a best 'click reaction' is the "Huisgen 1,3-dipolar cycloaddition of alkynes to azides to form 1,4-disubsituted-1,2,3-triazoles (anti) or 1,5-disubsituted-1,2,3-triazoles (syn)" (Scheme 2.10).

The click reaction is a slow kinetic process at room temperature without a catalyst and results in the mixture of regio-isomers. It has been demonstrated that the catalysis of this reaction by Cu(I) yields exclusively a 1,4-disubstituted triazole with a much faster rate (Rostovtsev, 2002). The reaction is mild and very efficient, requiring no purification in many cases (Rostovtsev, 2002). The formation of 1,5-disubstituted triazoles has been regioselectively mediated by ruthenium complexes (Krasinski, 2004; Tam, 2007), stereoelectronic effects (Coats, 2005) or biological selection (Krasinski, 2005; Manetsch, 2004).
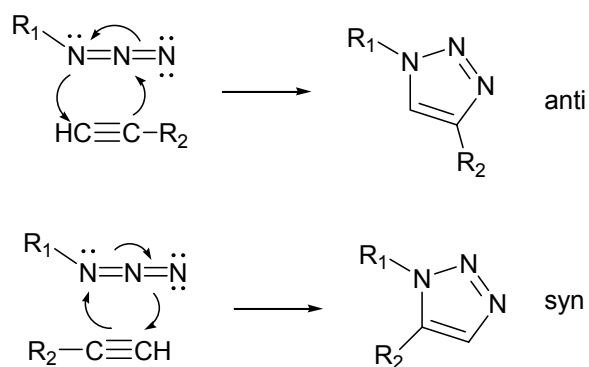
Scheme 2.10. Click chemistry.

The azide and alkyne groups are insensitive to most biological functional groups and aqueous environments, which allows the wide use of the click reaction in target guided synthesis (Manetsch, 2004). The resulting triazole ring has similarities to the ubiquitous amide moiety, but is not susceptible to hydrolysis and cleavage.

2.11 <u>Single Molecule Docking and FlexX</u>

Given a protein and an arbitrary small molecule, docking predicts whether the small molecule will bind to the protein and how the geometry of the binding is. Ligand-protein docking predictions determine the structure of the ligand-protein complex given the protein atomic coordinates. In certain cases, both protein and ligand are considered as rigid bodies to make an easier prediction of the interactions; in other cases, it might be necessary to consider either the ligand, or the protein or both molecules as completely or partially flexible when necessary conformational changes are considered in the binding process. The basic theory of docking program is that the configuration of the system (protein-ligand complex) has the minimum of free energy (potential energy + entropy).

As a relatively new approach to drug design, docking is largely dependent on the number of available protein crystal structures, which is increasing exponentially. The fast advancement in computer technology in the past few years has led to the development of several ligand-protein docking and drug-design tools (Joseph-McCarthy, 1999; Tao, 2001; Pei, 2004).

Some of the most commonly-used docking programs include AutoDock (Goodsell, 1990; Morris, 1996; Olson, 1998), DOCK (Kuntz, 2005), FADE (Fast Atomic Density Evaluator) and PADRE (Pairwise Atomic Density Reverse Engineering) programs (Mitchell, 2001; Law, 2003), Glide (Friesner, 2004; Halgren, 2004) and FlexX (Kramer, 1999). These docking programs use different construction algorithm and have various applications in molecular modeling studies, such as FADE and PADRE programs are used to rapidly discover the reactive regions of a protein and illuminate its interesting

structural features, AutoDock, FlexX and Glide are designed to predict interactions between small molecules (such as substrates and drug molecules) and proteins with known x-ray structure, and DOCK is mainly used to examine possible binding orientations of protein-protein and protein-DNA complexes.

Among these docking programs, FlexX was chosen to predict protein-ligand interactions in this study because of its fast rate, steadiness and flexibility. An overriding advantage of FlexX is that FlexX-Pharm in FlexX allows us to include pharmacophore type constraints in the docking calculation, which satisfies the requirement of the covalent modification between OP compounds and AChE in this study. A chemical reaction generally occurs only when the distance between the two reactive groups is less than 2.5 Å and a new chemical bond is formed after the reaction. To ensure a covalent modification of AChE, a 2.5 Å distance between the phosphorus atom of the ligand and the hydroxyl group of the active serine is defined in FlexX-Pharm as a necessary constraint, consequently, the protein with configurations in the resulting docking resolutions presumably can be irreversibly modified by the ligand. This will be discussed in detail in experimental section.

By using an incremental construction algorithm (Kramer, 1999), FlexX finds the most favorable position of the fragments in the active site by calculating torsion angles (intramolecular energy) and protein-ligand interactions (intermolecular energy). Besides defining a constraint, a reference ligand file and a protein file also need to be constructed before docking. The reference ligand provides the proper structure of ligand before being docked into the active site. The preparation of ligand converts data into readable format so that SYBYL can read and build proper structure of the ligand. Protein properties, such

as active site, ionization stage, and acceptable torsions, are defined in the protein

preparation step. After docking, FlexX ranks a series of possible protein-ligand

complexes based on various scoring systems.

CHAPTER 3

OBJECTIVES

1. To prepare a panel of chromophores linked to a reactive fluorophosphonate (FPs) head group and address a variety of chromophore-linked FPs different in chromophore structure and length.

2. To determine the inhibition potency (inhibition rate k_i) of chromophore-FPs against purified recombinant mouse AChE (rMAChE) and commercial electric eel AChE (EEAChE) and evaluate the binding effects of the chromophore and FP moiety to protein.

3. To visualize and calculate positioning of the chromophore-FP-AChE relative to the protein active site/gorge/peripheral site by molecular modeling.

4. To synthesize the asymmetric phosphonothiolates as anti-AChE inhibitors.

5. To examine the AChE stereospecificity by studying the anti-AChE potency of S_p- and R_p- phosphonothiolate enantiomers.

CHAPTER 4

SYNTHESIS

4.1 <u>Chromophore-linked Fluorophosphonates (FPs)</u>

A panel of chromophore-FPs was synthesized to ensure: 1) the synthetic routes to chromophore-linked OPs were functional; 2) the designed chromophore-linked OPs were still inhibitors against AChEs, which means that the added linker and chromophores did not impede inhibition; and 3) the chromophore and OP parts were positioned at the P-site and A-site, respectively, in the active gorge. In addition, the role of the chromophore in binding to AChEs could be evaluated by using a fluorophosphonate analog holding the tether constant (Saltmarsh, 2000). The fluoro atom has been chosen as an excellent leaving group and the phosphorus stereochemistry is not being discussed in this section.

The overall strategy was to synthesize a reactive phosphorus group containing an azo group and a chromophore part containing acetylene group and to use click chemistry to link the two building blocks together via a triazole ring. Fluoro groups would be added to phosphorus in the last step to ensure effective phosphorylation.

Considering the depth of the AChE gorge is 20 Å, the length of the target synthesized FPs was adjusted to approximately 16 Å (chromophore excluded) to optimize the inhibition ability (Scheme 4.1). With counting the length of triazole ring linker and

chromophore, three methylene (3-CH$_2$, n = 3) or four methylene (4-CH$_2$, n = 4) units

between phosphorus and azo group were desired.
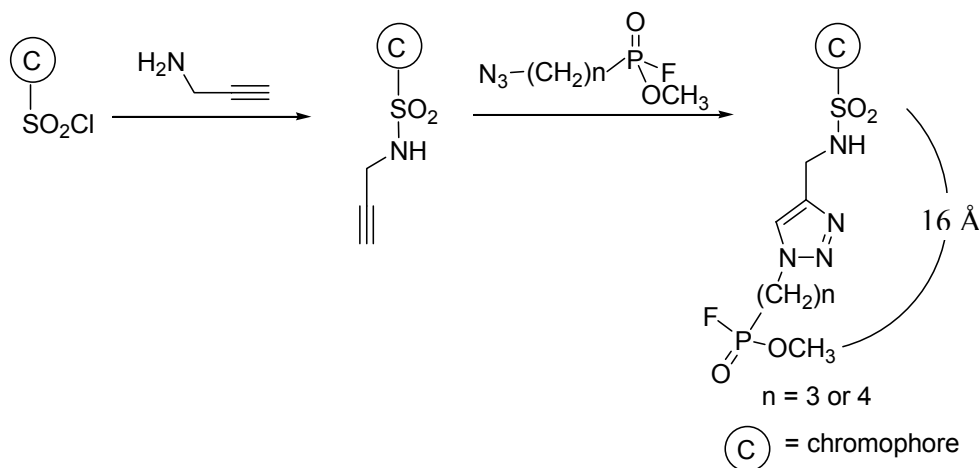
Scheme 4.1. Design of chromophore-linked FPs (chromophore is not included in distance calculation).

4.1.1   Dansyl-linked Fluorophosphonates (FPs)

5-Dimethylaminonaphthalene-1-sulfonyl chloride (dansyl chloride) (Gray, 1972) is a very stable chromophore with a strong color (large ε), good solubility, and ease of reaction with amines. These factors combined with the availability and inexpensive price of this source have made it the chromophore of choice for conducting preliminary synthesis studies.

The synthesis of dansyl-linked FPs is outlined in Scheme 4.2. Trimethyl phosphite was used as the starting material, followed by Arbuzov reaction with 1,3-dibromopropane (3-CH$_2$) or 1,4-diromobutane (4-CH$_2$) to produce *O,O*-dimethyl, bromo propyl/butyl phosphonate **1a/1b** (Maguire, 2001). Four equivalents of the dibromo compounds were used to reduce any double addition by-product. ^{31}P NMR showed that

the reaction was complete (from 140 ppm to 34 ppm) after refluxing at 140 ºC for 4 h. The desired products were bulb-to-bulb distilled into the cold trap under reduced pressure (0.5 mmHg) at a temperature of 90 °C to 130 °C. Substitution of a bromine atom with an azo group using sodium azide produced *O,O*-dimethyl, azo propyl/butyl phosphonate **2a/2b**. Various organic solvents including dimethylformamide (DMF), methanol, acetonitrile, and acetone were examined with 10% DI water as co-solvent and we found that DMF was the best solvent, which could facilitate a complete conversion in 12 h with best yield and purity. Catalysis of the reaction with sodium iodide (NaI) in acetone was also attempted, however, more by-products made the purification process more complicated and lower yield.

For the chromophore part, dansyl chloride was coupled with propargyl amine, thus adding an acetylene group to the amine-reactive chromophore (Bolletta, 1996). The reaction went from a bright yellow sulfonyl chloride to a florescent sulfonamide. After quenching with phosphate buffer (pH = 7) and extraction with CH_2Cl_2, sulfonamide **3** was obtained as a yellow solid in a quantitative yield. Click chemistry was conducted between the acetylene **3** and azo groups of **2a/2b** in co-solvents of t-butanol (t-BuOH) and water and afforded a robust triazole ring (Kolb, 2001) to form compound **4a/4b**. The quantitative yield and high reaction rate of click reaction under Cu(I) catalysis provided a new, easy, efficient way to link the two building blocks and form chromophore-linked OPs.

Dansyl-linked *O,O*-dimethyl phosphonate **4a/4b** was hydrolyzed at a single P-OCH_3 with sodium hydroxide (NaOH, 2 N, reflux) to afford phosphorus monoacid **5a/5b** and was converted to the corresponding fluorophosphonate (FP) **6a/6a'** with cyanuric

fluoride ($C_3N_3F_3$) in CH_2Cl_2 (Kokotos, 1996). Diethylamino sulfur trifluoride (DAST) was also examined as a reagent to introduce the P-F bond but did not work with our phosphonic acids. The conversion of the phosphonic acids to FPs was monitored by ^{31}P NMR: the 3 ppm upfield shift from the diester $P(OCH_3)_2$ (33.9 ppm) to the phosphorus monoacid (30.6 ppm) and finally, formation of the characteristic P-F coupling constant (J_{P-F} = 1072 Hz), which was centered at 31.6 ppm.
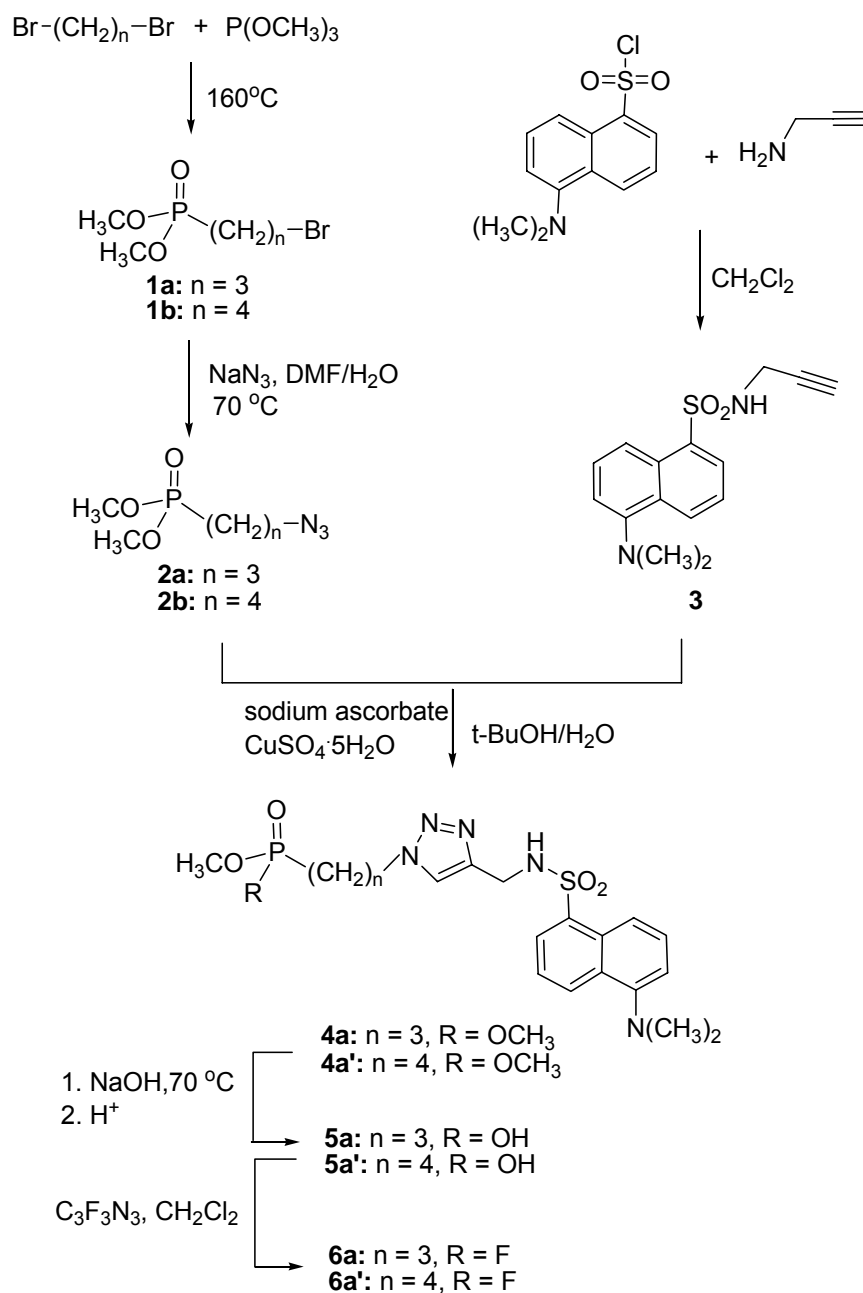
Scheme 4.2. Synthesis of dansyl-linked FPs.

In addition, the synthesis of azo-FPs **8a/8b** was undertaken in an effort to provide a control molecule of the FP part without attaching chromophores. Compounds **8a/8b** would enable the study of the OP portion without the chromophore as an AChE inhibitor.

Similar hydrolysis and FP conversion methods were applied to compound **2a/2b** (Scheme 4.3) and again, the reaction sequence was monitored by ^{31}P NMR.
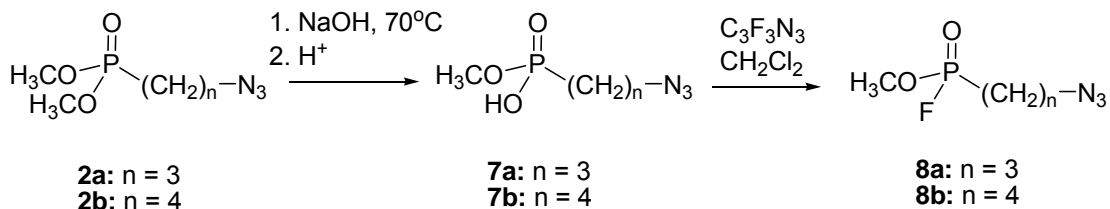
Scheme 4.3. Synthesis of azo-FPs.

^{31}P NMR data is shown in Table 4.1 and illustrates what a powerful tool it can be. As there is considerable difference in the chemical shift as one goes from P-OCH$_3$ to P-OH to P-F, it is easy to follow the course of reactions. It is worth noting that the unique phosphorus-fluoro (P-F) coupling constant is an identity unique to FP compounds.

Furthermore, as each phosphorus atom in a molecule produces only one sharp definitive peak with a chemical shift (as listed in Table 4.1) that is directly related to the phosphorus atom's immediate environment, compounds containing impurities are easily spotted. To simplify discussion, only compounds with 3-CH$_2$ units (n = 3) were presented and 4-CH$_2$ (n = 4) analogs have very similar properties.

Table 4.1: ^{31}P NMR chemical shifts of FPs.

compounds	^{31}P NMR (δ) ppm
P(OCH$_3$)$_3$	140.0
(H$_3$CO)$_2$P(O)(CH$_2$)$_3$-Br (**1a**)	34.3
(H$_3$CO)$_2$P(O)(CH$_2$)$_3$-N$_3$ (**2a**)	34.5
(H$_3$CO)$_2$P(O)(CH$_2$)$_3$-(triazole)-CH$_2$SO$_2$-dansyl (**4a**)	33.9
(H$_3$CO)(HO) P(O)(CH$_2$)$_3$-(triazole)-CH$_2$SO$_2$- dansyl (**5a**)	30.6
(H$_3$CO)(F) P(O)(CH$_2$)$_3$-(triazole)-CH$_2$SO$_2$-dansyl (**6a**)	31.6 (d, J = 1072 Hz)
(H$_3$CO)(HO)P(O)(CH$_2$)$_3$-N$_3$ (**7a**)	31.2
(H$_3$CO)(F)P(O)(CH$_2$)$_3$-N$_3$ (**8a**)	32.2 (d, J = 1075 Hz)

Triazole: 1,4-substituted, 1,2,3-triazole ring.

4.1.2   Other Chromophore-linked FPs
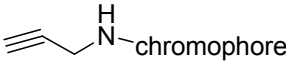
Since many amine-reactive chromophores are commercially available as sulfonyl chlorides or carboxylic acids, the synthesis approach in Scheme 4.2 was rationalized to be the most applicable and general to a panel of structures.

Using a similar scheme described above, FPs with either 3 methylene (n = 3) or 4 methylene (n = 4) units were prepared bearing different chromophore groups, thereby expanding the structure and chromophore diversity. Seven chromophores (Table 2.1) were selected and coupled with propargyl amine to form compounds **3a-3f** (Table 4.2). Their corresponding chromophore-linked FPs were synthesized from **3a-3f** and **2a-2b** in collaboration with Dr. Alirica Suarez. Fourteen chromophore-linked FPs (Table 4.3) and

two azo-linked FPs (controls) were prepared as inhibitors against AChE, and as potential probes of other protein targets.

In order to know exactly which part of chromophore-linked FP contributes to the inhibition of AChE, seven acetylene-containing chromophores (**3a - 3g**, Table 4.2) were also prepared for inhibition studies against AChEs.

Table 4.2: Synthesized chromophore amides.

chromophore	compounds
dansyl	**3a**
pyrene	**3b**
dabsyl	**3c**
diethylamino coumarin	**3d**
methoxycoumarin	**3e**
Lissamine rhodamine B	**3f**
Texas Red	**3g**

Note: Chromophore structures are drawn in Table 4.3.

Table 4.3: All chromophore-linked fluorophosphonates synthesized.

(n = 3, 4)

chromophore		n = 3	n = 4
dansyl		**6a**	**6a'**
pyrene		**6b**	**6b'**
dabsyl		**6c**	**6c'**
diethylamino coumarin		**6d**	**6d'**
methoxy coumarin		**6e**	**6e'**
Lissamine rhodamine B		**6f**	**6f'**
Texas Red		**6g**	**6g'**

4.2 Dansyl-linked Phosphonothiolates

Phosphonothioates are AChE-reactive molecules that typically contain an asymmetric phosphorus atom. It was established that asymmetric phosphonothiolates undergo reactions with AChE with high stereoselectivity concomitant with ejection of a thiol group (Doorn, 2000; Ryu, 1991).

A model compound, dansyl-linked *O,S*-dimethyl phosphonate (Fig 4.1) as a racemate was first studied to ensure the success of the synthetic steps and to estimate the inhibition potency of phosphonothioates. For comparison, dansyl-linked *O*-methyl, *S*-choline phosphonate (Fig 4.1) was synthesized because of the structural similarity to acetylcholine, the AChE's endogenous substrate. The synthesis of the phosphonothiolates were undertaken with three methylene units (n = 3) only.

Dansyl-linked *O,S*-dimethyl phosphonate

Dansyl-linked *O*-methyl, *S*-choline phosphonate
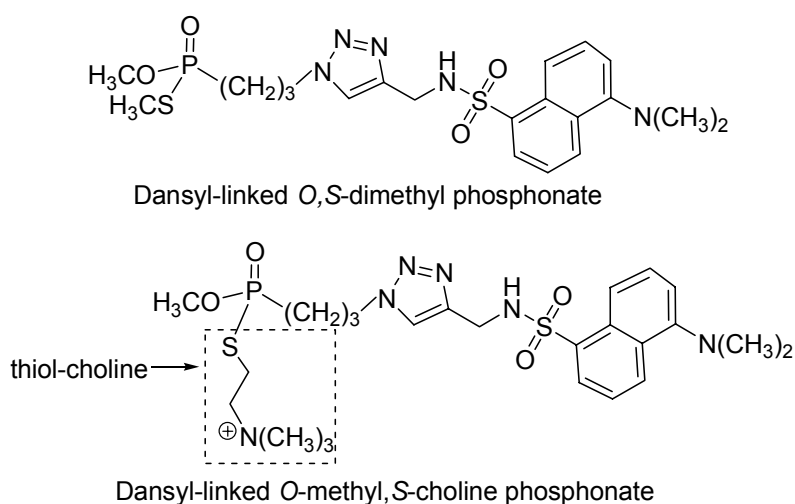
Figure 4.1. Structures of the target dansyl-linked phosphonothiolates.

4.2.1 Synthetic Approach A: Conversion of P=O to P=S in 4a with Lawesson Reagent (LR)

Lawesson reagent (LR) (Figure 4.2) is a widely-used reagent to transform P=O to P=S (Horner, 1982; Lecher, 1956).
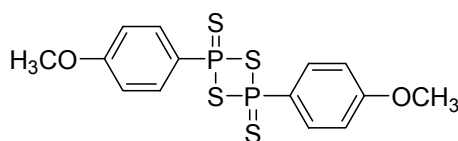
Figure 4.2. Structure of Lawesson reagent (LR).

The most straightforward strategy to synthesize the desired dansyl-linked phosphonothiolates is to first modify the already synthesized dimethyl phosphonate **4a** to dimethyl phosphonothionate by converting the P=O (oxon) to P=S (thionate). The target dimethyl phosphonothionates can be dealkylated and realkylated on sulfur over oxygen to give *O*-methyl, *S*-alkyl phosphonates (Scheme 4.4).
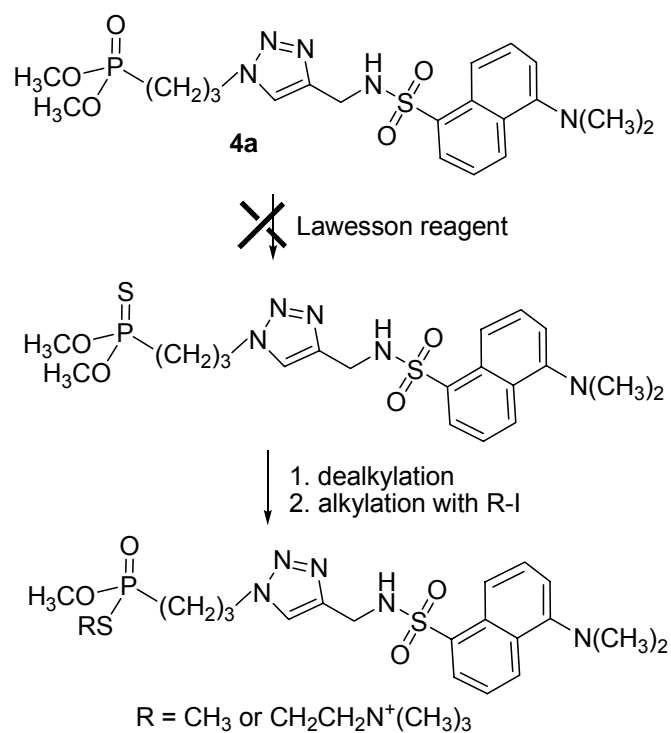
Scheme 4.4. Attempted synthesis of dansyl-linked phosphonothioates with LR.

The reaction between **4a** and LR was monitored by ^{31}P NMR. The starting material **4a** was consumed completely, however, no desired product was obtained. Experiments showed that LR also decomposed either the triazole ring or other functional groups in the molecule. So, compounds synthesized prior to click chemistry, **1a** or **2a**, would be reacted with LR to attempt converting the phosphonyl to a thiophosphonyl without the triazole or chromophore present (next section).

4.2.2 Synthetic Approach B: Reacting Bromo/Azo-phosphonates (Compound 1a or 2a) with LR

From the observations of synthetic approach A, it was decided to conduct the P=O to P=S conversion before click chemistry so that LR would not react with the triazole ring or the chromophore (Scheme 4.5). Both bromo-phosphonate (**1a**) and azo-phosphonate (**2a**) were examined in reaction with LR, and it was shown that both bromo- and azo- groups were reactive toward LR. However, it is worth noting that a lot of peaks in ^{31}P NMR originated from the decomposition of LR, which brought trouble in keeping track of the reaction progress using ^{31}P NMR. Moreover, it was not clear in spectral monitoring that we were seeing desired formation of the thionates.
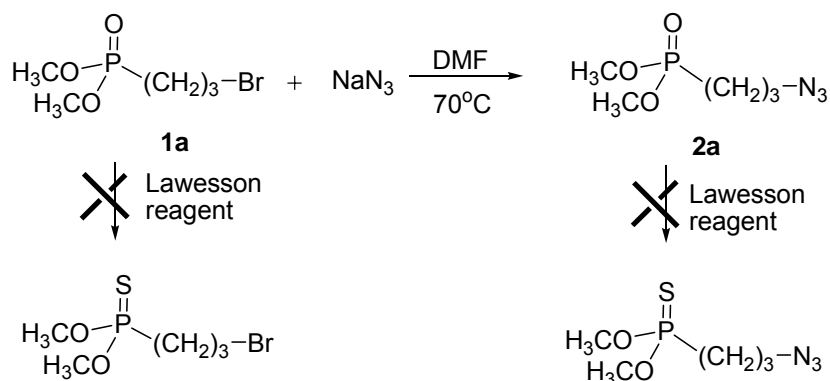
Scheme 4.5. Attempted synthesis of bromo-/azo- phosphonothionates with LR.

4.2.3 Synthetic Approach C: Using Sodium Hydrosulfide (NaSH) As a Nucleophile to Produce Phosphonothioic Acids [P(O)SH]

Because of the complexity of using LR in our studies, sodium hydrosulfide (NaSH) was selected to react with azo-phosphonate **2a** and dansyl-linked phosphonate **4a**

to prepare a phosphonothioic acid. The displacement of a methoxy ester by –SH group

was not observed under reflux after 48 h. The reaction with NaSH was also studied with

the reactive FP compounds **6a** and **8a**. A reaction occurred but no desired product was

observed in either reaction according to ^{31}P NMR. In these experiments, either a side

reaction was predominating (e.g. dealkylation) or the product was decomposing upon

formation as some thioic acids are known to do.

4.2.4   **Synthetic Approach D: Using a New Synthesis Strategy Starting with**

   Dimethyl Thiophosphite

   With the difficulties of adding sulfur to phosphorus on the previously synthesized

compounds, a new synthetic scheme starting with dimethyl thiophosphite (DMTP) was

designed (Scheme 4.6).
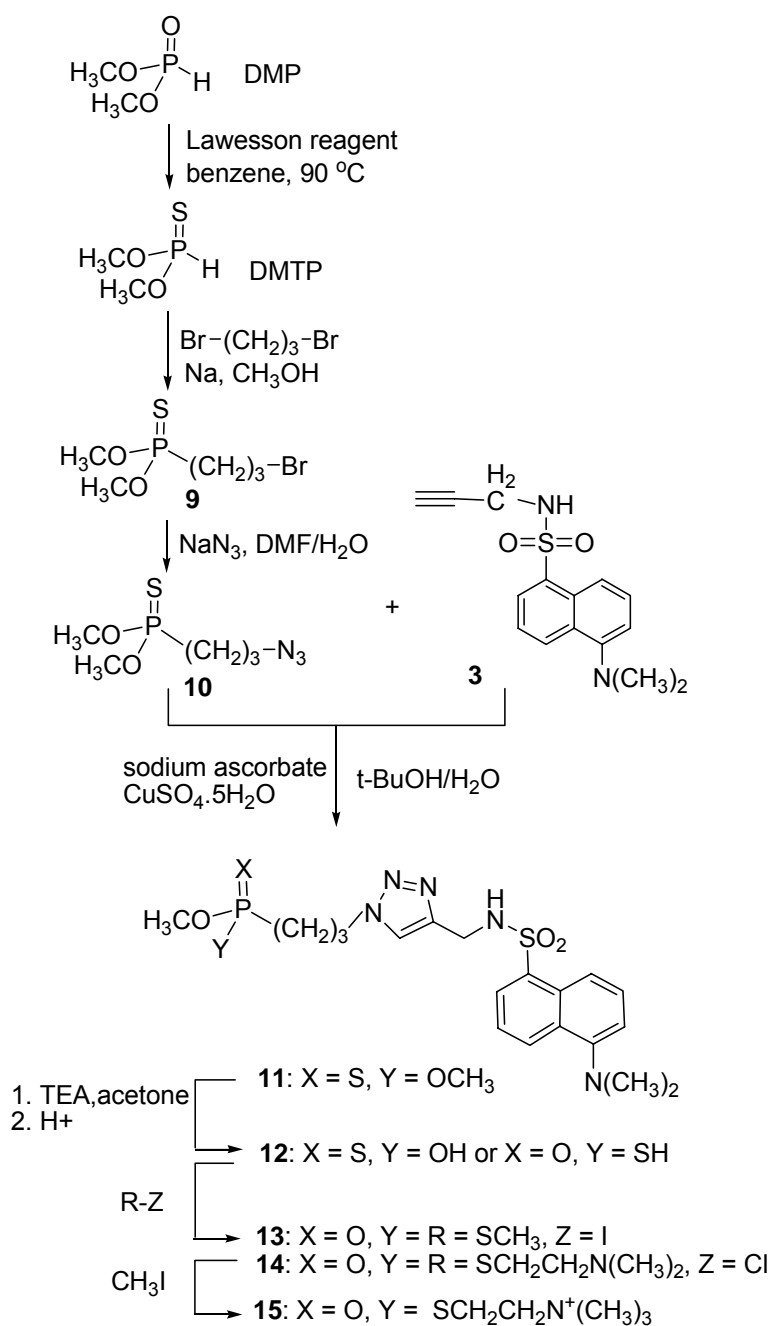
Scheme 4.6. Synthesis of dansyl-linked phosphonothiolates.

Commercially available DMTP gets oxidized easily and commonly contains impurities, so freshly synthesized DMTP is preferred. Dimethyl thiophosphite (DMTP) was prepared from dimethyl phosphate (DMP) using LR (Tongcharoensirikul, 2004).

The reaction was heated at 90 – 100 ºC for 2 h and ^{31}P NMR showed complete

conversion (from 11.5 ppm to 74.9 ppm). Sulfur- and phosphorus-containing by-

products were precipitated with adding hexane and filtered off. The solution was

concentrated and distilled under reduced pressure to give high purity DMTP.

A solution of sodium dimethyl thiophosphonate (prepared from DMTP and an

equivalent sodium in anhydrous methanol) was added dropwise to 1,3-dibromopropane to

afford *O,O*-dimethyl (3-bromopropyl) thiophosphonate **9**. Bromine substitution of **9** with

sodium azide provided *O,O*-dimethyl (3-azopropyl) thiophosphonate **10**, which is now

ready for the click reaction with compound **3**, which proceeded without problem to afford.

Dansyl-linked phosphonothionate **11** after click reaction was purified by a flash

chromatography. The synthesis of phosphonothionates (**9**, **10**, and **11**) was similar to the

synthesis of the corresponding phosphonates (**1a**, **2a**, and **4a**) in section 4.1, however,

inert argon gas was mandatory for each step of the synthesis, purification and storage

processes to prevent oxidization of phosphonothionates by air or moisture.

Dealkylation of phosphonothionate **11** was achieved by triethylamine and the

resulting solution was acidified (pH = 1) to obtain the phosphonothioic acid (P-SH) **12**.

Tautomerization of **12** was equilibrated between P-SH and P-OH products, which

produced two corresponding peaks in ^{31}P NMR spectrum (93.1 and 49.7 ppm).

Alkylation of **12** was achieved by reaction with the methyl iodide and 2-chloro-N,N-

dimethylethylamine and the target phosphonothiolates **13** and **14** were synthesized. To a

solution of compound **14** in chloroform, methyl iodide was added to obtain dansyl-linked

O-methyl, *S*-choline phosphonate **15**.

Again, as a simple and straightforward analytical method, ^{31}P NMR analysis was

used to follow the course of reactions. Data associated with the synthesis of

phosphonothioates are listed in Table 4.4. Compared with phosphonate compounds (P=O)

listed in Table 4.1, phosphonothionates (P=S) have higher or downfield chemical shifts.

In addition, phosphonothiolate **13** changes ~ 40 ppm downfield from phosphonothionates

11. All the data were collected with reference to 85% H_3PO_4 as an external standard.

Table 4.4: ^{31}P NMR chemical shifts of phosphonothioates.

compounds	^{31}P NMR (δ) ppm
$(CH_3O)_2P(O)H$	11.5
$(CH_3O)_2P(S)H$	74.9
$(CH_3O)_2P(S)(CH_2)_3$-Br (**9**)	102.7
$(CH_3O)_2P(S)(CH_2)_3$-N_3 (**10**)	103.2
$(CH_3O)_2P(S)(CH_2)_3$-(triazole)-CH_2SO_2-dansyl (**11**)	102.1
$(CH_3O)(HO)P(S)(CH_2)_3$-(triazole)-CH_2SO_2-dansyl or $(CH_3O)(HS)P(O)(CH_2)_3$-(triazole)-CH_2SO_2-dansyl (**12**)	93.1 & 49.7
$(CH_3O)(CH_3S)P(O)(CH_2)_3$-(triazole)-$CH_2SO_2$-dansyl (**13**)	59.1
$(CH_3O)[(CH_3)_2NCH_2CH_2S]P(O)(CH_2)_3$-(triazole)-$CH_2SO_2$-dansyl (**14**)	59.0
$(CH_3O)[(CH_3)_3N^+CH_2CH_2S]P(O)(CH_2)_3$-(triazole)-$CH_2SO_2$-dansyl (**15**)	58.8

Triazole: 1,4-substituted, 1,2,3-triazole ring.

4.2.5   <u>Summary</u>

Different approaches to the synthesis of the target phosphonothiolates were attempted and a robust, uncomplicated, and practical way was discovered (in section 4.2.4). The two designed dansyl-linked phosphonothiolates were successfully synthesized and their inhibition potency against AChEs was studied (in chapter 5). It is worth noting that the phosphonothiolates and phosphonothionates are sensitive to air/water and thus have to be stored in an inert atmosphere to prevent oxidization.

4.3 Asymmetric Phosphonothiolates

The model phosphonothiolates **13/14/15** synthesized previously are actually a 1:1 mixture of two enantiomers. To study their stereoselective interaction with AChEs, enantiopure isomers need to be synthesized. In general, enantiomers of smaller molecules are easier to be resolved, so asymmetric phosphonothionates with an azo-group (before click reaction) were prepared first in this section and then reacted with different alkyne-based chromophores to form CLAPs bearing an asymmetric phosphorus.

Basically, there were two synthetic routes to obtain the asymmetric phosphonothiolates: 1) The first method involves dealkylation with an alkaloid to form two alkaloid salts of phosphonothioic acids (*Rp* and *Sp*). Repeated fractional crystallization of the resulting diastereomeric mixtures results in separation of the individual, "resolved" diastereomers. The individual phosphonothioic salts were then converted to each isomer of phosphonothiolates by removal of alkaloid. This method has been used in the synthesis of asymmetric phosphonothiolates (Valentine, 1984; Aaron, 1960; Berkman, 1993). 2) The second pathway uses a chiral auxiliary instead of the alkaloid to resolve the phosphorus stereocenter. A covalent bond is formed between an amine enantiomer and one more chiral center was added to phosphonothioates. The resulting two diastereomers were separated by HPLC and the added chiral center is removed to offer two enantiopure isomers (Valentine, 1984; Koizumi, 1978; Wu, 1994; Reddy, 2002).

4.3.1   Attempted Synthesis of Asymmetric Phosphonothioates via Alkaloid

       Resolution

       Several prior studies showed that alkaloid resolution was an effective way to prepare enantioenriched phosphonothiolates (Valentine, 1984; Aaron, 1960). In addition, our group also has experience in successfully separating phosphonothioic acids via alkaloid resolution (Berkman, 1993). The general method for this type of resolution involves either conducting an acid-base reaction with a phosphonothioic acid and the alkaloid, or dealkylating a phosphonothioate methyl ester with the alkaloid to directly form the alkylated alkaloid/phosphonothioic acid diastereomer salts.

       Strychnine, brucine and quinine (Fig 4.3) are three widely known and used alkaloids in resolution of phosphorus compounds (Drabowicz, 1988; Michalski, 1963).
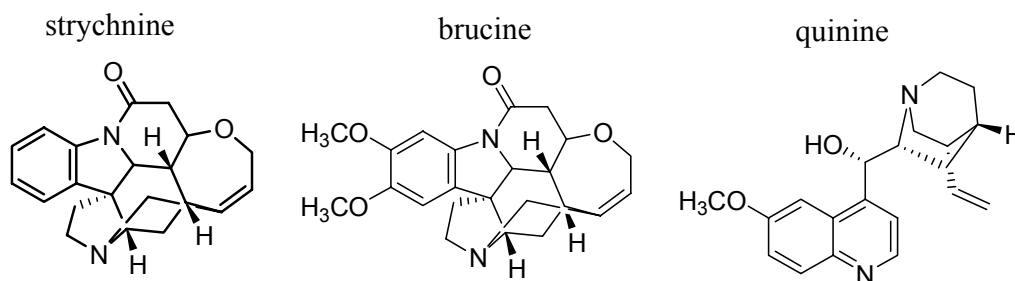
Figure 4.3. Strychnine, brucine and quinine structures.

       Dealkylation of *O,O*-dimethyl (3-azopropyl) thiophosphonate **10** with strychnine, brucine and quinine was examined and ^{31}P NMR was used to monitor the reaction. However only reaction with brucine occurred (Scheme 4.7). Repeated dealkylations of **10** with brucine were then performed followed by attempts at fractional crystallization of the resulting alkaloid salts. Fractional crystallization of phosphonothioate-alkaloid salt is

commonly performed in methanol or ethanol followed by addition of ether or other non-polar solvents. However, the brucine salts of **10** failed to produce any crystals under these conditions.
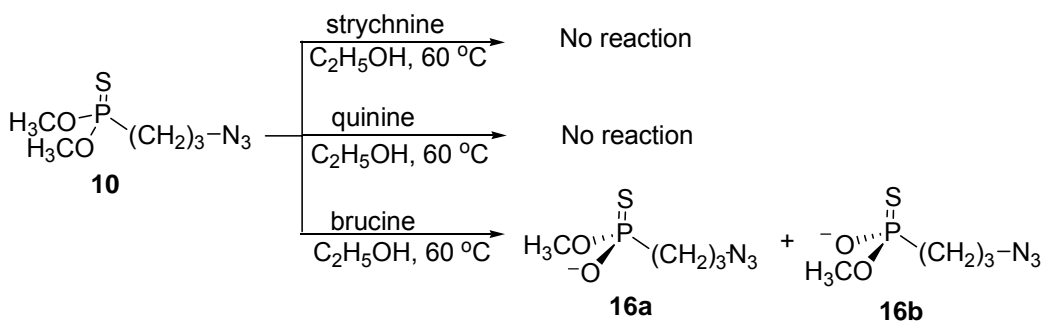
Scheme 4.7. Attempted dealkylation of phosphonothiolate with alkaloids.

Different solvent mixtures were examined and heat was also applied to effect a crystallization, which in most cases was subsequently stored at 0 °C. Despite this exploration of reactions, crystals of the brucine salt **16a/16b** were only observed in chloroform/ethyl ether or chloroform/ethyl acetate/ethyl ether, and unfortunately, the crystals formed are not hard enough to be separated from solutions. Examination of the reaction also showed that the two diastereomers **16a** and **16b** have overlapped peaks in ^{31}P NMR, making it difficult to examine the level of separation.

Acid-base reactions were next studied between proper phosphonothioic acid and the alkaloids. These reactions occurred more easily and provided us more opportunities to develop fractional crystallization. Strychnine, brucine and quinine were all able to form ionic parts with phosphonothioic acid **17** successfully (Scheme 4.8) and result in two distinct resonances (~ 0.05 ppm difference) for the diastereomers in the ^{31}P NMR.

S
H₃CO–P
H₃CO   (CH₂)₃–N₃
10

$\xrightarrow[40°C]{NaOH}$

S
H₃CO–P
HO   (CH₂)₃–N₃
17

strychnine / C₂H₅OH → **18a, 18b**

quinine / C₂H₅OH → **19a, 19b**

brucine / C₂H₅OH → **20a, 20b**

⁺NH alkaloid   S
H₃CO'''P
⁻O   (CH₂)₃—N₃
18a - 20a

⁺NH alkaloid   S
⁻O'''P
H₃CO   (CH₂)₃—N₃
18b - 20b
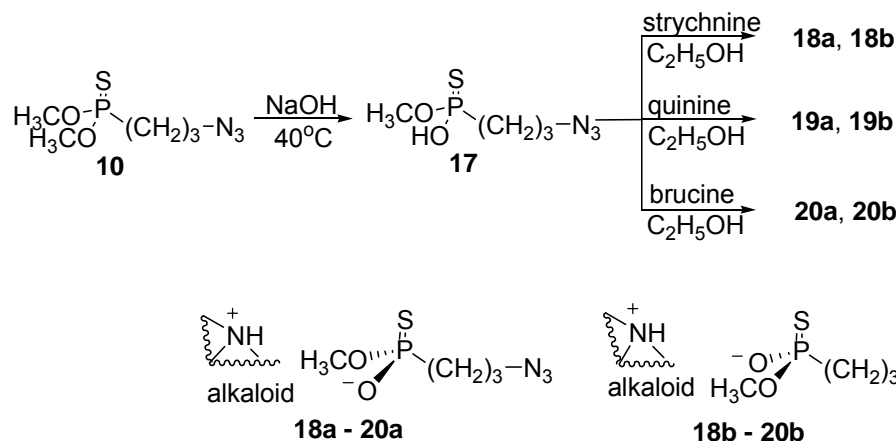
Scheme 4.8. Acid-base reactions between the phosphonothioic acid **17** and alkaloids.

Various solvent mixtures were examined to form crystals. A first crop of crystals was obtained for strychnine salts in ethanol/ethyl ether while brucine and quinine salts failed to produce any crystals. These first crops were analyzed by ^{1}H, ^{13}C, and ^{31}P NMR and enrichment of the diastereomers of strychnine salts (**18a/18b**) was easily observed in the ^{31}P NMR spectrum as revealed by two resonances differing by about 0.05 ppm. The most significant enrichment of the alkaloid salts from the first crop was observed for the strychnine/phosphonothioic acid salt in which ^{31}P NMR revealed approximately 70% enrichment of the downfield diastereomer (Figure 4.4-A). Further fractional crystallization of the downfield diastereomer was achieved stepwise, through repeated crystallization from ethanol-ethyl ether solutions. However, the limit of diastereomeric purity achieved by repeated crystallization was approximately 90%. To achieve higher resolution of the downfield diastereomer, several solvent mixtures for recrystallization were examined. A mixture of isopropanol and ethyl ether eventually provided the downfield alkaloid salt in a maximum of 95% diastereomeric purity by ^{31}P NMR (Figure 4.4-B).
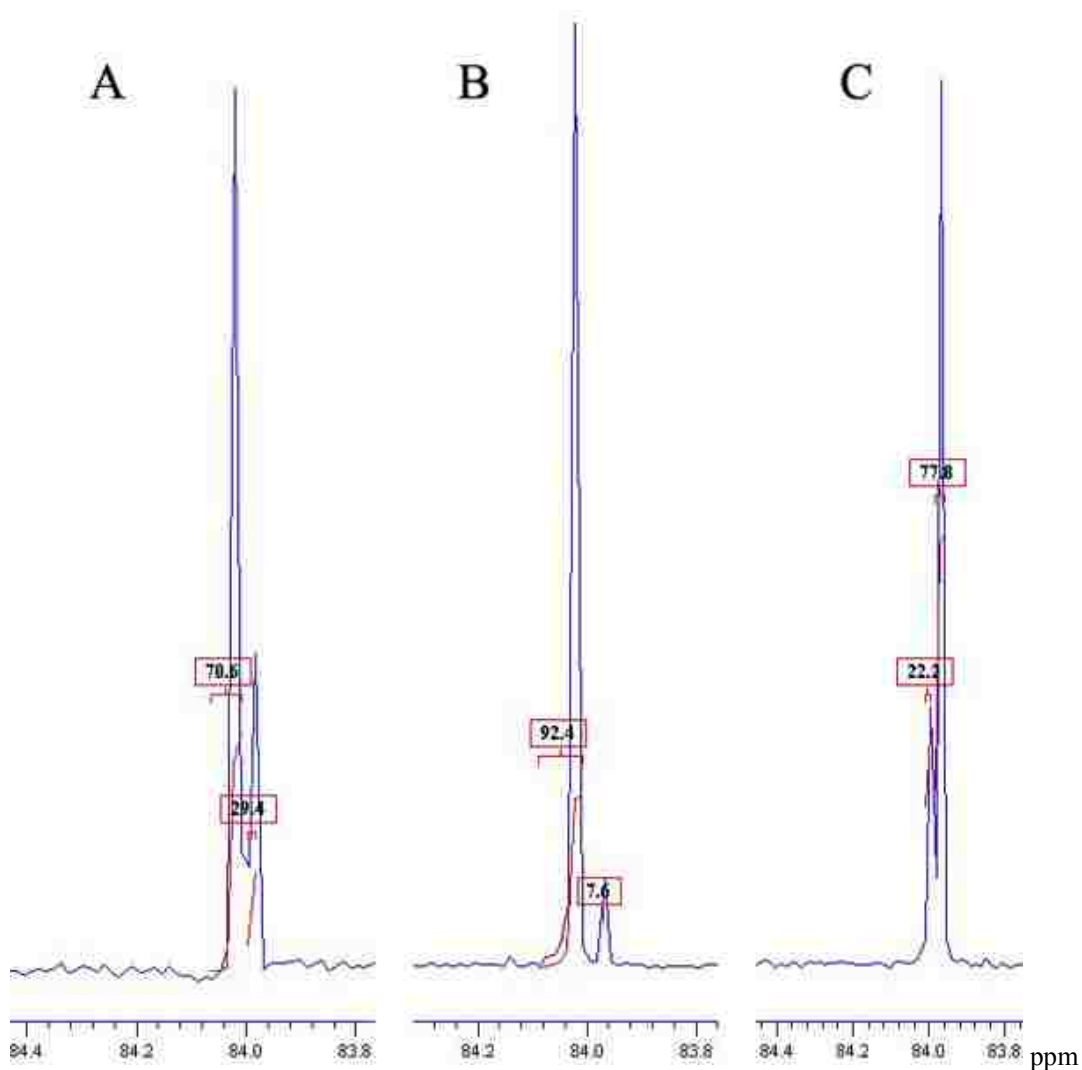
Figure 4.4. ^{31}P NMR spectra of strychnine salts **18a** and **18b**: (A) crystallized in ethanol/ethyl ether, (B) recrystallized in isopropanol/ethyl ether, and (C) remaining mother liquor; integration included.

The mother liquor from the first crystallization of the strychnine salts was concentrated to a smaller volume and crystallized repeatedly 4-5 times until no more crystals were formed. The last mother liquor was concentrated to a glassy oil/solid that showed approximately 80% enrichment of the upfield diastereomer by ^{31}P NMR (Figure 4.4-C). Several solvent mixtures were attempted to further enhance the diastereomeric

purity of this upfield diastereomer. However, no further enrichment of the resulting salt was obtained.

It's worth noting that the phosphonothioic acid-strychnine salts are not stable in solution. The possible reason for this is that it may be oxidized to the corresponding phosphonate compounds (loss of sulfur) after 1-2 days as determined by ^{31}P NMR. This observation severely limited the practicality of the fractional crystallization approach.

Fractional crystallization is largely dependent on the solvent system, physical and chemical properties of the target diastereomers, and other environmental uncertainties. With the method used above, it would not have allowed fully separating the two diastereomeric salts. As a result, the synthesis of CLAP stereoisomers using a chiral auxiliary to form two diastereomers via a covalent chemical bond was proposed and chromatographic separation of the resulting diastereomers was attempted.

4.3.2   Synthesis of Asymmetric Phosphonothioates Using a Chiral Auxiliary

A chiral auxiliary is an optically active compound that is temporarily incorporated into an organic synthesis so that the two diastereomers created from original enantiomers can be differentiated and separated from each other. After the separation of the two original stereocenters the auxiliary will be removed.

Previous experiments indicated that resolution of certain phosphonothioates could be achieved by the use of chiral auxiliaries (Valentine, 1984; Koizumi, 1978; Wu, 1994; Reddy, 2002). With a second stereocenter added, the diastereomers synthesized from phosphonothionate enantiomers would be analyzed and differentiated by ^{31}P NMR and separated.

71

Step 1: Adding a chiral auxiliary to phosphonothionate.

Because it has been proved to be useful for the preparation of phosphonothionate diastereomers followed by successful HPLC separation (Wu, 1994; Lee, 1992; Purnanand, 1994; Reddy, 2002), the enantiopure compound, *(R)*-methylbenzylamine was selected as the chiral auxiliary to resolve the diastereomeric phosphonamidothioates formed. Methanolysis of phosphonamidothioates with boron trifluoride would be attempted after diastereomeric resolution to replace the chiral auxiliary with a methoxyl group (Ryu, 1991).

To add the second chiral center to phosphorus, phosphonothionate **10** was converted to the amine-reactive phosphonochloridothionate **22** (Scheme 4.9). There were many reported routes to achieve this. The most convenient method to synthesize phosphonochloridothionates was reported by He (1998). *O,O*-Dimethyl (3-azopropyl) phosphonothioate **10** was dealkylated with diethylamine to form *O*-methyl ammonium phosphonothioate **21**, followed by conversion to P-Cl using phosphorus oxychloride (POCl$_3$) to give the corresponding *O*-methyl phosphonochloridothionate **22**. Reaction of **22** with two equivalent of *(R)*-methylbenzylamine yielded the desired phosphonamidothionate diastereomers, **23a** and **23b** (1:1).
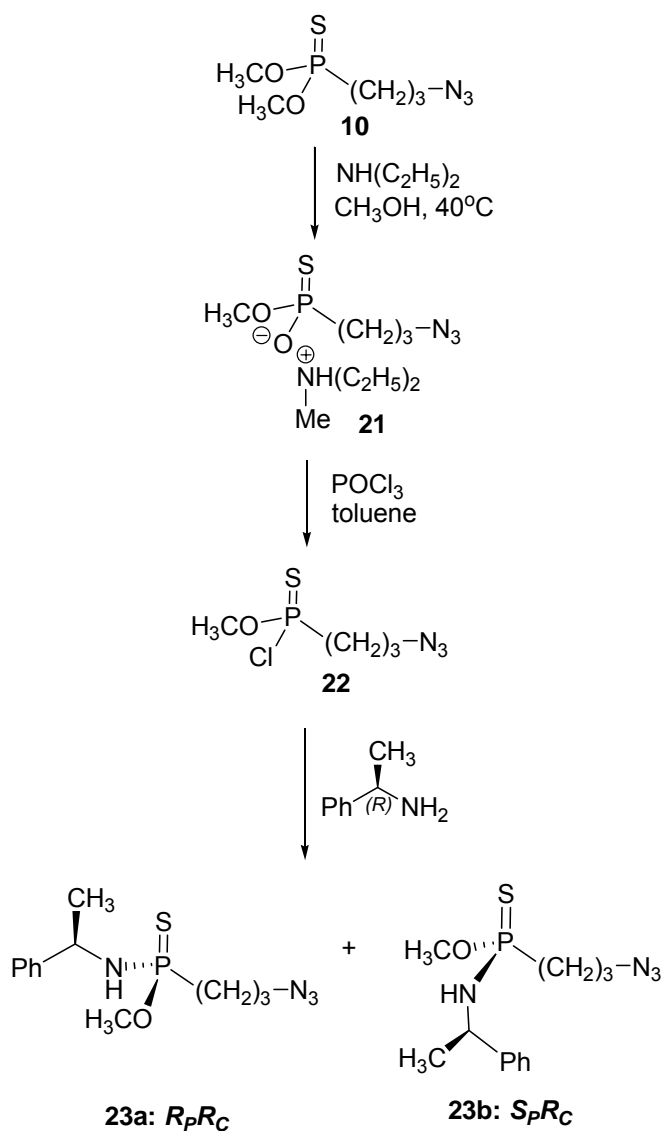
Scheme 4.9. Synthesis of phosphonamidothioate diastereomers.

The diastereomers **23a** and **23b** differed approximately 0.2 ppm from each other in the ^{31}P NMR spectrum but disappointingly were not separable to any great extent by flash chromatography. Phosphonamidothionate **23** was next converted to a phosphonamidothiolate to achieve a better separation.

Step 2: Converting phosphonamidothionate to phosphonamidothiolate and

separation.

Hydrolysis or dealkylation of phosphonamidothionate, followed by desired

alkylation, can afford corresponding phosphonamidothioate. However, hydrolysis or

dealkylation of phosphonamidothionate **23** was studied in various conditions without any

success (Scheme 4.10). In general, it was found that phosphonamidothionates such as

compound **23**, with a phosphonamide bond, were much more resistant to hydrolysis or

dealkylation than the corresponding phosphonothionates.
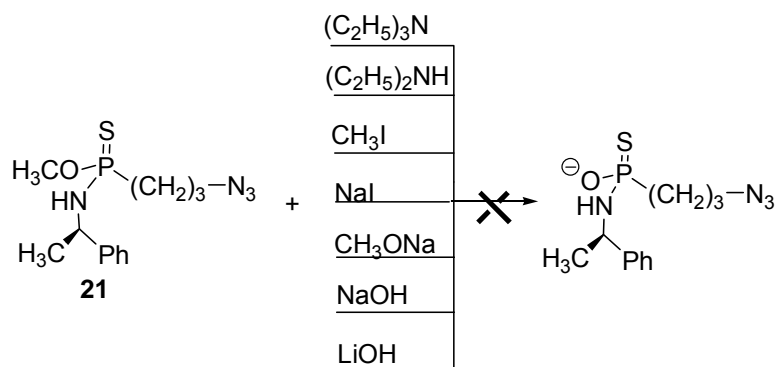
Scheme 4.10. Attempted hydrolysis or dealkylation of phosphonamidothionate **23**.

With the difficulties of stepwise dealkylation-alkylation, reversing the sequence to

alkylation first and dealkylation second was attempted. This change ensured the success

of the chemistry, however, the flexibility of the target compounds was restricted due to

the availability of the alkylation reagents that would act in the first step. Methyl triflate

was known as a methylation reagent and used on phosphonothionates (Mikolajczyk,

1988). Alkylation of phosphonamidothionate **23** resulted in the derived phosphonium

salt, which was treated with lithium chloride to make *S*-substituted

phosphonamidothiolate **24** (Scheme 4.11). It was found later that the compound **24** could also be synthesized by treating **23** with methyl iodide as solvent/reagent (Scheme 4.11) under extreme conditions (heating and long time). The methyl iodide reaction took a long time (6 days) under reflux to achieve 100% conversion. Besides ^{31}P NMR, TLC analysis staining with 2,6-dibromoquinone-4-chloroimide (DBQ) were also used to monitor the conversion reaction from P=S to P=O. Visualization of the color change from orange to yellow provided a convenient way to identify the conversion progress.
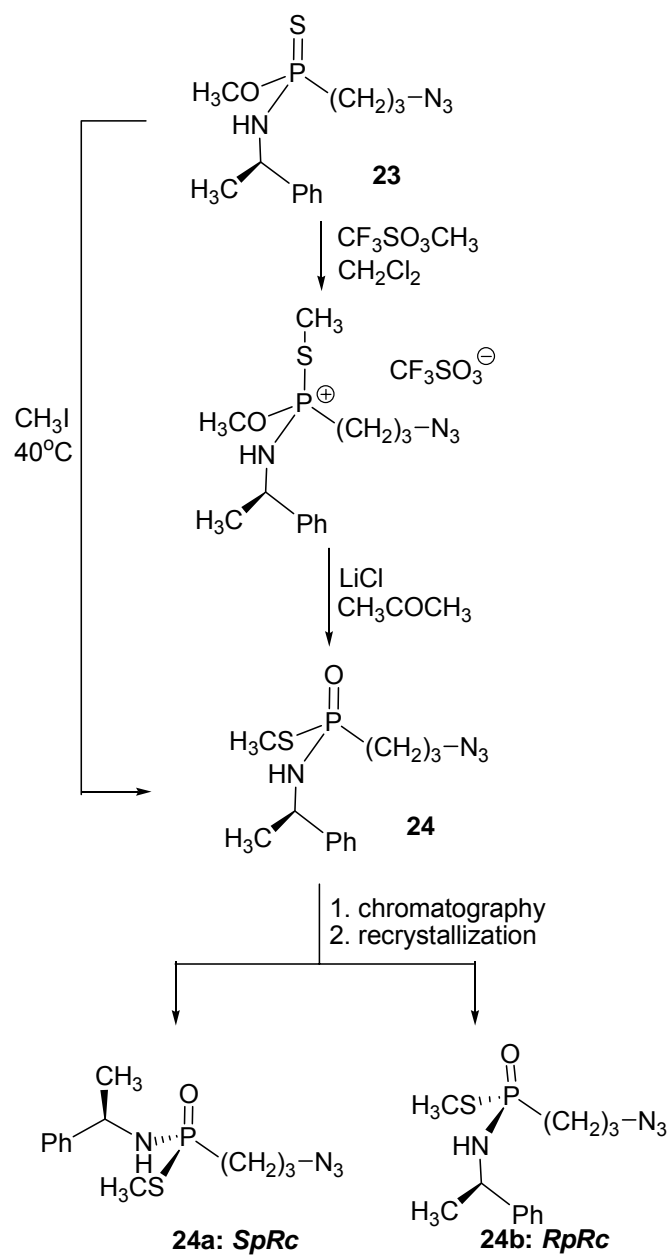
Scheme 4.11. Synthesis of *S*-substituted phosphonamidothioate.

The phosphonamidothiolate **24** was confirmed by ^{1}H, ^{13}C, ^{31}P NMR and elemental analysis. Diastereomers **24a** and **24b** showed a 1.4 ppm difference in the ^{31}P NMR spectrum and were effectively separated by flash chromatography using 1-2%

methanol in chloroform. The separation was reconfirmed by ^{31}P NMR: 1) integration

showed 50:50 of the two diastereomers **24a/24b** after reaction (Figure 4.5-A); 2) the first

fraction was collected and there is a single chemical shift at 48.6 ppm in ^{31}P NMR

analysis (Figure 4.5-B); and 3) the second fraction was collected and the chemical shift of

the second diastereomer is 50.0 ppm (Figure 4.5-C). The overlapped fractions were

collected and separated once again with same chromatographic conditions.
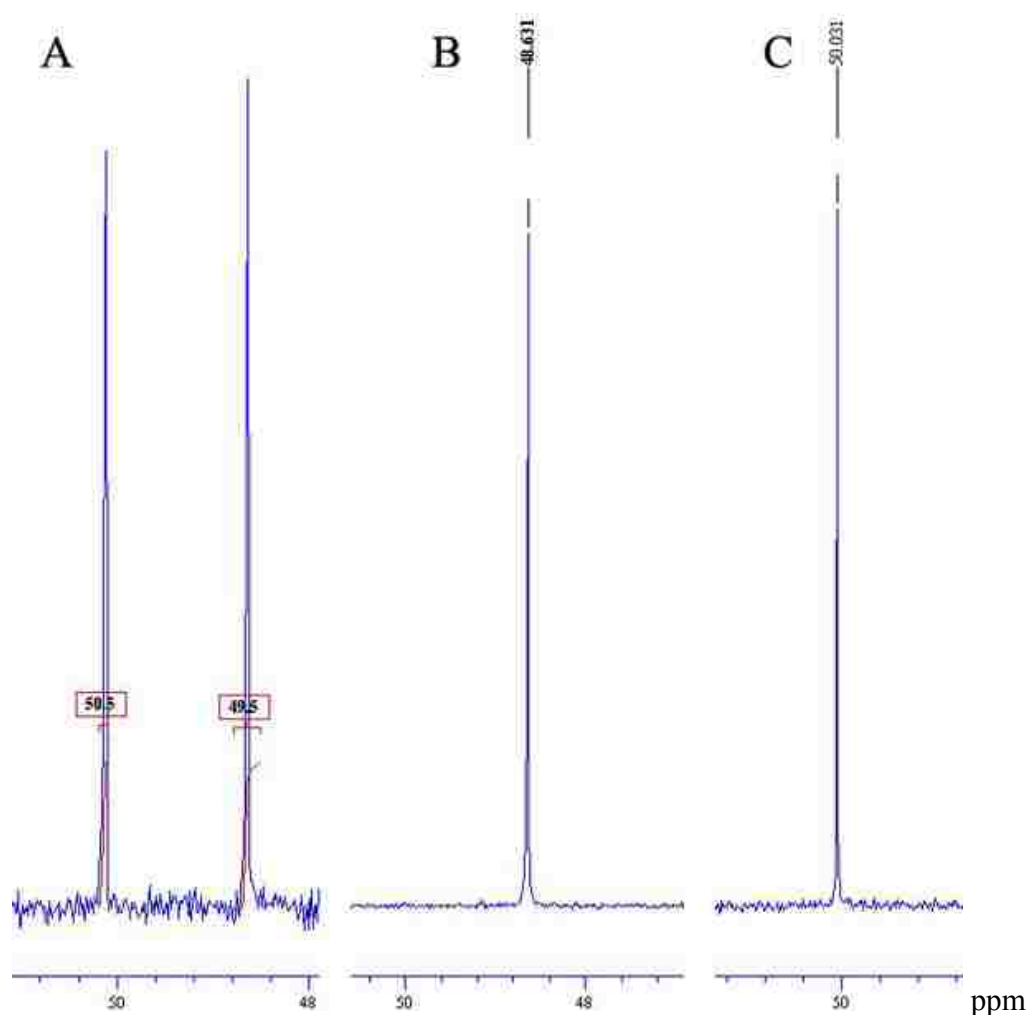
Figure 4.5. ^{31}P NMR spectra of compound (A) **24a** and **24b** before chromatographic
separation, (B) **24a**, and (C) **24b**.

Isomer **24a** was further crystallized from ether and afforded needle-like crystals.

Diastereomer **24b** was dissolved in the necessary amount of methanol and crystallized as

ether was added to afford needle-like crystals. In addition to NMR analysis of the

diastereomers **24a** and **24b**, specific rotations and melting points were also obtained

(Table 4.5). The diastereomers were identified as the levorotatory or dextrorotatory

stereoisomer with respect to the phosphorus stereochemistry because the carbon

configuration was known as 100% enantiopure. The phosphorus and carbon

configurations were later analyzed and confirmed by x-ray crystallography.

Table 4.5: Physical data of the diastereomers **24a** and **24b**.

compounds	$[\alpha]_D^{22}$ (conc.) [a]	^{31}P NMR (δ) ppm	mp(ºC) [b]
24a (*SpRc*)	+23.6 (1.40)	48.6 (4)	95.5-95.8
24b (*RpRc*)	+60.1 (1.04)	50.0 (3)	88.5-88.8

[a] rotations performed in CHCl$_3$; concentrations in g/100 mL; [b] melting point
analysis calibrated with 4-nitrobenzyl chloride (mp 70.0 ºC).

Step 3: Identifying the absolute configurations of compounds **24a/24b**.

In an effort to assign the absolute configuration of the carbon and phosphorus

stereocenters of the resolved diastereomers **24a/24b**, x-ray crystallographic analysis was

desired. In order to prepare crystals for x-ray crystallography, recrystallization of the

resolved diastereoisomers **24a** and **24b** was preformed in the respective solvent mixtures

at a high dilution to afford crystals of high quality.

The structure of the crystal **24a** was solved and revealed an orthorhombic unit cell with dimensions of 5 x 12 x 24 Å (Table 4.6). As a result of this analysis, stereochemistry was assigned (Figure 4.6) as C9(*R*) P1(*S*) and the packing diagram was illustrated in Figure 4.7 for diastereomer **24a.**

Table 4.6: Crystal data for diastereomer **24a**.

Empirical formula	C12 H19 N4 O P S	
Formula weight	298.34	
Temperature	90(2) K	
Wavelength	0.71073 Å	
Crystal system	Orthorhombic	
Space group	P2(1)2(1)2(1)	
Unit cell dimensions	a = 5.1896(2) Å	$\alpha = 90°$
	b = 12.1755(4) Å	$\beta = 90°$
	c = 23.6534(8) Å	$\gamma = 90°$
Volume	1494.56(9) Å^3	
Z	4	
Density (calculated)	1.326 mg/m^3	
Absorption coefficient	0.322 mm^{-1}	
F(000)	632	
Crystal size	0.39 x 0.19 x 0.17 mm^3	
Crystal color and habit	colorless needle	
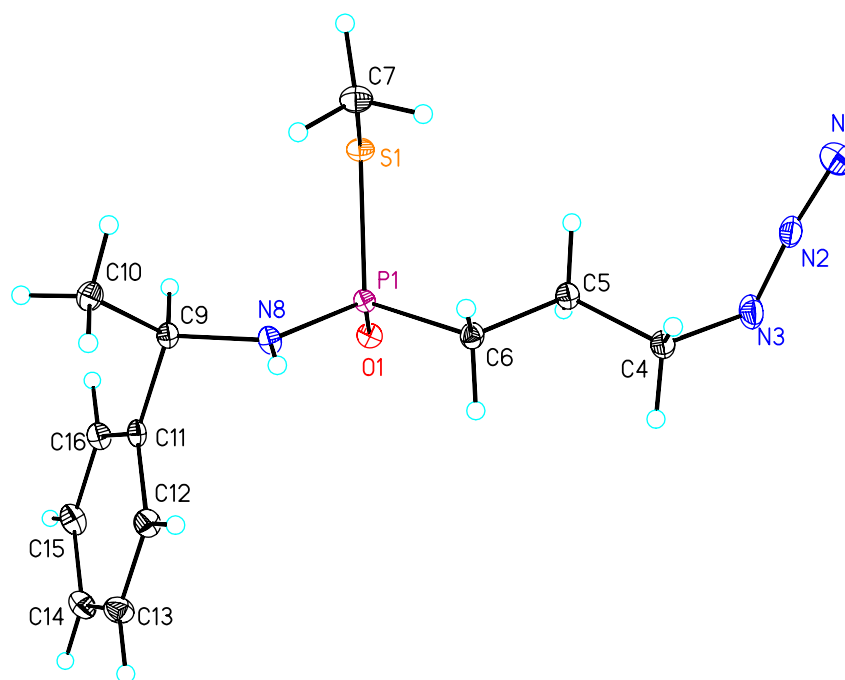
Figure 4.6. The structure of the diastereomer **24a** as determined by x-ray crystallographic analysis.
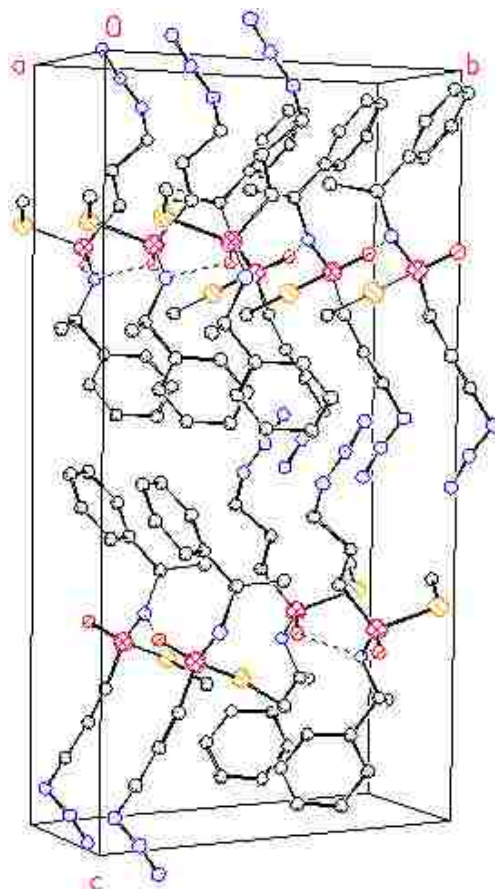
Figure 4.7. Packing diagram of **24a** (hydrogen atoms omitted for clarity and dashed lines indicate hydrogen bonding).

The crystal structure of the crystal **24b** was also solved and revealed an orthorhombic unit cell with smaller dimensions of 5 x 12 x 22 Å (Table 4.7) compared with **24a**. Stereochemistry of this crystal was assigned (Figure 4.8) as C9(*R*) P1(*R*) and the packing diagram was illustrated in Figure 4.9 for diastereomer **24b.**

Table 4.7: Crystal data for diastereomer **24b**.

Empirical formula	C12 H19 N4 O P S
Formula weight	298.34
Temperature	90(2) K
Wavelength	0.71073 Å
Crystal system	Orthorhombic
Space group	P2(1)2(1)2(1)
Unit cell dimensions	$a = 5.4509(3)$ Å $\quad \alpha = 90°$
	$b = 12.0987(6)$ Å $\quad \beta = 90°$
	$c = 22.2882(11)$ Å $\quad \gamma = 90°$
Volume	1469.88(13) Å^3
Z	4
Density (calculated)	1.348 mg/m^3
Absorption coefficient	0.327 mm^{-1}
F(000)	632
Crystal size	0.48 x 0.08 x 0.05 mm^3
Crystal color and habit	colorless needle
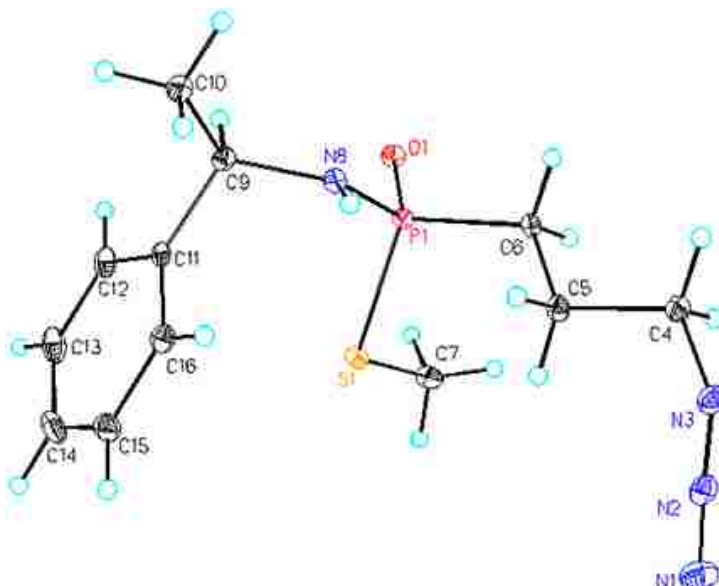
Figure 4.8. The structure of the diastereomer **24b** as determined by x-ray crystallographic analysis.
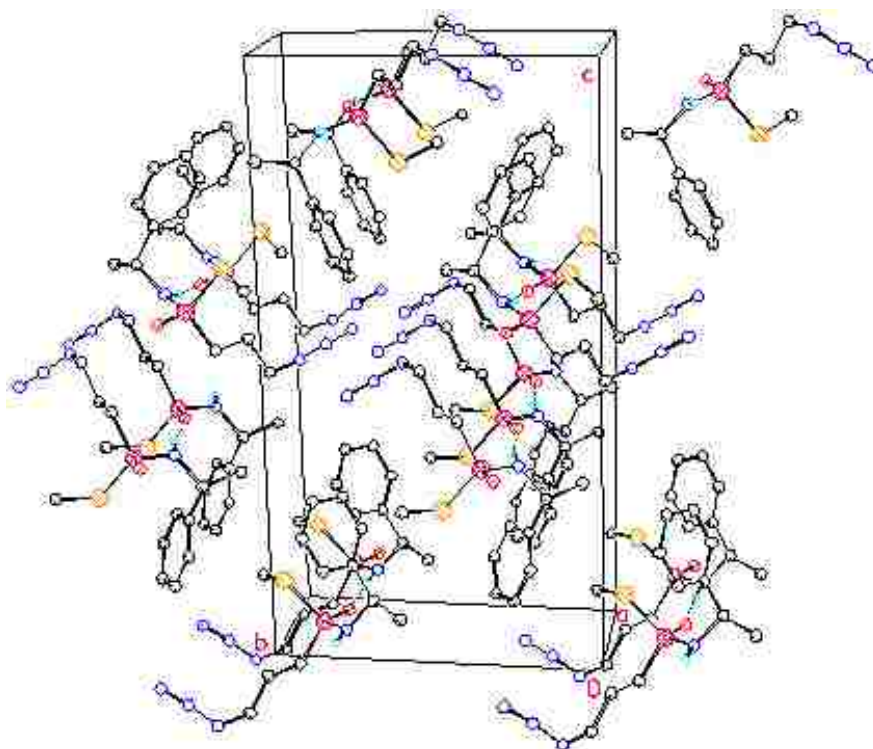
Figure 4.9. Packing diagram of **24b** (hydrogen atoms omitted for clarity and dashed lines indicate hydrogen bonding).

Step 4: Removing the chiral auxiliary with retention of configuration at phosphorus.

With the two diastereomers resolved, removal of the chiral auxiliary group to form the respective enantiopure isomers was conducted. Seungmin Ryu (1991) discovered an effective way to chemoselectively transform sulfur-containing phosphoramidates to the corresponding phosphonate methyl ester by using boron trifuoride-methanol (BF_3-CH_3OH) complex. The reaction proceeds with net inversion of stereochemistry. Reported higher yields, ease of reaction manipulation, the commercial availability of reagent, and the successful preparation of chiral phosphorus thiol ester made it the methanolysis method of choice in this study.

Reactions with each diastereomer (**24a/24b**) with BF$_3$-CH$_3$OH complex gave the corresponding chiral *O,S*-dimethyl 3-azidopropylphosphonothioate **25a** (*Sp*, [α]$^{22}_D$ = -48°) /**25b** (*Rp*, [α]$^{22}_D$ = +48°) (Scheme 4.12). It was observed that the methanolysis of phosphonothiolates **24a/24b** took much longer time (5-6 d) to be completed than previously reported phosphorothiolate compounds (< 12 h).
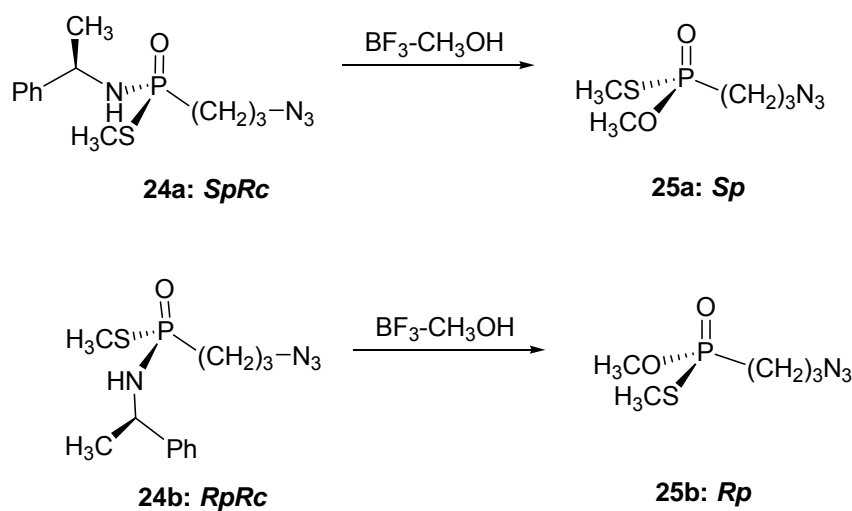
Scheme 4.12. Synthesis of phosphonamidothiolate diastereomers.

In summary, the azo-linked phosphonothiolates **24a/24b** were successfully synthesized and separated using an auxiliary. X-ray analysis showed the absolute configuration of phosphorus and chromophore-linked asymmetric phosphonothiolates (CLAPs) would be synthesized now.

4.4 Chromophore-linked Asymmetric Phosphonothiolates (CLAPs)

The racemates of chromophore-linked phosphonothiolates were synthesized in section 4.2.4 with click chemistry. However, whether click chemistry would work with the synthesized phosphonothiolates **25a/25b** remains unclear. Click chemistry with the phosphonothiolate as a racemate was studied first to ensure that Cu(I) used as the catalyst has no negative effect on the thiol-group (Scheme 4.13).
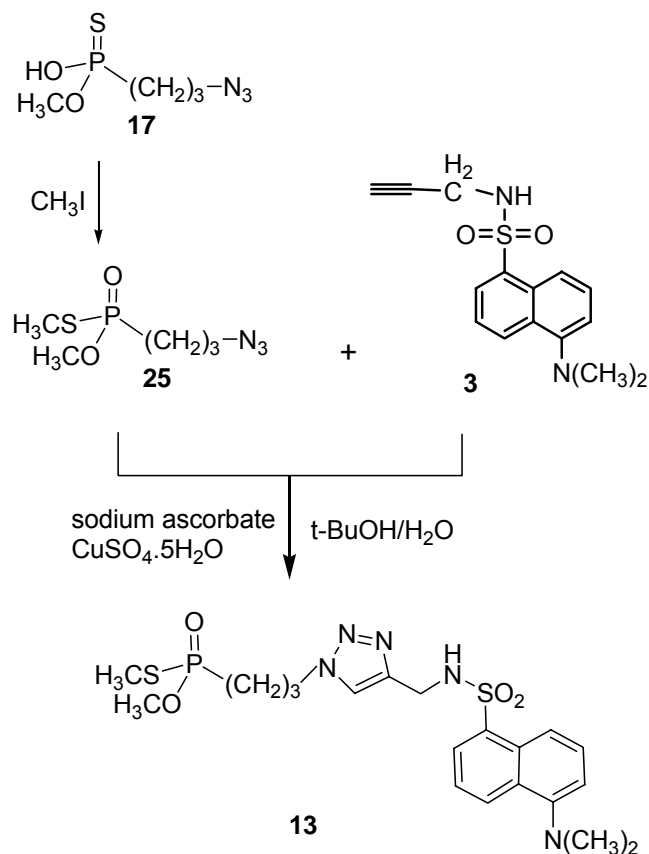
Scheme 4.13. Click reaction with phosphonothiolates.

Racemic phosphonothiolate **25** was synthesized from phosphonothionate **17** by hydrolysis and methylation. Click reaction occurred fabulously under 1% Cu(I) catalysis, which showed that chromophore-linked asymmetric phosphonothiolates (CLAPs) could be synthesized from **25a** and **25b** in this way (Scheme 4.14).
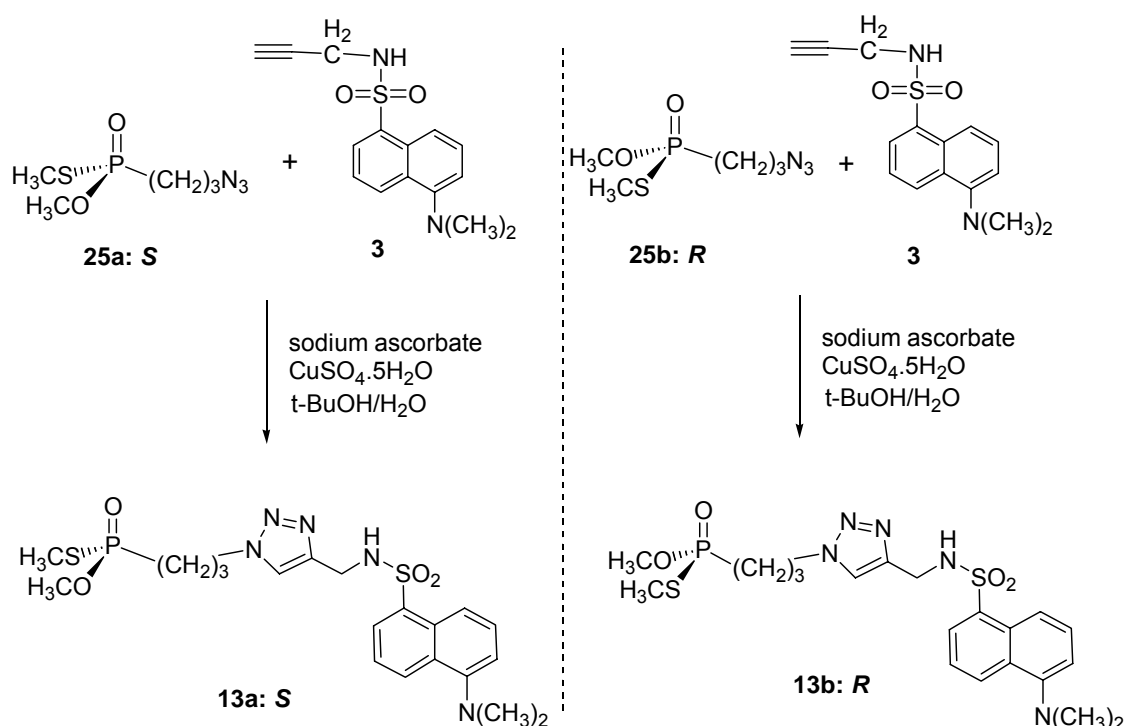
Scheme 4.14. Synthesis of chromophore-linked asymmetric phosphonamidothiolates.

4.5 Meta-Inhibitor (m-Trimethylaminophenyl Amine) Coupled to Sepharose Resin

Meta-trimethylaminophenyl amine, also referred as meta-inhibitor, was synthesized and coupled to sepharose resin through a successively coupled succinic acid and diaminodipropylamine arm for purification purpose of recombinant mouse AChE. The expressed recombinant mouse AChE (rMAChE) in HEK 293 cells would be purified by an affinity chromatography packed with this modified resin (Taylor & Jacobs, 1974; Marchot, 1996; and Bourne, 1999).

4.5.1 Meta-Inhibitor (m-trimethylaminophenyl amine)

Meta-trimethylaminophenyl amine, also referred as meta-inhibitor (**26**) against recombinant mouse AChE, was synthesized as illustrated in Scheme 4.15.
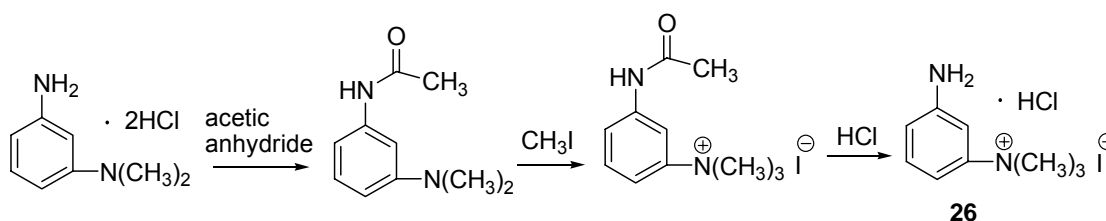
Scheme 4.15. Synthesis of meta-inhibitor.

The free primary amino group of *N,N*-dimethyl-1,3-phenylenediamine was first protected by an acetyl group, followed by addition of methyl iodide to from the tertiary amine at meta-position. Hydrochloric acid was used to deprotect and give the meta-inhibitor (20-25% total yield). Due to the salt form of the final compound containing iodide, it must be shielded from light.

4.5.2   Meta-Inhibitor Coupled Resin

When the meta-inhibitor is coupled to the resin, a proper linker is necessary to ensure that the meta-inhibitor can reach the active site of rMAChE, so that the tertiary amine on the meta-inhibitor can reversibly interact with AChE. The meta-inhibitor coupled resin with a proper linker length was illustrated in Scheme 4.16.
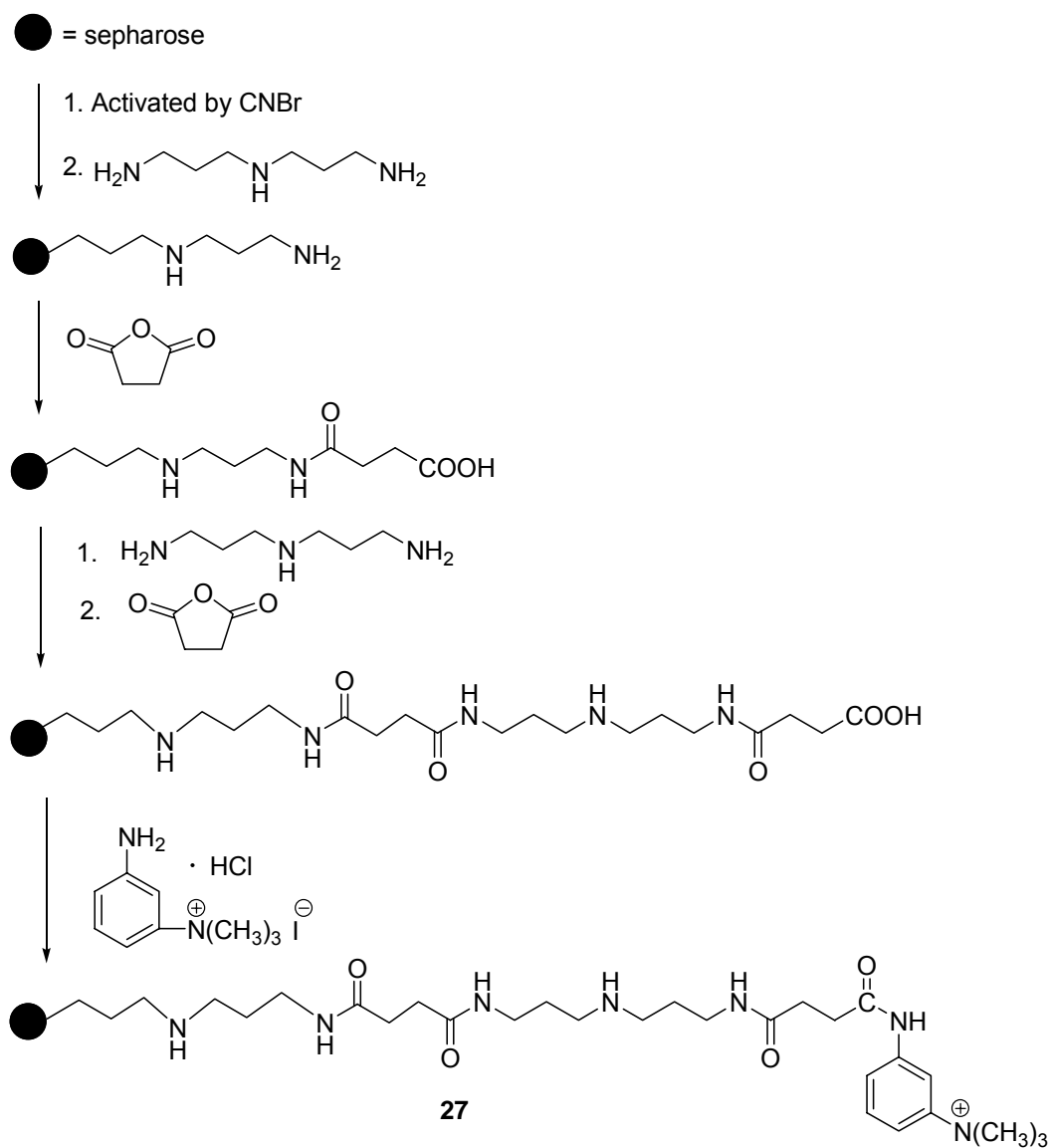
Scheme 4.16. Synthesis of meta-inhibitor coupled resin.

Sepharose CL-4B resin was activated by cyanogen bromide (CNBr), followed by reaction with 3, 3'- iminobispropylamine. The success of reaction was examined by a bead testing using picryl sulfonic acid solution (3%), which would show an orange color for the resulting primary amine group. The resulting amine coupled resin reacted with succinic anhydride through a peptide bond and offered a carboxylic acid coupled resin, which would not show color change in the bead testing. These reactions were repeated once again to achieve appropriate length of the coupling linker. The primary amine in the meta-inhibitor was added to the carboxylic acid coupled resin at last and offered a tertiary amine linked resin with appropriate linker length, which was used as affinity column for purification of rMAChE

The total length of linker is approximately 25 Å, which is long enough to reach and interact with the active site at the bottom of the gorge of AChE. The conjugated resin was stored as a 50% suspension in 100 mM NaCl, 40 mM $MgCl_2$, 10 mM $NaHCO_3$, pH 8.0, containing NaN_3, 0.02% (w/v) before packing an affinity column.

CHAPTER 5

RESULTS AND DISCUSSIONS

5.1   Solvent Effect on the Activity of AChE

The synthesized organophosphonate compounds with leaving groups (compound **6**, and **25**) are reactive toward most solvents including water. Any nucleophilic attack to phosphorus atom causes displacement of the leaving group of the OP inhibitors. ^{31}P NMR analysis was used to investigate the stability of OP inhibitors and showed that most fluorophosphonate compounds (FPs) were hydrolyzed in water after 0.5 h, so all kinetic experiments in 0.1 M phosphate buffer solution (PBS) were designed to be completed in less than 0.5 h to ensure the purity of the OP inhibitors. Meanwhile, organic solvent with the least effect on AChE was desired to store OP inhibitors and was selected to dissolve FPs and be mutually soluble with PBS.

Acetylcholinesterase is sensitive to most organic solvents, so the amount of the solvent used in inhibition study was first examined. Experiments with rMAChE and EEAChE demonstrated that rMAChE is particularly sensitive to the effect of solvents while EEAChE is more robust. Solutions containing 0.5% (vol/vol) of acetone, methanol, DMSO, or DMF decreased the enzyme activity more than 20%. In contrast, acetonitrile (ACN) was found to be the best solvent with least effect to both AChEs' activity. Less

than 10% reduction in activity was observed for solutions containing 0.5% (vol/vol) of

ACN (Fig 5.1 and 5.2) for both enzymes, and subsequently, less than 0.5% of ACN

would be used in all the following kinetic studies to ensure that more than 90% activity of

AChE is retained.
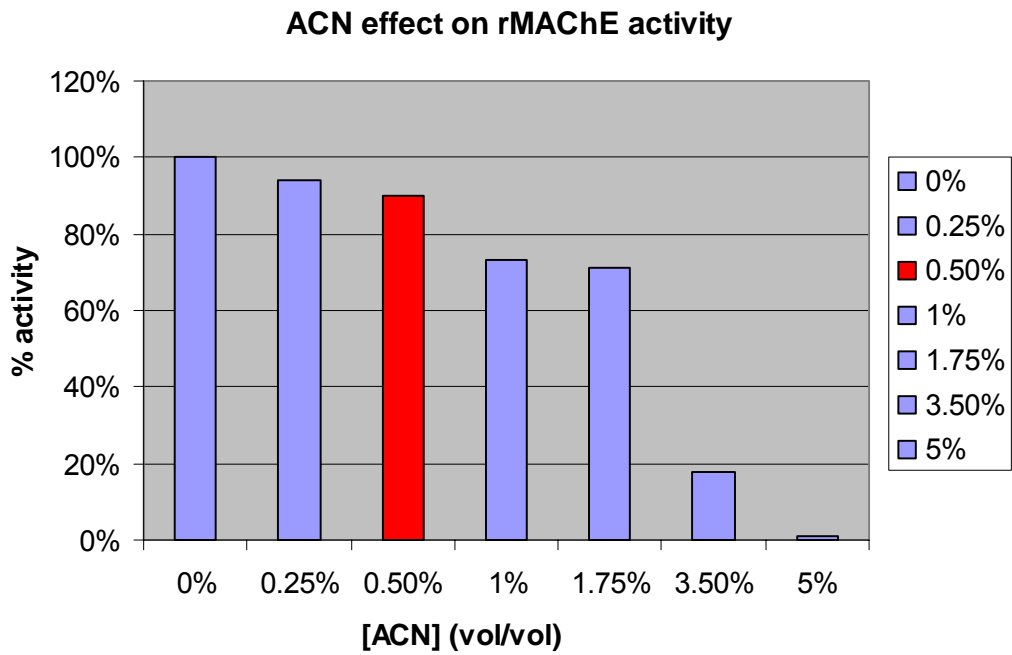
Figure 5.1. Effect of composition of ACN in 0.1 M PBS 7.6 on rMAChE activity**.**
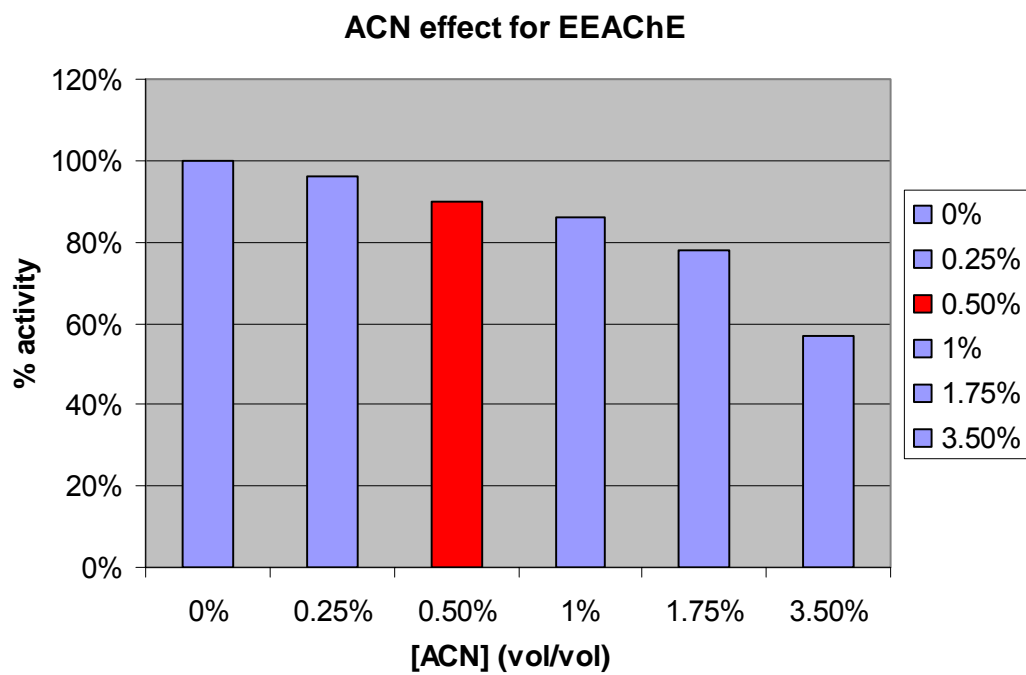
Figure 5.2. Effect of composition of ACN in 0.1 M PBS 7.6 on EEAChE activity.

5.2 Inactivation of rMAChE and EEAChE by Chromophore-linked FPs

All synthesized fluorophosphonate compounds are designed to inactivate AChE by covalently binding to the active site serine, which is an irreversible process. Thus, the inhibition potencies of fluorophosphonates were determined in a concentration-dependent method and the kinetic parameters k_i and K_D were calculated. The contributions to the inhibitory activity of the chromophore moiety and fluorophosphonate moiety were studied individually. It is worth noting that the chromophore moiety by itself cannot irreversibly inhibit AChE and a different kinetic analysis was required.

All data are expressed as mean ± S.E.M. from three or more replicate experiments.

5.2.1 Inhibition of rMAChE and EEAChE by fluorophosphonoazides 8a and 8b

The inhibitory action of fluorophosphonate portion of the target molecules was first studied to define its contribution to the overall inactivation process. The FP compounds with no chromophore, $(CH_3O)(F)P(O)(CH_2)_3N_3$ (**8a**) and $(CH_3O)(F)P(O)(CH_2)_4N_3$ (**8b**), were examined as irreversible inhibitors in a concentration-dependent manner against rMAChE and EEAChE and the kinetic parameters (k_i and K_D) were determined in Table 5.1 and 5.2.

Table 5.1: Inhibition of rMAChE by **8a** and **8b.**

compound	k_i ($M^{-1}min^{-1}$)	K_D (M)	$\overline{k_i}$ ($M^{-1}min^{-1}$)	$\overline{K_D}$ (M)
8a	1.3×10^7	2.1×10^{-8}		
	1.4×10^7	2.1×10^{-8}	$1.3 \pm 0.1 \times 10^7$	$2.7 \pm 0.6 \times 10^{-8}$
	1.3×10^7	3.8×10^{-8}		
8b	1.0×10^6	0.98×10^{-6}		
	0.93×10^6	1.7×10^{-6}	$1.0 \pm 0.1 \times 10^6$	$1.7 \pm 0.4 \times 10^{-6}$
	1.2×10^6	2.4×10^{-6}		

The bimolecular rate constant k_i describes the overall interaction rate, which represents the potency of an inhibitor. For fluorophosphonates **8a** and **8b** against rMAChE, it is determined that k_i(s) are 1.3×10^7 and 0.98×10^6 $M^{-1}min^{-1}$, respectively. Compared with a well-studied potent inhibitor, paraoxon, with k_i of 4×10^5 $M^{-1}min^{-1}$ for rMAChE (Amitai, 1998; Kardos, 2000), compounds **8a** and **8b** both have larger k_i values and therefore are more potent inhibitors for rMAChE than paraoxon, and are deemed extremely potent.

The smaller fluorophosphonate **8a** (with 3 CH_2 groups) shows a ten-fold higher inhibitory activity than **8b** (with 4 CH_2 groups). The fact that smaller FP inhibitor has stronger inhibition indicates the rigid structure of the active gorge of rMAChE. A FP with a longer chain would have a harder time getting into the active gorge and inactivate

rMAChE. The longer alkyl group also adds a slightly greater margin of electron donation thereby causing the phosphoryl to be less reactive toward nucleophilic attack.

The dissociation constant K_D is generally considered a measure of an inhibitor's affinity to the enzyme active site (Fukuto, 1990). A smaller K_D indicates easier formation of reversible enzyme-inhibitor complex. Comparing fluorophosphonates **8a** and **8b**, higher affinity of **8a** (smaller K_D) demonstrates that smaller inhibitors enter the active gorge and form the complex more easily than bigger ones.

Similar trends were observed in the study of inactivation of EEAChE by **8a** and **8b**. The bimolecular rate constants k_i for fluorophosphonates **8a** and **8b** were determined to be 7.7 x 10^6 and 0.96 x 10^6 $M^{-1}min^{-1}$, respectively. Both are potent inhibitors against EEAChE as compared with paraoxon with k_i of approximately 3 x 10^5 $M^{-1}min^{-1}$ (Herzsprung, 1989; Mionetto, 1997). The smaller fluorophosphonate **8a** also exhibits roughly eight times stronger inhibitory potency than **8b**, which is consistent with the observation in the study of rMAChE. The dissociation constants (K_D) also show agreement with the data for rMAChE: a smaller molecule (fluorophosphonate **8a)** has higher affinity (a smaller K_D) for the enzyme than a larger molecule (**8b**).

Comparing the kinetic results from the two sources of AChE, a higher k_i was observed in rMAChE, indicating that it is more sensitive to the phosphonoazides **8a** and **8b** than EEAChE.

With the potency of these compounds established, the kinetic studies of the chromophore-linked FPs (section 5.2.2) containing the fragment can be compared to evaluate the effect of chromophores in inhibition of AChEs.

Table 5.2: Inhibition of EEAChE by **8a** and **8b.**
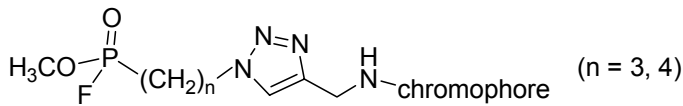
compounds	k_i ($M^{-1}min^{-1}$)	K_D (M)	$\overline{k_i}$ ($M^{-1}min^{-1}$)	$\overline{K_D}$ (M)
8a	7.8×10^6	1.2×10^{-7}	$7.7 \pm 0.1 \times 10^6$	$1.7 \pm 0.4 \times 10^{-7}$
	7.4×10^6	1.6×10^{-7}		
	7.9×10^6	2.4×10^{-7}		
8b	1.1×10^6	0.86×10^{-6}	$0.96 \pm 0.08 \times 10^6$	$2.9 \pm 1.1 \times 10^{-6}$
	0.89×10^6	2.9×10^{-6}		
	0.86×10^6	4.8×10^{-6}		

5.2.2 Inhibition of rMAChE and EEAChE by Chromophore-linked FPs

As described for experiments in the previous section, the inactivation of AChEs by chromophore-linked fluorophosphonates was also kinetically treated as an irreversible, pseudo-first order reaction. The inhibition of AChEs by fourteen synthesized chromophore-linked FPs were determined in the concentration-dependent manner and examined more than three times to attain reproducible data.
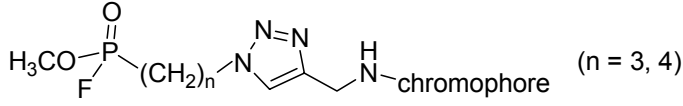
The kinetic parameters k_i and K_D were determined and presented in Table 5.3 and 5.4. The pyrene-linked FP with the four methylene (n = 4) linker showed poor solubility in ACN and thus no data was reported. The precise kinetic data for Lissamine-linked FPs was not obtained due to the high concentration requirement of the inhibitor, which would cause strong color contamination from the inhibitor and swamp the UV signal in the assay, which is determined at 412 nm.

Table 5.3: Inhibition of rMAChE by chromophore-linked FPs.

chromophore	n = 3		n = 4	
	$k_i\ (M^{-1}min^{-1})$	$K_D\ (M)$	$k_i\ (M^{-1}min^{-1})$	$K_D\ (M)$
dansyl	$1.0 \pm 0.1 \times 10^6$	$4.6 \pm 1.3 \times 10^{-7}$	$1.9 \pm 0.5 \times 10^5$	$3.2 \pm 1.2 \times 10^{-6}$
pyrene	$4.0 \pm 0.6 \times 10^5$	$7.9 \pm 0.4 \times 10^{-7}$	N/A	N/A
dabsyl	$7.5 \pm 1.0 \times 10^5$	$3.7 \pm 0.5 \times 10^{-7}$	$6.5 \pm 1.1 \times 10^4$	$1.8 \pm 0.1 \times 10^{-6}$
diethylamino coumarin	$2.1 \pm 0.7 \times 10^5$	$2.7 \pm 1.2 \times 10^{-6}$	$1.4 \pm 0.2 \times 10^5$	$4.7 \pm 0.8 \times 10^{-7}$
methoxy coumarin	$6.5 \pm 0.6 \times 10^5$	$2.4 \pm 0.3 \times 10^{-7}$	$3.5 \pm 0.6 \times 10^4$	$4.8 \pm 0.7 \times 10^{-6}$
Lissamine rhodamine B	$\sim 1 \times 10^4$	N/A	$\sim 1 \times 10^4$	N/A
Texas Red	$8.4 \pm 0.7 \times 10^4$	$5.0 \pm 0.9 \times 10^{-6}$	$3.1 \pm 0.1 \times 10^5$	$1.4 \pm 0.2 \times 10^{-6}$

N/A: not acquired.

Table 5.4: Inhibition of EEAChE by chromophore-linked FPs.

(n = 3, 4)

chromophore	n = 3		n = 4	
	$k_i\ (M^{-1}min^{-1})$	$K_D\ (M)$	$k_i\ (M^{-1}min^{-1})$	$K_D\ (M)$
dansyl	$1.3 \pm 0.0 \times 10^5$	$3.1 \pm 0.6 \times 10^{-5}$	$6.2 \pm 0.1 \times 10^4$	$9.0 \pm 0.4 \times 10^{-6}$
pyrene	$1.8 \pm 0.3 \times 10^5$	$1.1 \pm 0.4 \times 10^{-6}$	N/A	N/A
dabsyl	$3.0 \pm 0.3 \times 10^5$	$1.9 \pm 0.3 \times 10^{-6}$	$1.1 \pm 0.0 \times 10^5$	$1.7 \pm 0.1 \times 10^{-6}$
diethylamino coumarin	$2.5 \pm 0.4 \times 10^5$	$1.4 \pm 0.4 \times 10^{-6}$	$3.3 \pm 0.8 \times 10^4$	$6.8 \pm 0.7 \times 10^{-6}$
methoxy coumarin	$1.8 \pm 0.1 \times 10^4$	$1.5 \pm 0.4 \times 10^{-4}$	$2.7 \pm 1.0 \times 10^4$	$5.0 \pm 2.1 \times 10^{-5}$
Lissamine rhodamine B	$\sim 1 \times 10^4$	N/A	$\sim 1 \times 10^4$	N/A
Texas Red	$3.1 \pm 0.2 \times 10^4$	$6.7 \pm 1.3 \times 10^{-6}$	$6.7 \pm 0.4 \times 10^4$	$1.6 \pm 0.6 \times 10^{-5}$

N/A: not acquired.

All chromophore linked FPs but Lissamine were potent inhibitors against rMAChE (Table 5.3). However, no chromophore-linked FP had a larger k_i than the k_i for phosphonoazides **8a** and **8b** (section 5.2.1), indicating that the attached chromophore decreases the overall inhibition potency. This observation is consistent with the previous assumption that smaller molecules inactivate AChE more potently than larger ones.

It is also worth pointing out that both Texas Red-linked FPs exhibit relatively weak inhibition activity against rMAChE compared with other chromophores-linked FPs. The same trend was observed in Lissamine-linked FPs. Texas Red and Lissamine are large polycyclic chromophores and it is likely that a different mechanism by which these two large size chromophores inactivate AChEs.

For dansyl, dabsyl and methoxycoumarin, the k_i(s) of their linked FPs with 3-CH_2 linker are roughly 10 times greater than the k_i(s) of the corresponding FPs with 4-CH_2 linker (Fig 5.3). This difference is the same as was observed for the phosphonoazides **8a** and **8b** (section 5.2.1). In contrast, the k_i of Texas Red-linked FP with 3-CH_2 linker is less than that of corresponding FP with 4-CH_2. The two diethylamino coumarin-linked FPs showed similar inhibitory activity.
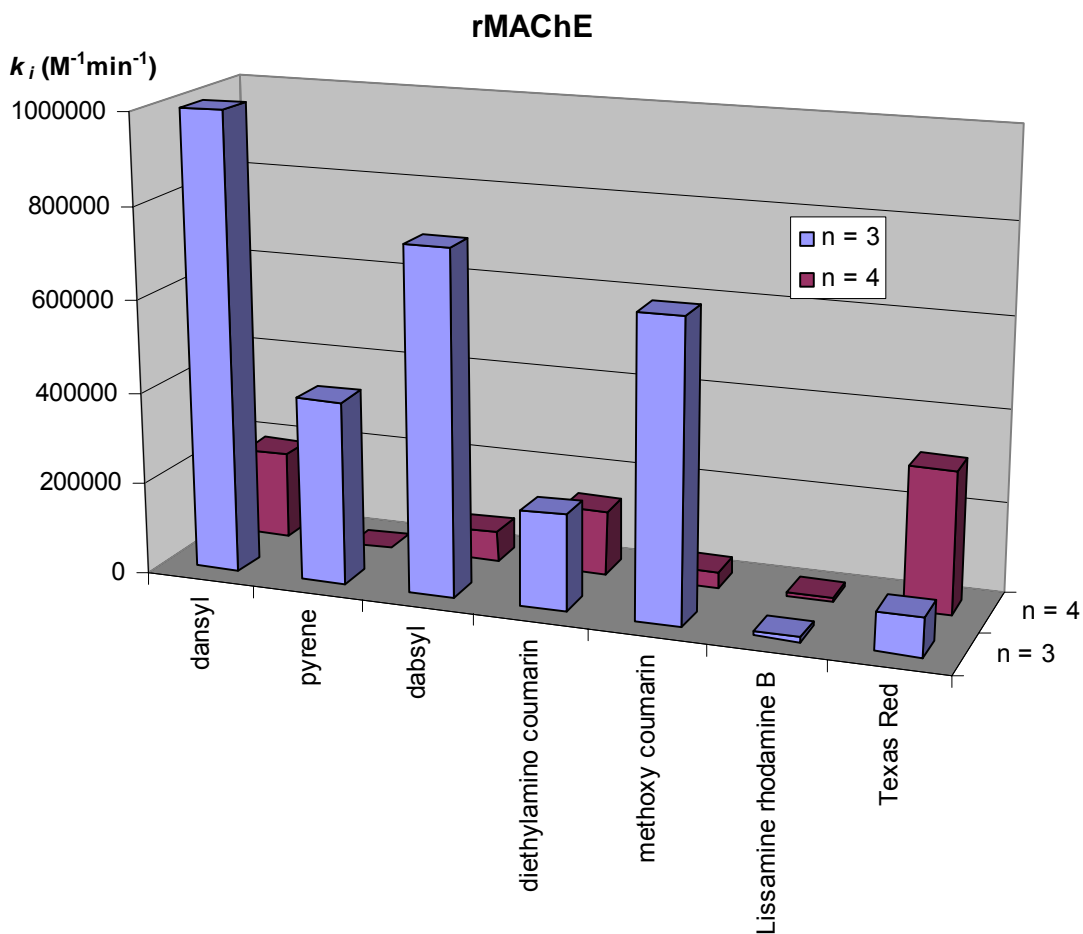
Figure 5.3. Comparison of inactivation potency of chromophore-linked FPs with n = 3, 4 linker length against rMAChE.

In terms of chemical structures, Lissamine and Texas Red are positively charged, larger and more complicated than dansyl, dabsyl and the other small chromophores. It is suggested that these complex chromophores may have effect on binding to the peripheral active site (PAS) of rMAChE and the proper length is necessary for their FP moiety to access the enzyme active site and fit in the gorge.

Similar observations were also made for EEAChE (Table 5.4). All chromophore-linked FPs were less potent than the fluorophosphonates **8a** and **8b**, indicating that the attached chromophores decrease the inhibition potency. For small chromophores such as dansyl and dabsyl, their linked FPs with shorter linker (3-CH_2) also exhibit higher inhibition activities over ones with longer linker (4-CH_2) against EEAChE. In contrast, for Texas Red -linked FPs, 4-CH_2 linker FP exhibits stronger inhibition activity compared with the 3-CH_2 linker one (Fig 5. 4).
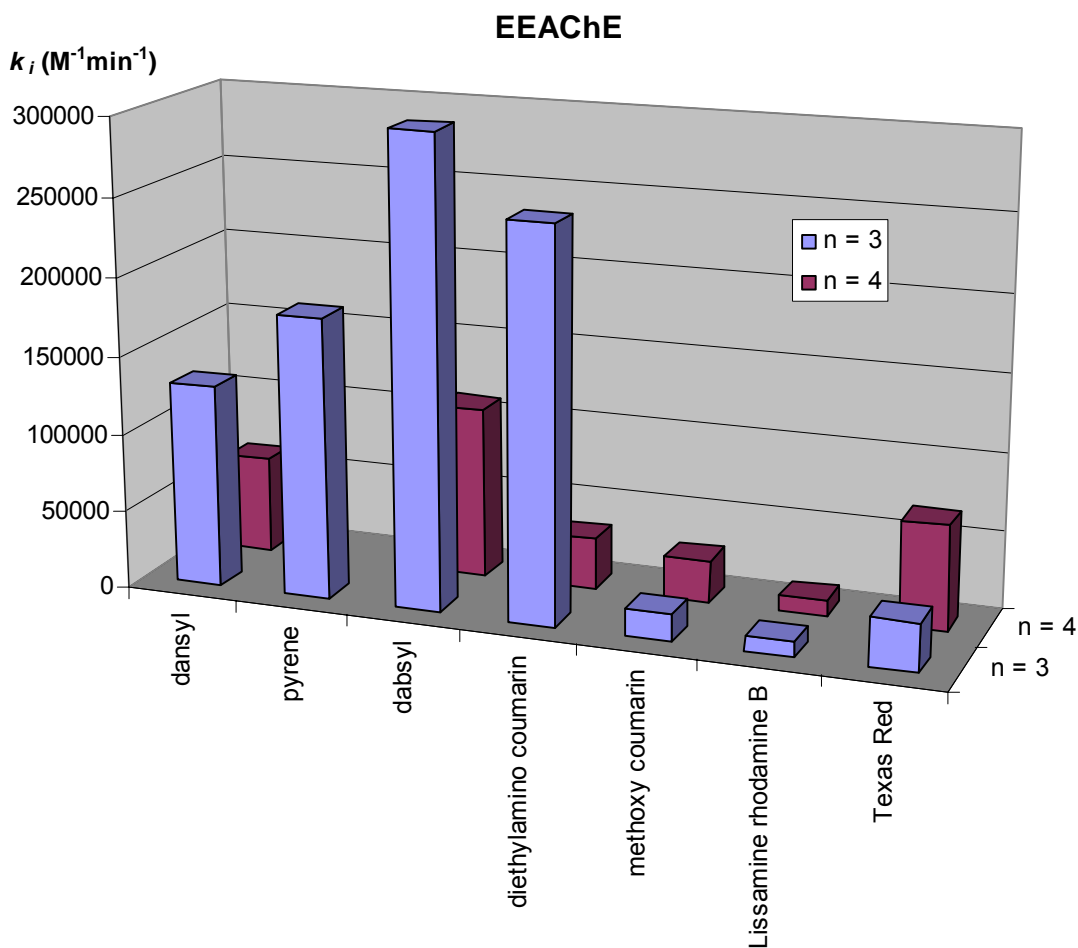
Figure 5.4. Comparison of inactivation potency of chromophore-linked FPs with n = 3, 4 linker length against EEAChE.

It was also found that Texas Red-linked FPs have larger K_D values compared to the other FPs, indicating that it is harder for these inhibitors to access the active site of AChEs and subsequently form the complex. These observations suggest that the complicated structure of Texas Red interacts with the peripheral site of AChE and requires a minimum length of the linker to access the active site to irreversibly inactivate the enzyme.

Comparing data against EEAChE and rMAChE, most chromophore-linked FPs showed similar inhibition activities. However, the difference in kinetic data of EEAChE between shorter and longer linker FPs is less pronounced than that of rMAChE, which further illustrates that rMAChE has a more rigid structure in the active site.

If a chromophore-linked FP can covalently modify the active site (using phosphorous moiety) and the peripheral active site (using the chromophore moiety) at the same time, the strength of its inhibition should be the sum of both parts, which is called 'double-site binding'. The chromophore moiety of the chromophore-linked FPs is designed to be positioned at the PAS when the organophosphorus moiety reacts with the active site, however, all the chromophore-FPs have k_i (s) smaller than that of the corresponding azo-FP compounds (**8a** or **8b**). These observations demonstrate that the length or the structure of our designed chromophore-linked FPs does not fit to allow for double-site binding on AChEs. As a result, the chromophores attached on FPs do not increase the inhibition activities, on the contrary, they decrease the inactivation.

Texas Red shows inhibition against both AChEs, however, the k_i(s) of Texas Red-linked FPs (3-CH$_2$ or 4-CH$_2$, $1 \times 10^4 \sim 1 \times 10^5$ M^{-1}min^{-1}) demonstrate less inhibition

activity on either AChE compared to other chromophores-linked FPs, which indicates that the charge and/or the bulky structure of Texas Red hinders binding to AChE.

In additional to the Texas Red-linked FPs, another relatively big chromophore-linked FP, Lissamine-linked, displayed similar weak inhibitory potency (small k_i). The different inactivation behavior of these large chromophores linked FPs indicates a negative effect of chromophore moiety in binding to the enzyme. This phenomenon was further examined by studying the effect of chromophore moiety without the covalently modification of the enzyme. Specifically, we sought to determine the interaction of the chromophores (analogs of compound **3**) with AChEs.

5.2.3   Inhibition of rMAChE and EEAChE by Chromophore Groups

The chromophore moiety may interact with AChE by binding to the active site, the peripheral active site, or non-competitively at other sites. Without the fluorophosphonate moiety to form the covalent bond to the enzyme, the chromophore moiety only reversibly binds to the enzyme. To elucidate how the chromophores interact with the enzyme and how much inhibition activity is resulted from this effect, the kinetic studies of chromophore moiety with no fluorophosphonate part (analogs of compound **3**) against both AChEs were carried out. The interaction between the chromophores and the enzyme is no longer a covalent modification, so a different data analysis method is required to characterize these compounds as reversible inhibitors.
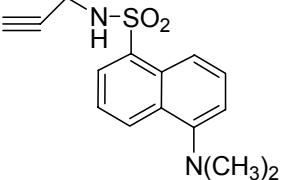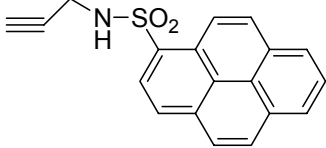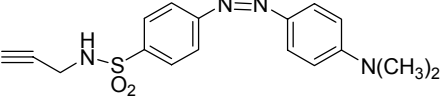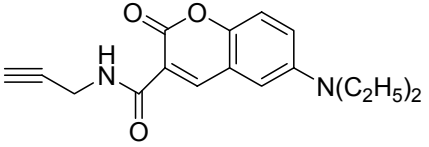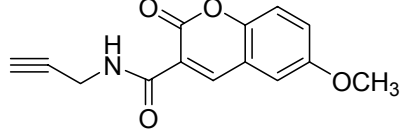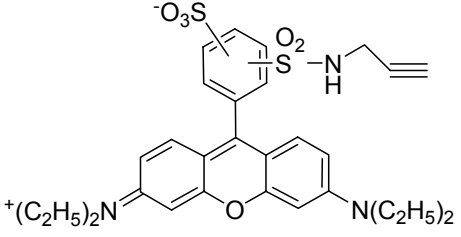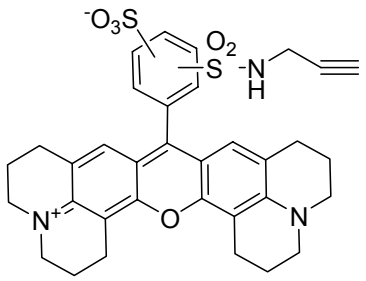
The chromophores with sulfonyl chloride or carboxylic chloride groups from Aldrich-sigma were first prepared by reacting with propargyl amine to obtain the corresponding propargyl amides (Table 5.5).

All chromophore-linked propargyl amides (**3a - 3g**) were first dissolved in acetonitrile (ACN) to make concentrated solutions with final concentrations of 20 μM and tested to see whether they were able to inactivate rMAChE. Only diethylcoumarin, Lissamine and Texas Red showed apparent inhibition (more than 50%), while dansyl, dabsyl, methoxycoumarin and pyrene did not. Higher concentrations of chromophores were not attempted due to solubility problem and interference with the assay.

The effect of diethylcoumarin, Lissamine and Texas Red on the activity of rMAChE was further investigated in the concentration-dependent method. As shown in Figure 5.5, the data were analyzed by Kaleidagraph 3.6 (Synergy Software, Reading, PA) and the concentration of the compound required to inhibit rMAChE and EEAChE by 50% at 6 min incubation (IC_{50}) was determined from the inhibition curve for each compound (Table 5.5).

Lissamine (**3f**) showed an IC_{50} value of 50 nM range against rMAChE, indicating a strongest enzyme inactivation among all chromophores (**3a - 3g**). Both Lissamine and Texas Red showed inhibition activity, suggesting that the positive charge on these molecules might contribute to the inactivation. It is also possible for diethylcoumarin to obtain a proton and form a positive charge.

Table 5.5: rMAChE and EEAChE inhibitory activity (IC_{50}) of chromophores.

compound	structure	rMAChE	EEAChE
		colspan	$IC_{50} \pm SE$ (μM)
3a (dansyl)		N/A	N/A
3b (pyrene)		N/A	N/A
3c (dabsyl)		N/A	N/A
3d (diethylamino coumarin)		1.00 ± 0.47	N/A
3e (methoxy coumarin)		N/A	N/A
3f (Lissamine rhodamine B)		0.05 ± 0.02	3.57 ± 1.45
3g (Texas Red)		0.70 ± 0.08	10.4 ± 2.1

N/A: not acquired, indicating that less than 20% inhibition activity was observed when inhibitor concentration is 20 μM.
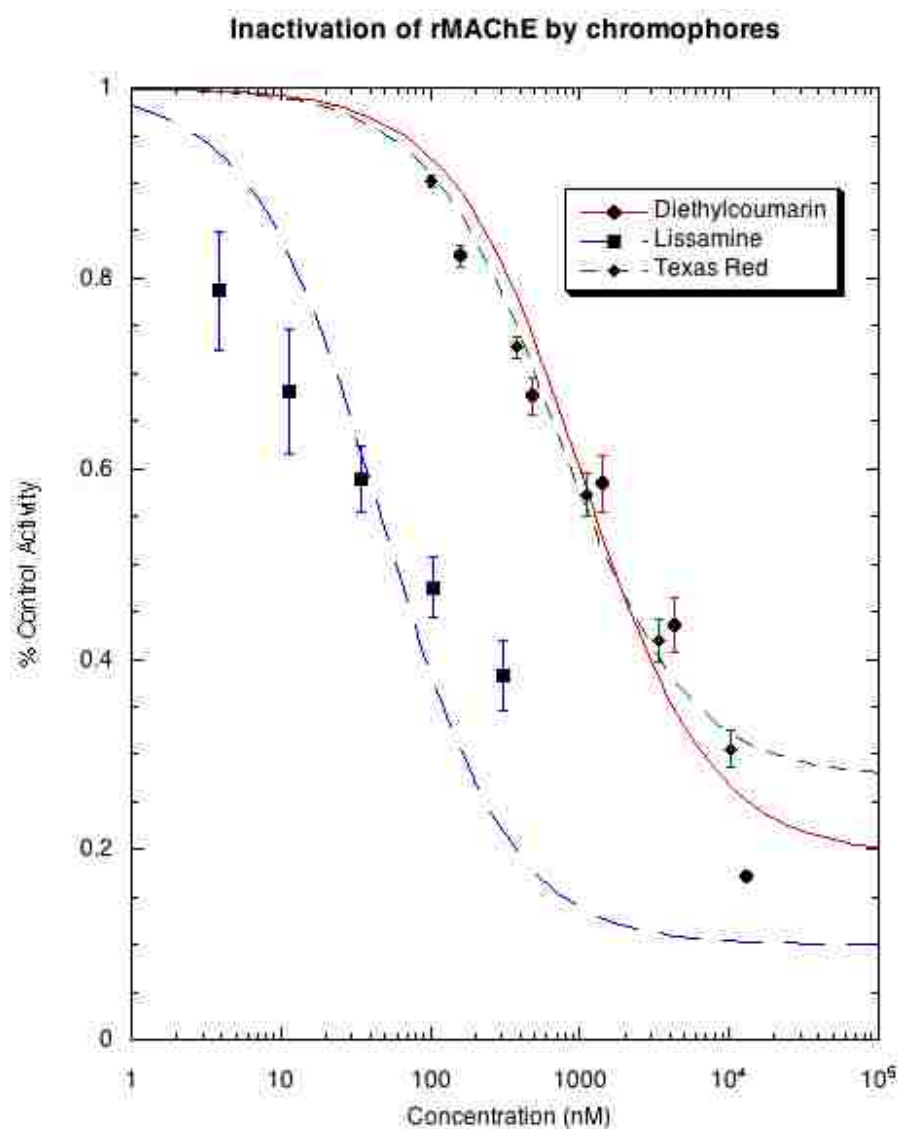
Figure 5.5. Concentration-dependence of rMAChE inhibition by diethylcoumarin (**3d**), Lissamine (**3f**), and Texas Red (**3g**); three chromophores that cause more than 20% inhibition at 10 μM.

Similar studies were also performed for EEAChE (Table 5.5) and Lissamine and Texas Red were found to be inhibitors with IC_{50} of 3.57 and 10.4 μM, respectively (Fig 5.6). Previous reported studies on inactivation of EEAChE by polycyclic aromatic

hydrocarbons showed that pyrene was an inhibitor with IC_{50} of 5.22 μM (Kang, 1997).
However, the inhibition potency of the pyrene-linked propargyl amide (**3b**) was not
reported in this study.
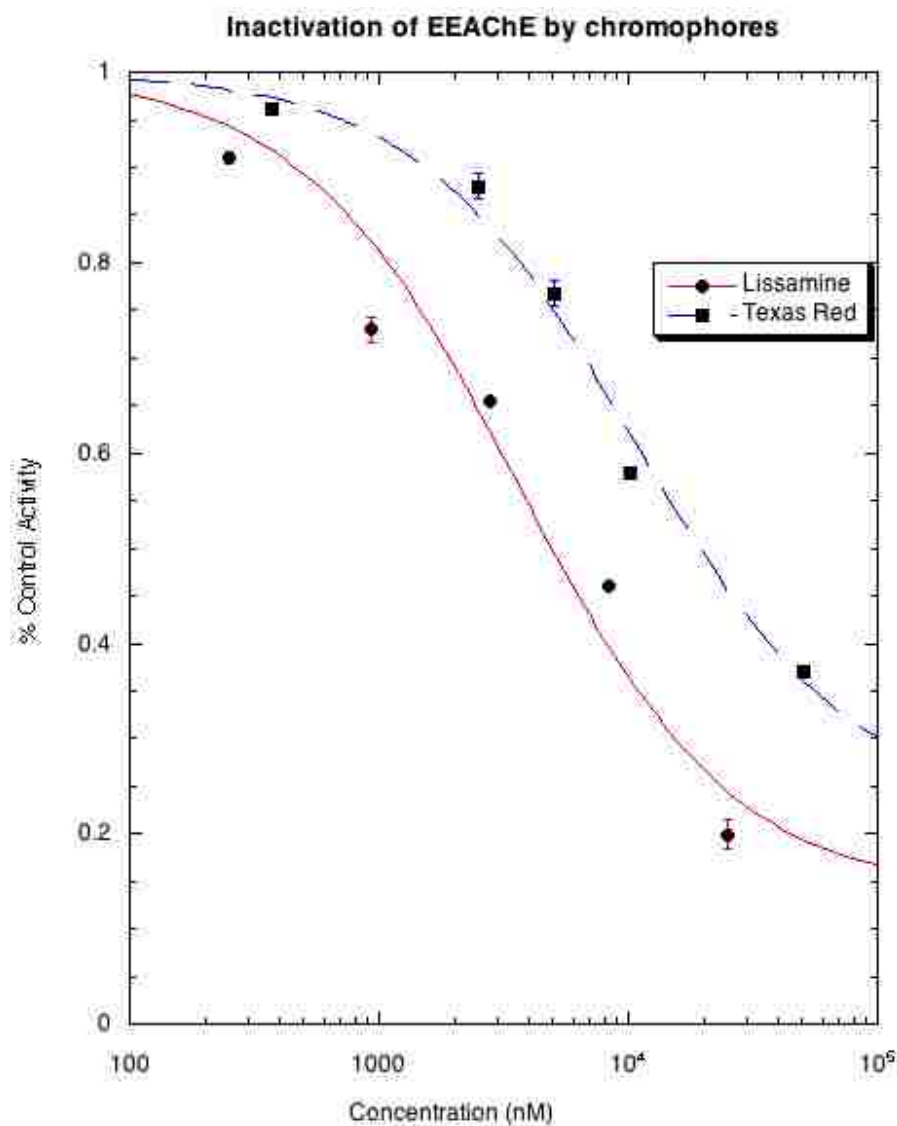
Figure 5.6. Concentration-dependence of EEAChE inhibition by Lissamine (**3f**) and
Texas Red (**3g**); chromophores that cause more than 20% inhibition at 10 μM.

To further delineate the inhibitory mechanism of these chromophores against AChE, the compound with stronger inhibition potency (lower IC_{50}), Lissamine, was further assayed against EEAChE at five substrate concentrations (duplicate experiments). Different concentrations of substrate were applied after 10 min of incubation with the inhibitor and the enzyme activity was recorded. Lineweaver-Burk analysis in the presence of different substrate and inhibitor concentration was conducted with Lissamine (Fig 5.7).

Double reciprocal Lineweaver-Burk plot

$y = 1.6525x + 5.4208$
$R^2 = 0.9975$

$y = 1.0634 x + 4.1473$
$R^2 = 1.0000$

$y = 0.7378x + 3.2475$
$R^2 = 0.9984$

$y = 0.6045x + 2.8817$
$R^2 = 0.9935$

$y = 0.5648x + 2.7919$
$R^2 = 0.9918$

Legend:
- [I]=0
- [I] = 25 uM
- [I] = 12.5 uM
- [I] = 5 uM
- [I] = 2.5 uM

Y-axis: $1/v$ (minA^{-1})

X-axis: $1/[S]$ (mM^{-1})
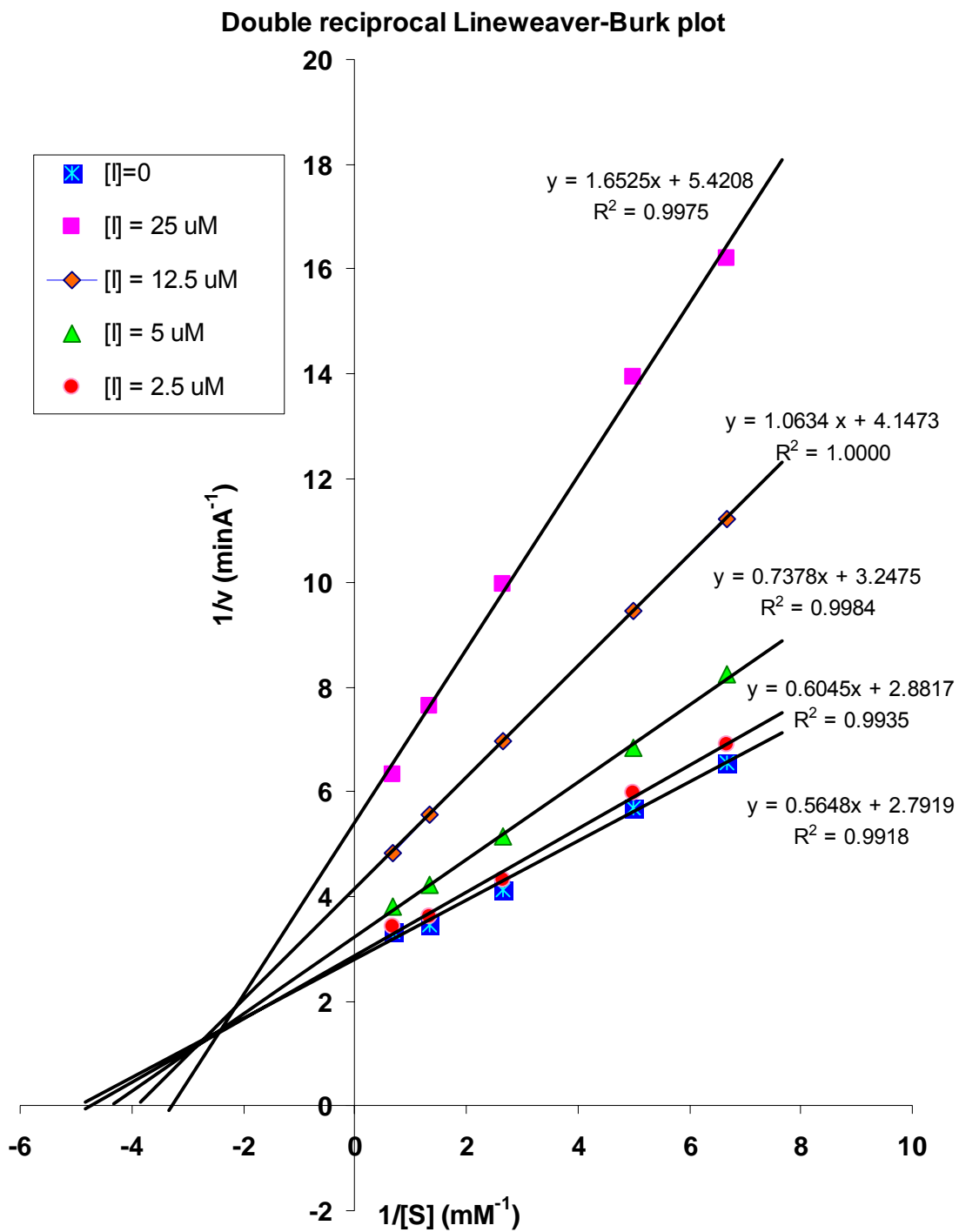
Figure 5.7. Double reciprocal Lineweaver-Burk plot of Lissamine on the EEAChE activity.

109

Figure 5.7 shows both slopes and intercepts increase with higher inhibitor concentration. This pattern indicates a mixed inhibition between competitive and noncompetitive inhibition, suggesting that Lissamine may interact with both the active site of free enzyme and some other site of the enzyme-substrate complex.

The competitive inhibition constant K_i is obtained by secondary plot of the slope versus the inhibitor concentration (Fig 5.8). The x axis intercept indicates a $K_i = 11.7$ μM of the inhibitor.
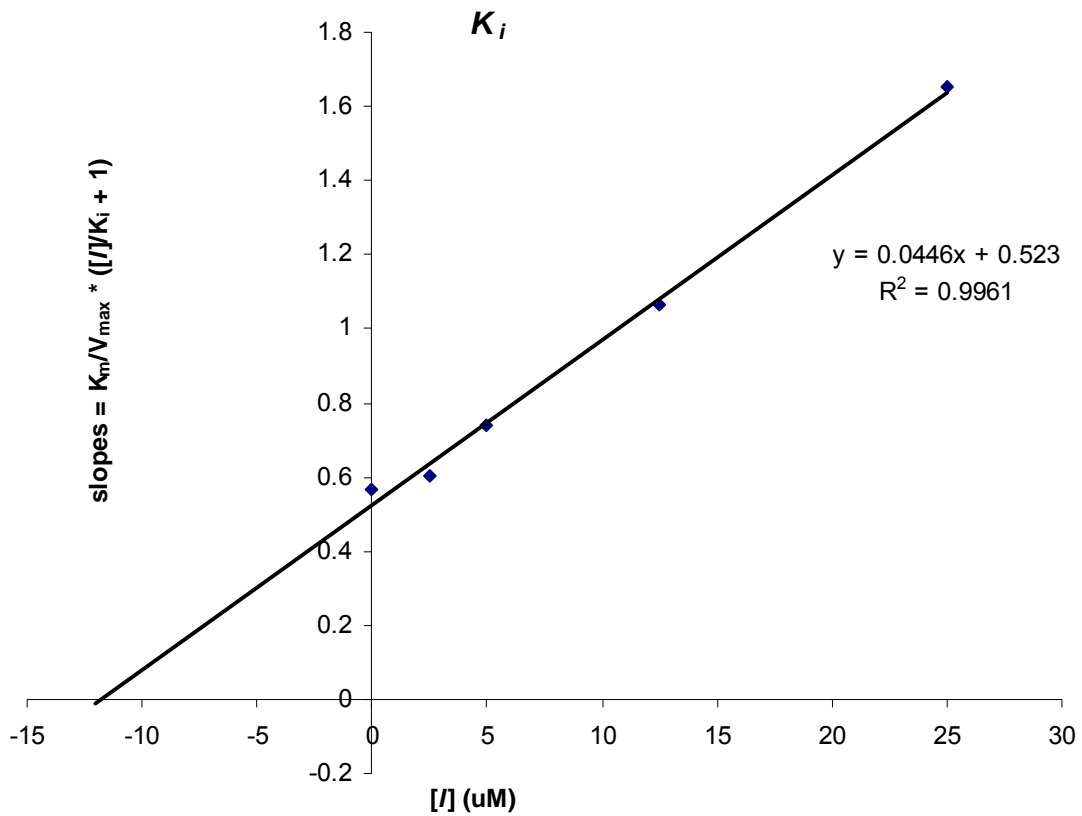
Figure 5.8. Replots of the reciprocal plots: slope versus inhibitor (Lissamine, **3f**) concentration.

The noncompetitive inhibition constant K_i' is obtained by secondary plot of the intercept versus the inhibitor concentration (Fig 5.9). The x axis intercept represents K_i = 24.9 μM of the inhibitor.
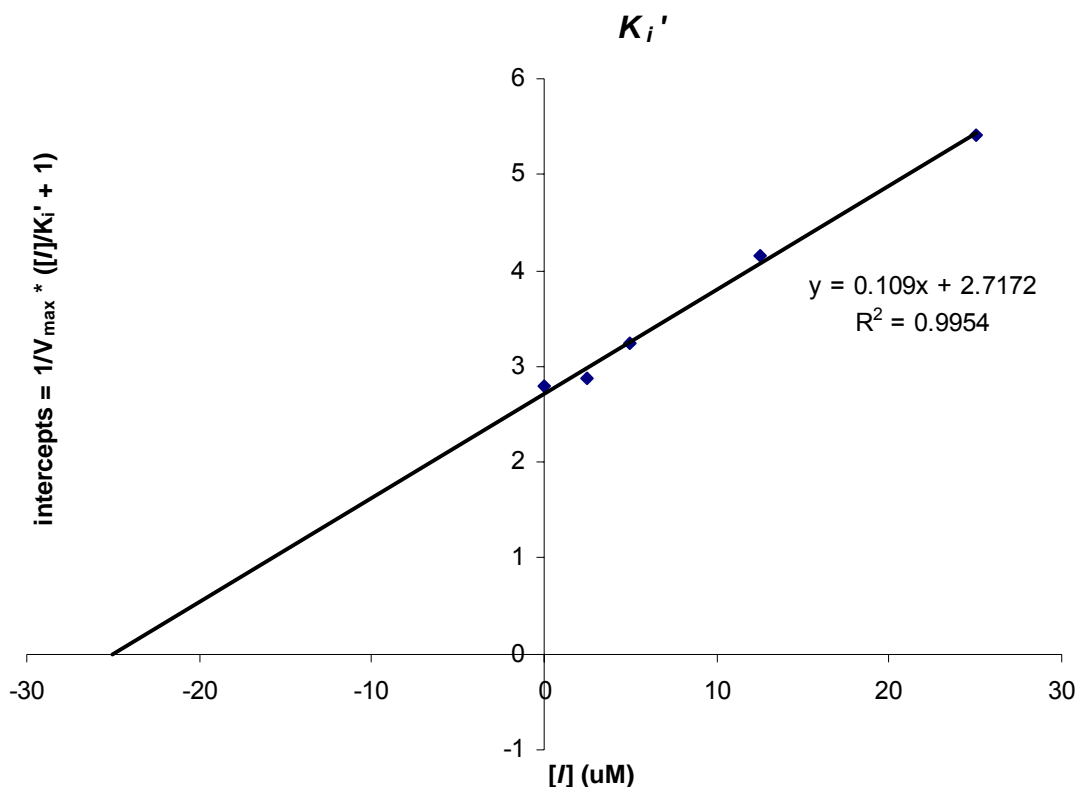
Figure 5.9. Replots of the reciprocal plots: intercept versus inhibitor (Lissamine, **3f**) concentration.

Kinetic data reveals the likely mechanism of EEAChE inactivation by Lissamine as an interaction with the entrance of the active gorge; namely, the peripheral active site (PAS). When Lissamine interacts with the PAS of EEAChE, which is a noncompetitive process for both free enzyme and the substrate-enzyme complex. When the EEAChE-

Lissamine complex is formed, it prevents the substrate from entering the active site, making it a competitive inhibitor at the same time. The mixed type property of the chromophores agrees with previous assumption and demonstrates that the bulky chromophores such as Lissamine and Texas Red inhibit AChEs by binding to the PAS and thereby blocking the gorge entrance.

Chromophores with inhibition activity in this study are relatively weak reversible inhibitors against AChE compared with most well-known reversible inhibitors (e.g. E2020 with a mixed competitive K_i of 4.27 nM. Saxena, 2003). In the studies with chromophore-linked FPs, considering the fast phosphorylation step, the irreversibly binding by FP moiety is much more predominant than the reversible binding from the chromophore moiety and thus the whole ligand can still be treated as an irreversible OP inhibitor.

For both rMAChE and EEAChE, small chromophores such as dansyl and dabsyl show no inhibition activity, indicating no effect from small, uncharged chromophores on binding to AChEs.

5.2.4   Molecular Modeling of Chromophore-linked FPs

All kinetic analyses suggest that the large chromophores (Texas Red and Lissamine) interact with the peripheral active site of AChE. To visualize this hypothesis and examine the orientation of the protein-ligand complexes, the smallest chromophore-linked FP, dansyl-linked FP with 3-CH2, and the largest FP, Texas Red-FP with 3-CH2, were selected and compared using molecular modeling. Both molecules were docked into the active gorge of AChE, followed by the comparison of the results.

Crystal structures of various types of AChE are available in the RCSB Protein

Data Bank (PDB) (http://www.rcsb.org). In order to be consistent with previous

experiments, a crystal structure of rMAChE (1maa, resolution 2.90 Å) (Fig 3.1) (Bourne,

1999) was chosen for simulation. FlexX was used as the docking program because it

offers specification of the tailored active site and customization of any kind of constraint

between ligand and protein is allowed. The phosphorus moiety of the inhibitor was first

manually positioned into the active site to optimize the opportunity for phosphor-serine

formation and then the docking program minimized the total energy of the protein-ligand

complex to offer the possible docked configurations.

1) Dansyl-linked FP (3-CH$_2$):

For dansyl-linked FP (3-CH$_2$), four docking solutions were found when the

constraint of distance from phosphorus to the hydroxyl of the active site serine was set up

to be less than 2.5 Å, which is generally a distance for a chemical reaction to occur.

FlexX provided various scoring for each of them (Table 5.6).

Table 5.6: Docking solutions for dansyl-linked FP (3-CH$_2$) in FlexX.

1	2	3	4	5	6	7	8	9	10	11	12	13	14	15
1	-5.5	-13.6	-9.5	-7.8	7.5	12.6	5.4	4.9	8	-169	-71	-133	-28	5
2	-4.9	-12.3	-10.9	-7.4	7.6	12.6	5.5	5.0	8	-156	-63	-132	-27	1
3	-4.6	-13.0	-9.2	-8.1	7.6	12.6	5.7	5.2	9	-161	-67	-130	-27	1
4	-4.5	-12.3	-10.8	-7.2	7.8	12.6	5.5	5.0	8	-164	-63	-133	-27	2

1.Solution_Rank 2.Total_Score 3.Match_Score 4.Lipo_Score 5.Ambig_Score
6.Clash_Score 7.Rot_Score 8.RMS 9.Similarity 10.Match 11.G_Score
12.PMF_Acore 13.D_Score 14.CHEMSCORE 15.CScore

The four docking solutions have high similarity. The first one with the highest

CScore (column 15, Table 5.6) represents the most reasonable structure of enzyme-OP

complex (Fig 5.10).
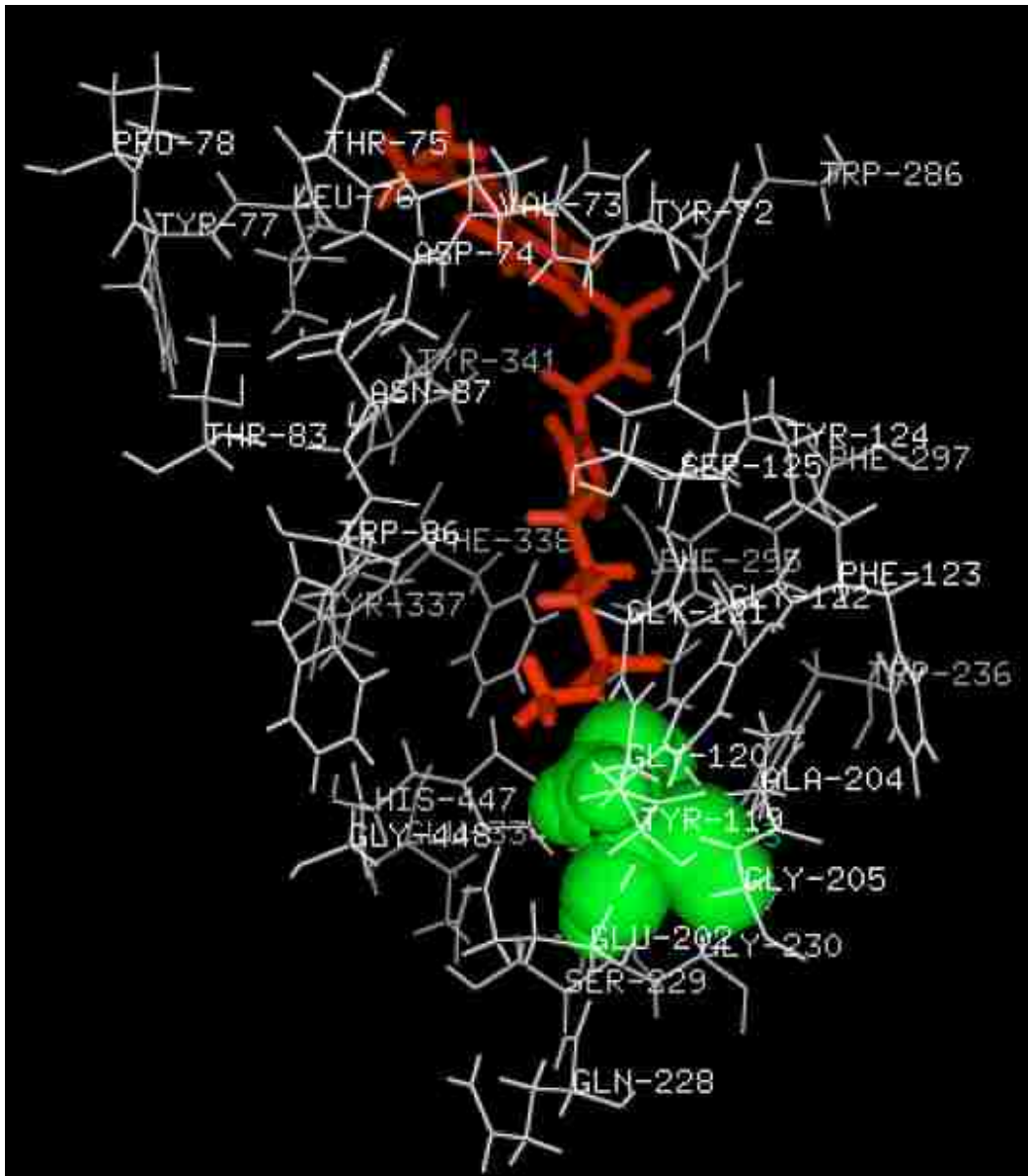
Figure 5.10. Best docking solution of dansyl-linked FP (3-CH$_2$).

In this best docking solution, the distances were measured as (Fig 5.11):

Phosphorus (ligand) – Oxygen (Ser203) = 2.5 Å;

Phosphorus (P9) – Carbon (C19) = 14.6 Å;

Phosphorus (P9) – Carbon (C13) = 11.6 Å.
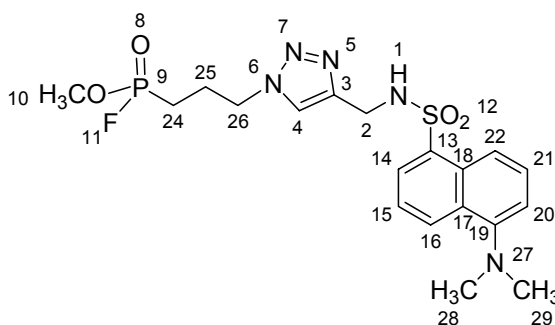
Figure 5.11. Structure of dansyl-linked FP (3-CH$_2$).

The distance of 2.5 Å from the Ser203-O and the phosphorus atom P is close enough for a chemical reaction to occur in assistance of small changes of protein structure. Meanwhile, the whole dansyl-linked FP is smoothly placed along the active gorge in this structure.

2) Texas Red-linked FP (3-CH$_2$):

Texas Red was the largest chromophore molecule used in the study. The compound obtained from Invitrogen, Inc is a mixture of ortho- and para- isomers that relate to the position of amide link to propargyl amine.

2a) (o-)Texas Red-linked FP (3-CH$_2$):
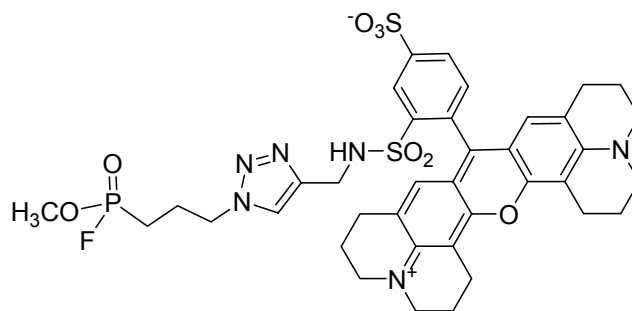
Figure 5.12. Structure of (o-) Texas Red-linked FP (3-CH$_2$).

The structure of (o-)Texas Red-linked FP (3-CH$_2$) was drawn in SYBYL. After minimizing the free energy of this ligand, the most stable structure was bent and the length of the molecule in this configuration is approximate 13.1 Å, which is much shorter than the length of the gorge.

No docking solution was found when the distance between phosphorus of the inhibitor and the hydroxyl of Ser203 was constrained to 3.0 Å or less. The docking results indicate that the possibility for fluorophosphonate moiety to access the hydroxyl serine is relatively low for (o-)Texas Red-linked FP (3-CH$_2$).

The constraint was later set to be "optional" to show all possible docking solutions. Among the first 30 docking solutions produced (about 200 solutions generated), most of them showed that the docked ligand was outside of the enzyme, which is not desired. The best docking solution with highest scores is shown in Fig 5.13.
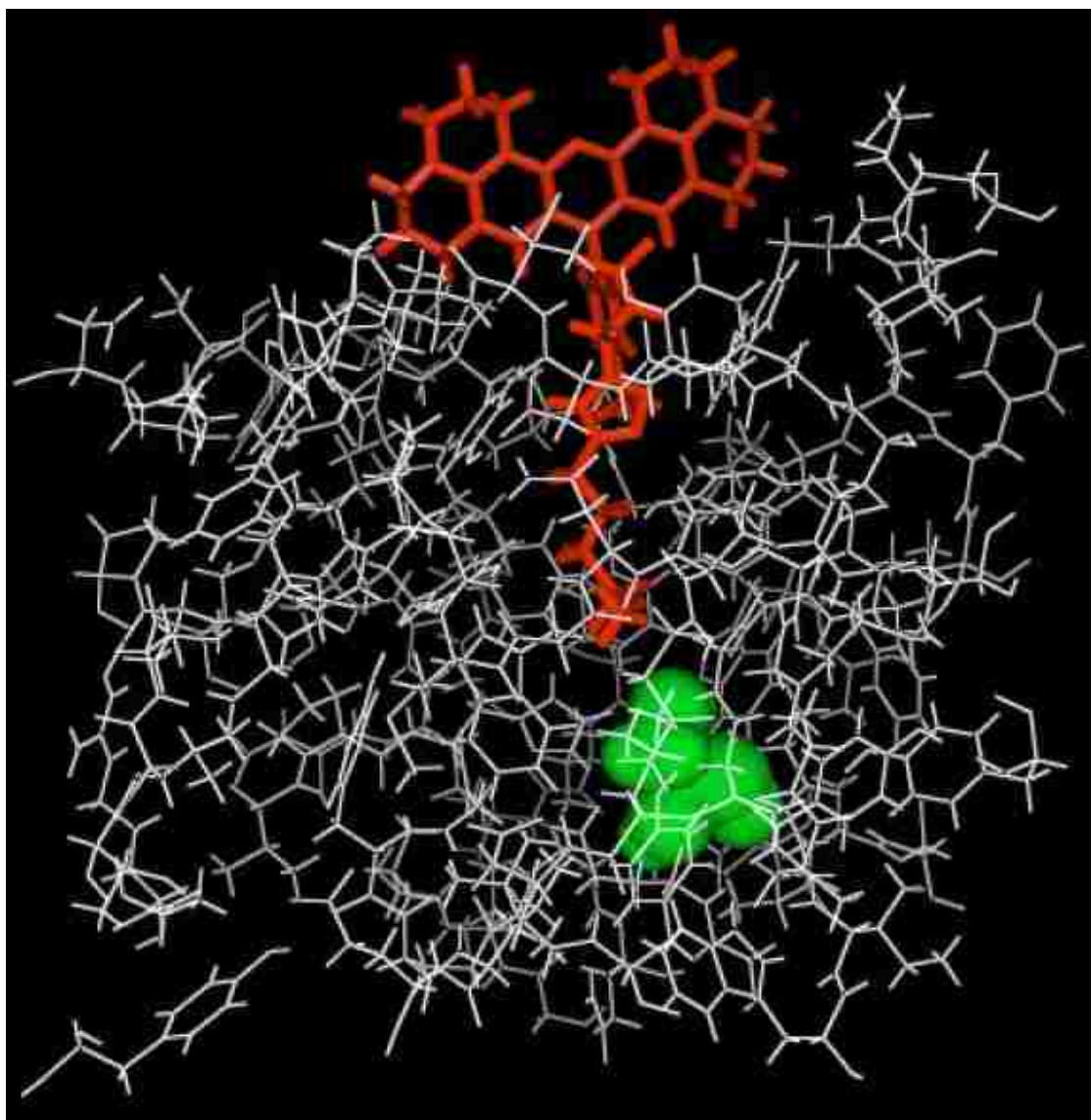
Figure 5.13. Best docking solution of (o-)Texas Red-linked FP (3-CH$_2$).

In the docking solution, the chromophore moiety is placed outside of the gorge entrance (Fig 5.14), either because the size of the chromophore is bigger than the entrance or because the interaction between the chromophore and the entrance is strong. Considering the ligand length about 13.1 Å, it is unsurprising that the linker is not long

enough for the phosphorus to access the bottom of the gorge if its big chromophore

moiety cannot pass through the gorge entrance.
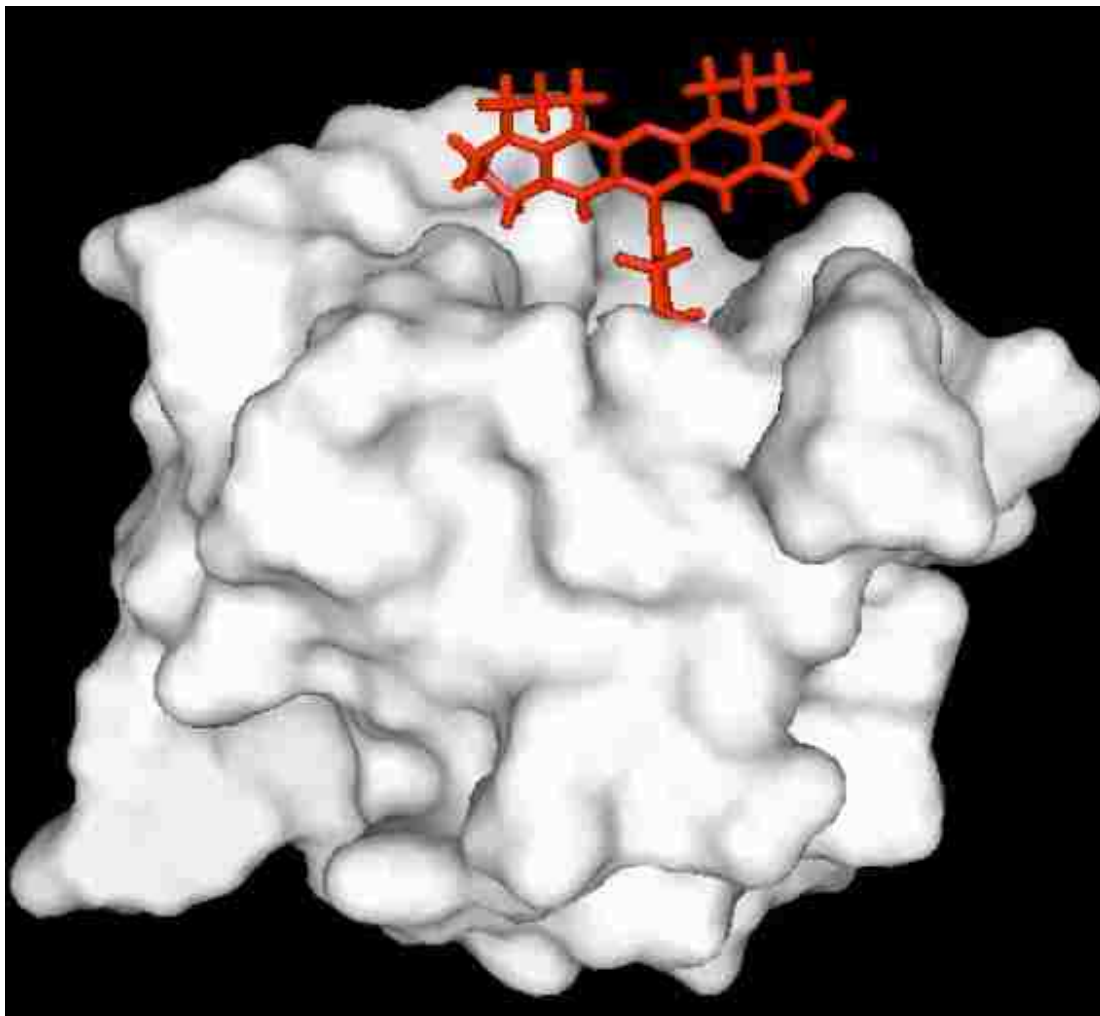
Figure 5.14. A docking solution for (o-)Texas Red-linked FP (3-CH$_2$) in rMAChE
(surface view), showing that the chromophore portion remains external to the enzyme.

In the solution, the distances were:

Phosphorus (ligand) – Oxygen (Ser203) = 4.5 Å;

Phosphorus (ligand) – Oxygen (ligand, in the ring) = 15.5 Å.

The 4.5 Å distance from the phosphorus of the ligand to the hydroxyl serine, is too far for a chemical reaction to take place, unless the protein structure changes dramatically to help the reaction. It is proposed that (o-)Texas Red-linked FP (3-CH$_2$) can not slide into the active gorge completely due to its big chromophore moiety. Both the big size and the charge of the Teas Red could be the reasons for this unfavorable configuration.

2b) (p-)Texas Red-linked FP (3-CH$_2$):
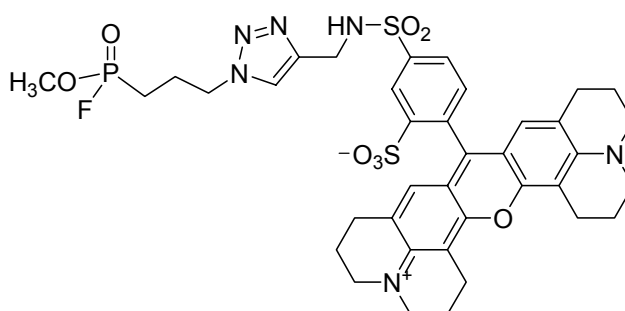
Figure 5.15. Structure of (p-) Texas Red-linked FP (3-CH$_2$).

Compared with (o-)Texas Red-linked FP (3-CH$_2$), the other isomer, (p-)Texas Red-linked FP (3-CH$_2$) (Fig 5.15), has a longer linker. The most stable structure after minimizing free energy showed that the direct molecule length is 14.8 Å, which provides a better chance for the FP moiety to access the hydroxyl serine at the bottom of the gorge.

Two similar solutions were produced by the docking program when the distance between phosphorus of the ligand and the hydroxyl Ser203 is less than 2.5 Å. The one with better scores was shown in Figure 5.16 and 5.17.
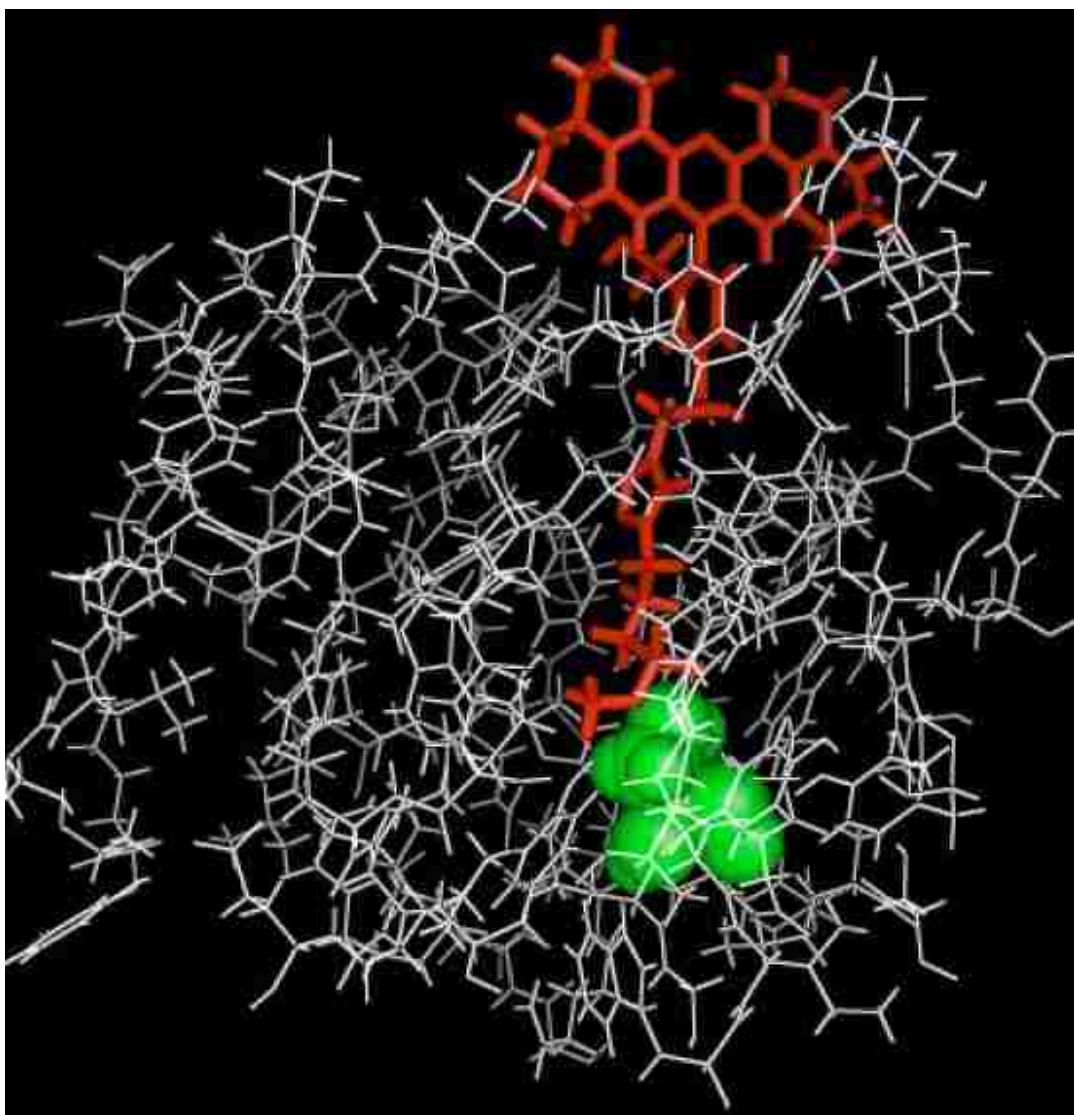
Figure 5.16. Best docking solution of (p-)Texas Red-linked FP (3-CH$_2$).

The distances were:

Phosphorus (ligand) – Oxygen (Ser203) = 2.5 Å;

Phosphorus (ligand) – Oxygen (on the ring of the ligand) = 17.8 Å.
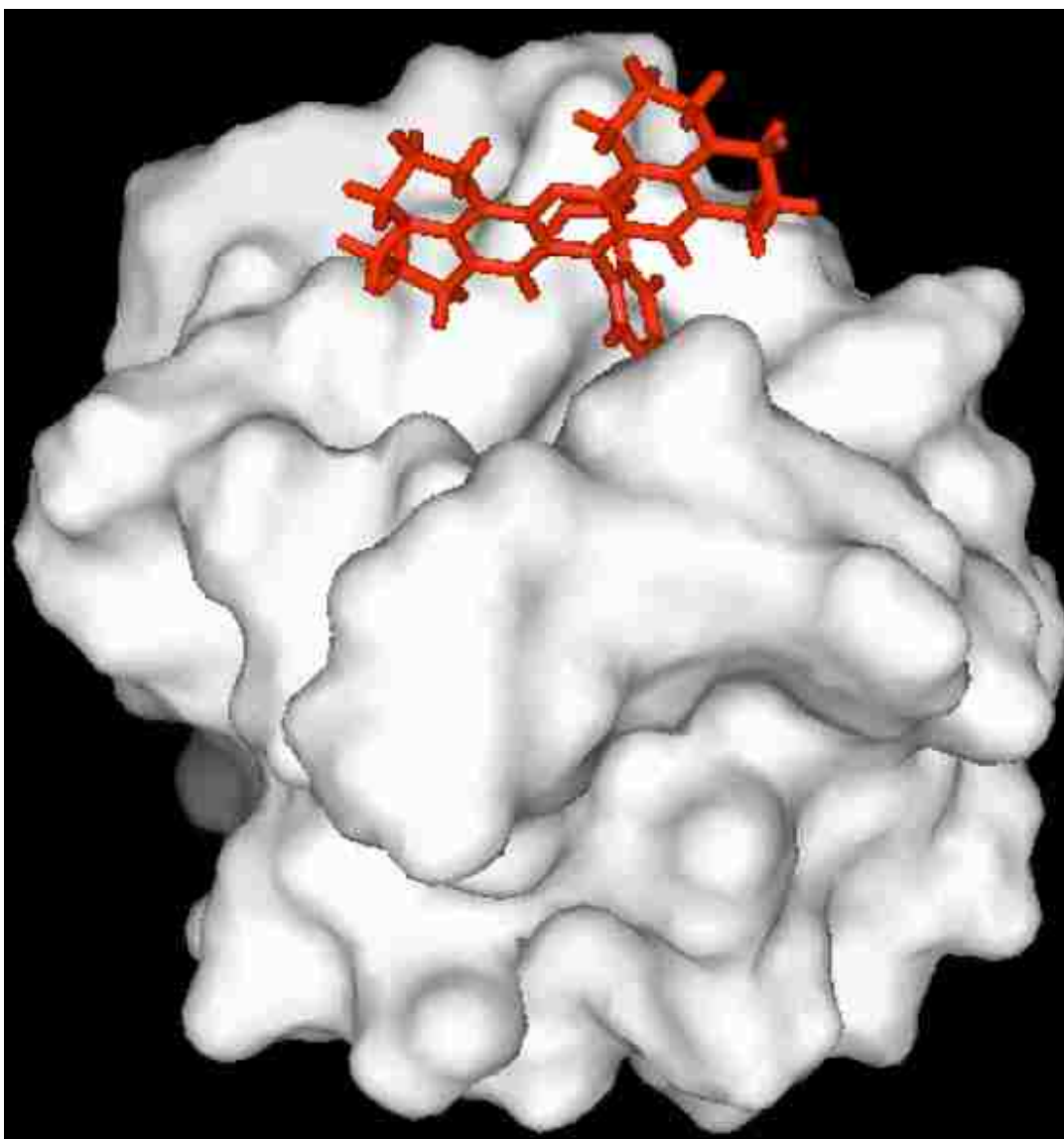
Figure 5.17. A docking solution for (p-)Texas Red-linked FP (3-CH$_2$) in rMAChE (surface view), showing that the chromophore portion remains external to the enzyme.

As shown in figure 5.17, the chromophore moiety was again placed outside of the gorge entrance. For (p-)Texas Red-linked FP (3-CH$_2$), the phosphorylation step is easier to take place than the ortho- isomer because of the longer molecular length, although the chromophore group is positioned out of the gorge entrance in both cases.

Based upon all the docking experiments, it is proposed that (o-)Texas Red-linked FP (3-CH$_2$) is not able to covalently modify the enzyme while the (p-)Texas Red-linked FP (3-CH$_2$) possibly can. The mixture of isomers of Texas Red makes the interaction with enzyme complicated and unpredictable. However, it is clear that Texas Red moiety interacts with the enzyme by blocking the entrance of the active site.

5.2.5 **Summary**

In summary, large chromophores such as Texas Red and Lissamine interact with AChE by blocking its gorge entrance, which further block the enzyme activity. On the other hand, small chromophores such as dansyl and dabsyl, do not have much interaction with the enzyme by themselves and their linked FPs demonstrate similar inhibition potency. Both docking observations and kinetic data show agreement on this conclusion.

In the docking studies, Texas Red moiety restricts the FP moiety from reacting with Ser203, either by sterically hindering the entrance, or by strongly binding to the PAS on the entrance with their cations. Either mechanism prevents this type of chromophore-linked FPs from phosphorylating the active site unless long enough linker is attached. This explains why the big chromophore linked FPs show relatively low inhibition activity. Longer linker FP inhibitors with these chromophores are better than shorter linker ones because the longer linker provides a better chance for the FP moiety to access the active site on the bottom of the gorge.

Texas Red and Lissamine linked propargyl amide behave as reversible inhibitors against AChE, both competitively and noncompetitively, indicating that the big

chromophores inactivate the enzyme by both binding to the PAS and blocking the gorge entrance.

To avoid the binding from the chromophore moiety, smaller, uncharged chromophores are preferred for investigating the stereoselectivity of the gorge in the future. It is also possible to increase the chain length of big chromophore-linked FPs to decrease the effect. The big chromophores with complicated interactions with the enzyme can be used in the future to study the PAS of AChE or build the double-site binding inhibitors by optimizing the length of the molecule.

5.3 Post-inhibition Analysis of Inactivated EEAChE by Chromophore-linked FPs

The post-inhibition phases of inhibited acetylcholinesterase by irreversible fluorophosphonate inhibitors are illustrated in Figure 5.18.
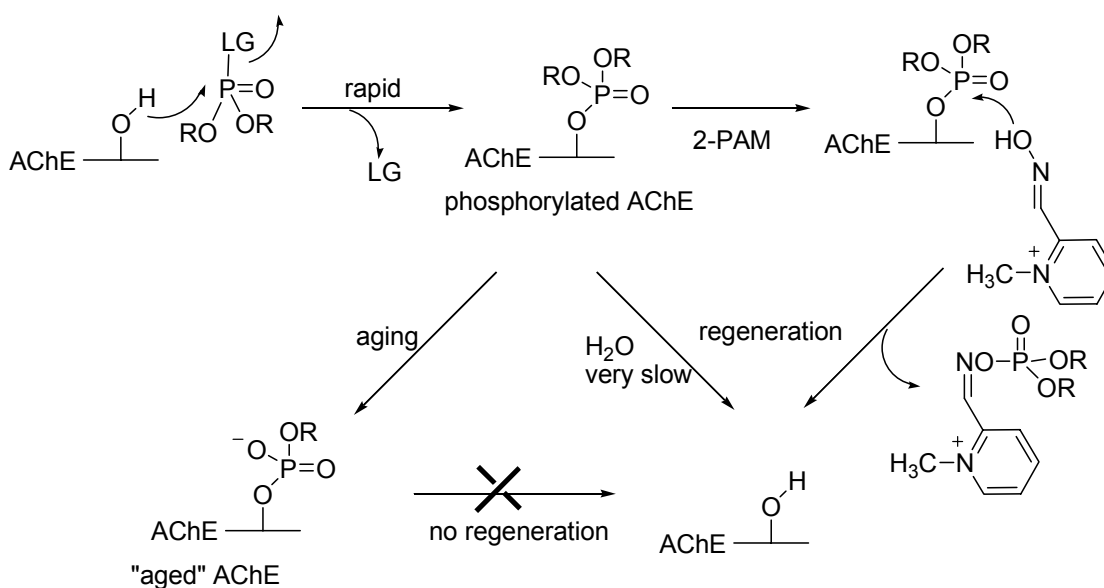
Figure 5.18. Inhibition of AChE and post-inhibitory mechanism.

The post-inhibition phases of inhibited acetylcholinesterase are supposed to be the same for all fluorophosphonate inhibitors because the fluorophosphonate moiety is the only target involved in these processes. Preliminary study of reactivation process was made and fluorophosphonate inhibitors with different inhibition potency were examined.

Because the reactivation experiments require a high concentration of enzyme, only EEAChE was studied. Spontaneous reactivation was studied for fluorophosphonate

8a, which is the strongest inhibitor among all FPs. Following the method described in section 7.4.3, more than 90% inactivated EEAChE by inhibitor **8a** was diluted 100-fold, and the reactivation rate was studied. At a 100-fold dilution, the inhibitor concentration is no longer a factor in further inactivating the enzyme and only reactivation, aging or inhibited species exist. No reactivation of inhibited EEAChE was observed. Spontaneous reactivation was also analyzed for dansyl-linked FP ($4-CH_2$), an inhibitor with average inhibition strength and no reactivation was observed. A weaker inhibitor, Texas Red-linked FP ($3-CH_2$) was studied under the same conditions and no reactivation was observed.

The activity of the control aliquot started decreasing after 3 h inhibition, thus no study was attempted more than 3 h. To get more than 90% inhibition of AChE in 3 h, excess amount of inhibitors was used. The amount of inhibitors should be better controlled to investigate the reactivation process more precisely in the future.

2-PAM solution (0.1 mM) was used in mediated reactivation of EEAChE inhibited by Texas Red-linked FP ($3-CH_2$) and dansyl-linked FP ($3-CH_2$). Again, no reactivation was found. Further study with more concentrated 2-PAM is desired to study this process in more details.

Current observations showed that EEAChE inhibited by FPs was not reactivated, implying that the aging is the dominant post-inhibitory process or that the chromophore moiety around the gorge entrance prevents the nucleophile (oxime) from accessing the active site. The fact that no reactivation was observed is beneficial to the purpose of separation and purification of protein-inhibitor complex in the future.

5.4 Inactivation of rMAChE and EEAChE by Dansyl-linked Phosphonothiolates

The inhibition activities of the synthesized dansyl-linked phosphonothiolates **13** and **15** are the average activities of its chromophore-linked asymmetric phosphonothiolates (CLAPs) (Fig 5.19).

13: R = SCH$_3$
15: R = SCH$_2$CH$_2$N$^+$(CH$_3$)$_3$
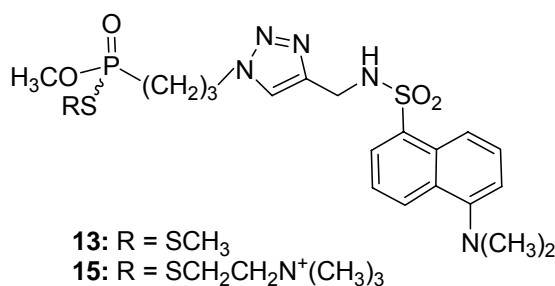
Figure 5.19. Structures of dansyl-linked phosphonothiolates **13** and **15** (racemate).

To evaluate the inhibitory potency of the CLAPs, the inhibition abilities of racemic dansyl-linked phosphonothiolates (compound **13** and **15**) were examined. Phosphonothiolates were examined as phosphorylated inhibitors in a concentration dependent manner and the k_i and K_D values were presented in Table 5.7. Each compound was tested more than three times and data were only included when R^2 of the plot is over 0.95.

Table 5.7: Inhibition of rMAChE and EEAChE by phosphonothiolates **13** and **15** (racemate).

compound	rMAChE		EEAChE	
	k_i $(M^{-1}min^{-1})$	K_D (M)	k_i $(M^{-1}min^{-1})$	K_D (M)
13	$< 10^3$	NA	$< 10^3$	NA
15	$2.0 \pm 0.4 \times 10^5$	$2.5 \pm 0.7 \times 10^{-6}$	$3.3 \pm 0.4 \times 10^3$	$1.2 \pm 0.5 \times 10^{-5}$

N/A: not acquired.

Compared with dansyl-linked FP compounds, dansyl -linked phosphonothiolates have lower inhibition potency against rMAChE and EEAChE. The phosphonothiolate **15** is more potent than compound **13**. Considering the structure difference in the two compounds, the thiocholine group of compound **15** makes the phosphorus moiety bind to the active site better and thus increases the inhibition ability.

Modest inhibition ability of phosphonothiolates may provide longer time course in studying the stereoselectivity of AChE later, however, the low inhibition potency of compound **13** may add difficulty in obtaining the kinetic data at the same time.

5.5 Inactivation of rHuAChE and EEAChE by Asymmetric Phosphonothiolates

Asymmetric phosphonothiolates **25a** and **25b** were prepared in chapter 4 and used to determine the stereospecific inhibition of recombinant human and electric eel AChE. Recombinant human AChE selected in this section has comparable properties as rMAChE but more practical application due to its human source.

5.2.1 Stereoselective Inactivation of rHuAChE by Asymmetric Phosphonothiolates

The racemate *O, S*-dimethyl (3-azopropyl) phosphonothiolate **25** and the corresponding enantiopure isomers **25a** and **25b** were studied against rHuAChE as irreversible inhibitors, respectively. The inhibition rates (k_i) and dissociation constants (K_D) were determined in the concentration-dependent manner and presented in Table 5.8.

Table 5.8: Inhibition of rHuAChE by phosphonothiolates **25, 25a** and **25b**.

compound	k_i $(M^{-1}min^{-1})$	K_D (M)	$\overline{k_i}$ $(M^{-1}min^{-1})$	$\overline{K_D}$ (M)
25	8.1×10^3	6.1×10^{-5}	$7.9 \pm 0.3 \times 10^3$	$8.5 \pm 1.8 \times 10^{-5}$
	8.2×10^3	7.3×10^{-5}		
	7.2×10^3	12.1×10^{-5}		
25a **(S) (-)**	1.7×10^3	9.8×10^{-5}	$1.7 \pm 0.1 \times 10^3$	$10.3 \pm 0.5 \times 10^{-5}$
	1.7×10^3	9.8×10^{-5}		
	1.9×10^3	11.2×10^{-5}		
25b **(R) (+)**	9.4×10^3	2.4×10^{-5}	$9.0 \pm 0.6 \times 10^3$	$3.1 \pm 0.8 \times 10^{-5}$
	9.7×10^3	2.8×10^{-5}		
	7.8×10^3	4.7×10^{-5}		

The extent of stereoselective inhibition is revealed by the kinetic rate constants (k_i). *(S)*-Phosphonothiolate **25a** exhibits five times less inhibitory potency than *(R)*-phosphonothiolate **25b** on recombinant human AChE, showing that the enzyme is *(R)*-selectively inactivated.

The dissociation constant K_D, which describes the formation of the OP-AChE complex, is restricted by the steric hindrance, possibly suggesting a selective configuration favored by the active site of rHuAChE. *(R)*-Phosphonothiolate **25b** has three times higher affinity (lower K_D) than *(S)*-**25a**, indicating that the first inhibition step of complex formation is largely dependent on the chirality of the inhibitor due to the configuration refinement. In contrast, phosphorylation step proceeds rapidly and the rate constant ($k_p = k_i$ x K_D) is less dependent of the chirality of the inhibitor.

5.5.2 Inhibition of EEAChE by Asymmetric Phosphonothiolates

Similar stereoselective inactivation of EEAChE was observed with the asymmetric phosphonothiolates **25a** and **25b**. However, the racemate compound **25** shows a small k_i of 5.3 x 10^2 $M^{-1}Min^{-1}$ against EEAChE, indicating that the inhibition potency of this inhibitor is too weak to study the stereoselectivity.

Both **25a** and **25b** slightly inactivated EEAChE however the kinetic parameter k_i(s) were not determined and only estimated to be less than 10^3 $M^{-1}Min^{-1}$. It is hard to obtain data of a weak inhibitor ($k_i < 10^3$ $M^{-1}Min^{-1}$) in the kinetic studies because either longer incubation time or more concentrated sample is required. However, a longer incubation time induces the decrease of the enzyme activity according to the control

129

study, and a more concentrated sample is not applicable in most cases due to solubility problem. It was decided that only k_i larger than 10^3 ($M^{-1}Min^{-1}$) is attempted.

In contrast to EEAChE, recombinant Human AChE is more sensitive to phosphonothiolate inhibitors. Recombinant acetylcholinesterases from different sources are desired to examine the stereoselectivity in the future.

5.6 Attempted Analysis of Inactivation of rHuAChE by CLAPs

Before attempting inactivation analysis with CLAPs, dansyl-linked racemic phosphonothiolate **13** was studied first. Previous data in section 5.4 have already demonstrated the weak inhibitory activity of this compound against rMAChE and EEAChE. Current kinetic study on rHuAChE showed that the k_i of compound **13** is approximately 0.8×10^3 $M^{-1}Min^{-1}$. Considering the larger effect added by other chromophores than dansyl, study of two different chromophores-linked asymmetric phosphonothiolate compounds was not attempted.

In order to increase the inhibition potency of the asymmetric phosphonothiolate inhibitors, chromophore-linked *O*-methyl, *S*-choline phosphonates (analog of compound **15**) are desired in the future study. Based on studies in section 5.4, *S*-choline group increases the inhibition activity by binding to the active site with its tertiary amine. *O*-methyl, *S*-choline (3-azopropyl) phosphonate is to be synthesized as an asymmetric inhibitor and more stereoselectivity is expected due to the structural bulkiness.

CHAPTER 6

CONCLUSIONS

1. A flexible and reliable synthetic route for the generation of an array of chromophore-linked fluorophosphonate (FPs) was found to be successful and a panel of chromophore-linked FPs with different chromophore and length was synthesized via click chemistry.

2. The chromophore-linked FPs showed potent inhibitory activity against both recombinant mouse AChE (rMAChE) and electric eel AChE (EEAChE). Compared with the inhibitory activity for the FP moiety without chromophore, a decrease in inhibition potency demonstrated a negative effect of the chromophore in the inactivation of AChEs. This negative effect is especially evident when the chromophore is bulky and positively charged.

3. Detailed analysis of one chromophore (Lissamine) as a reversible inhibitor that transiently binds to AChE confirmed the inhibition effect of the chromophore. A mixed inhibitory activity (both competitive and non-competitive) of Lissamine was observed, indicating the steric blockage effect of bulky chromophore.

4. Molecular modeling of chromophore-linked FPs in AChE verified that bulky chromophores were positioned outside the gorge entrance and small chromophores were seated within the gorge. The blockage of the gorge entrance by big chromophores in docking observations verified their kinetic inhibition activity.

5. A new synthetic route for preparation of the phosphonothiolate analogs of chromophore-OPs was proposed and the synthesized chromophore-linked phosphonothiolates showed inhibitory activity on both rMAChE and EEAChE.

6. The asymmetric synthesis of the phosphonothiolate building block of chromophore-linked phosphonothiolates was accomplished by using a chiral auxiliary to form separable phosphorus diastereomers. X-ray analysis assigned the absolute configuration at phosphorus for both stereoisomers.

7. Anti-AChE potency of phosphonothiolate enantiomers demonstrated a 4-fold favoring of R_p–isomer over S_p–isomer by the recombinant human acetylcholinesterase (rHuAChE).

CHAPTER 7

EXPERIMENTAL

7.1 <u>General</u>

Commercially available reagents were purchased from Aldrich Chemical Co., Millwaukee, WI. All solvents and reagents were purified when necessary by standard literature methods. Melting points were determined on a Fisher-Johns melting point apparatus with calibration in an appropriate temperature range. Analytical thin-layer chromatography (TLC) was conducted on E. Merck aluminum-backed, 0.2 mm silica gel, TLC plates. Flash chromatography was performed with Kieselgel 60, 230-400 mesh (Merck). Elemental analyses were performed by Midwest Microlab Ltd., Indianapolis, IN. High resolution mass spectra (HRMS) were obtained by electrospray ionization (ESI) on a Micromass LCT using caffeine as a mass standard at *m/z* 195.0882.

All proton (^{1}H), carbon (^{13}C) and phosphorus (^{31}P) nuclear magnetic resonance spectra were recorded on a Varian VXR 400-NMR instrument (400 MHz, 100 MHz and 162 MHz, respectively) in deuterated chloroform ($CDCl_3$) unless specified otherwise. Pertinent proton NMR frequencies are tabulated in the following order: chemical shift (in ppm), multiplicity (s, singlet; d, doublet; t, triplet; q, quartet; m, multiplet), coupling constant (*J* in hertz) and the number of hydrogens. Proton and carbon frequencies of

134

spectra obtained are relative to chloroform (^{1}H, 7.26 ppm; ^{13}C, 77.0 ppm) as an internal standard unless specified otherwise. Phosphorus chemical shifts are relative to phosphoric acid (H_3PO_4) in $CDCl_3$ as an external standard.

      Caution: *The OP chemicals synthesized and used in this study are hazardous anticholinesterases and should be handled only by trained personnel in a well-ventilated hood. The OP chemicals described are hydrolyzed by 5N NaOH to render them inactive as phosphorylating agents.*

7.2 Synthesis
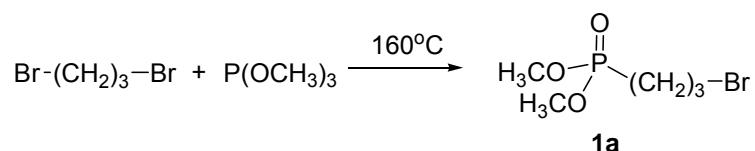
O,O-Dimethyl (3-bromopropyl) phosphonate (1a). This compound has been described previously (Maguire, 2001). Slight modifications in the reaction conditions are presented here to prevent double addition by-product. Trimethylphosphite (3.55 mL, 30 mmol) and 1,3-dibromopropane (12.2 mL, 120 mmol) were placed in a round bottom flask fitted with a reflux condenser and heated to 150 °C (external temperature) in an oil-bath for 1 h. Once cooled to rt, the excess dibromopropane was removed by distillation at 60–62 °C under reduced pressure (1 mmHg). Purification by Kugelrohr distillation at 120 °C at 0.1 mmHg gave a clear, colorless oil (3.28 g, 47%).

^{1}H NMR (CDCl$_3$): δ 1.86 (m, 2 H), 2.09 (m, 2 H), 3.42 (t, J = 6.0 Hz, 2 H), 3.69 (d, $^3J_{HP}$ = 8.2 Hz, 6 H).

^{13}C NMR (CDCl$_3$): δ 23.5 (d, $^1J_{CP}$ = 143.0 Hz), 25.9 (d, $^2J_{CP}$ = 4.8 Hz), 33.6 (d, $^3J_{CP}$ = 18.4 Hz), 52.6 (d, $^2J_{CP}$ = 6.4 Hz).

^{31}P NMR (CDCl$_3$): δ 34.2 (s).

136

Br-(CH$_2$)$_4$-Br + P(OCH$_3$)$_3$ $\xrightarrow{\text{160°C}}$ (H$_3$CO)(H$_3$CO)P(=O)(CH$_2$)$_4$-Br

1b
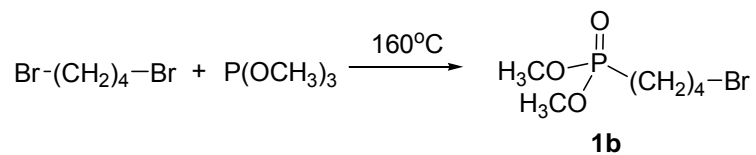
_O,O_-Dimethyl (4-bromobutyl) phosphonate (1b). This procedure is identical to that described in **1a** except that it started with 1,4-dibromobutane.

^{1}H NMR (CDCl$_3$): δ 1.57 (m, 2 H), 1.60 (m, 2 H), 1.78 (m, 2 H), 3.24 (t, J = 6.6 Hz, 2 H), 3.56 (d, $^3J_{HP}$ = 10.7 Hz, 6 H).

^{13}C NMR (CDCl$_3$): δ 20.7 (d, $^2J_{CP}$ = 6.0 Hz), 23.3 (d, $^1J_{CP}$ = 141.9 Hz), 32.4, 32.6 (d, $^3J_{CP}$ = 15.0 Hz), 51.9 (d, $^2J_{CP}$ = 7.6 Hz).

^{31}P NMR (CDCl$_3$): δ 34.8 (s).

(A)

(B)

(C)

Figure 7.1. (A) ^{1}H, (B) ^{13}C and (C) ^{31}P NMR spectra of *O,O*-dimethyl (4-bromobutyl) phosphonate (**1b).**
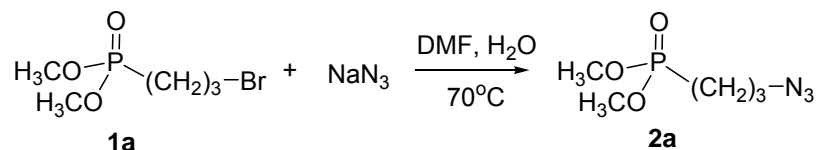
_O,O_-Dimethyl (3-azopropyl) phosphonate (2a). A reaction mixture of compound **1a** (2.00 g, 8.67 mmol) and sodium azide (1.13 g, 17.00 mmol) in a 10:1 mixture of acetonitrile-water (15 mL) was heated at 70 °C for 12 h. After cooling to rt, ethyl acetate was added and the organic layer was washed with water, collected and dried over anhydrous $MgSO_4$. Evaporation under reduced pressure gave 1.20 g (72%) of the title compound as light yellow oil.

^{1}H NMR ($CDCl_3$): δ 1.77 (m, 2 H), 1.86 (m, 2 H), 3.36 (t, J = 4.3 Hz, 2 H), 3.73 (d, $^3J_{HP}$ = 11.0 Hz, 6 H).

^{13}C NMR ($CDCl_3$): δ 21.3 (d, $^1J_{CP}$ = 142.9 Hz), 22.6 (d, $^2J_{CP}$ = 4.1 Hz), 51.6 (d, $^3J_{CP}$ = 16.4 Hz), 52.6 (d, $^2J_{CP}$ = 6.8 Hz).

^{31}P NMR ($CDCl_3$): δ 34.5 (s).

MS (ESI-TOF): Calcd for $C_5H_{12}N_3O_3P$ (M+H) 194.0695; found 194.0615.

IR (NaCl, $CHCl_3$): ν 3464, 2954, 2852, 2099, 1459, 1248, 1031, 818 cm^{-1}.

(A)

(B)

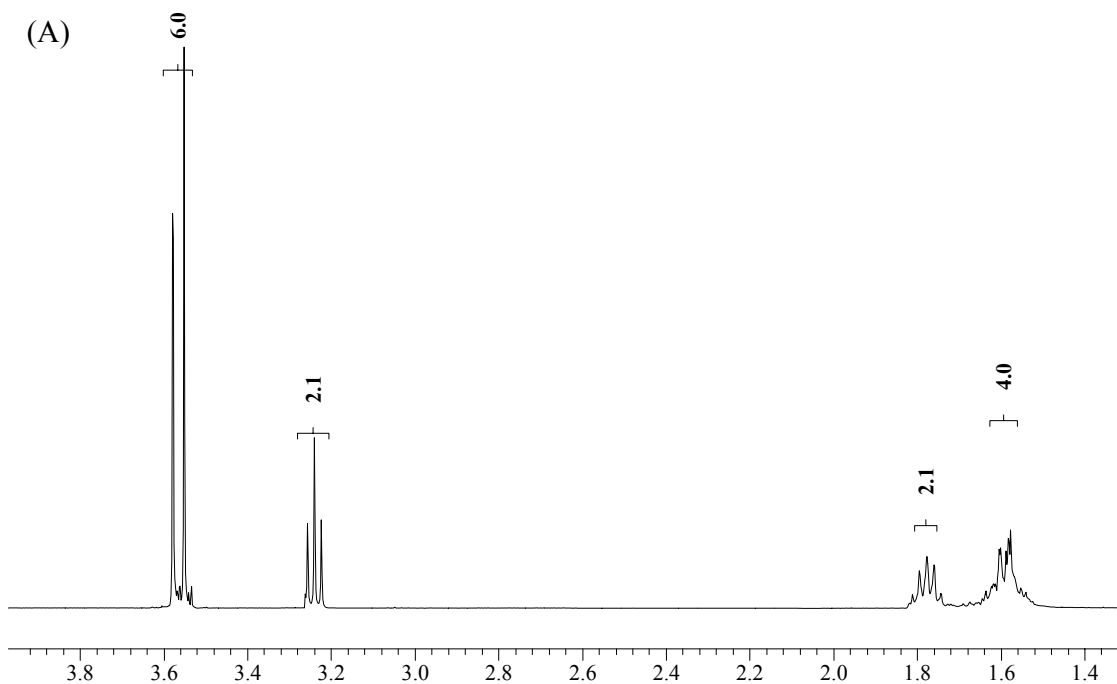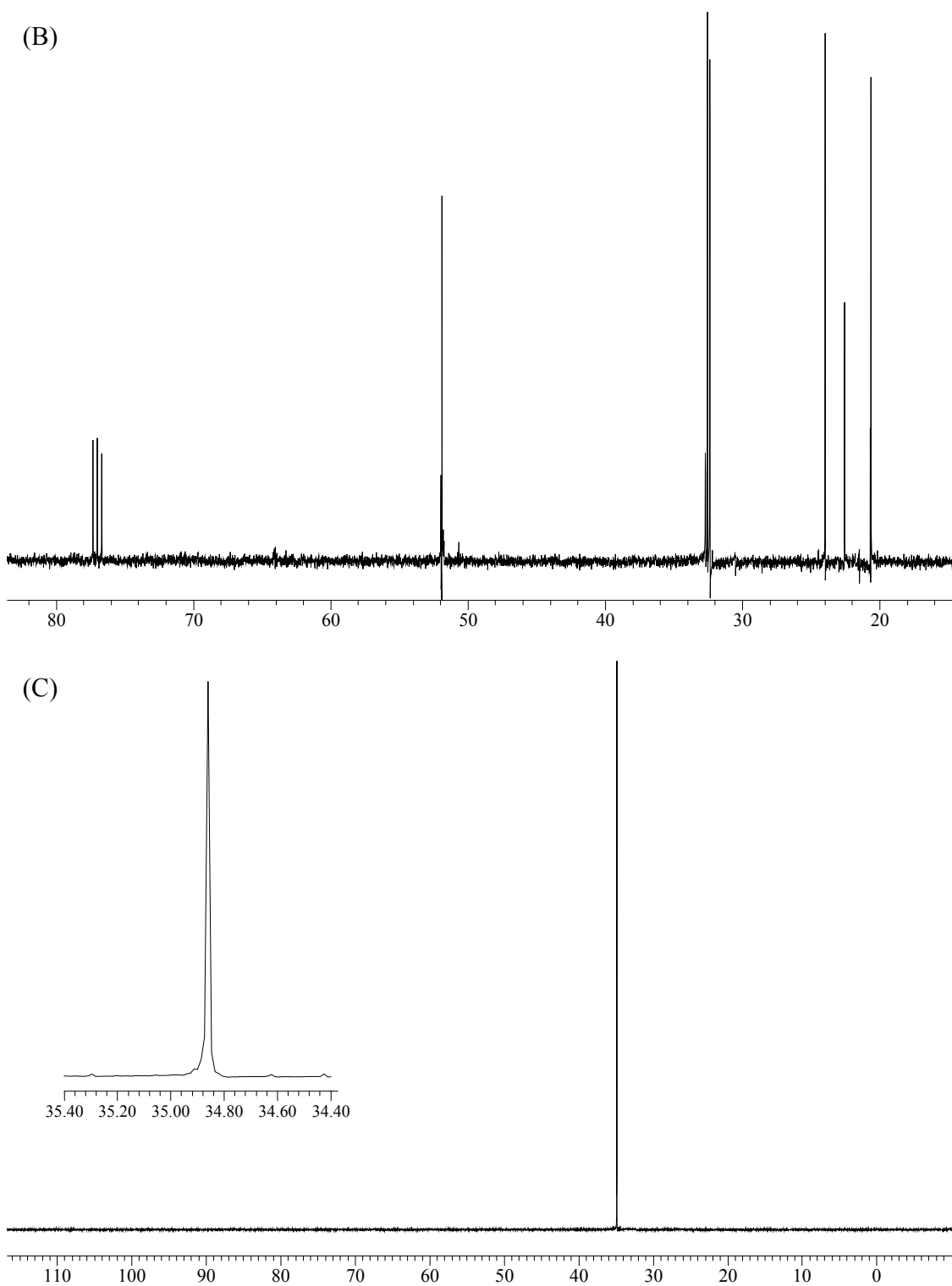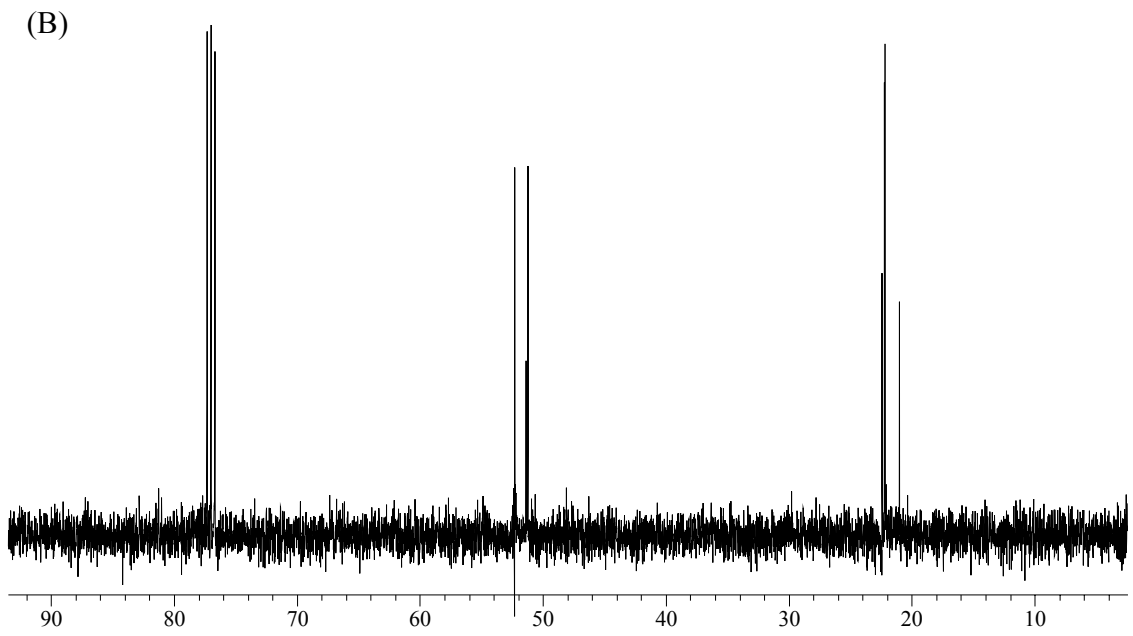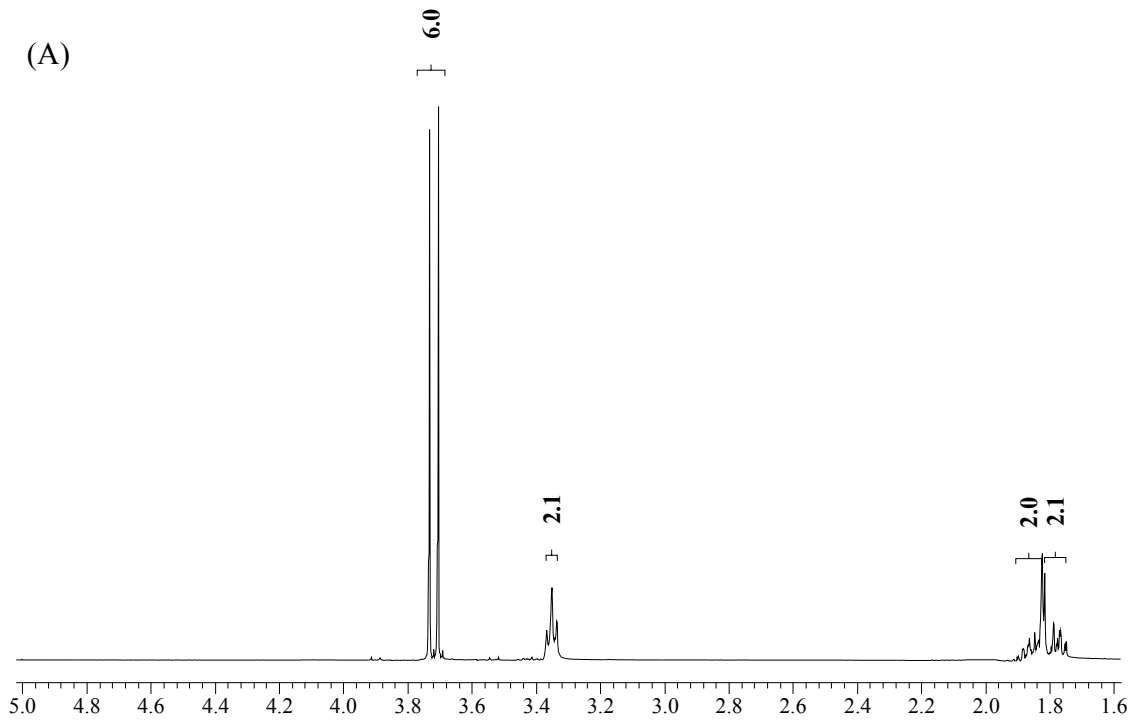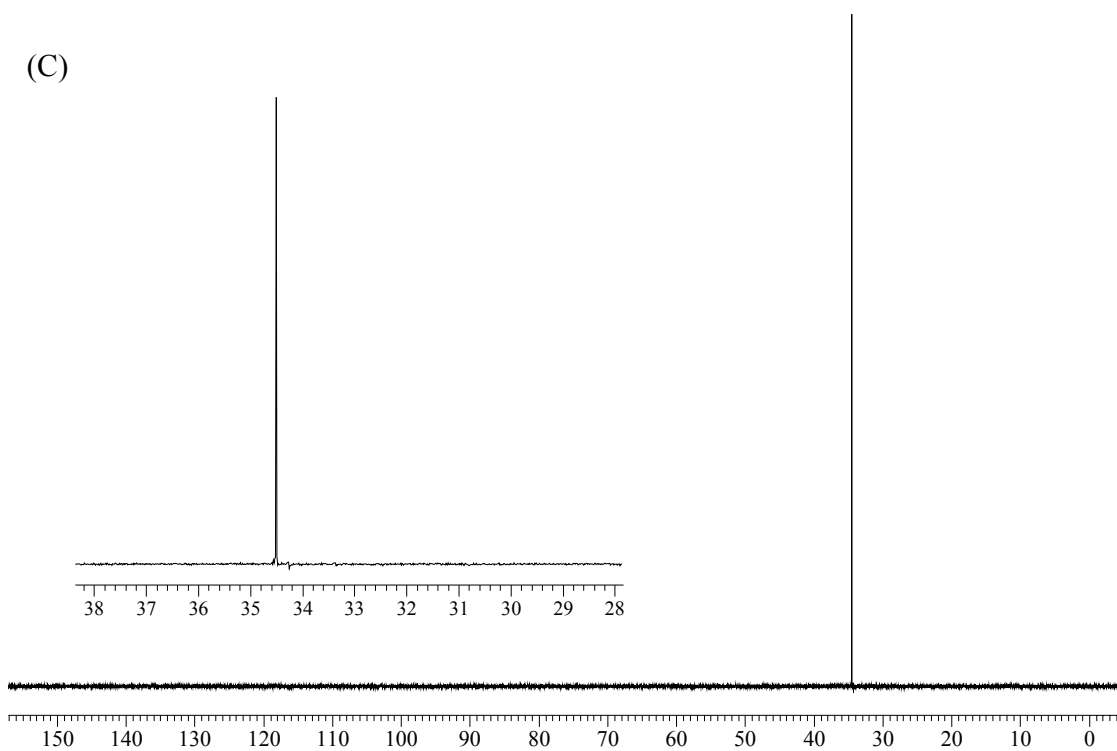**Figure 7.2.** (A) ^{1}H, (B) ^{13}C and (C) ^{31}P NMR spectra of *O,O*-dimethyl (3-azopropyl) phosphonate (**2a**).
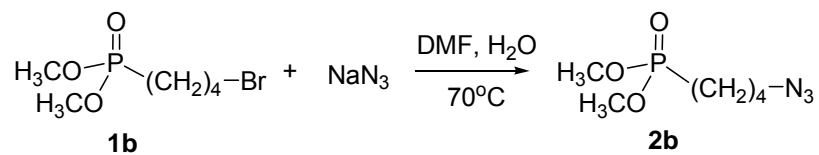
O,O-Dimethyl (4-azobutyl) phosphonate (2b). This procedure is identical to that described in **2a** except that it started with *O,O*-dimethyl (4-bromobutyl) phosphonate **1b**.

^{1}H NMR (CDCl$_3$): δ 1.66(m, 4 H), 1.77 (m, 2 H), 3.28 (t, *J* = 6.5 Hz, 2 H), 3.72 (d, $^3J_{HP}$ = 11.0 Hz, 6 H).

^{13}C NMR (CDCl$_3$): δ 19.5 (d, $^2J_{CP}$ = 6.1 Hz), 23.8 (d, $^1J_{CP}$ = 141.9 Hz), 29.2 (d, $^3J_{CP}$ = 16.2 Hz), 50.5, 52.1 (d, $^2J_{CP}$ = 7.6 Hz).

^{31}P NMR (CDCl$_3$): δ 34.6 (s).

(A)

(B)

143

(C)

35.00 34.80 34.60 34.40 34.20 34.00

130   120   110   100   90   80   70   60   50   40   30   20   10   0
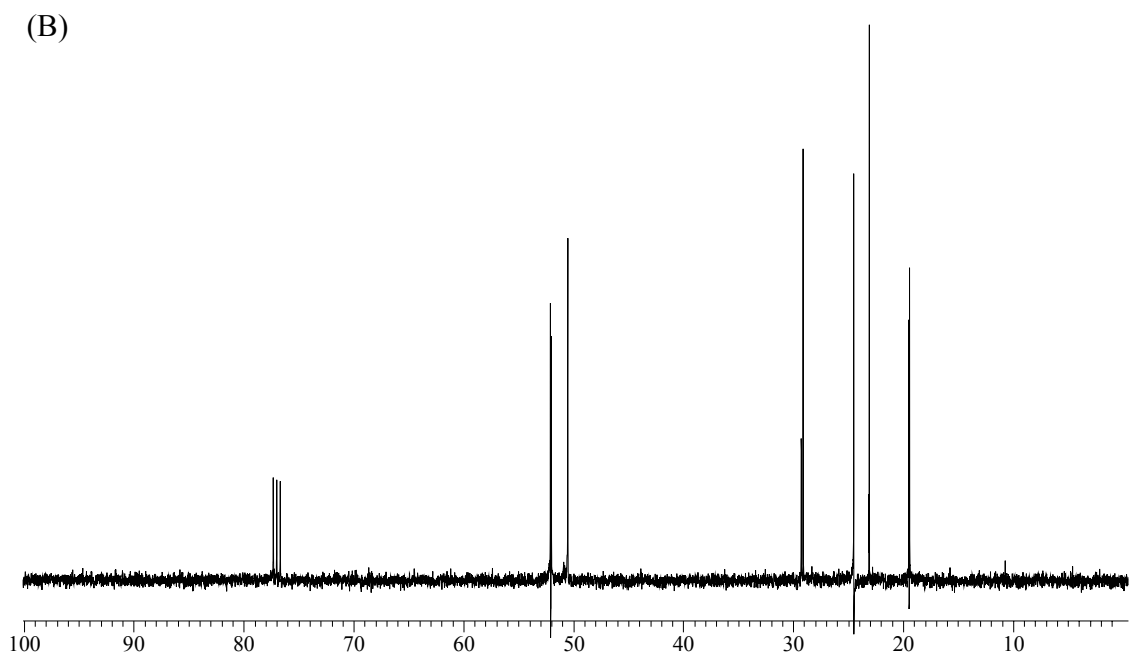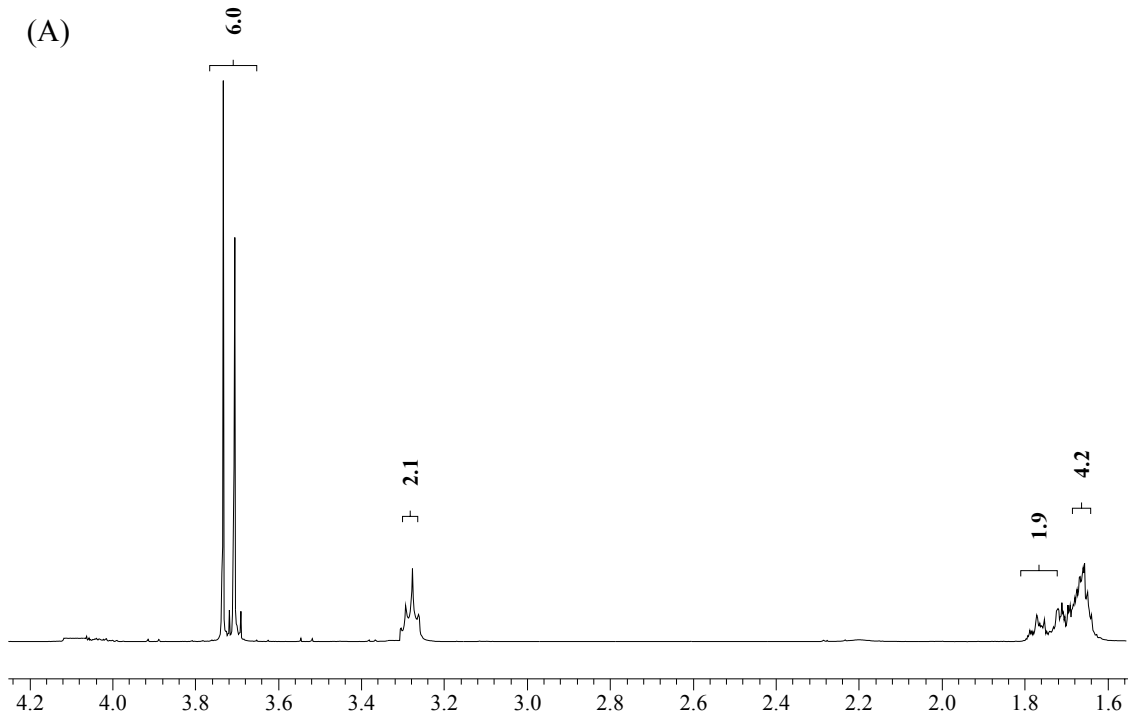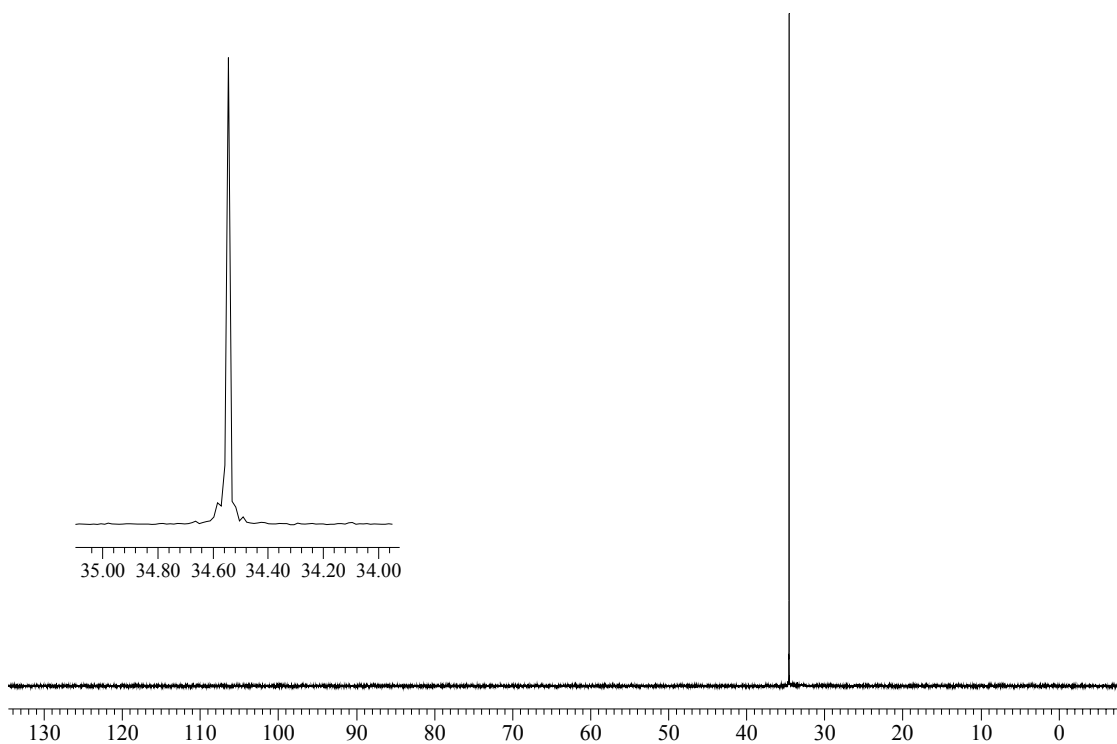
Figure 7.3. (A) ^{1}H, (B) ^{13}C and (C) ^{31}P NMR spectra of *O,O*-dimethyl (4-azobutyl) phosphonate (**2b**).

144
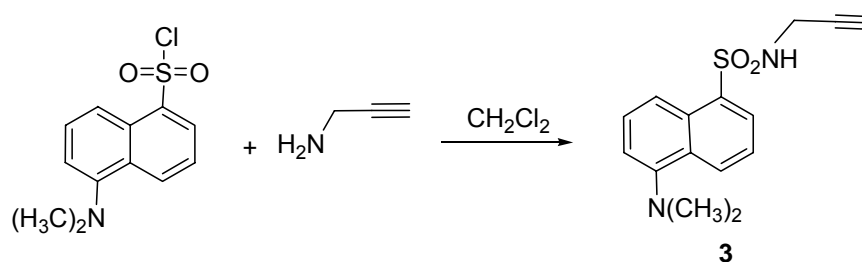
5-(Dimethylamino)-*N*-(2-propynyl)-1-naphthalenesulfonamide (3) (Bolletta, 1996). To a solution of 5-(dimethylamino)naphthalene-1-sulfonyl chloride (1.00 g, 3.70 mmol) in anhydrous dichloromethane (CH_2Cl_2, 10 mL) were added triethylamine (0.55 mL, 4.00 mmol) and propargylamine (0.28 mL, 4.00 mmol). The solution immediately turned from bright yellow to fluorescent. After quenching with 0.1 M phosphate buffer (pH 7.0, 20 mL) and extraction with CH_2Cl_2 (25 mL), the organic layer was collected and dried over anhydrous $MgSO_4$. Further purification by flash chromatography using silica (5:95 methanol-chloroform) gave a yellow solid (0.95 g, 89%) of pure compound **3**.

^{1}H NMR (CDCl$_3$): δ 1.90 (t, *J* = 2.5 Hz, 1 H), 2.88 (s, 6 H), 3.76 (dd, *J* = 6.0, 2.5 Hz, 2 H), 4.81 (t, *J* = 6.0 Hz, 1 H), 7.19 (d, *J* = 7.8 Hz, 1 H), 7.55 (q, *J* = 7.8 Hz, 2 H), 8.25 (t, *J* = 7.8 Hz, 2 H), 8.55 (d, *J* = 7.8 Hz, 1 H).

^{13}C NMR (CDCl$_3$): δ 158.0, 152.2, 134.5, 131.0, 130.1, 130.0, 128.8, 123.4, 118.8, 115.4, 78.1, 72.9, 45.6, 33.2.
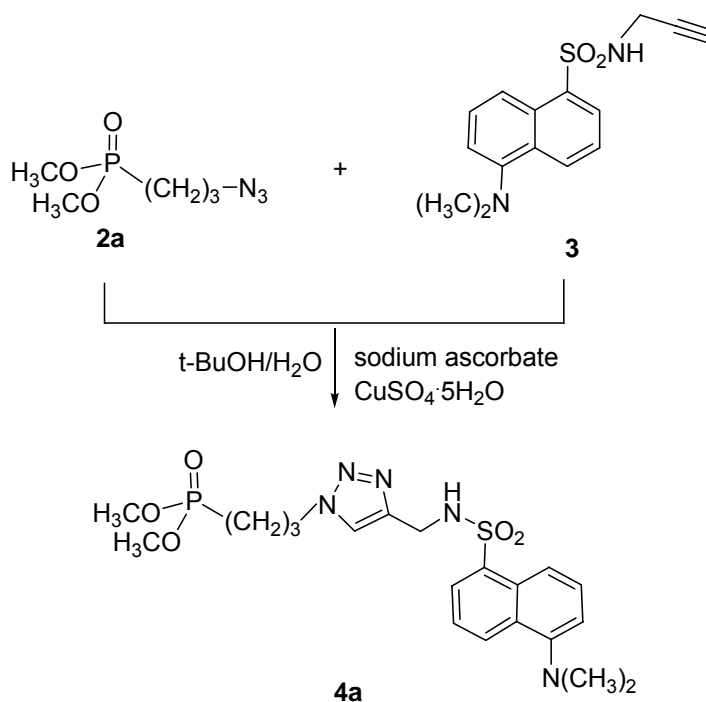
Dansyl-linked phosphonate (4a). Dimethyl (3-azopropyl) phosphonate (**2a**) (0.33 g, 1.70 mmol) and dansyl sulfonamide **3** (0.49 g, 1.70 mmol) were suspended in a 1:1 mixture of water and *tert*-butyl alcohol (8 mL). Sodium ascorbate solution (0.17 mmol; 0.17 mL of freshly prepared 1 M solution in water) was added, followed by copper (II) sulfate pentahydrate solution (7.50 mg, 0.10 mmol, in 0.20 mL of water). The heterogeneous mixture was stirred vigorously overnight, at which point it cleared and TLC analysis indicated complete consumption of the reactants. Ethyl acetate (30 mL) was added and washed with water twice. The organic layer was collected and dried over anhydrous $MgSO_4$. Evaporation under reduced pressure and purification by flash chromatography using silica (5:95 methanol-chloroform) gave 0.63 g (78%) of pure product as a yellow powder.

^{1}H NMR (CDCl$_3$): δ 1.57 (m, 2 H), 1.99 (m, 2 H), 2.77 (s, 6 H), 3.59 (d, $^{3}J_{HP}$ = 10.8 Hz, 6 H), 4.11 (dd, J = 6.9, 5.1 Hz, 2 H), 4.16 (t, J = 6.9 Hz, 2 H), 6.87 (t, J = 5.1 Hz, 1 H), 7.04 (d, J = 7.6 Hz, 1 H), 7.33 (s, 1 H), 7.39 (q, J = 7.6 Hz, 2 H), 8.14 (d, J = 7.6 Hz, 1 H), 8.22 (d, J = 9.0 Hz, 1 H), 8.41 (d, J = 7.6 Hz, 1 H).

^{13}C NMR (CDCl$_3$): δ 20.5 (d, $^{1}J_{CP}$ = 142.3 Hz), 23.1 (d, $^{2}J_{CP}$ = 4.5 Hz), 38.3, 45.1, 49.5 (d, $^{3}J_{CP}$ = 17.5 Hz), 52.2 (d, $^{2}J_{CP}$ = 6.0 Hz), 77.2, 114.9, 118.7, 122.5, 122.9, 128.5, 129.3, 130.0, 134.6, 144.0, 151.5.

^{31}P NMR (CDCl$_3$): δ 33.9 (s).

MS (ESI-TOF): Calcd for C$_{20}$H$_{29}$N$_5$O$_5$PS (M+H) 482.1627; found 482.1633; Calcd for C$_{20}$H$_{28}$N$_5$O$_5$PSNa (M+Na) 504.1446; found 504.1433.

(A)

147

(B)

(C)
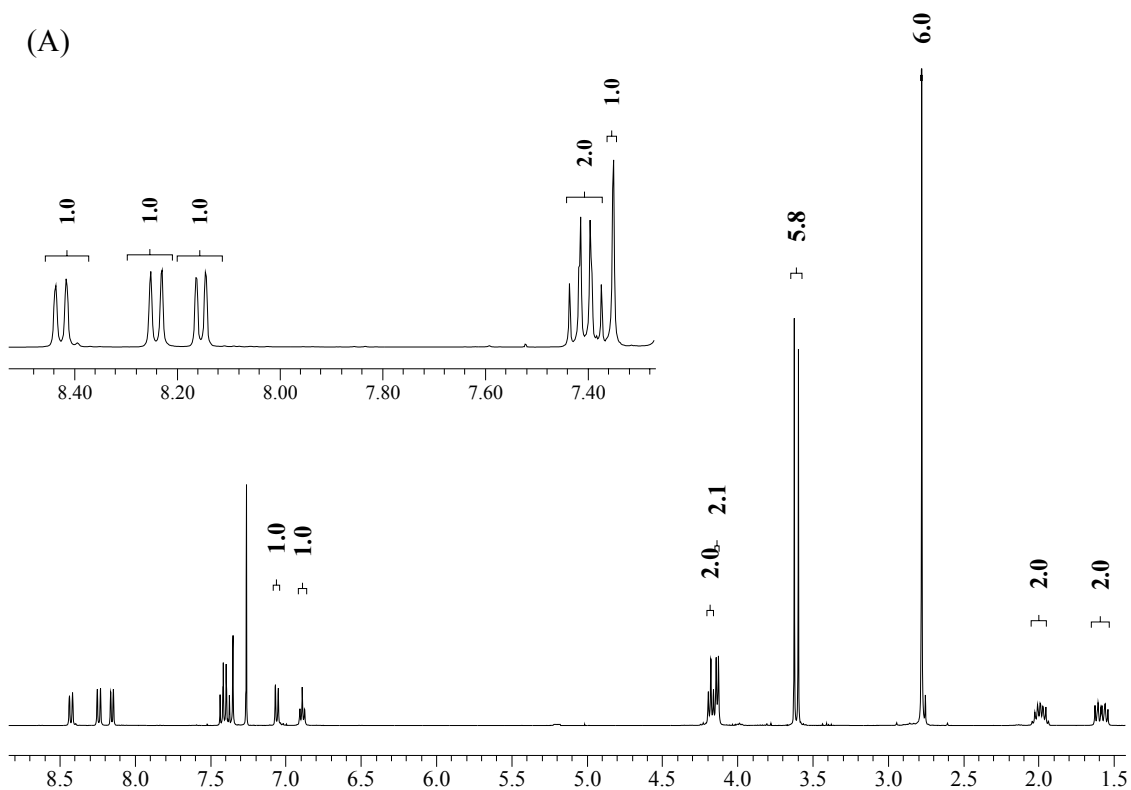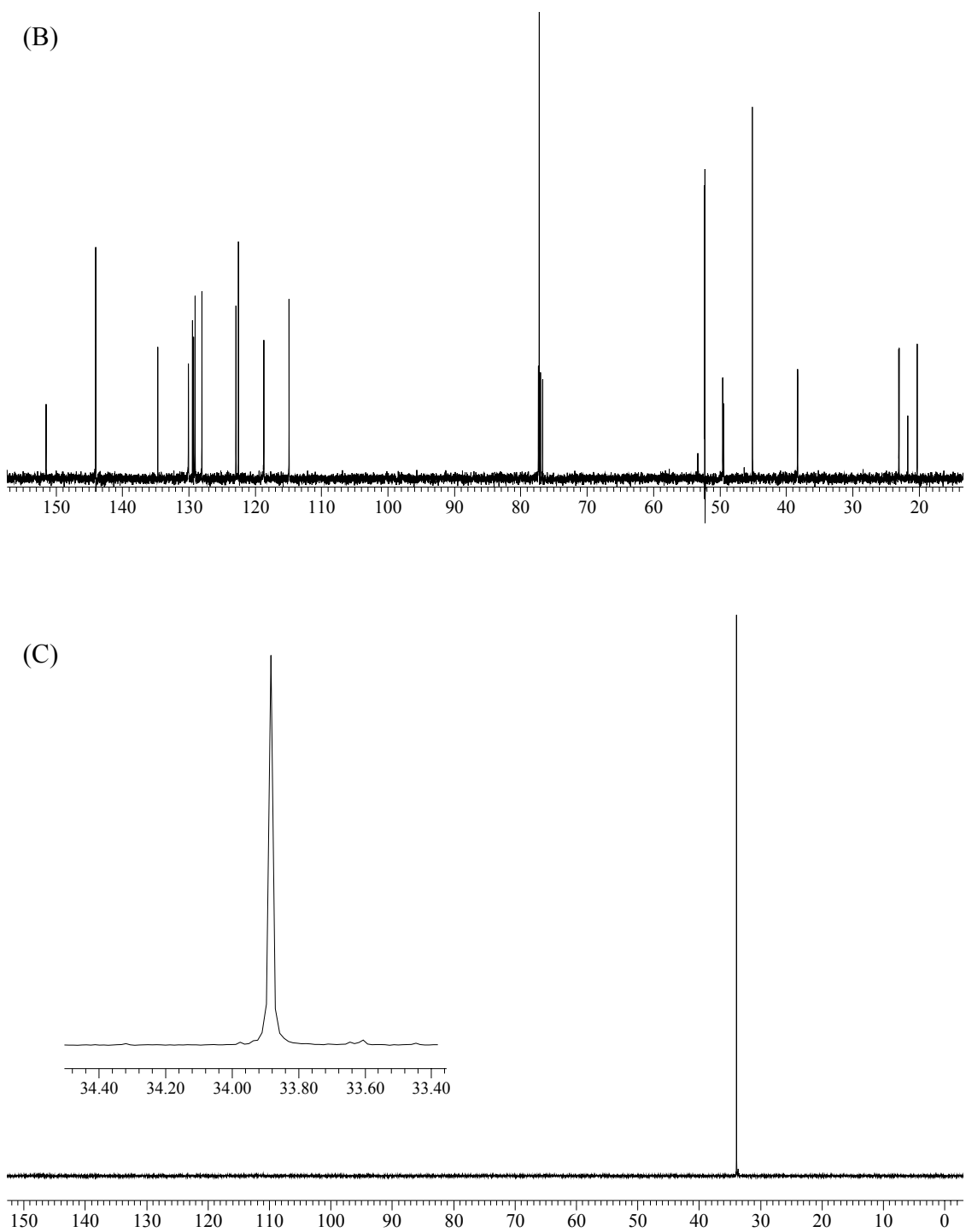
Figure 7.4. (A) ^{1}H, (B) ^{13}C and (C) ^{31}P NMR spectra of dansyl-linked phosphonate (**4a**).
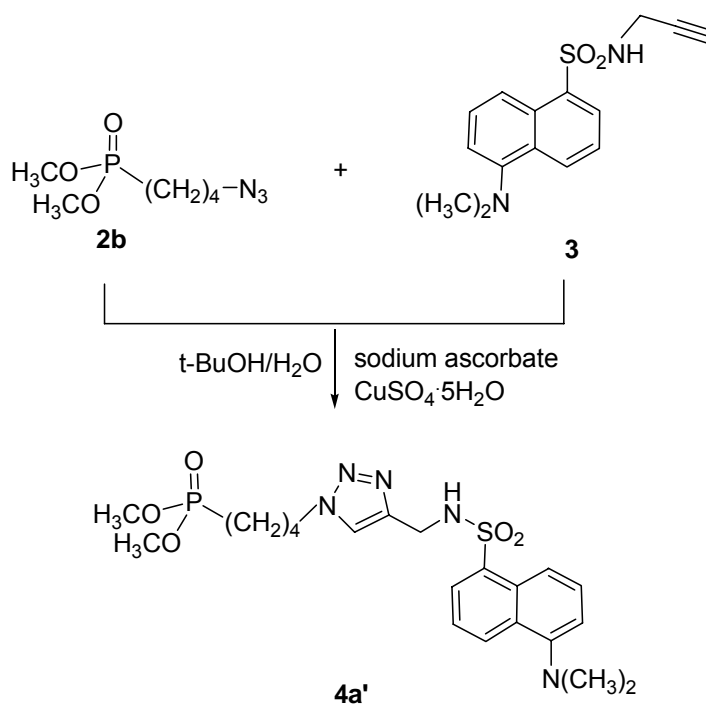
Dansyl-linked phosphonate (4a'). This procedure is identical to that described in **4a** except that it started with *O,O*-dimethyl (4-azobutyl) phosphonate **2b**.

^{1}H NMR (CDCl$_3$): δ 1.50 (m, 2 H), 1.69 (m, 2 H), 1.83 (m, 2 H), 2.84 (s, 6 H), 3.66 (d, $^3J_{HP}$ = 11.2 Hz, 6 H), 4.15 (t, J = 7.2 Hz, 2 H), 4.16 (dd, J = 6.9, 3.5 Hz, 2 H), 6.52 (t, J = 5.1 Hz, 1 H), 7.13 (d, J = 7.8 Hz, 1 H), 7.28 (s, 1 H), 7.47 (q, J = 7.3 Hz, 2 H), 8.21 (d, J = 7.3 Hz, 1 H), 8.25 (d, J = 8.8 Hz, 1 H), 8.49 (d, J = 8.1 Hz, 1 H).

^{13}C NMR (CDCl$_3$): δ 22.2 (d, $^1J_{CP}$ = 143.5 Hz), 23.6 (d, $^2J_{CP}$ = 4.5 Hz), 31.5 (d, $^3J_{CP}$ = 16.5 Hz), 38.4, 45.6, 50.0 (d, $^4J_{CP}$ = 15.1 Hz), 51.8 (d, $^2J_{CP}$ = 6.2 Hz), 76.8, 115.7, 119.8, 122.8, 123.5, 128.3, 129.3, 129.5, 130.0, 135.1, 143.9, 150.3.

^{31}P NMR (CDCl$_3$): δ 34.7 (s).

(A)

(B)
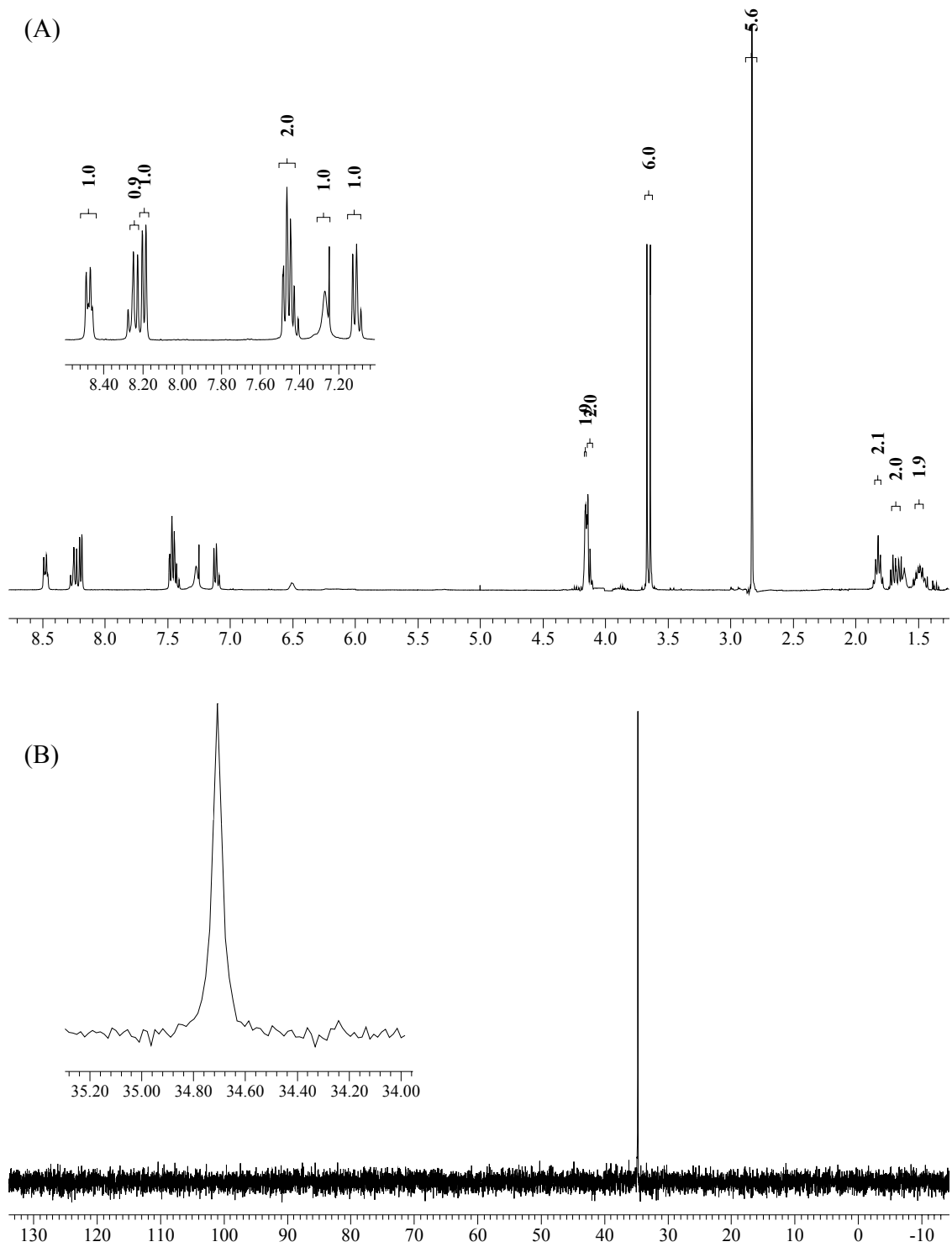
Figure 7.5. (A) ^{1}H and (B) ^{31}P NMR spectra of dansyl-linked phosphonate (**4a'**).
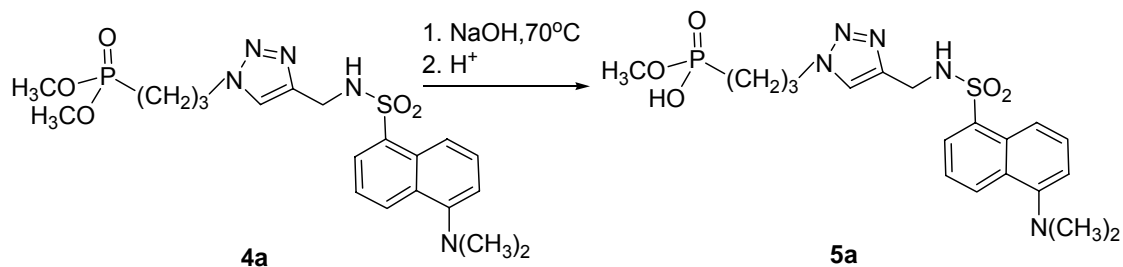
Dansyl-linked phosphonic acid (5a). Hydrolysis of dansyl-linked phosphonate **4a** was achieved by dissolving **4a** (0.52 g, 1.10 mmol) into isopropanol (20 mL) with 1 N NaOH (3 mL). The mixture was heated at 70 °C for 12 h while refluxing. After cooling to rt, the solution mixture was diluted with water (20 mL) and washed with ethyl acetate (2 x 20 mL). The aqueous part was acidified by 1 N HCl to adjust to pH 2. A mixture of chloroform and isopropanol (30 mL, 1:3) was added and the extracted product was collected and dried over anhydrous $MgSO_4$. Evaporation under reduced pressure gave 0.32 g (62%) of pure product **5a** as light yellow oil.

^{1}H NMR (CDCl$_3$): δ 1.54 (m, 2 H), 1.93 (m, 2 H), 2.89 (s, 6 H), 3.55 (d, $^3J_{HP}$ = 9.5 Hz, 3 H), 4.10 (dd, J = 6.9, 2.1 Hz, 2 H), 4.18 (t, J = 6.9 Hz, 2 H), 5.98 (t, J = 5.1 Hz, 1 H), 7.21 (d, J = 7.2 Hz, 1 H), 7.41 (s, 1 H), 7.45 (q, J = 7.6 Hz, 2 H), 8.25 (t, J = 8.1 Hz, 2 H), 8.45 (d, J = 8.1 Hz, 1 H).

^{13}C NMR (CD$_3$OD): δ 22.2 (d, $^1J_{CP}$ = 138.1 Hz), 23.0 (d, $^2J_{CP}$ = 3.3 Hz), 37.7, 45.0, 50.0 (d, $^3J_{CP}$ = 16.1 Hz), 51.0 (d, $^2J_{CP}$ = 6.1 Hz), 75.7, 116.3, 121.3, 123.1, 124.1, 127.9, 128.8, 129.1, 129.5, 136.3, 148.6.

^{31}P NMR (CDCl$_3$): δ 30.1 (s).

MS (ESI-TOF): Calcd for $C_{19}H_{27}N_5O_5PS$ (M+H) 468.1471; found 468.1499;

Calcd for $C_{19}H_{26}N_5O_5PSNa$ (M+Na) 490.1290; found 490.1394.
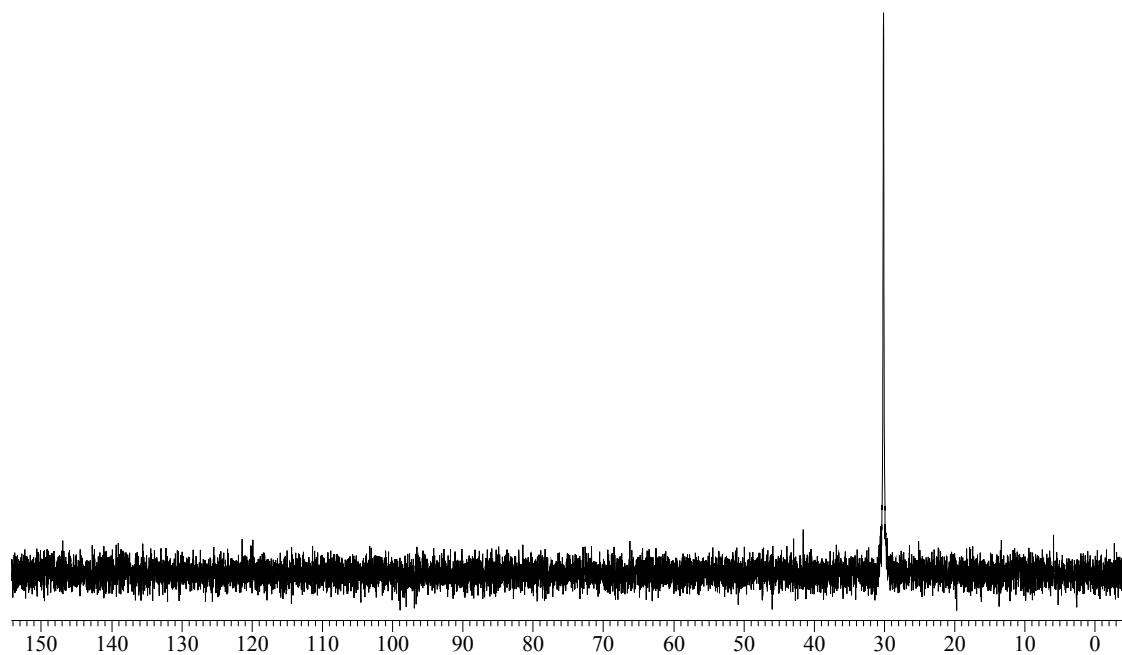
Figure 7.6. ^{31}P NMR spectrum of dansyl-linked phosphonic acid (**5a**).
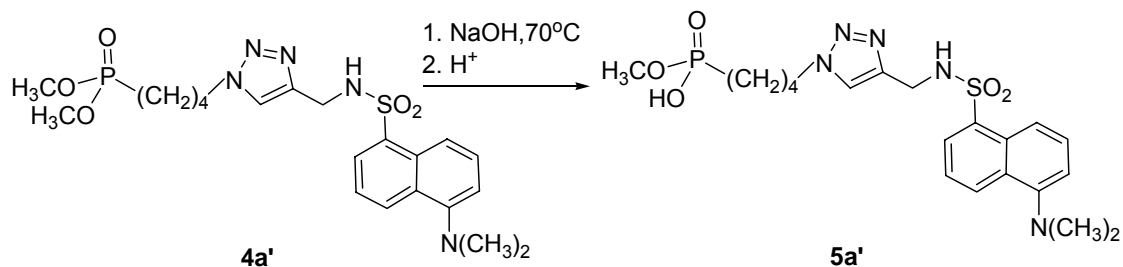
Dansyl-linked phosphonic acid (5a'). This procedure is identical to that described in **5a** except that it started with dansyl-linked phosphonate **4a'**.

^{1}H NMR (CDCl$_3$): δ 1.47 (m, 4 H), 1.85 (m, 2 H), 2.83 (s, 6 H), 3.46 (d, $^{3}J_{HP}$ = 7.2 Hz, 3 H), 4.08 (t, J = 6.9 Hz, 2 H), 4.12 (dd, J = 6.9, 2.1 Hz, 2 H), 6.55 (s, 1 H), 7.03 (d, J = 7.4 Hz, 1 H), 7.21 (s, 1 H), 7.46 (q, J = 7.6 Hz, 2 H), 8.06 (d, J = 7.3 Hz, 1 H), 8.21 (d, J = 8.5 Hz, 1 H), 8.39 (d, J = 9.0 Hz, 1 H).

^{13}C NMR (CD$_3$OD): δ 22.5 (d, $^{1}J_{CP}$ = 141.1 Hz), 23.7 (d, $^{2}J_{CP}$ = 3.3 Hz), 29.2, 38.6, 45.8, 50.0 (d, $^{3}J_{CP}$ = 15.2 Hz), 52.0 (d, $^{2}J_{CP}$ = 6.1 Hz), 75.7, 115.9, 120.1, 123.8, 128.6, 129.5, 129.7(2), 129.8, 130.3, 135.4, 144.2.

^{31}P NMR (CDCl$_3$): δ 32.2 (s).
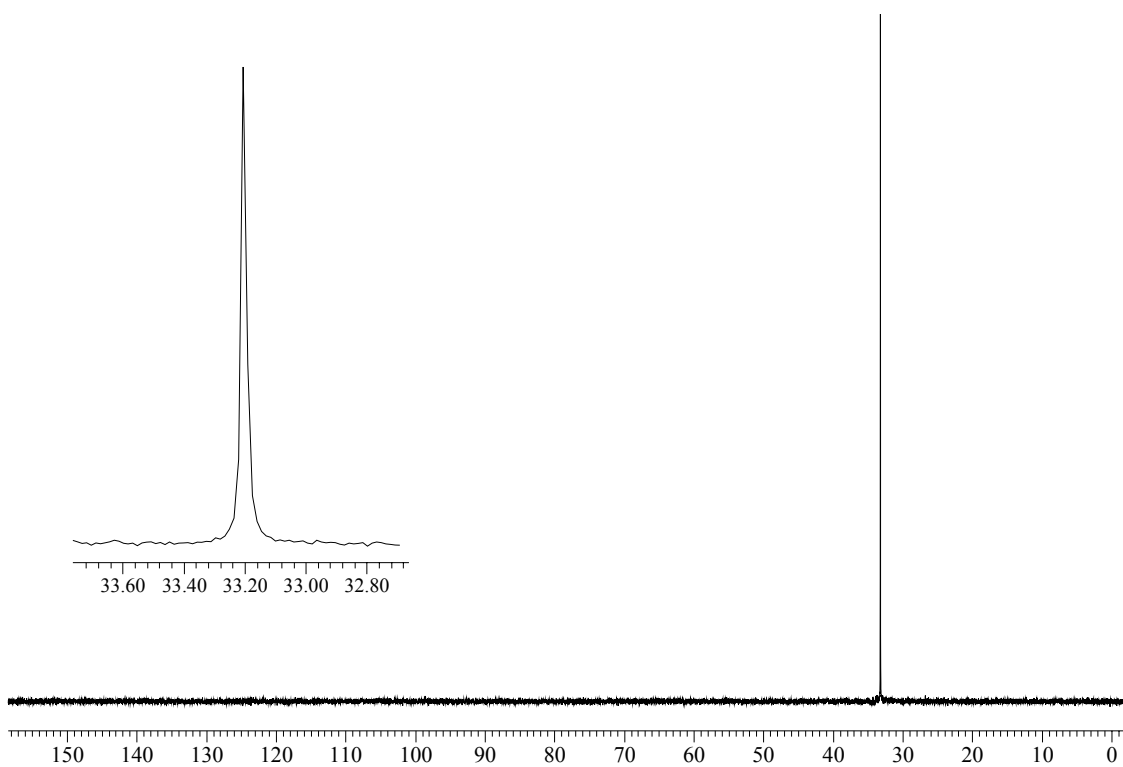
Figure 7.7. ^{31}P NMR spectrum of dansyl-linked phosphonic acid (**5a'**).
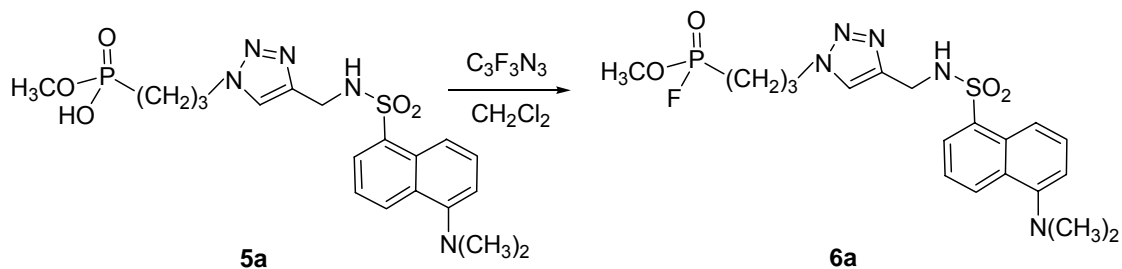
Dansyl-linked fluorophosphonate (6a). To a solution of compound **5a** (0.060 g, 0.13 mmol) in CH$_2$Cl$_2$ (5 mL) was added cyanuric fluoride (0.018 g, 0.13 mmol). The reaction mixture was stirred at rt for 0.5 h until ^{31}P NMR showed a complete conversion from P-OH to P-F. After evaporation under vacuum, compound **6a** (0.060 g, 0.13 mmol) was isolated as a yellow solid.

^{1}H NMR (CDCl$_3$): δ 1.69 (m, 2 H), 1.87 (m, 2 H), 2.87 (s, 6 H), 3.78 (d, $^3J_{HP}$ = 9.0 Hz, 3 H), 4.21 (dd, J = 4.9, 2.1 Hz, 2 H), 4.27 (t, J = 6.6 Hz, 2 H), 5.78 (t, J = 5.1 Hz, 1 H), 7.24 (d, J = 8.1 Hz, 1 H), 7.34 (s, 1 H), 7.55 (q, J = 8.0 Hz, 2 H), 8.38 (t, J = 8.2 Hz, 2 H), 8.45 (d, J = 8.1 Hz, 1 H).

^{31}P NMR (CDCl$_3$) δ 31.6 (d, J = 1072 Hz).
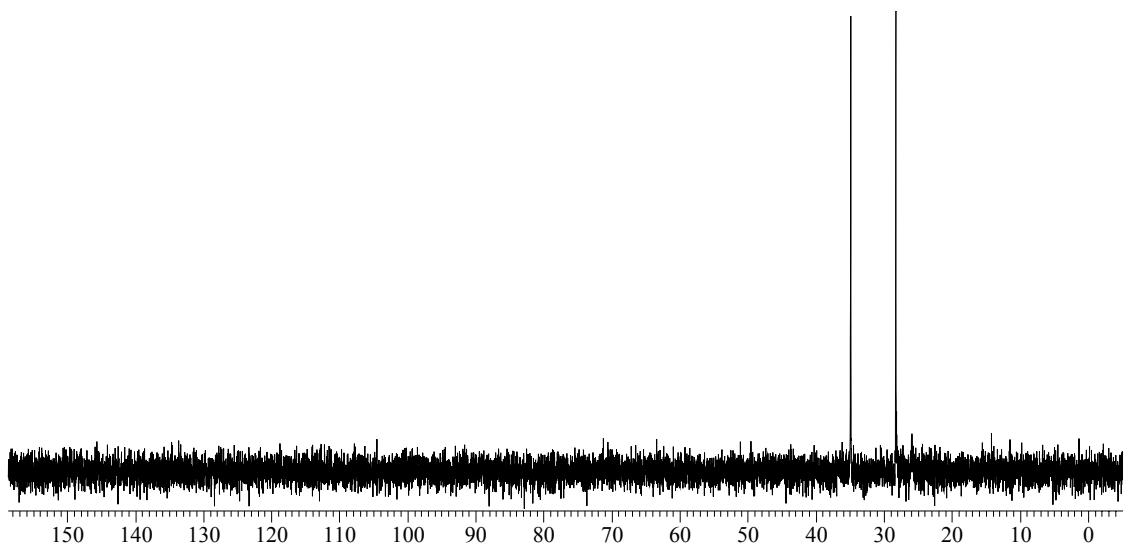
Figure 7.8. ^{31}P NMR spectrum of dansyl-linked fluorophosphonate (**6a**).

5a'   **6a'**
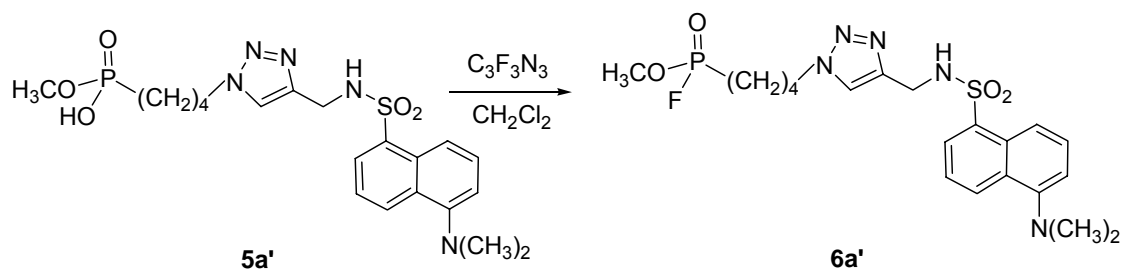
Dansyl-linked fluorophosphonate (6a'). This procedure is identical to that described in **6a** except that it started with dansyl-linked phosphonic acid **5a'**.

^{1}H NMR (CDCl$_3$): δ 1.65 (m, 4 H), 2.00 (m, 2 H), 2.90 (s, 6 H), 3.67 (d, $^3J_{HP}$ = 8.2 Hz, 3 H), 4.23 (dd, J = 6.9, 2.1 Hz, 2 H), 4.25 (t, J = 6.9 Hz, 2 H), 6.55 (s, 1 H), 7.20 (d, J = 7.4 Hz, 1 H), 7.37 (s, 1 H), 7.48 (q, J = 7.6 Hz, 2 H), 8.23 (d, J = 7.3 Hz, 1 H), 8.31 (d, J = 8.5 Hz, 1 H), 8.50 (d, J = 9.0 Hz, 1 H).

^{31}P NMR (CDCl$_3$) δ 32.2 (d, J = 1070 Hz).

2a   **7a**
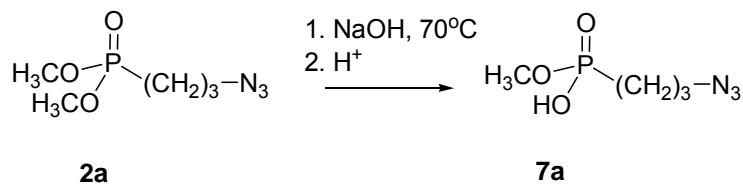
O-Methyl (3-azopropyl) phosphonic acid (7a). Hydrolysis of *O,O*-dimethyl (3-azopropyl) phosphonate **2a** was accomplished by dissolving **2a** (0.33 g, 1.71 mmol) into isopropanol (10 mL), followed by adding 1 N NaOH solution (3 mL). The mixture was heated at 70 °C for 12 h while refluxing until ^{31}P NMR showed a complete conversion (PONa, $\delta = 27.7$ ppm). After cooling to rt, the solution mixture was diluted by water (15 mL) and washed with ethyl acetate (2 x 15 mL). The aqueous part was acidified by 1 N HCl to adjust to pH 1. A mixture of chloroform and isopropanol (15 mL, 1:3) was added and the extracted product was collected and dried over anhydrous $MgSO_4$. Evaporation under reduced pressure gave 0.23 g (75%) of pure product **7a** as light yellow oil.

^{1}H NMR (CDCl$_3$): δ 1.76 (m, 2 H), 1.83 (m, 2 H), 3.32 (t, $J = 6.6$ Hz, 2 H), 3.66 (d, $^{3}J_{HP} = 10.4$ Hz, 3 H).

^{13}C NMR (CDCl$_3$): δ 22.0 (d, $^{2}J_{CP} = 4.4$ Hz), 22.3 (d, $^{1}J_{CP} = 144.9$ Hz), 51.1 (d, $^{3}J_{CP} = 16.7$ Hz), 51.6 (d, $^{2}J_{CP} = 6.1$ Hz).

^{31}P NMR (CDCl$_3$): δ 33.7 (s).

MS (ESI-TOF): Calcd for $C_4H_{10}N_3O_3P$ (M+H) 180.0493; found 180.0671.

IR (NaCl, CHCl$_3$): ν 2954, 2852, 2100, 1248, 1031 cm^{-1}.

(A)

3.0

1.9

4.0

7.5 7.0 6.5 6.0 5.5 5.0 4.5 4.0 3.5 3.0 2.5 2.0 1.5 1.0 0.5

(B)

100 90 80 70 60 50 40 30 20 10

159

(C)

| 60 | 50 | 40 | 30 | 20 | 10 |
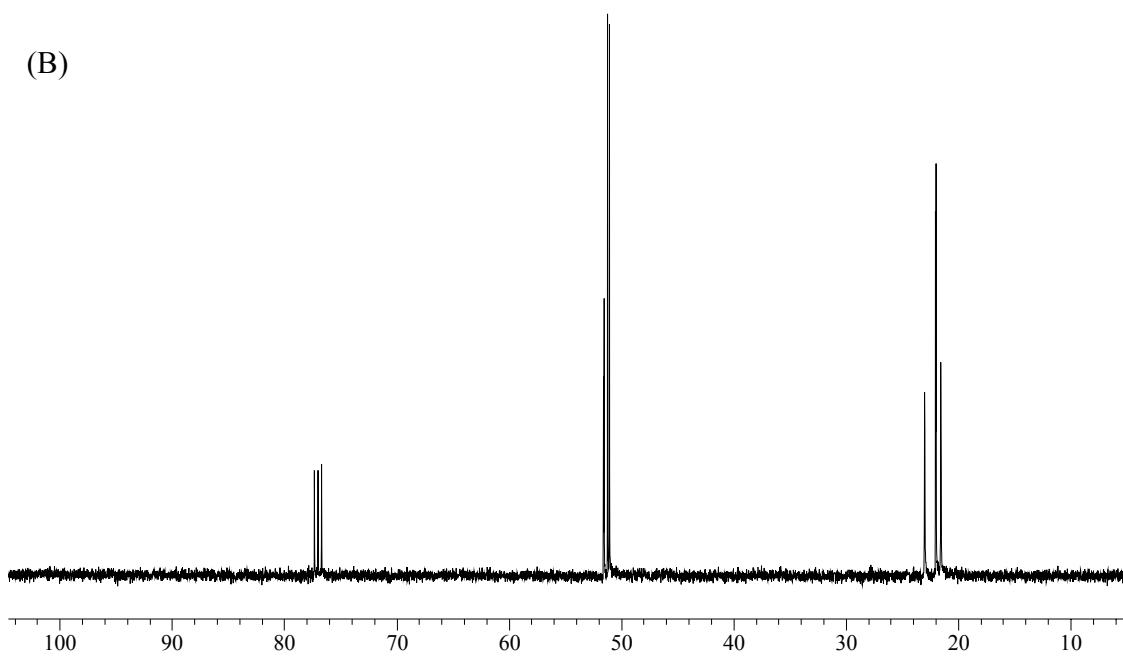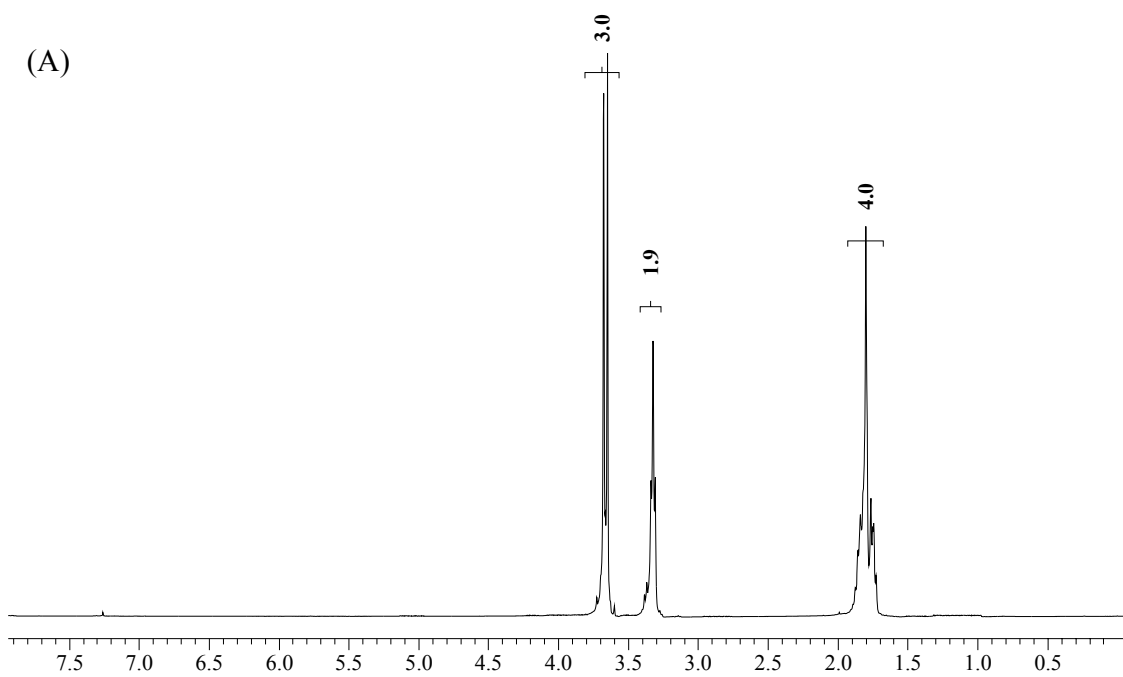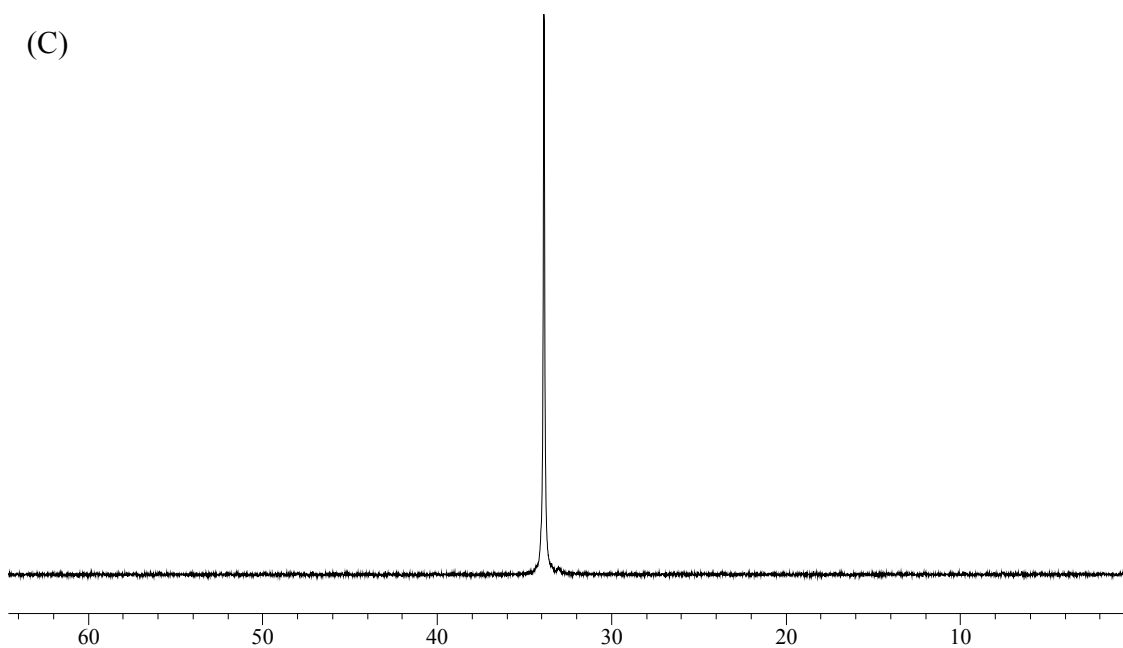
Figure 7.9. (A) ^{1}H, (B) ^{13}C and (C) ^{31}P NMR spectra of *O*-methyl (3-azopropyl) phosphonic acid (**7a**).

2b → **7b**

1. NaOH, 70°C
2. H⁺
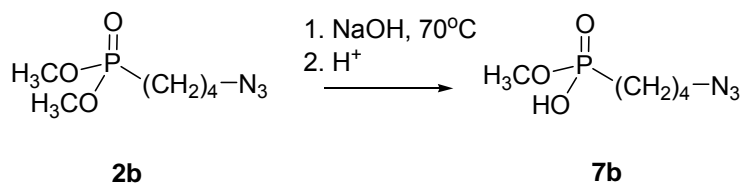
O-Methyl (4-azobutyl) phosphonic acid (7b). This procedure is identical to that described in **7a** except that it started with O,O-dimethyl (4-azobutyl) phosphonate **2b**.

^{1}H NMR (CDCl$_3$): δ 1.64 (m, 4 H), 1.76 (m, 2 H), 3.25 (t, J = 6.7 Hz, 2 H), 3.67 (d, $^3J_{HP}$ = 11.1 Hz, 3 H).

^{13}C NMR (CDCl$_3$): δ 19.5 (d, $^2J_{CP}$ = 6.2 Hz), 23.8 (d, $^1J_{CP}$ = 141.9 Hz), 29.3 (d, $^3J_{CP}$ = 16.9 Hz), 51.1, 51.4 (d, $^2J_{CP}$ = 7.7 Hz).

^{31}P NMR (CDCl$_3$): δ 33.7 (s).

(A)

(B)

(C)
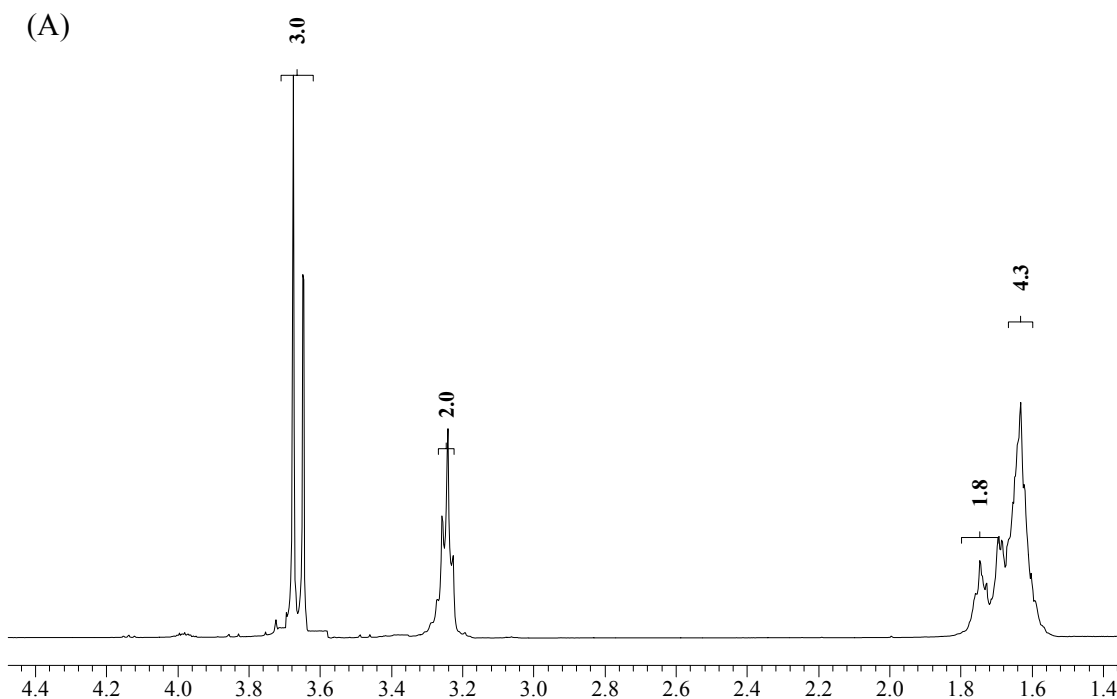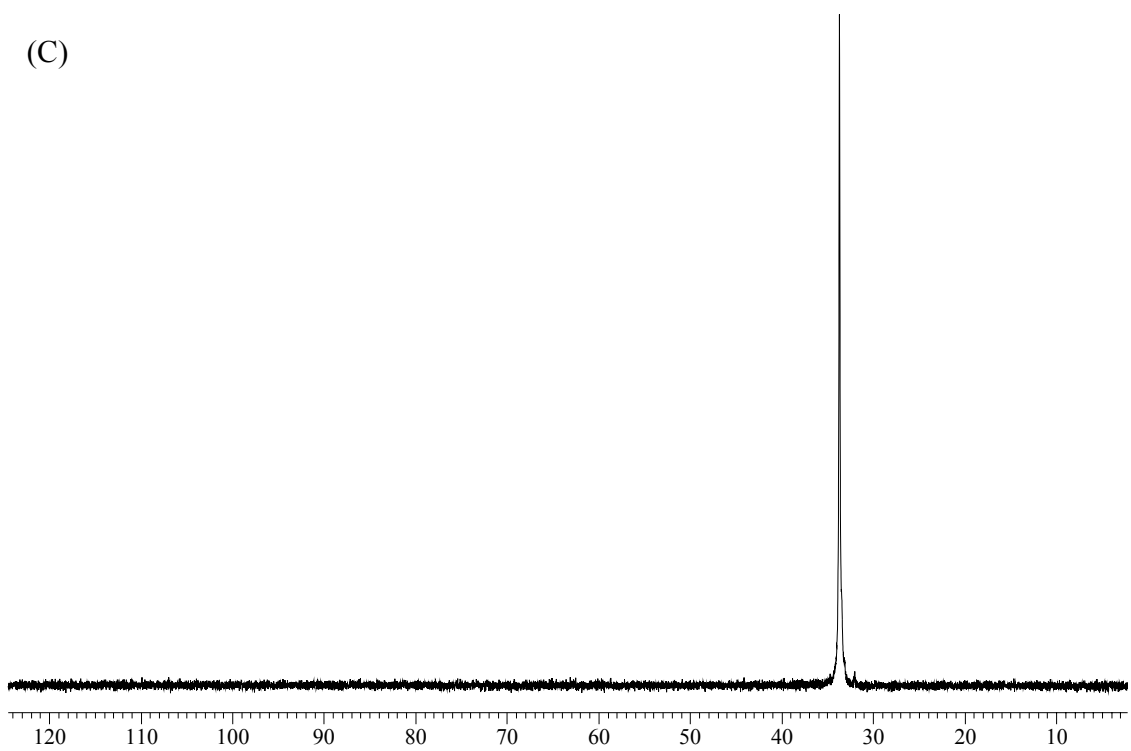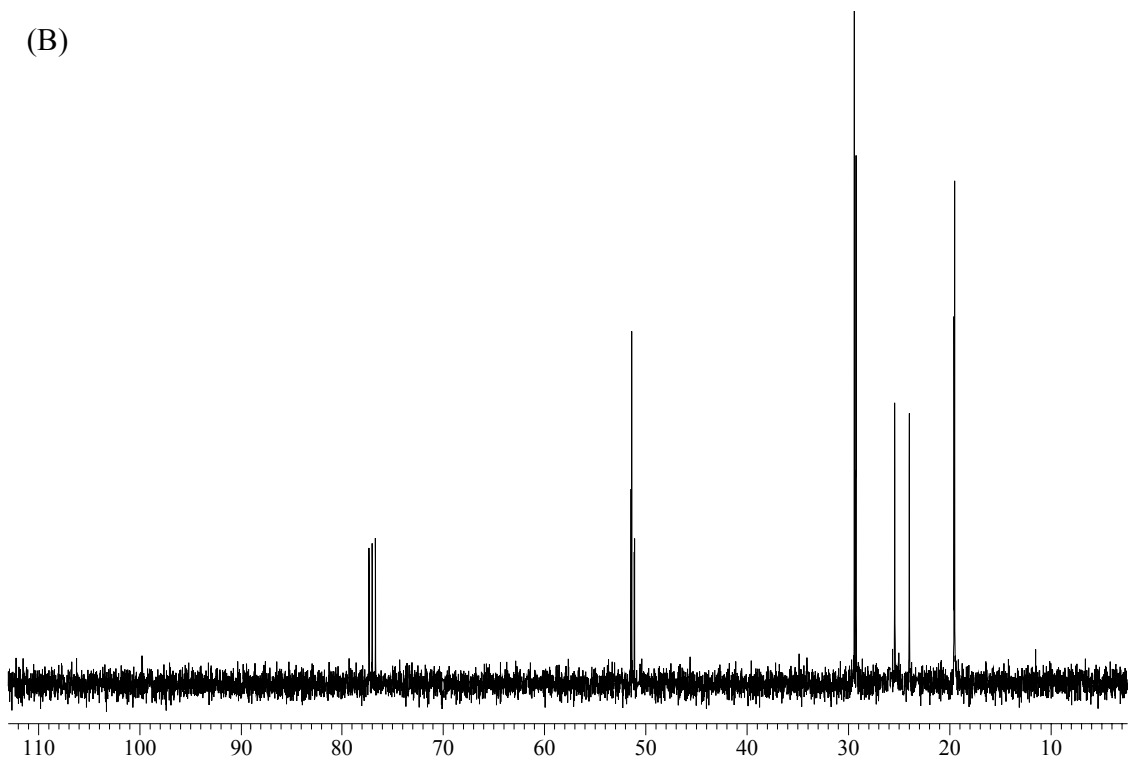
Figure 7.10. (A) ^{1}H, (B) ^{13}C and (C) ^{31}P NMR spectra of *O*-methyl (4-azobutyl) phosphonic acid (**7b**).

7a   **8a**
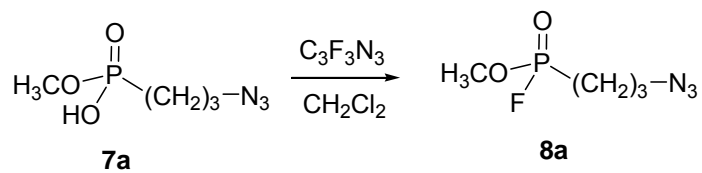
_O_-Methyl (3-azopropyl) fluorophosphonate (8a). To a solution of compound

7a (0.060 g, 0.34 mmol) in dichloromethane (5 mL), cyanuric fluoride (0.050 g, 0.34

mmol) was added. The reaction mixture was stirred at rt for 0.5 h until ^{31}P NMR showed

a complete conversion from P-OH to P-F. After evaporation under vacuum, compound

6a (0.060 g, 0.33 mmol) was isolated as a yellow oil.

^{1}H NMR (CDCl$_3$): δ 1.88 (m, 2 H), 1.95 (m, 2 H), 3.41 (t, J = 6.4 Hz, 2 H), 3.86

(d, $^3J_{HP}$ = 11.1 Hz, 3 H).

^{13}C NMR (CDCl$_3$): δ 21.0 (d, $^1J_{CP}$ = 146.3 Hz), 21.7 (d, $^2J_{CP}$ = 4.6 Hz), 51.3 (d,

$^3J_{CP}$ = 16.4 Hz), 51.6 (d, $^2J_{CP}$ = 7.3 Hz).

^{31}P NMR (CDCl$_3$): δ 31.9 (d, J = 1071 Hz).
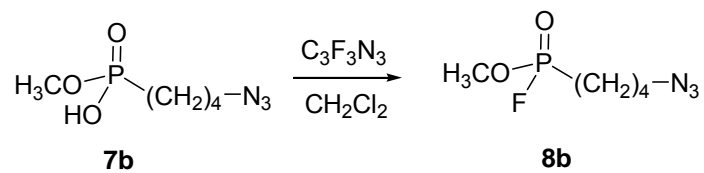
_O_-Methyl (4-azobutyl) fluorophosphonate (8b). This procedure is identical to that described in **8a** except that it started with _O_-methyl (4-azobutyl) phosphonic acid **7b**.

^{1}H NMR (CDCl$_3$): δ 1.68 (m, 4 H), 1.89 (m, 2 H), 3.30 (t, J = 6.0 Hz, 2 H), 3.82 (d, $^{3}J_{HP}$ = 10.6 Hz, 3 H).

^{13}C NMR (CDCl$_3$): δ 19.3 (d, $^{2}J_{CP}$ = 4.6 Hz), 23.2 (d, $^{1}J_{CP}$ = 144.5 Hz), 29.2 (d, $^{3}J_{CP}$ = 15.1 Hz), 50.6, 53.0 (d, $^{2}J_{CP}$ = 8.2 Hz).

^{31}P NMR (CDCl$_3$): δ 32.9 (d, J = 1074 Hz).
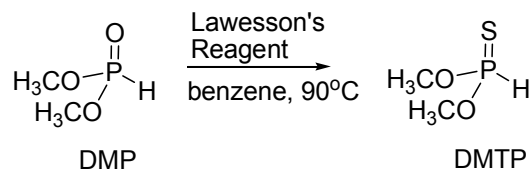
Dimethyl thiophosphonate (DMTP, 28) (Tongcharoensirikul, 2004).

Although dimethyl thiophosphonate is commercially available, it always contains dimethyl phosphonate (according to ^{31}P NMR). We synthesized and distilled it in the lab to improve purity and subsequently reactivity.

A solution of 2,4-bis(4-methoxyphenyl)-1,3-dithia-2,4-diphosphetane-2,4-disulfide (Lawesson reagent; 22.7 g, 0.056 mol) and freshly distilled dimethyl phosphonate (10 mL, 12.0 g, 0.11 mol) in benzene (80 mL) was heated at 90-100 ºC for 2 h until the reaction was complete indicated by ^{31}P NMR (from 11.5 ppm to 74.9 ppm in benzene). The reaction mixture was cooled to room temperature, and hexane (80 mL) was added to precipitate sulfur- and phosphorus-containing by-products. The reaction mixture was passed through filter paper, and the solution was concentrated to oil under reduced pressure. The product, dimethyl thiophosphonate, distilled bulb-to-bulb as a colorless liquid (8.45 g, 0.067 mol, 61%).

^{1}H NMR (CDCl$_3$): δ 3.72 (d, J = 15.0 Hz, 6 H), 7.68 (m, 1 H).

^{13}C NMR (CDCl$_3$): δ 52.7 (d, J_{CP} = 6.2 Hz).

^{31}P NMR (CDCl$_3$): δ 74.9 (s).

S
‖
H₃CO—P—H   +   Br–(CH₂)₃–Br   →(Na, CH₃OH)→   H₃CO—P(=S)—(CH₂)₃–Br
H₃CO   H₃CO

DMTP   9

$$\underset{\text{DMTP}}{\overset{\displaystyle S}{H_3CO-\overset{\|}{P}-H}} \;+\; Br-(CH_2)_3-Br \;\xrightarrow{\;Na,\;CH_3OH\;}\; \underset{\mathbf{9}}{\overset{\displaystyle S}{H_3CO-\overset{\|}{P}-(CH_2)_3-Br}}$$
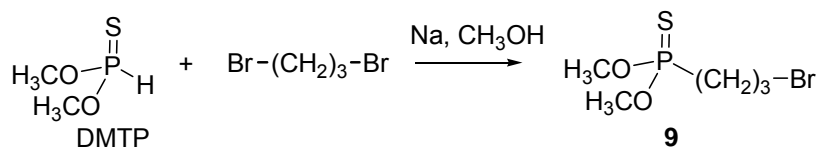
O,O-Dimethyl (3-bromopropyl) phosphonothionate (9). The synthesis of O,O-diethyl (3-chloropropyl) thiophosphonate from diethyl thiophosphonate has been reported (Reznik, 2001). By a similar way, O,O-dimethyl (3-bromopropyl) thiophosphonate can be obtained.

A solution of sodium dimethyl thiophosphonate was prepared from dimethyl thiophosphonate (1.30 g, 10.00 mmol) and sodium (0.24 g, 10.00 mmol) in anhydrous methanol (6 mL). The sodium dimethyl thiophosphonate solution was added dropwise with stirring at 30-35 ºC to a solution of 1,3-dibromopropane (3.00 mL, 24.00 mmol) in 4 mL of anhydrous methanol. The reaction mixture was refluxed for 5 h until the ^{31}P NMR showed that loss of the starting material was complete. The sodium bromide precipitate (NaBr) was filtered off, and the filtrate was concentrated under reduced pressure. The product was extracted with ethyl ether, washed with water, and dried over MgSO₄. Ethyl ether was then removed, and the residue was distilled *in vacuo* to give compound **9** as a light yellow oil (1.28 g, 5.00 mmol, 50%).

^{1}H NMR (CDCl₃): δ 2.02 (m, 4 H), 3.36 (t, J = 5.2 Hz, 2 H), 3.58 (d, J = 8.3 Hz, 6 H).

^{13}C NMR (CDCl₃): δ 26.5 (d, $^{3}J_{CP}$ = 3.1 Hz), 31.3 (d, $^{1}J_{CP}$ = 115.0 Hz), 33.6 (d, $^{2}J_{CP}$ = 19.2 Hz), 53.2 (d, $^{2}J_{CP}$ = 7.6 Hz).

^{31}P NMR (CDCl₃): δ 102.7 (s).

(A)

(B)

167
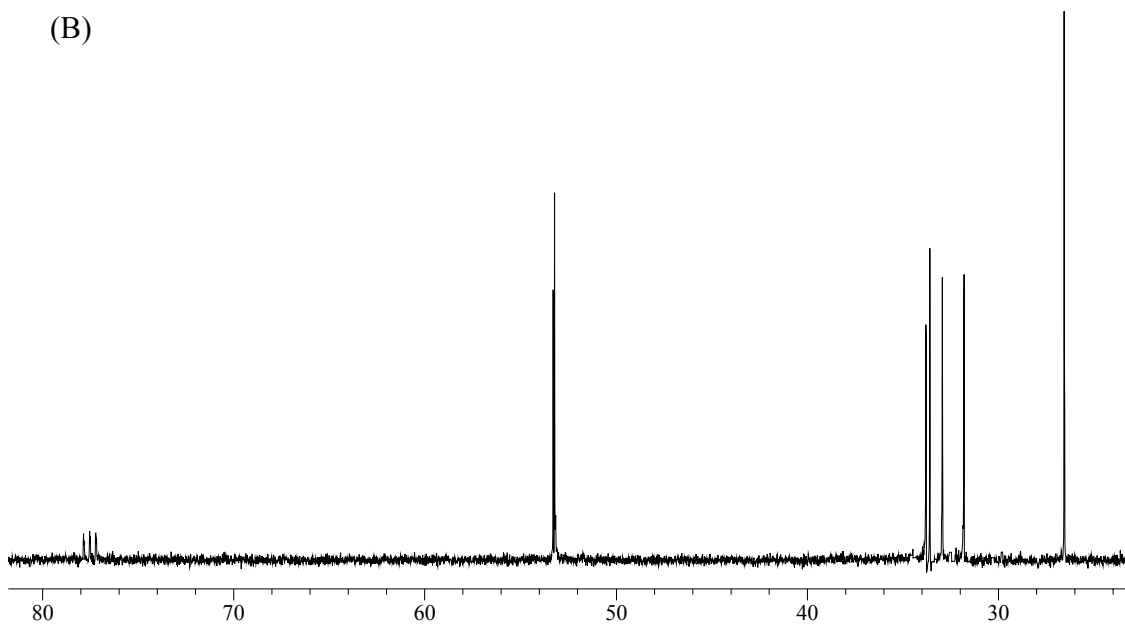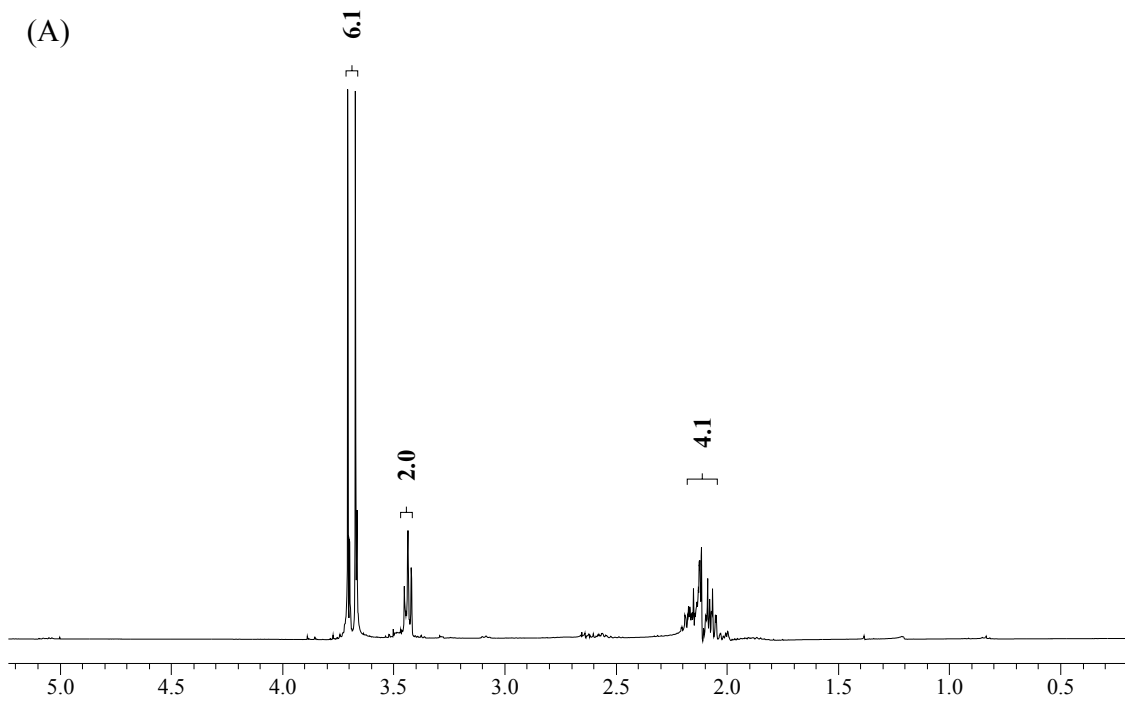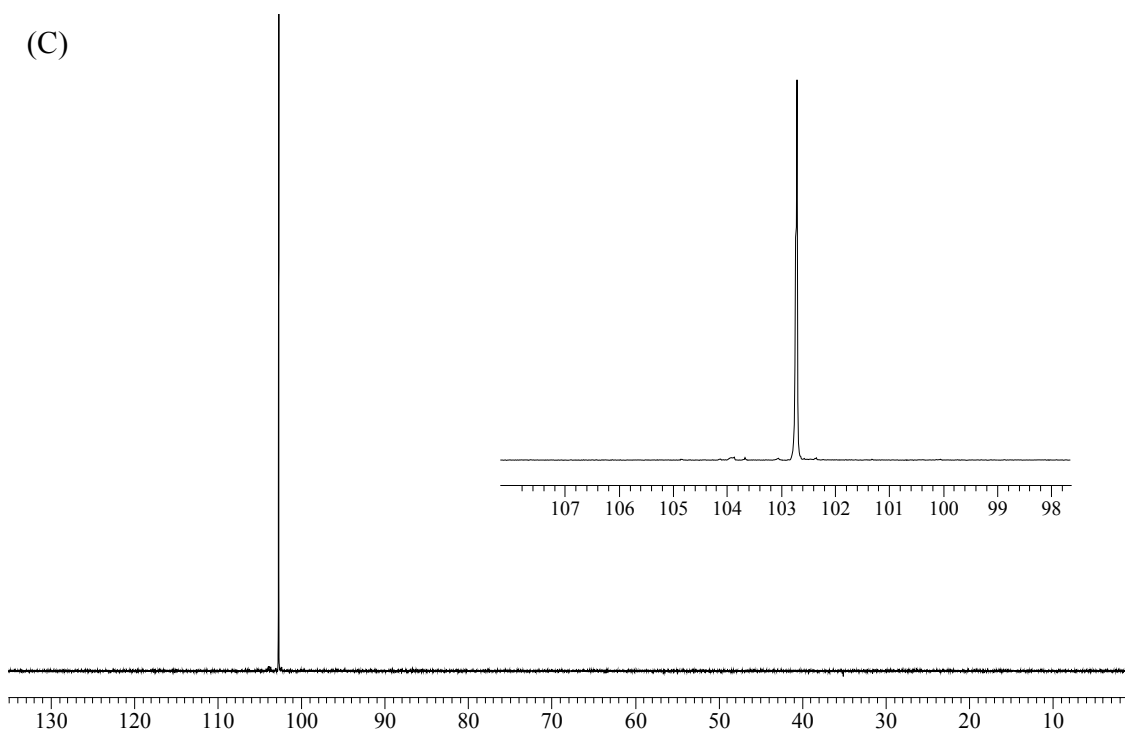
Figure 7.11. (A) ^{1}H, (B) ^{13}C and (C) ^{31}P NMR spectra of *O,O*-dimethyl (3-bromopropyl) phosphonothionate (**9**).

S
||
H₃CO—P
   | ＼(CH₂)₃–Br   +   NaN₃ $\xrightarrow{\text{DMF/H}_2\text{O}}$ H₃CO—P
H₃CO | ＼(CH₂)₃–N₃
                                                                               H₃CO
9   **10**
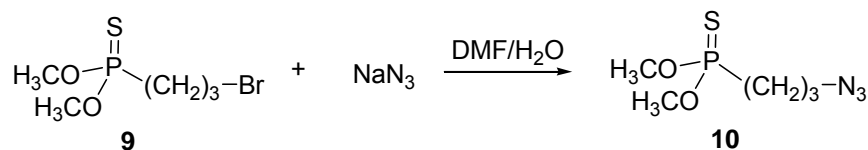
O,O-**Dimethyl (3-azopropyl) phosphonothionate (10).** A solution of compound

phosphonothionate **9** (0.73 g, 2.95 mmol) in dimethylformamide (DMF, 5 mL) was

stirred at rt under argon. Sodium azide (0.38 g, 5.85 mmol) was added, followed with

several drops of deionized water (0.5 mL) to help sodium azide dissolve. Using a ^{31}P

NMR shift from 102.7 ppm to 103.2 ppm to assess reaction progress, the reaction was

completed in 24 h. The reaction mixture was concentrated under reduced pressure. Ethyl

acetate (30 mL) was added and washed with water (15 mL) twice. The organic layer was

collected and dried over anhydrous MgSO₄. Evaporation under reduced pressure and

purification by flash chromatography using silica (6:94 ethyl acetate-hexane) gave 0.31 g

(1.48 mmol, 50%) of pure product as a light yellow oil.

^{1}H NMR (CDCl₃): δ 1.76-1.83 (m, 2 H), 1.89-1.97 (m, 2 H), 3.28 (t, J = 6.6 Hz, 2

H), 3.61 (d, J = 12.8 Hz, 6 H).

^{13}C NMR (CDCl₃): δ 22.9 (d, $^3J_{CP}$ = 3.5 Hz), 30.7 (d, $^1J_{CP}$ = 112.8 Hz), 51.4 (d,

$^2J_{CP}$ = 18.3 Hz), 53.2 (d, $^2J_{CP}$ = 6.1 Hz).

^{31}P NMR (CDCl₃): δ 103.2 (s).

(A)

6.0

2.0

1.9 2.1

4.8   4.6   4.4   4.2   4.0   3.8   3.6   3.4   3.2   3.0   2.8   2.6   2.4   2.2   2.0   1.8

(B)

90   80   70   60   50   40   30   20   10

170

(C)
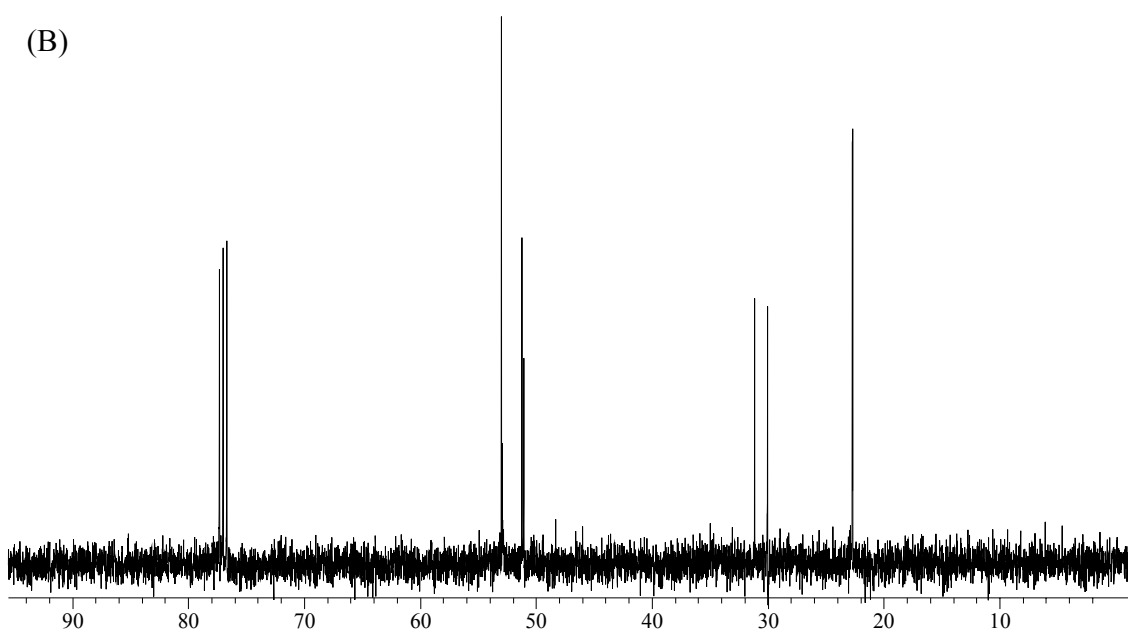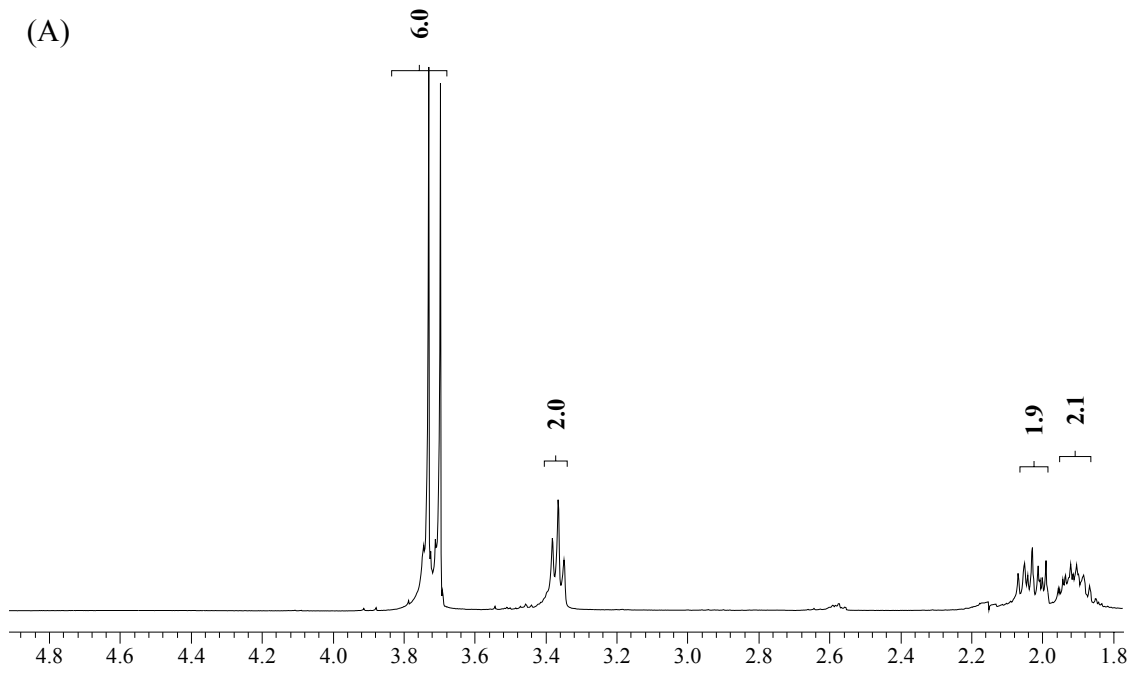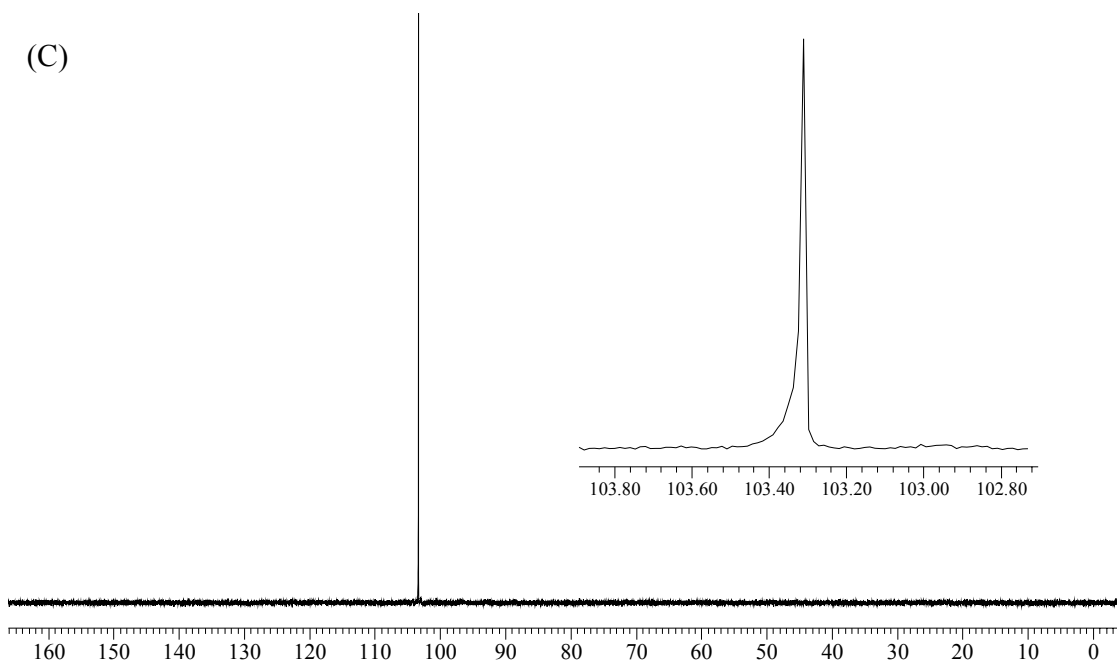
Figure 7.12. (A) ^{1}H, (B) ^{13}C and (C) ^{31}P NMR spectra of *O,O*-dimethyl (3-azopropyl) phosphonothionate (**10**).

171
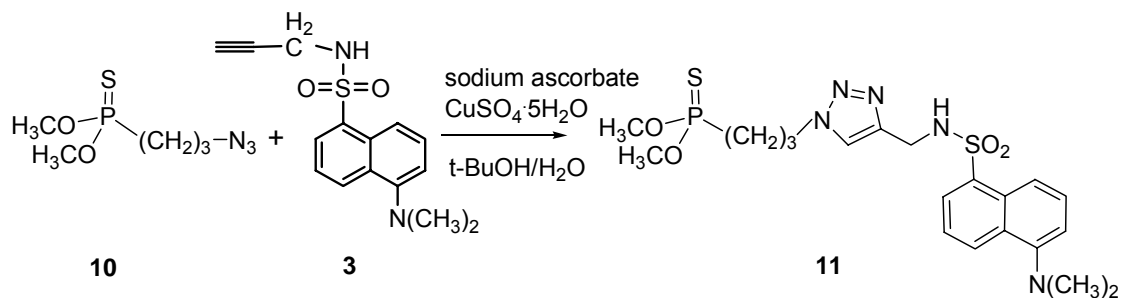
Dansyl-linked phosphonothionate (11). Phosphonothionate **10** (0.43 g, 2.06 mmol) and dansyl sulfonamide **3** (0.59 g, 2.05 mmol) were suspended in a 1:1 mixture of water and *tert*-butyl alcohol (8 mL total) under argon. Sodium ascorbate (0.50 mmol, 0.30 mL of freshly prepared 1 M solution in water) was added, followed by copper (II) sulfate pentahydrate solution (0.10 mmol, 0.20 mL of 0.5 M solution in water). The heterogeneous mixture was stirred vigorously overnight, at which point the mixture cleared and TLC analysis indicated complete consumption of the reactants. A mixture of chloroform-isopropanol (30 mL, 3:1) was added and the organic layer was washed with water, collected and dried over anhydrous $MgSO_4$. Evaporation under reduced pressure and purification by flash chromatography using silica (2:1 ethyl acetate-hexane) gave 0.92 g (1.86 mmol, 90%) of pure product as a yellow oil.

^{1}H NMR ($CDCl_3$): δ 1.86 (m, 2 H), 2.13 (m, 2 H), 2.87 (s, 6 H), 3.68 (d, $J = 13.8$ Hz, 6 H), 4.18 (dd, $J = 6.1, 5.7$ Hz, 2 H), 4.26 (t, $J = 7.0$ Hz, 2 H), 5.79 (t, $J = 6.1$ Hz, 1 H), 7.17 (d, $J = 8.1$ Hz, 1 H), 7.30 (s, 1 H), 7.39 (q, $J = 8.1$ Hz, 2 H), 8.24 (t, $J = 8.1$ Hz, 2 H), 8.53 (d, $J = 8.3$ Hz, 1 H).

^{13}C NMR (CDCl$_3$): δ 24.8 (d, $^1J_{CP}$ = 140.4 Hz), 29.8, 31.2 (d, $^3J_{CP}$ = 4.5 Hz), 38.9, 45.7, 50.0 (d, $^2J_{CP}$ = 16.8 Hz), 53.3, 64.6, 79.6, 115.6, 122.6, 123.4, 128.8, 129.7, 129.8, 130.0, 130.8, 144.2.

^{31}P NMR (CDCl$_3$): δ 102.1 (s).

(A)

(B)

(C)
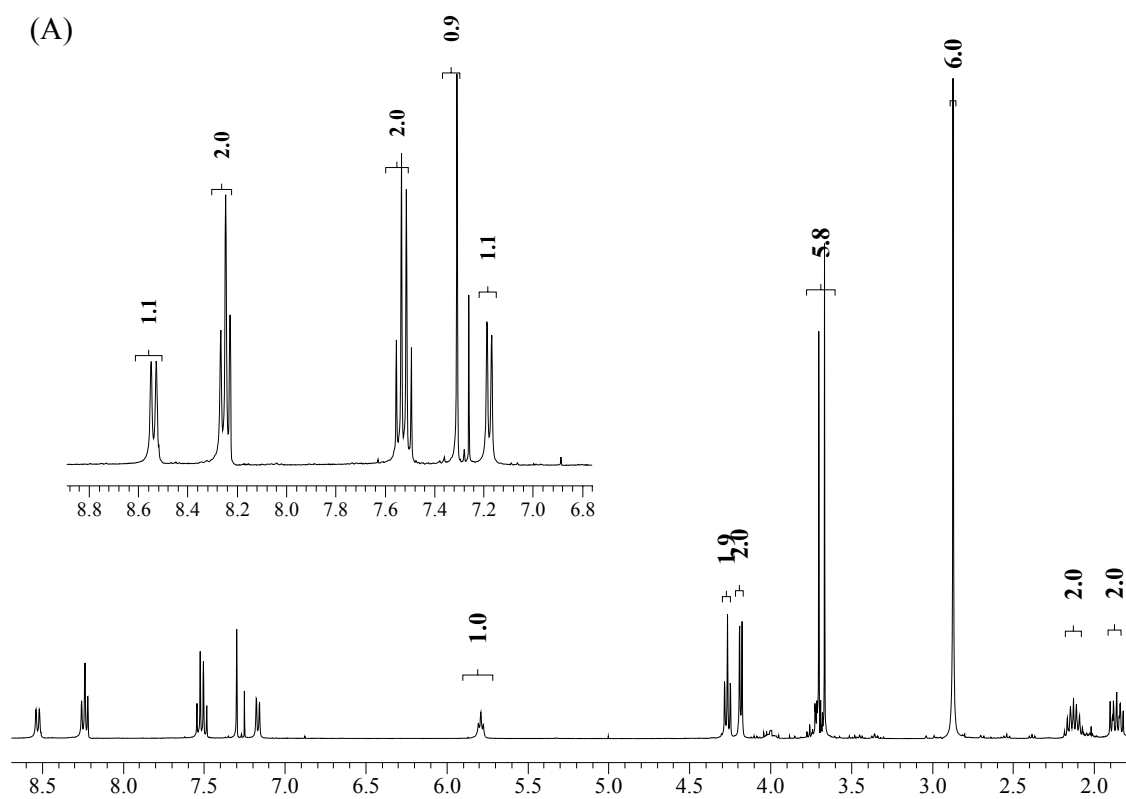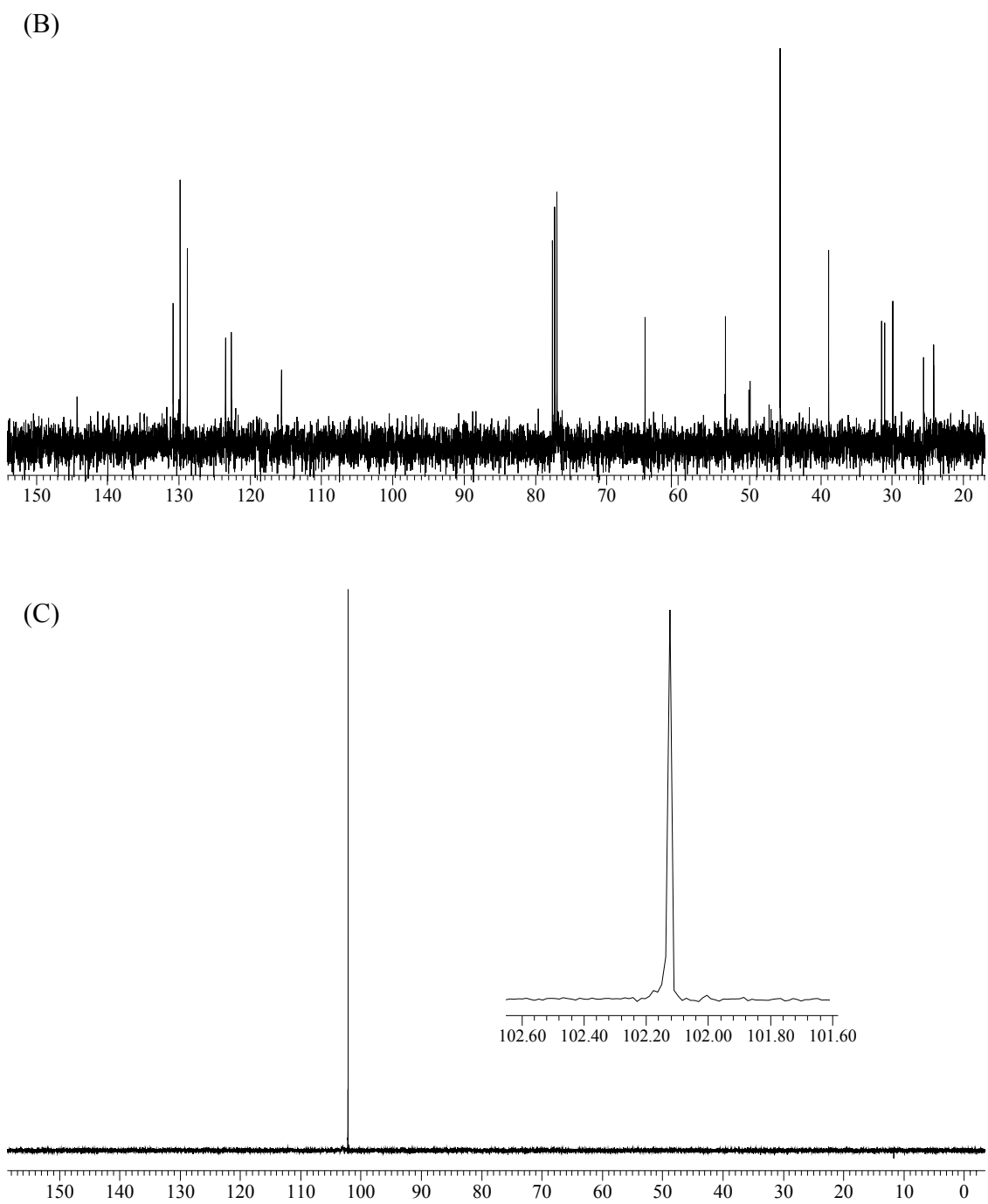
Figure 7.13. (A) ^{1}H, (B) ^{13}C and (C) ^{31}P NMR spectra of dansyl-linked phosphonothionate (**11**).

174
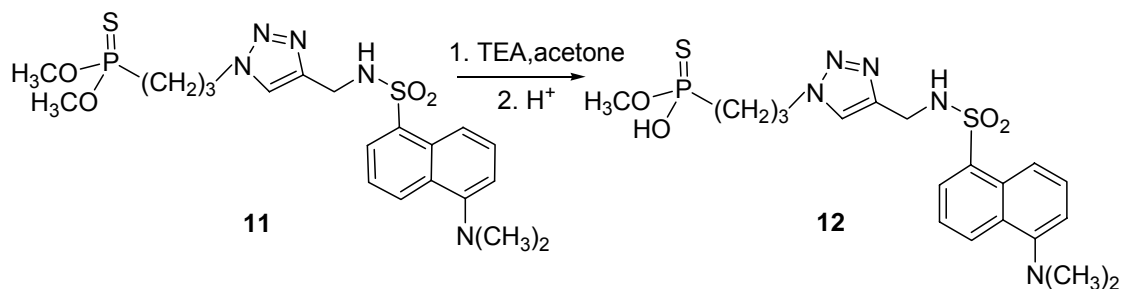
Dansyl-linked phosphonothioic acid (12). Dealkylation of dansyl-linked phosphonothionate **11** was achieved by dissolving it (0.30 g, 0.60 mmol) into acetone (1.5 mL) and adding triethylamine (TEA, 1 mL). The mixture was stirred under argon at 35 °C for 48 h while refluxing until the solution did not contain any ^{31}P NMR peak of the starting material. After cooling to rt, chloroform and water were added to extract by-products out. Hydrochloric acid (HCl, 1 N) was used to adjust to pH 1, and then a mixture of chloroform and isopropanol (3:1) was added to extract desired product from water. The organic layer was collected and dried over anhydrous MgSO$_4$. Evaporation under vacuum gave 0.17 g (0.35 mmol, 58%) of pure product **12** as light yellow oil.

^{1}H NMR (d-DMSO): δ 1.74 (m, 2 H), 1.97 (m, 2 H), 3.07 (s, 6 H), 3.68 (d, J = 13.1 Hz, 3 H), 4.22 (dd, J = 15.7, 6.6 Hz, 2 H), 4.31 (t, J = 5.2 Hz, 2 H), 6.62 (t, J = 5.8 Hz, 1 H), 7.13 (d, J = 7.1 Hz, 1 H), 7.39 (d, J = 7.8 Hz, 1 H), 7.57 (q, J = 4.3 Hz, 2 H), 8.22 (d, J = 7.3 Hz, 1 H), 8.49 (d, J = 8.9 Hz, 1 H), 8.63 (d, J = 8.1 Hz, 1 H).

^{31}P NMR (d-DMSO): δ 93.1 (s).

Compound **12** was found to undergo a proton oxo-thio shift under certain conditions as revealed by a second ^{31}P NMR shift at 49.7 ppm.

(A)

(B)
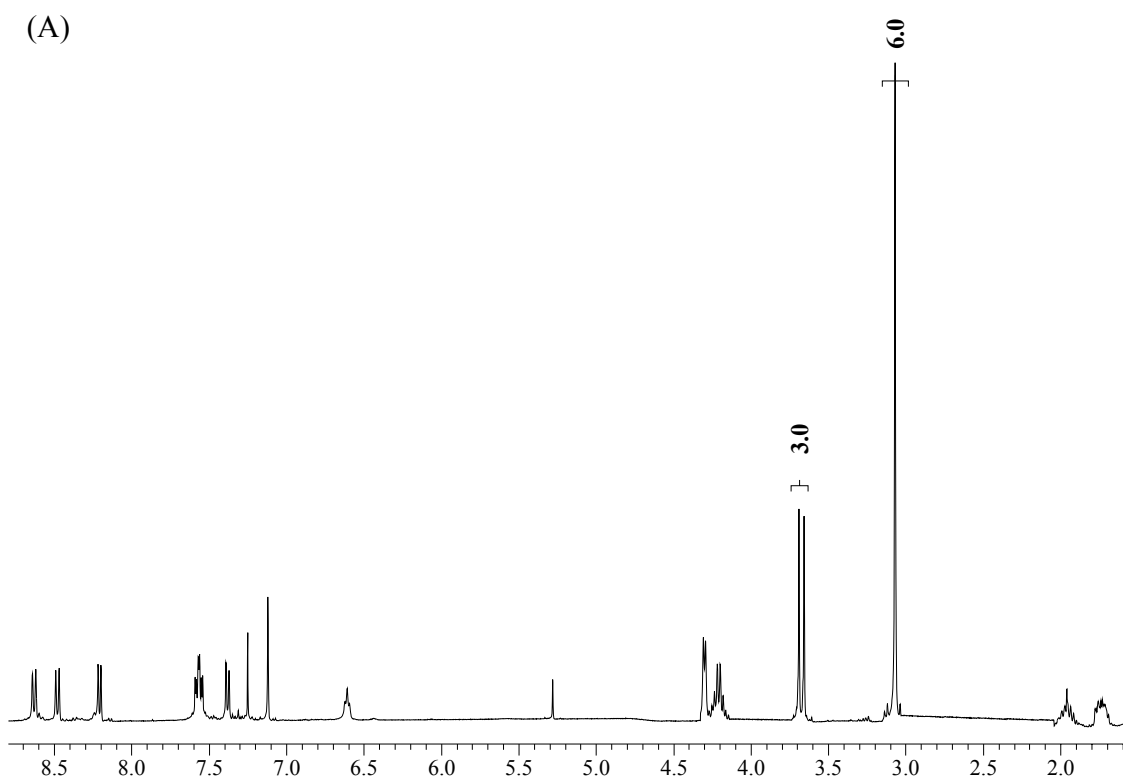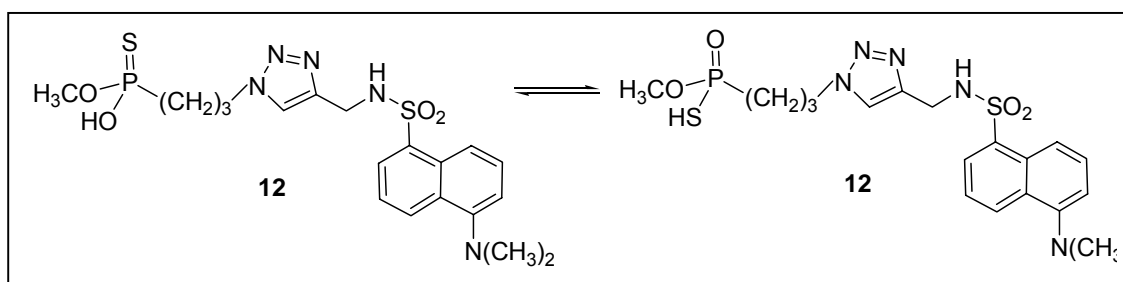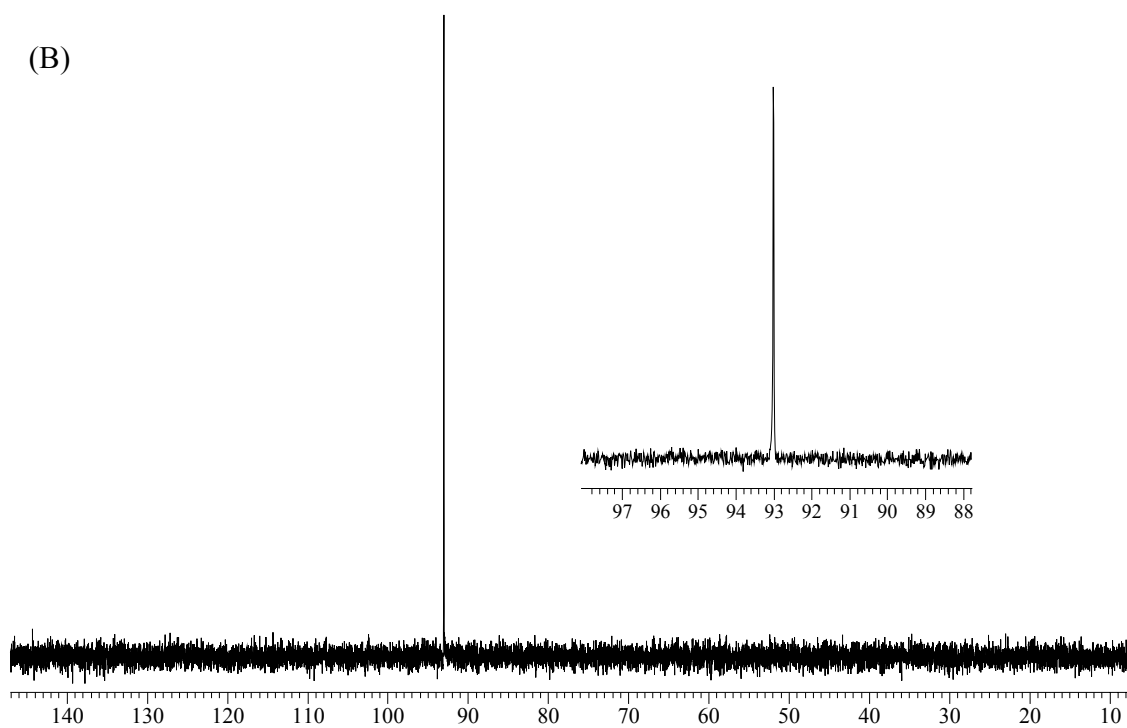
Figure 7.14. (A) ^{1}H and (B) ^{31}P NMR spectra of dansyl-linked phosphonothionic acid (**12**).
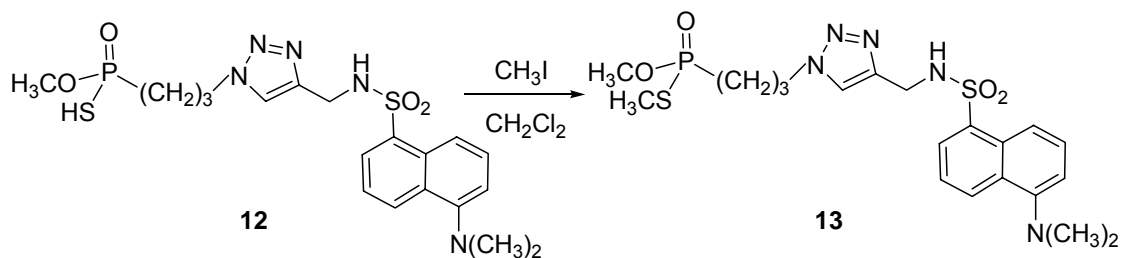
Dansyl-linked *O*, *S*-dimethyl phosphonate (13). To a solution of compound **12** (0.020 g, 0.041 mmol) in dichloromethane, triethylamine (TEA, 0.050 mL) and methyl iodide (0.014 g, 0.10 mmol) were added. The reaction mixture was stirred under argon at rt for 0.5 h until ^{31}P NMR showed a complete consumption of starting material. Water (1 mL) was added and then extracted with ethyl acetate (2 x 1 mL). The organic layer was collected and dried over anhydrous MgSO$_4$. Evaporation under reduced pressure gave 0.019 g (87%) of final compound **13** as a yellow oil.

^{1}H NMR (CDCl$_3$): δ 1.90 (m, 2 H), 2.21 (m, 2 H), 2.25 (d, $^3J_{PH}$ = 12.6 Hz, 3 H), 2.88 (s, 6 H), 3.75 (d, $^3J_{PH}$ = 12.5 Hz, 3 H), 4.20 (d, J = 6.3 Hz, 2 H), 4.34 (t, J = 6.4 Hz, 2 H), 5.66 (t, J = 4.5 Hz, 1 H), 7.17 (d, J = 8.1 Hz, 1 H), 7.37 (s, 1 H), 7.53 (q, J = 8.2 Hz, 2 H), 8.26 (t, J = 8.5 Hz, 2 H), 8.54 (d, J = 8.7 Hz, 1 H).

^{13}C NMR (CDCl$_3$): δ 12.1 (d, $^2J_{CP}$ = 3.1 Hz), 23.2 (d, $^2J_{CP}$ = 4.7 Hz), 28.0 (d, $^1J_{CP}$ = 108.3 Hz), 38.7, 45.4, 49.7 (d, $^3J_{CP}$ = 16.8 Hz), 51.6 (d, $^2J_{CP}$ = 6.2 Hz), 77.2, 115.3, 118.6, 122.5, 123.1, 128.5, 129.5, 129.6, 129.8, 130.6, 134.4, 144.0.

^{31}P NMR (CDCl$_3$): δ 58.9 (s).

(A)

(B)
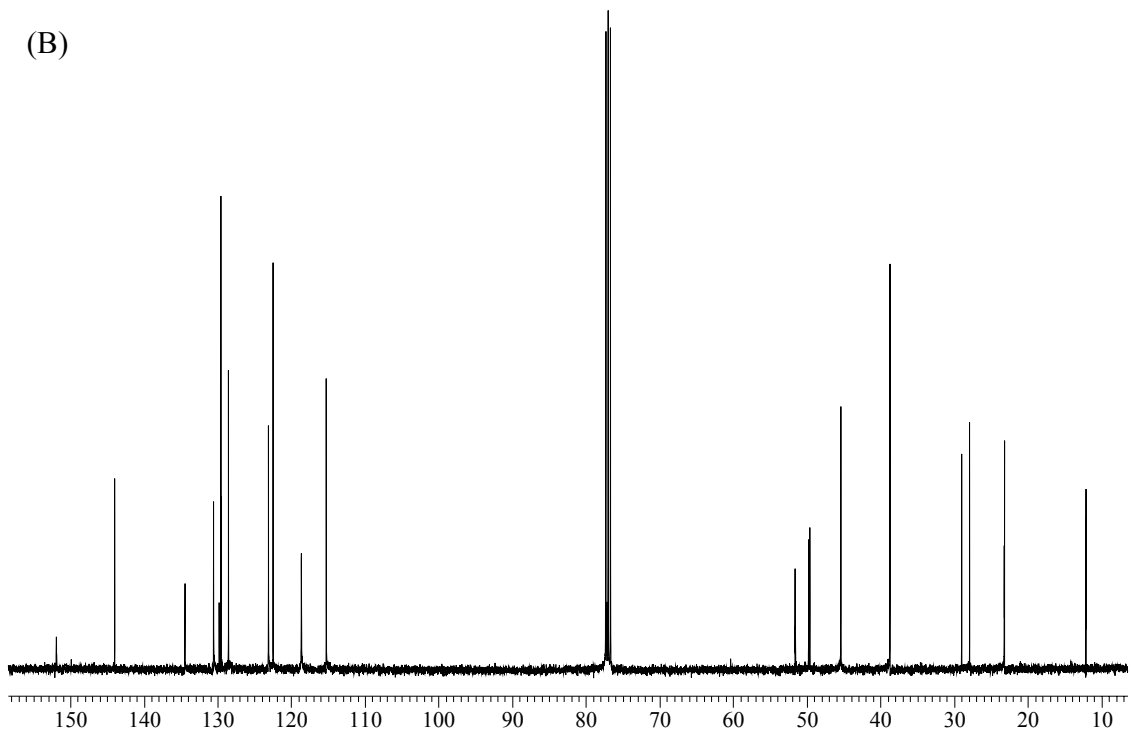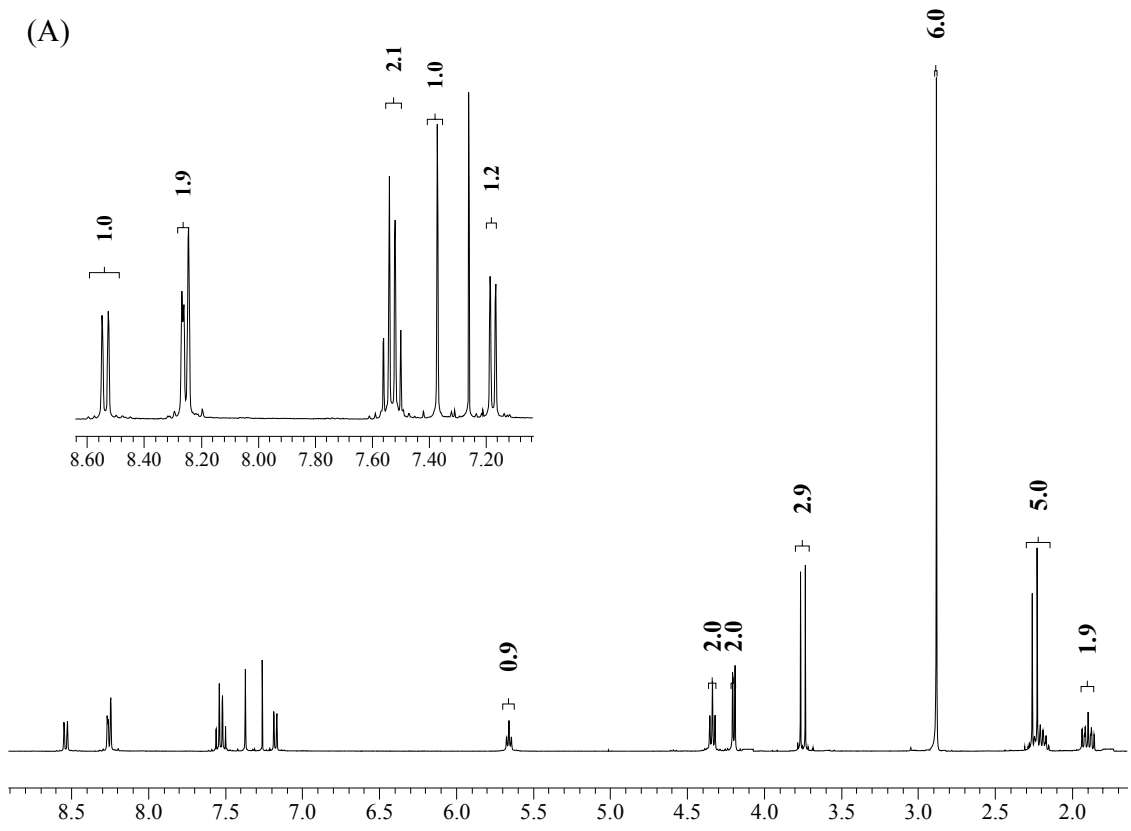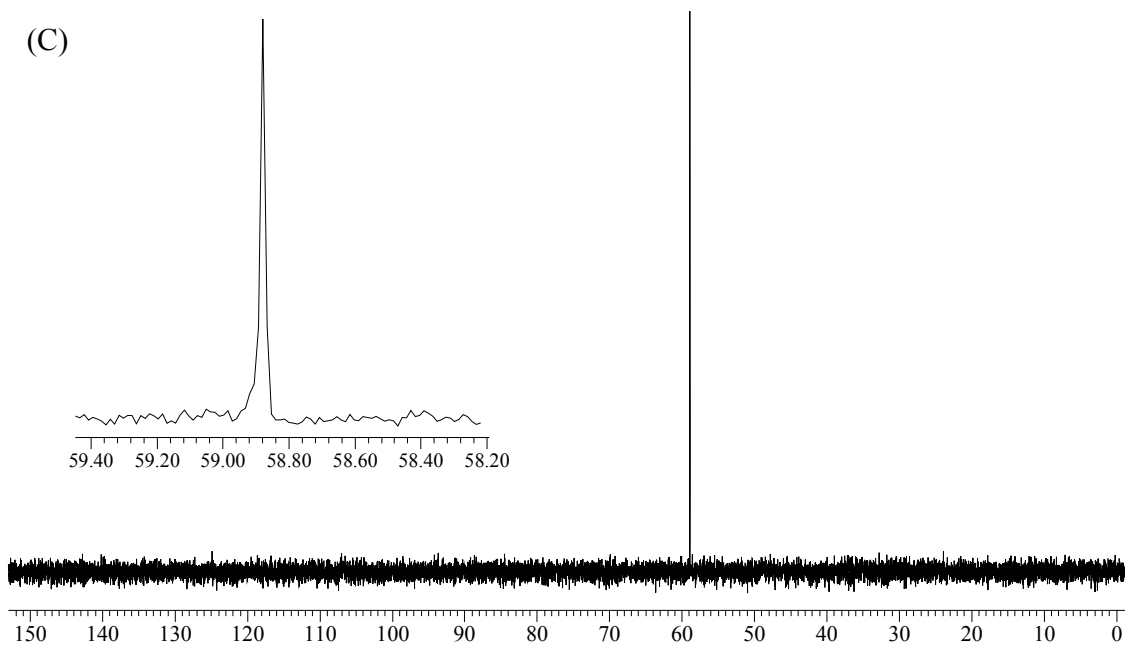
Figure 7.15. (A) ^{1}H, (B) ^{13}C and (C) ^{31}P NMR spectra of dansyl-linked *O, S*-dimethyl phosphonate (**13**).

H$_3$CO–P–(CH$_2$)$_3$ ... (CH$_3$)$_2$N(CH$_2$)$_2$Cl / DMSO ... **12** → **14**

N(CH$_3$)$_2$ N(CH$_3$)$_2$
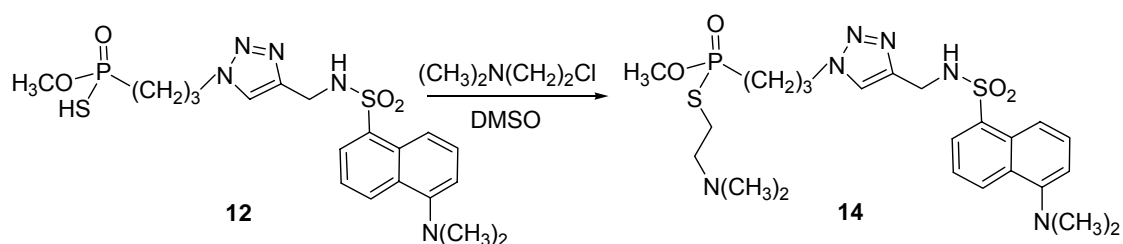
Dansyl-linked *O*-methyl, *S-2*-(dimethylamino)ethyl phosphonate (14). To a solution of compound **12** (0.040 g, 0.083 mmol) in dimethylsulfoxide (DMSO), potassium carbonate (K$_2$CO$_3$, 0.012 g, 0.083 mmol) and 2 drops of deionized water were added, followed with 2-chloro-*N,N*-dimethylethylamine (0.012 g, 0.083 mmol). The reaction mixture was stirred under argon at rt for 0.5 h until ^{31}P NMR showed a complete consumption of starting material. Water (1 mL) was added and washed with a 1:3 mixture of CHCl$_3$ - isopropanol. The organic layer was collected and dried over anhydrous MgSO$_4$. Evaporation under reduced pressure and purification by flash chromatography using silica (1:9 chloroform-methanol) gave 0.036 g (78%) of the final compound **14** as a yellow oil.

^{1}H NMR (CDCl$_3$): δ 1.89 (m, 2 H), 2.20 (m, 2 H), 2.32 (s, 6 H), 2.60 (m, 2 H), 2.88 (s, 6 H), 3.46 (t, J = 2.0 Hz, 2 H), 3.74 (d, [3]J_{PH} = 12.5 Hz, 3 H), 4.19 (d, J = 4.5 Hz, 2 H), 4.34 (t, J = 3.8 Hz, 2 H), 6.14 (t, J = 4.5 Hz, 1 H), 7.17 (d, J = 7.5 Hz, 1 H), 7.40 (s, 1 H), 7.53 (q, J = 8.0 Hz, 2 H), 8.26 (t, J = 8.5 Hz, 2 H), 8.53 (d, J = 8.9 Hz, 1 H).

^{13}C NMR (CDCl$_3$): δ 23.6, 28.5 (d, [1]J_{CP} = 158.8 Hz), 30.2 (d, [3]J_{CP} = 43.2 Hz), 39.0, 45.0, 45.6, 49.9 (d, [2]J_{CP} = 18.5 Hz), 51.0, 51.9, 59.7, 115.5, 119.0, 122.9, 123.4, 128.7, 129.7, 130.0, 134.9, 152.2.

^{31}P NMR (CDCl$_3$): δ 58.9 (s).
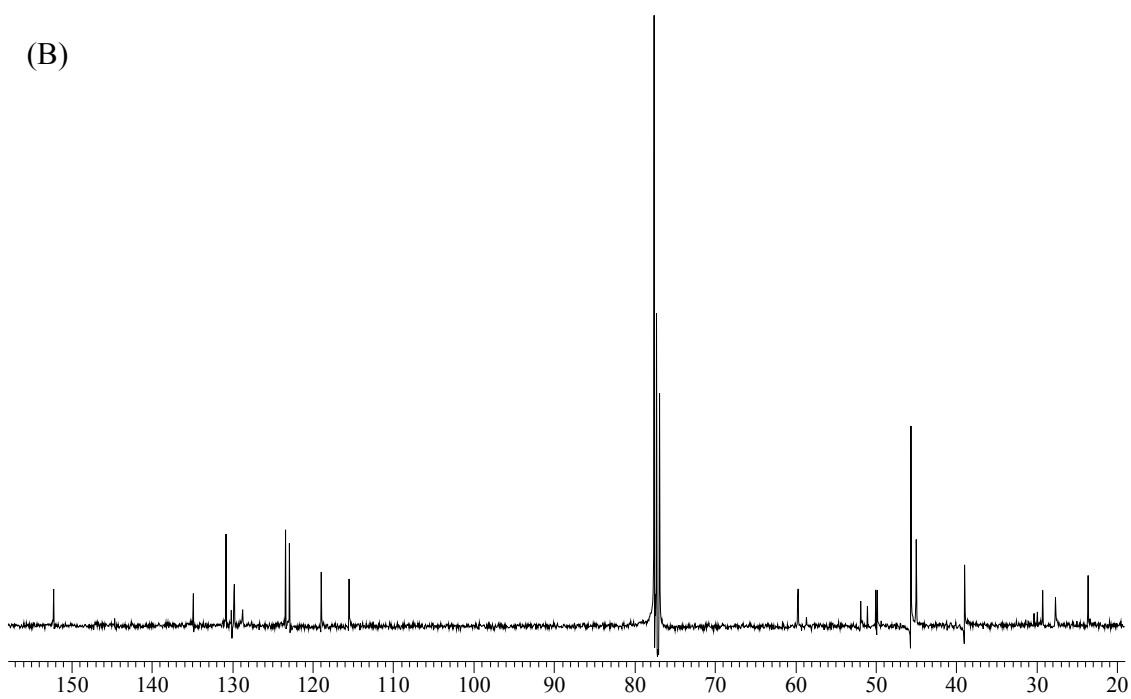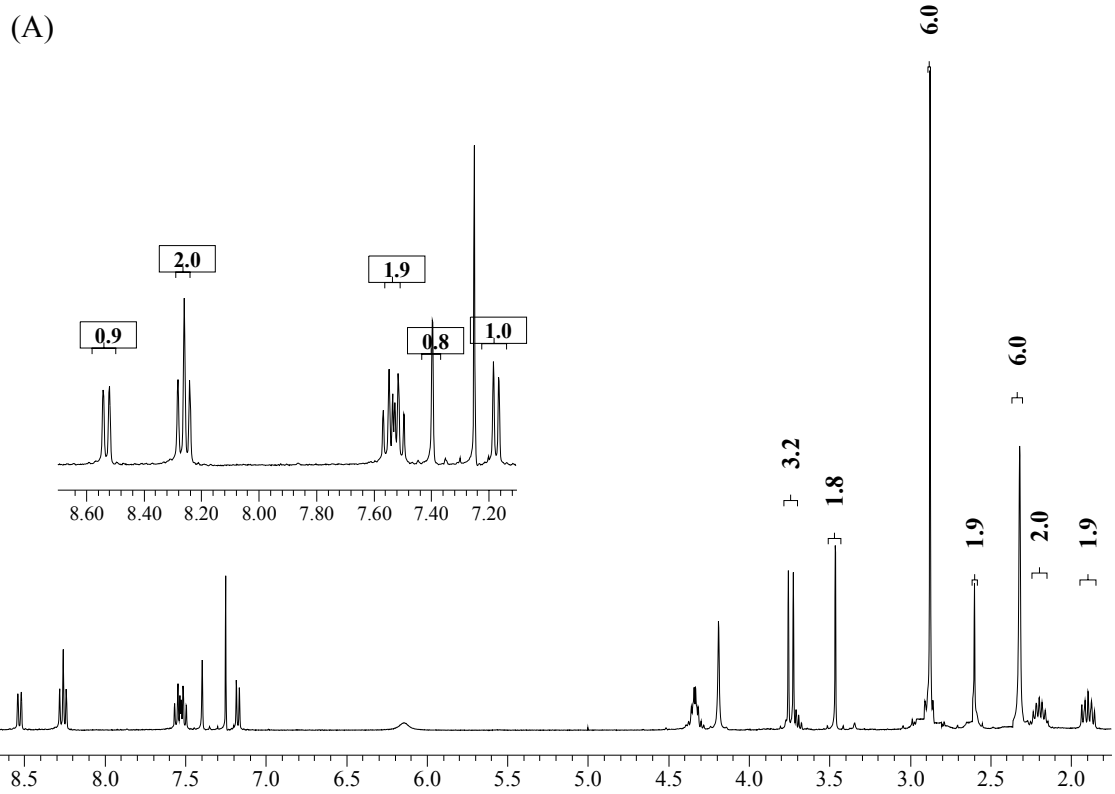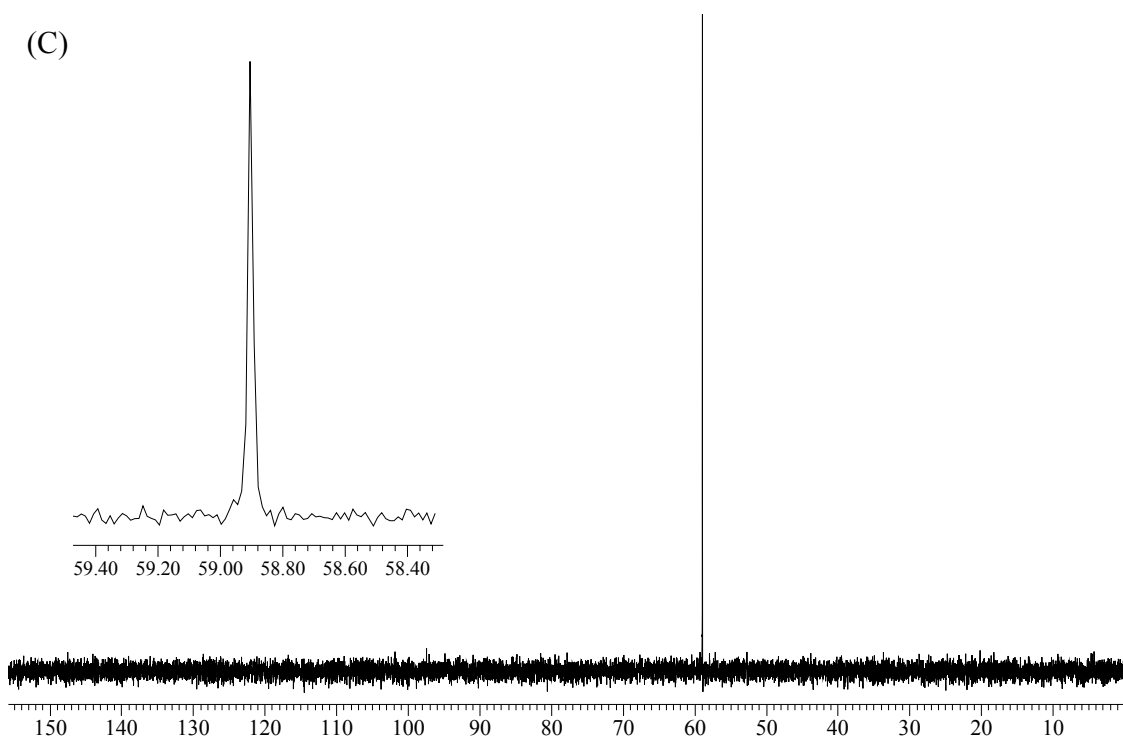
Figure 7.16. (A) ^{1}H, (B) ^{13}C and (C) ^{31}P NMR spectra of dansyl-linked *O*-methyl, *S*-2-(dimethylamino)ethyl phosphonate (**14**).
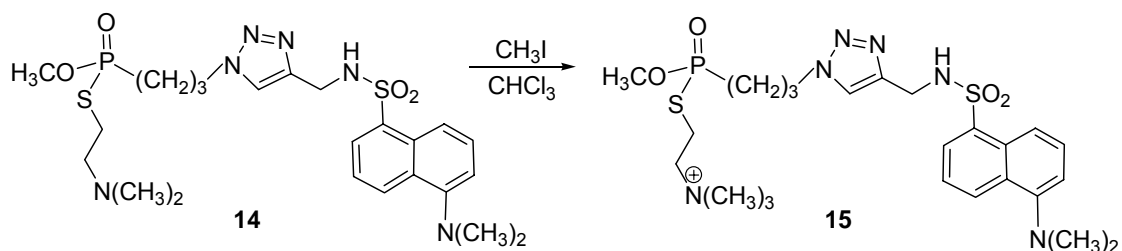
Dansyl-linked *O*-methyl, *S*-choline phosphonate (15). To a solution of compound **14** (0.036 g, 0.065 mmol) in chloroform, methyl iodide (2 equiv) was added. The reaction mixture was stirred at rt for 1 h until ^{31}P NMR spectral did not contain the peak of the starting material. After evaporation under vacuum, compound **15** was obtained as a yellow solid (quantitative yield).

^{1}H NMR (CDCl$_3$): δ 1.69 (m, 2 H), 2.04 (m, 2 H), 2.16 (s, 9 H), 2.70 (m, 2 H), 2.86 (s, 6 H), 3.46 (t, *J* = 2.0 Hz, 2 H), 3.45 (d, $^3J_{PH}$ = 14.5 Hz, 3 H), 3.90 (t, *J* = 5.7 Hz, 2 H), 4.14 (d, *J* = 5.9 Hz, 2 H), 7.08 (t, *J* = 6.0 Hz, 1 H), 7.15 (d, *J* = 7.5 Hz, 1 H), 7.53 (q, *J* = 7.8 Hz, 2 H), 7.78 (s, 1 H), 8.22 (d, *J* = 7.2 Hz, 1 H), 8.34 (d, *J* = 8.2 Hz, 1 H), 8.51 (d, *J* = 9.0 Hz, 1 H).

^{31}P NMR (CDCl$_3$): δ 58.8 (s).

MS (ESI-TOF): Calcd for C$_{24}$H$_{38}$N$_6$O$_4$PS$_2$ (M+H) 569.2134; found 569.2148.
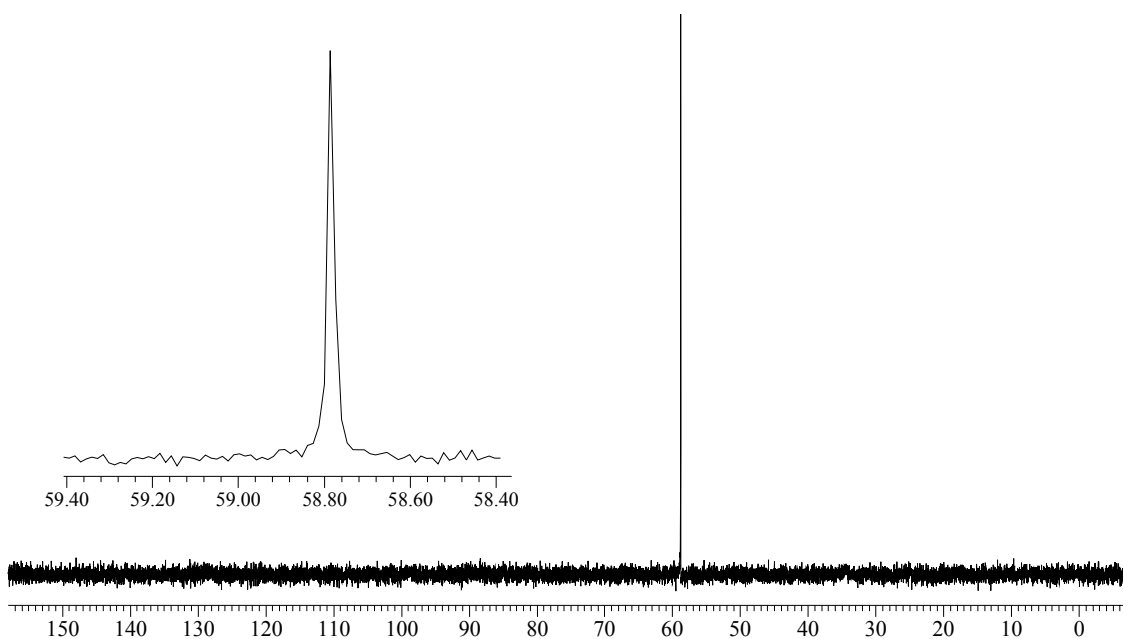
Figure 7.17. ^{31}P NMR spectrum of dansyl-linked *O*-methyl, *S*-choline phosphonate (**15**).

10 → **16a** + **16b**
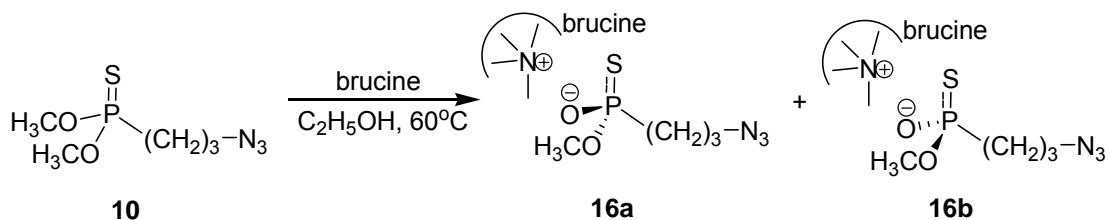
brucine
C₂H₅OH, 60°C

O-**Methyl (3-azopropyl) phosphonothioic acid, brucines salt (16).** Brucine
(1.65 g, 4.18 mmol) was added to a stirring solution of *O,O*-dimethyl (3-azopropyl)
phosphonothionate **10** (0.96 g, 4.59 mmol) in ethanol (10 mL). The reaction mixture was
brought to reflux at 50 °C for six days until ^{31}P NMR showed a complete conversion.
Ethanol was removed by rotary evaporation under reduced pressure and ethyl ether was
added to wash off the starting material and give the crude brucine salt **16**.

The separation of **16a/16b** was attempted. This separation was not able to be
monitored by ^{31}P NMR since the two peaks are largely overlapped.

^{1}H NMR (CDCl₃): δ

Brucine part: 1.21 (dt, *J* = 10.1, 4.2 Hz, 1 H), 1.53 (d, *J* = 15.3 Hz, 1 H), 1.69 (m,
2 H), 2.53 (dd, *J* = 20.4, 2.8 Hz, 1 H), 2.87 (d, *J* = 15.4 Hz, 1 H), 2.96 (m, 1 H), 3.59 (d, *J*
= 14.0 Hz, 1 H), 3.67 (s, 3 H), 3.70 (d, *J* = 13.7 Hz, 2 H), 3.77 (d, *J* = 27.3 Hz, 6 H), 3.85
(d, *J* = 20.4 Hz, 2 H), 4.04 (d, *J* = 13.7 Hz, 1 H), 4.11 (m, 1 H), 4.22 (t, *J* = 10.7 Hz, 2 H),
4.45 (s, 1 H), 6.37 (t, *J* = 8.7 Hz, 1 H), 7.11 (s, 1 H), 7.61 (s, 1 H).

Phosphonothionate part: 1.77 (m, 2 H), 2.10 (m, 2 H), 3.18 (t, *J* = 6.4 Hz, 2 H),
3.41 (d, *J* = 12.4 Hz, 3 H).

^{31}P NMR (CDCl₃): δ 76.1 (s) (2 single peaks for **16a** and **16b**).

(A)

(B)
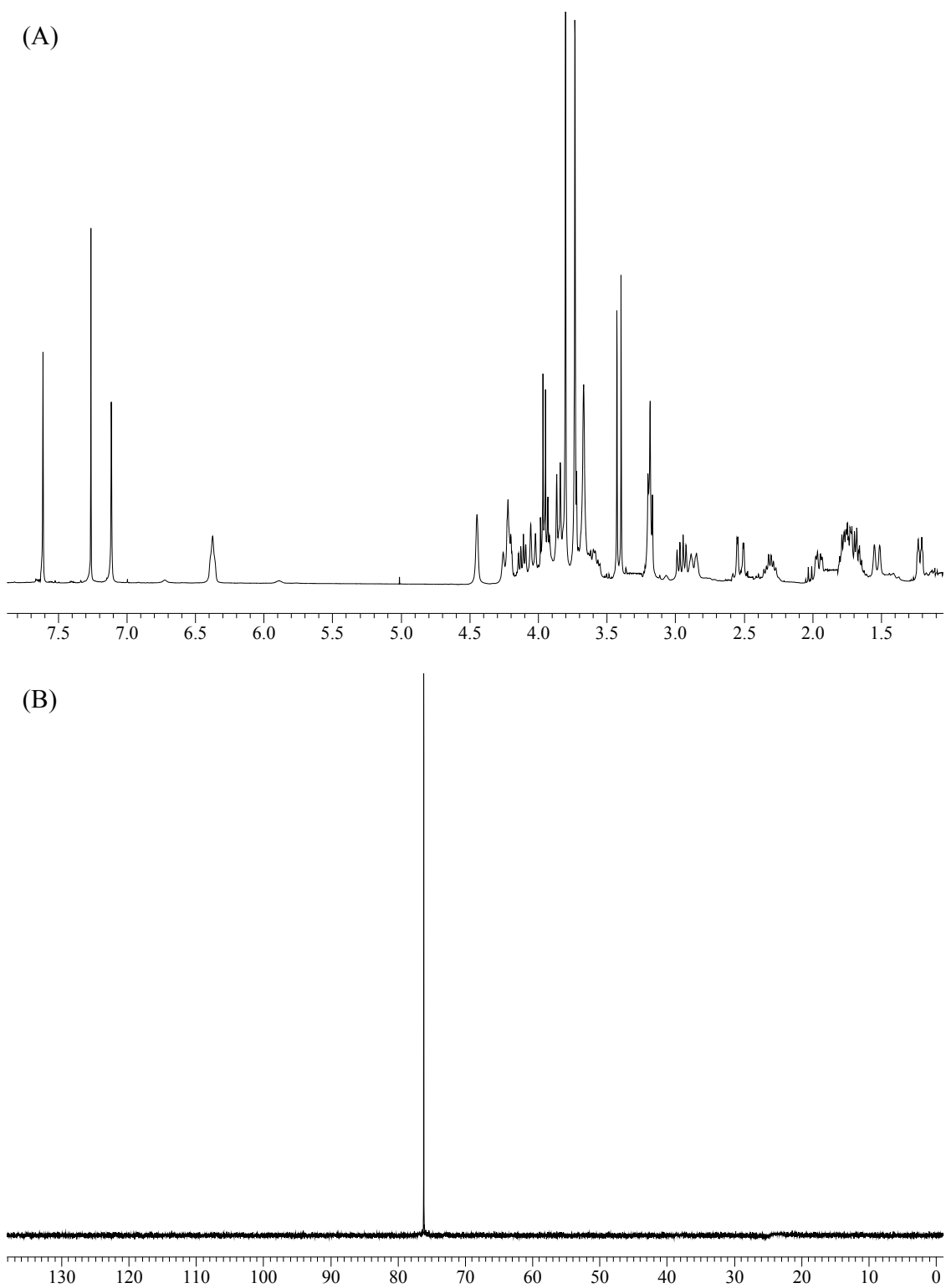
Figure 7.18. (A) ^{1}H and (B) ^{31}P NMR spectra of *O*-methyl (3-azopropyl) phosphonothioic acid, brucines salt (**16**).

10   **17**
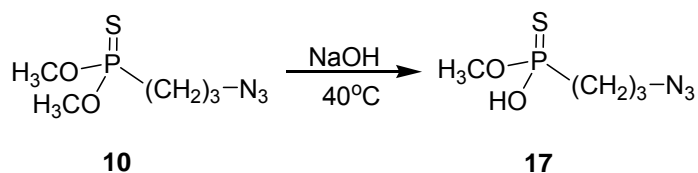
_O_-methyl (3-azopropyl) phosphonothioic acid (17). Hydrolysis of phosphonothionate **10** was performed by dissolving **10** (5.00 g, 23.92 mmol) into 20 mL methanol with 5 mL NaOH (5 M). The mixture was stirred at 55 °C under argon for 48 h while refluxing until ^{31}P NMR showed completion of the reaction. After cooling to rt, dichloromethane and water were added to extract the remaining starting material. Hydrochloric acid (HCl, 3 N) was used to adjust to pH 1, and then a mixture of chloroform and isopropanol (3:1) was added to extract the desired product from water. The organic layer was collected and dried over anhydrous MgSO$_4$. Evaporation under vacuum gave 3.19 g (16.36 mmol, 68%) of pure product **17** as light yellow oil.

^{1}H NMR (CDCl$_3$): δ 1.91-1.98 (m, 2 H), 2.04-2.12 (m, 2 H), 3.40 (t, J = 6.6 Hz, 2 H), 3.74 (d, J = 13.7 Hz, 3 H).

^{13}C NMR (CDCl$_3$): δ 22.9 (d, $^3J_{CP}$ = 3.5 Hz), 31.6 (d, $^1J_{CP}$ = 111.3 Hz), 51.3 (d, $^2J_{CP}$ = 18.4 Hz), 51.9 (d, $^2J_{CP}$ = 6.3 Hz).

^{31}P NMR (CDCl$_3$): δ 95.2 (s).
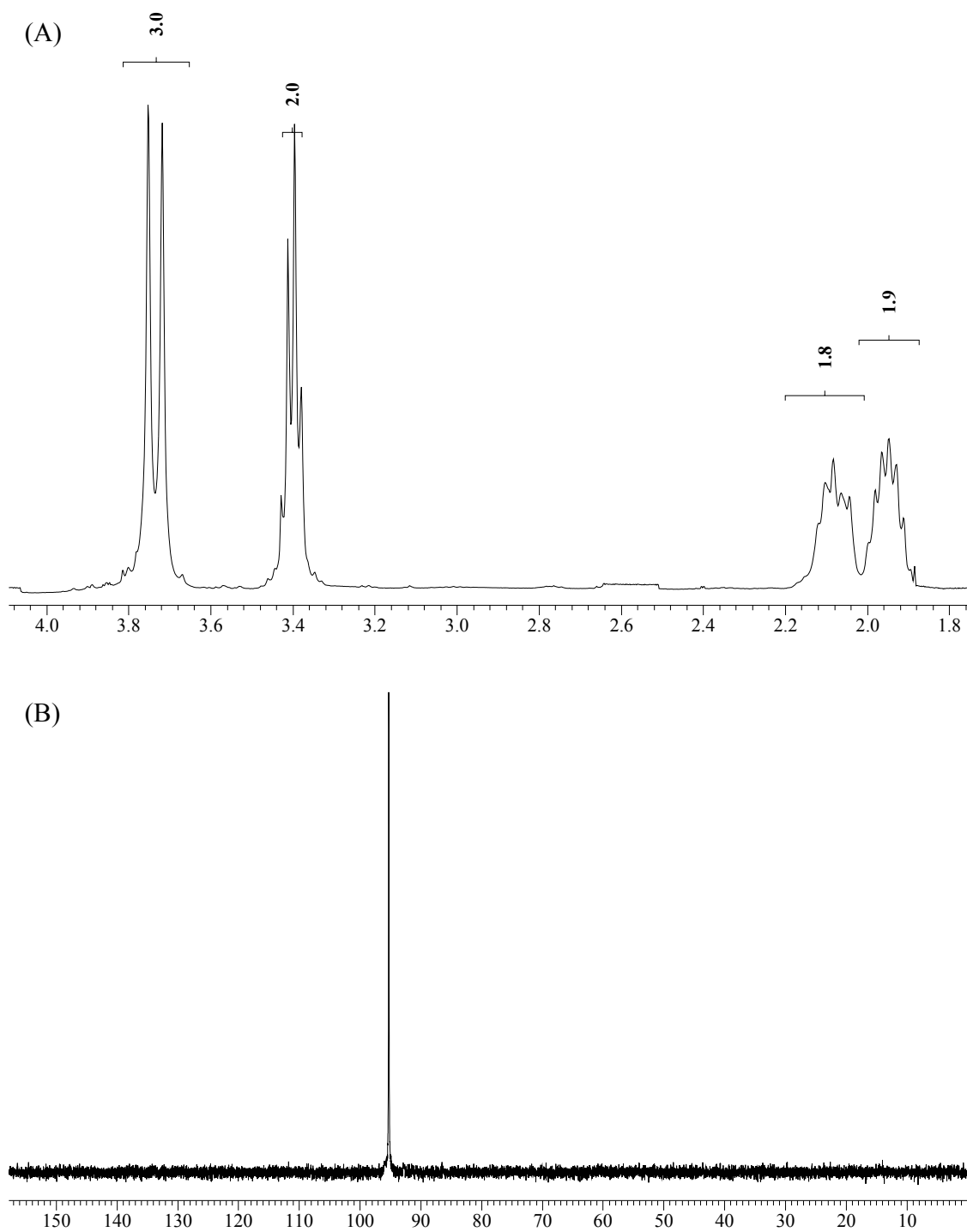
Figure 7.19. (A) ^{1}H and (B) ^{31}P NMR spectra of *O*-methyl (3-azopropyl) phosphonothioic acid (**17**).
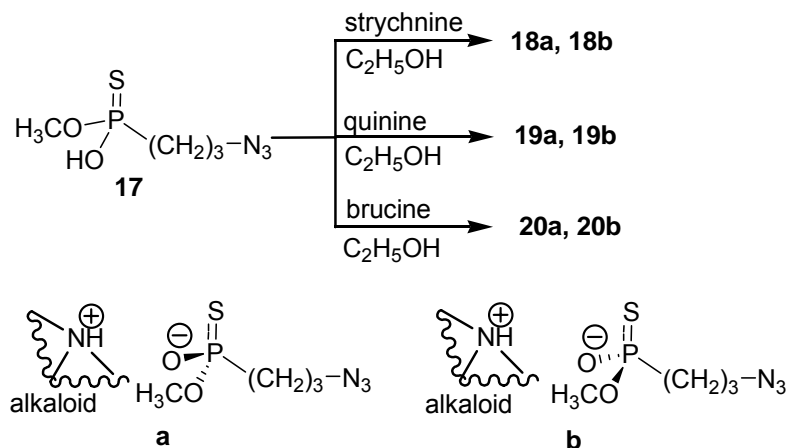
O-methyl (3-azopropyl) phosphonothioic acid – alkaloid salts (18, 19, 20).

One of three alkaloids (strychnine, brucine or quinine, 6.00 mmol) was added to a stirring solution of **17** (1.17 g, 6.00 mmol) in 10 mL ethanol. The reaction mixture was brought to 65 °C while refluxing. ^{31}P NMR showed a complete conversion after 3 h.

Strychnine 18a/18b: ^{31}P NMR (CDCl$_3$): δ 84.02 (s), 83.97 (s).

Brucine 19a/19b: ^{31}P NMR (CDCl$_3$): δ 83.77 (s), 83.66 (s).

Quinine 20a/20b: ^{31}P NMR (CDCl$_3$): δ 82.07 (s), 82.00 (s).

The strychnine salts **18a/18b** were selected for more detailed analysis. See subsequent experimental.

(A)

86.0 85.5 85.0 84.5 84.0 83.5 83.0 82.5 82.0 81.5

(B)

89 88 87 86 85 84 83 82 81 80 79

(C)
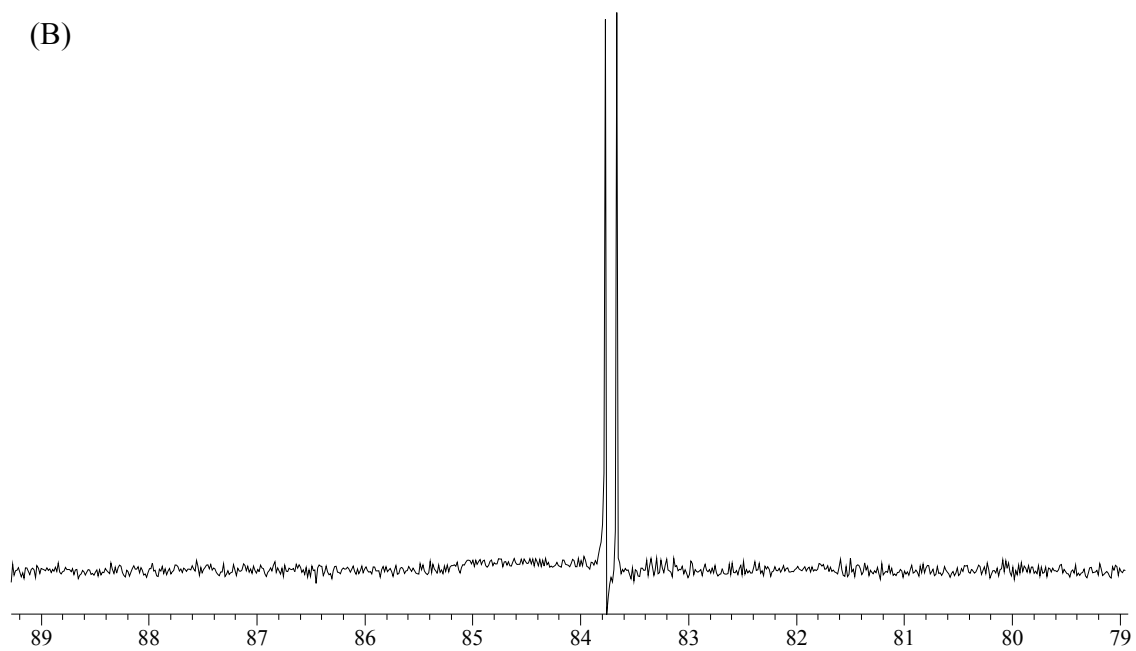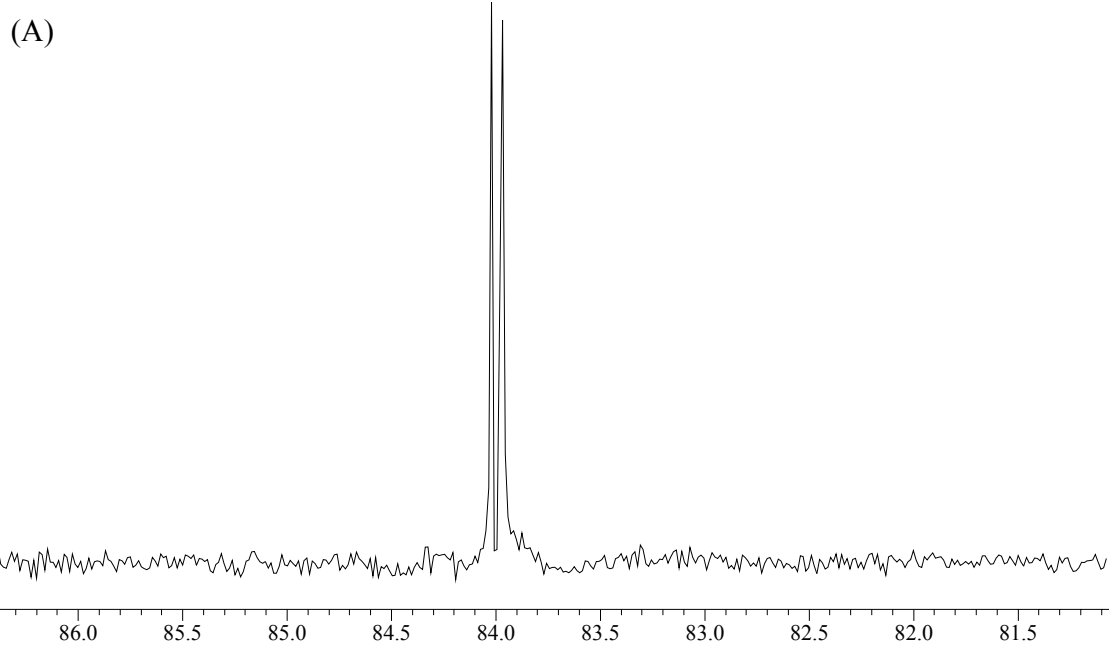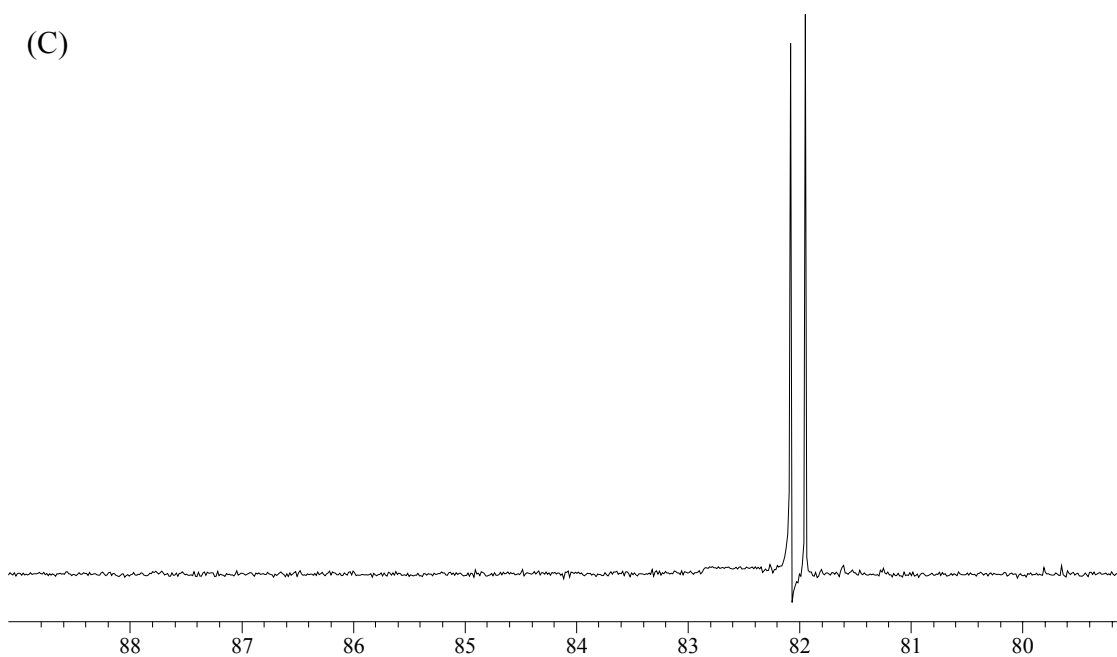
Figure 7.20. ^{31}P NMR spectra of (A) *O*-methyl (3-azopropyl) phosphonothioic acid – strychnine salts (**18a** and **18b**), (B) *O*-methyl (3-azopropyl) phosphonothioic acid – brucine salts (**19a** and **19b**) and (C) *O*-methyl (3-azopropyl) phosphonothioic acid – quinine salts (**20a** and **20b**).
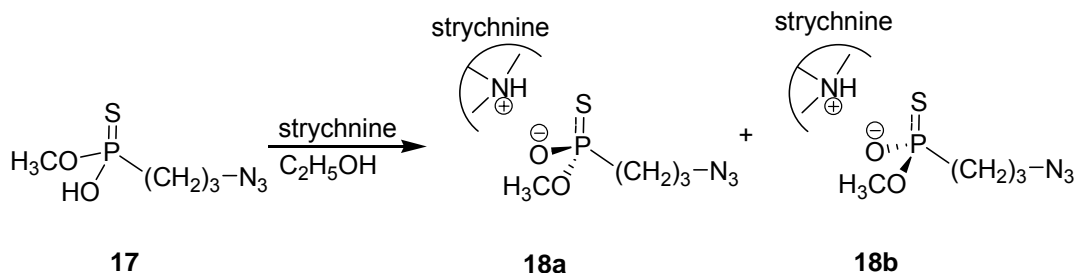
Experimental continued from general procedure to phosphonothioic acid –

alkaloid salts. **18a**: Ethyl ether was added to effect cloudiness. Upon cooling, crystals

precipitated a strychnine salt (**18**). The first crop of crystals was filtered, and washed

with a small portion of ethanol. The resulting crystals were dissolved into isopropanol

under heat and recrystallized twice. ^{31}P NMR of the first crop of crystal showed > 90% of

one diastereomer (**18a**).

^{1}H NMR (CDCl$_3$): δ

Strychnine part: 1.34 (dt, J = 10.4, 3.1 Hz, 1 H), 1.61 (d, J = 15.5 Hz, 1 H), 1.94

(d, J = 4.4 Hz, 2 H), 2.56 (dt, J = 15.4, 3.3 Hz, 1 H), 2.62 (dd, J = 18.2, 3.5 Hz, 1 H), 3.08

(d, J = 8.3 Hz, 1 H), 3.13 (d, J = 8.3 Hz, 1 H), 3.17 (d, J = 13.9 Hz, 1 H), 3.85 (dd, J =

11.3, 7.1 Hz, 1 H), 3.91 (s, 1 H), 3.95 (t, J = 6.0 Hz, 1 H), 4.02 (d, J = 6.0 Hz, 0.5 H),

4.06 (d, J = 5.8 Hz, 0.5 H), 4.12 (s, 1 H), 4.18 (m, 2 H), 4.29 (dt, J = 18.8, 3.2 Hz, 1 H),

4.69 (s, 1 H), 6.25 (t, J = 7.5 Hz, 1 H), 7.10 (t, J = 7.3 Hz, 1 H), 7.25 (t, J = 7.4 Hz, 1 H),

7.42 (d, J = 7.5 Hz, 1 H), 8.02 (d, J = 8.1 Hz, 1 H).

Phosphonothionate part: 1.88-1.93 (m, 2 H), 1.95-2.10 (m, 2 H), 3.34 (t, J = 6.4

Hz, 2 H), 3.64 (d, J = 13.2 Hz, 3 H).

^{31}P NMR (CDCl$_3$): δ 84.02 (s).

(A)

(B)
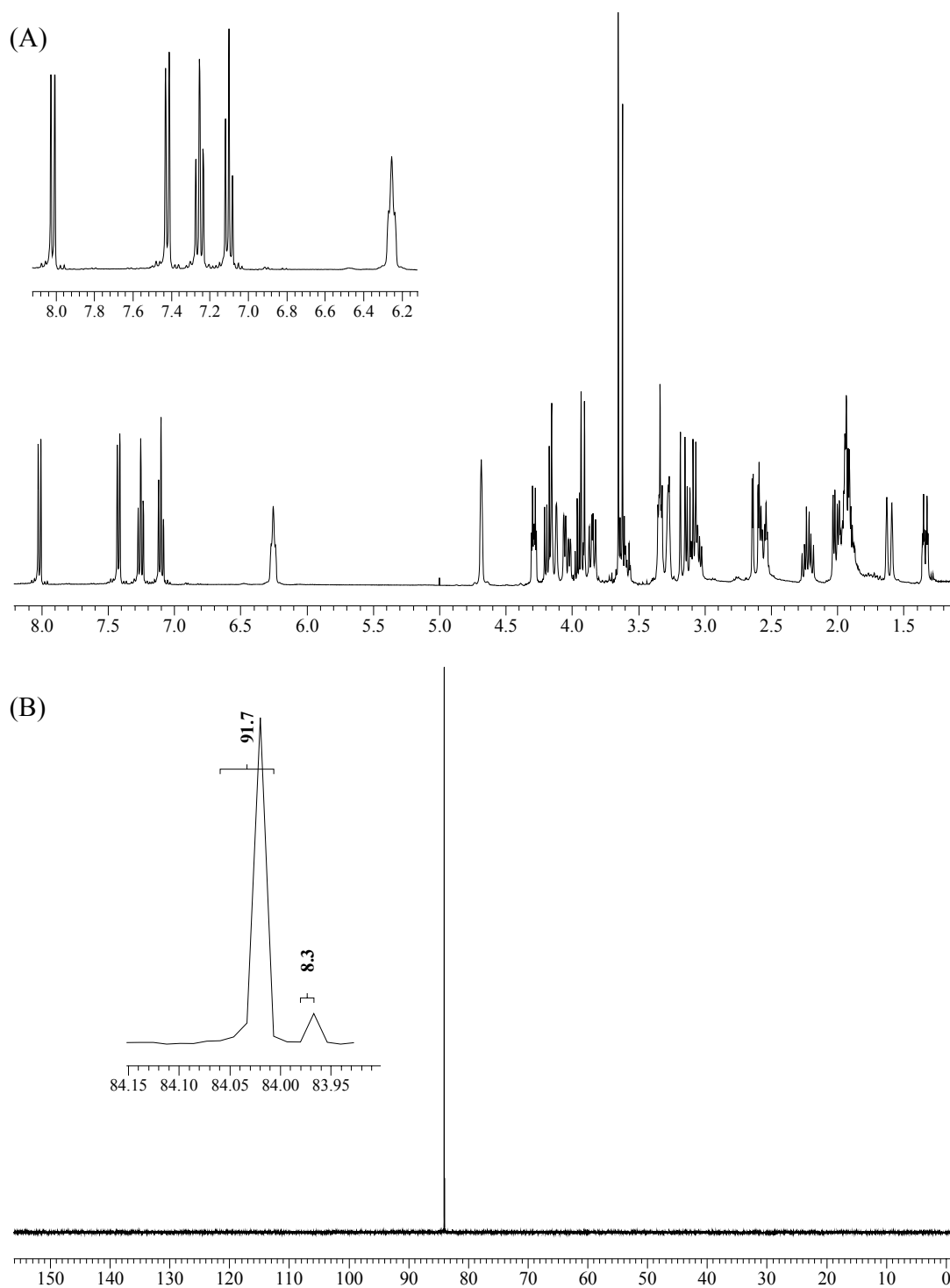
Figure 7.21. (A) ^{1}H and (B) ^{31}P NMR spectra of crystals (**18a**) formed from *O*-methyl (3-azopropyl) phosphonothioic acid – strychnine salts.

18b: 18b was in the mother liquor with approximate 20% **18a**.

Data for **18b** is same as **18a** except:

^{1}H NMR (CDCl$_3$): δ in phosphonothionate part: 3.62 (d, J = 13.2 Hz, 3 H), 3.33 (t, J = 6.4 Hz, 2 H).

^{31}P NMR (CDCl$_3$): δ 83.97 (s).

(A)
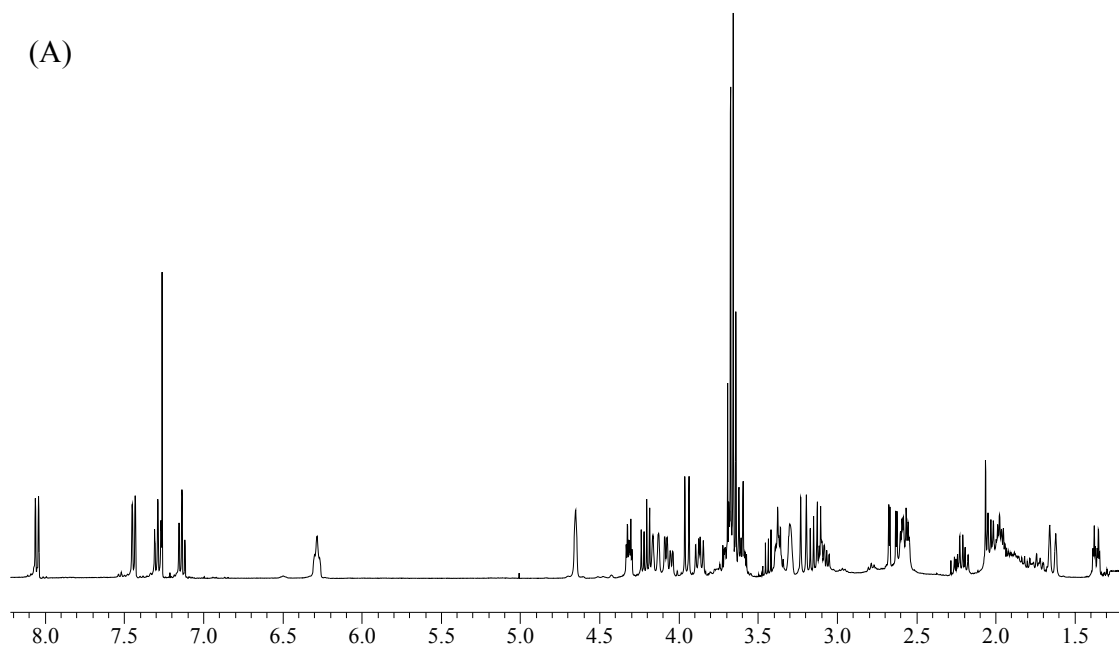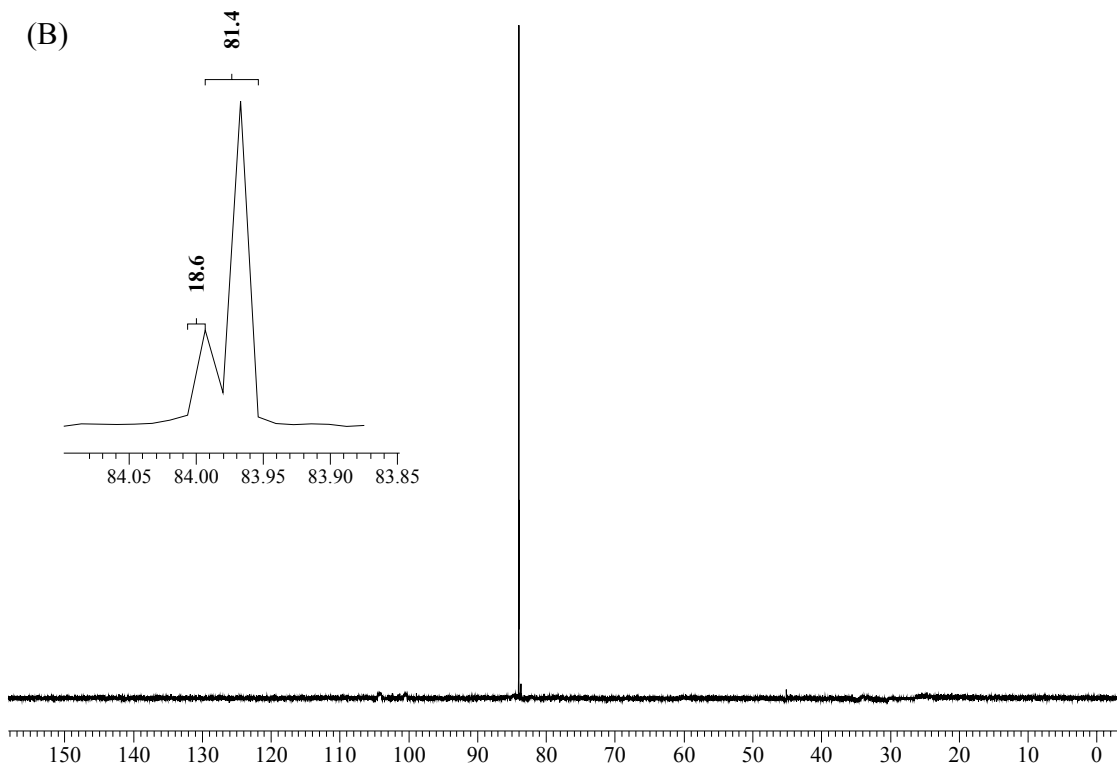
Figure 7.22. (A) ^{1}H and (B) ^{31}P NMR spectra of mother liquor (**18b**) formed from *O*-methyl (3-azopropyl) phosphonothioic acid – strychnine salts.

10 **21**
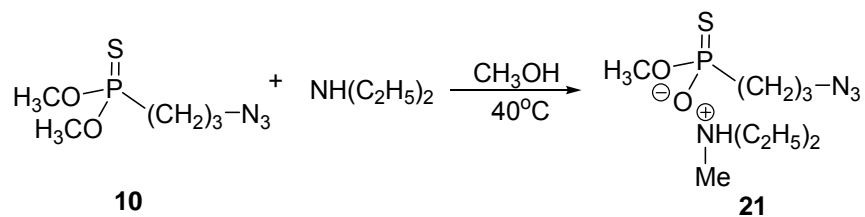
_O_-Methyl (3-azopropyl) ammonium phosphonothioic acid, ammonium salt (21). The mixture of **10** (0.53 g, 2.50 mmol) and diethylamine (1.04 mL, 10.00 mmol) in methanol (2 mL) was refluxed vigorously at 50-60 ℃ for 4 h with stirring until **10** disappeared in ^{31}P NMR. The excess diethylamine together with solvent was removed by rotary evaporation under reduced pressure to give the crude ammonium salt **21** as a viscous oil in a quantitative yield. The ammonium salt can be directly used without further purification.

^{31}P NMR (CH$_3$OH): δ 80.4 (s).
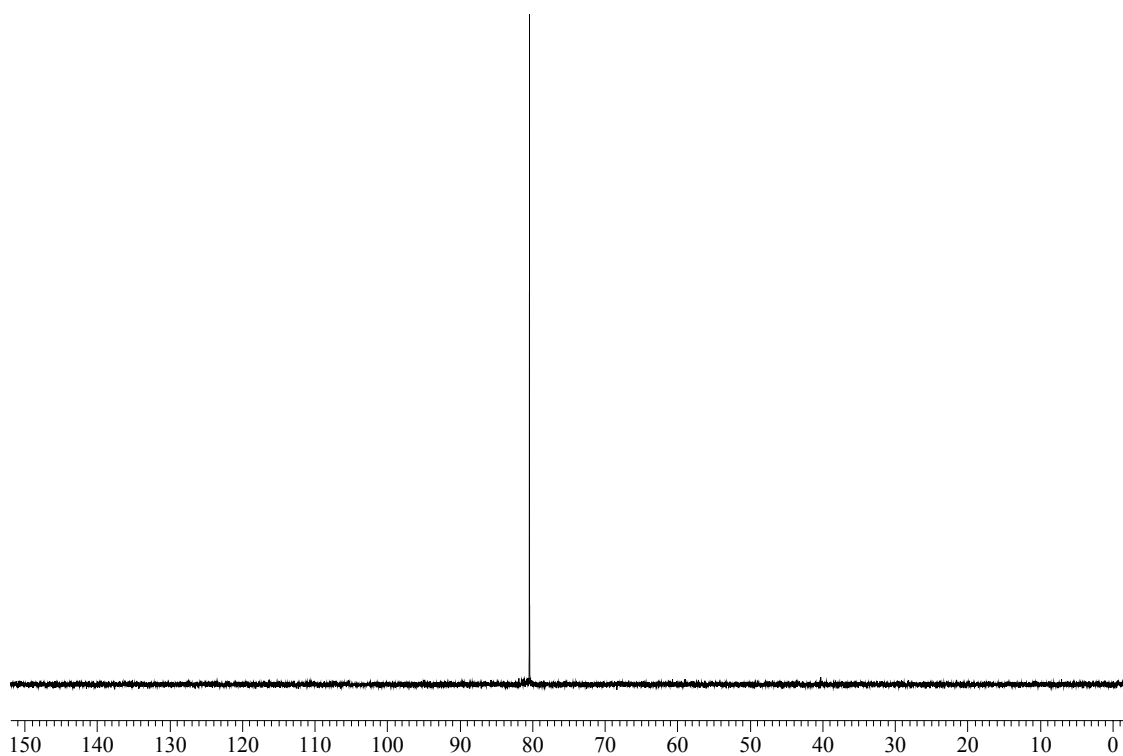
Figure 7.23. ^{31}P NMR spectrum (unlocked in methanol) of ammonium phosphonothionate **21**.

H₃CO—P(=S)(O⁻)(CH₂)₃—N₃ · ⁺NH(C₂H₅)₂ Me **21** →[POCl₃ / toluene]→ H₃CO—P(=S)(Cl)(CH₂)₃—N₃ **22**
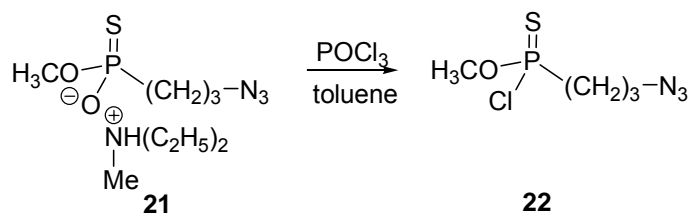
O-Methyl (3-azopropyl) phosphonochloridothionate (22). To a solution of phosphorus oxychloride (0.23 mL, 2.50 mmol) and toluene (1 mL) was added dropwise a suspension of the crude ammonium salt **21** (2.50 mmol) and toluene (1.5 mL) at rt under argon with rapid stirring. After addition, the reaction mixture was stirred at 40 ºC for 4 h, then cooled to rt and poured into cold water to consume excess phosphorous oxychloride. The organic layer was collected and dried over $MgSO_4$. Toluene was removed under reduced pressure to give the crude product **22** (0.49 g, 2.30 mmol, 92%). Further purification was performed in next step after synthesizing the stable phosphonamidothionates.

^{1}H NMR (CDCl₃): δ 2.01 (m, 2 H), 2.42-2.50 (m, 2 H), 3.43 (t, J = 6.1 Hz, 2 H), 3.83 (d, J = 12.8 Hz, 3 H).

^{31}P NMR (CDCl₃): δ 105.4 (s).
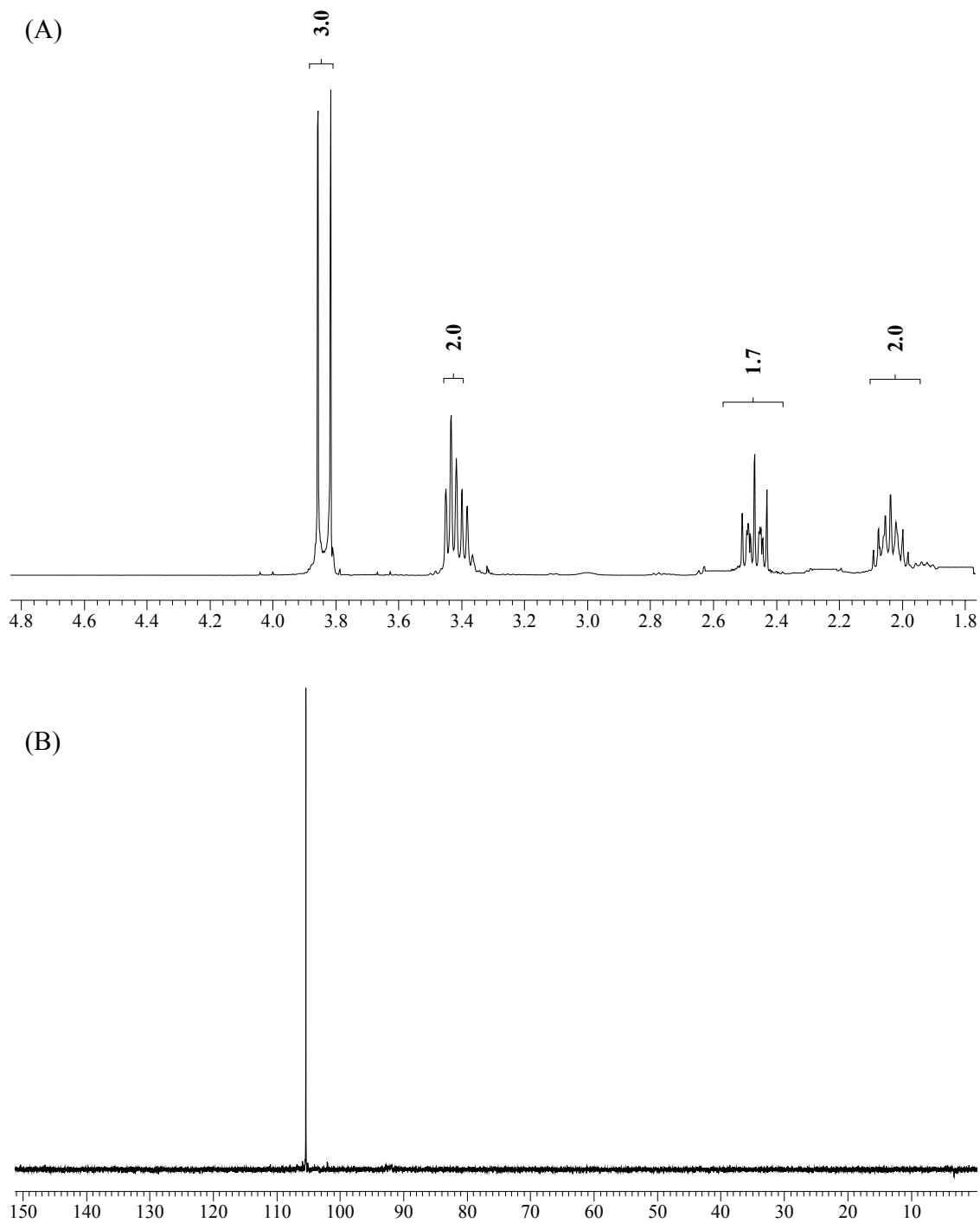
Figure 7.24. (A) ^{1}H and (B) ^{31}P NMR spectra of *O*-methyl (3-azopropyl) phosphonochloridothionate (**22**).
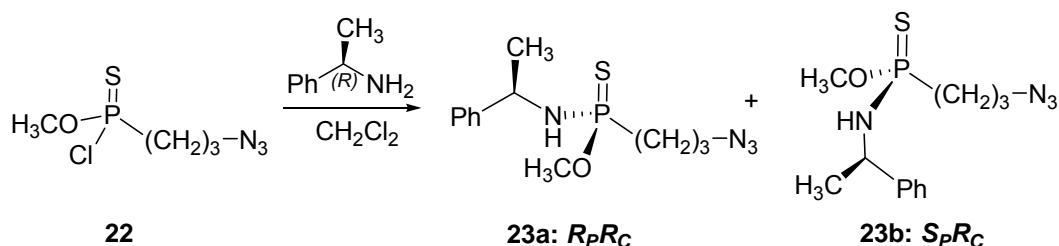
N-(1-Phenylethyl), O-methyl (3-azopropyl) phosphonamidothionate (23).

Phosphonochloridothionate **22** (0.49 g, 2.30 mmol) and (R)-(+)-methylbenzylamine (1.20 mL, 9.20 mmol) were mixed in dichloromethane (10 mL). ^{31}P NMR showed completion of the reaction after 12 h. The excess amine and solvent were removed under reduced pressure and the crude diastereomeric products **23a/23b** were purified by chromatography (1:4 ethyl ether-hexane) to give a light yellow oil (0.48 g, 1.60 mmol, 70%).

23a + **23b** (1:1):

^{1}H NMR (CDCl$_3$): δ 1.46 (d, J = 2.3 Hz, 3 H), 1.47 (d, J = 2.1 Hz, 3 H), 1.53-1.64 (m, 2 H), 1.72-1.81 (m, 2 H), 1.89-1.96 (m, 2 H), 2.00-2.07 (m, 2 H), 3.06 (q, J = 3.9 Hz, 2 H), 3.25 (d, J = 13.7 Hz, 3 H), 3.37 (q, J = 8.0 Hz, 2 H), 3.60 (d, J = 13.7 Hz, 3 H), 4.25-4.40 (m, 2 H), 7.35-7.23 (m, 10 H).

^{13}C NMR (CDCl$_3$): δ 22.7 (d, $^2J_{CP}$ = 4.2 Hz), 23.1, 25.5 (d, $^2J_{CP}$ = 7.6 Hz), 26.0 (d, $^2J_{CP}$ = 4.5 Hz), 51.8 (d, $^1J_{CP}$ = 64.1 Hz), 50.4 (d, $^2J_{CP}$ = 4.8 Hz), 50.5 (d, $^2J_{CP}$ = 4.8 Hz), 51.2 (d, $^2J_{CP}$ = 3.0 Hz), 51.3 (d, $^2J_{CP}$ = 3.0 Hz), 51.8 (d, $^2J_{CP}$ = 3.0 Hz), 52.0 (d, $^2J_{CP}$ = 3.0 Hz), 125.7, 127.4, 127.5, 128.6, 128.7, 144.6 (d, $^3J_{CP}$ = 3.0 Hz).

^{31}P NMR (CDCl$_3$): δ 88.93 (s), 88.76 (s).

(A)

(B)

202

(C)
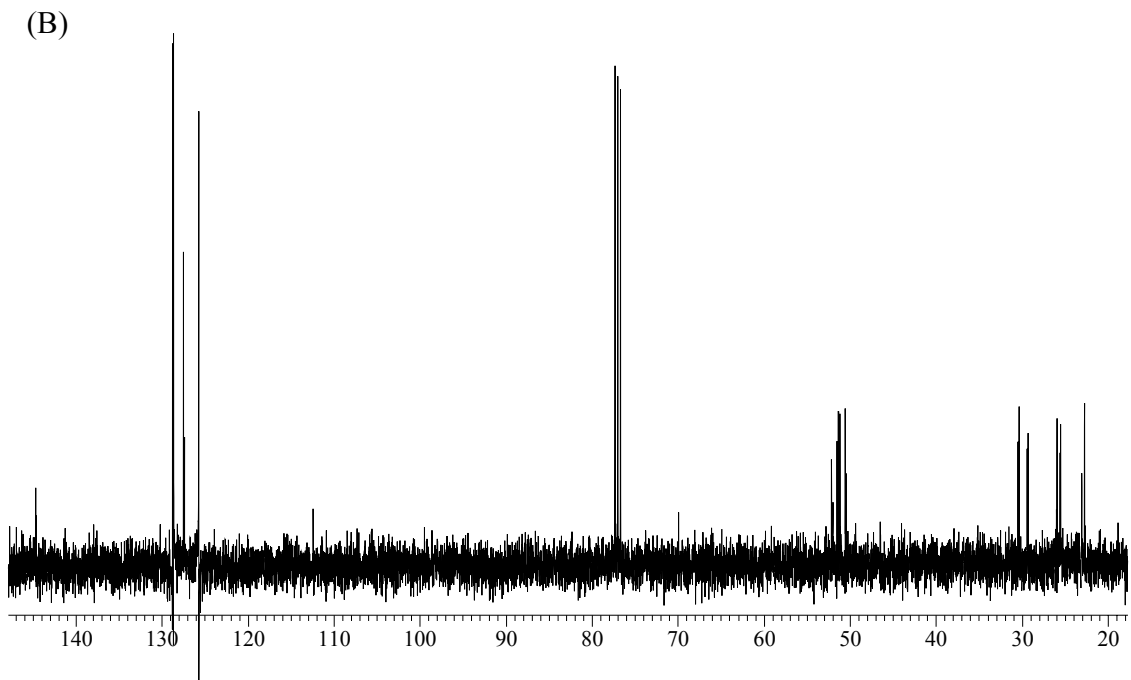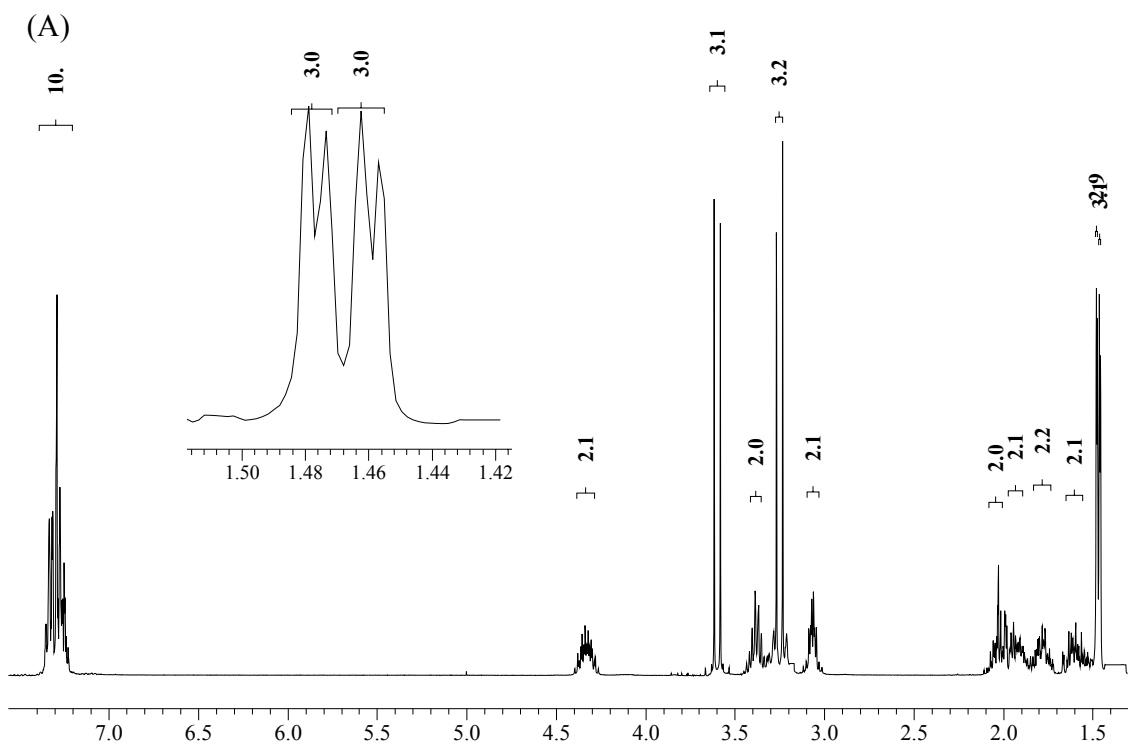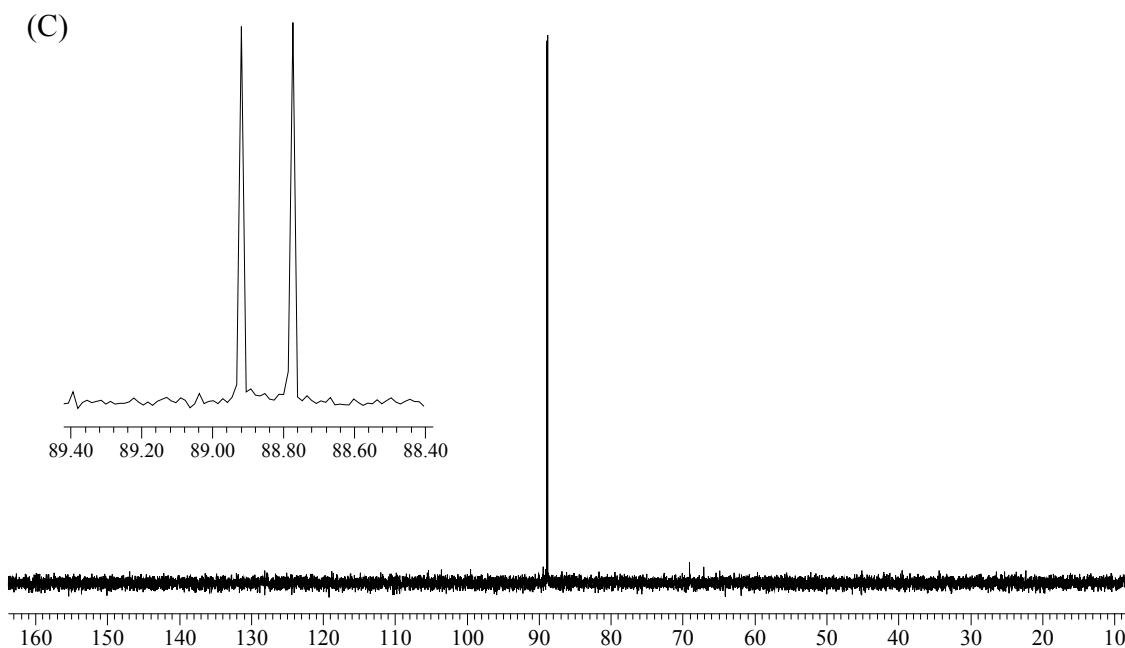
Figure 7.25. (A) ^{1}H, (B) ^{13}C and (C) ^{31}P NMR spectra of N-(1-phenylethyl), O-methyl (3-azopropyl) phosphonamidothionate (**23**).

Attempted separation of **23a** and **23b**: Separation of phosphonamidothionates **23a** and **23b** was attempted by a flash chromatography, however, separation was not obtained. The first fraction collected after chromatography showed approximately **24a**:**24b** = 3:1 and the last fraction collected contained approximately **24a**:**24b** = 1:4. As a result, diastereomers' separation would be attempted after dealkylation in the next step because the *S*-alkylated phosphonamidothiolates would be expected to differ on silica gel more easily than phosphonamidothionates because of greater bonding between the P=O and the silica surface.
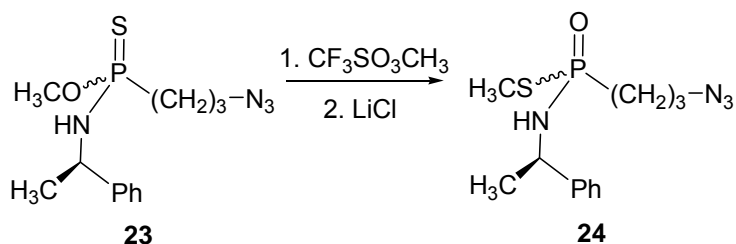
S-methyl-P-(3-azopropyl)-N-[(1R)-1-phenylethyl] phosphonamidothiolate

(24). Method A.

N-(1-Phenylethyl), *O*-methyl (3-azopropyl) phosphonamidothionate **23** (0.11 g, 0.37 mmol) and methyl triflate (0.050 mL, 0.37 mmol) were mixed in dichloromethane (2 mL) under argon at rt. ^{31}P NMR showed completion of reaction after 12 h. The reaction mixture was dried under reduced pressure and the resulting salt was dissolved in acetone (2 mL), followed with lithium chloride (0.015 g, 0.37 mmol). The reaction was complete in 12 h according to TLC (10% methanol in chloroform) with DBQ staining. The solution was concentrated and purified by chromatography (1:20 methanol-chloroform) to give a crude diastereomeric mixture of **24** (0.10 g, 0.33 mmol) in 91% yield and a diastereomeric ratio of 50:50.

For spectral data, see Method B.

S atom double-bonded to P; H₃CO and HN substituents; (CH₂)₃—N₃ chain

$$\text{23} \quad + \quad CH_3I \quad \xrightarrow{45^oC} \quad \text{24}$$

23   **24**
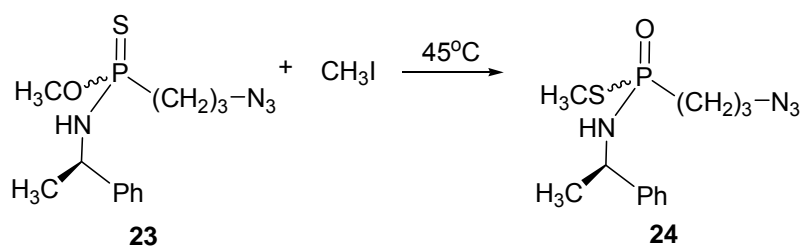
_S_-methyl-_P_-(3-azopropyl)-N-[(1_R_)-1-phenylethyl] phosphonamidothiolate

(24). Method B.

Phosphonamidothiolate (24) was also prepared by alkylation-dealkylation.

Methyl iodide (2 mL, 32.00 mmol) was added to phosphonamidothiolate 23 (0.30 g, 1.00

mmol). The reaction mixture was refluxed for 4 d until the TLC analysis or ^{31}P NMR

showed a complete conversion. The solution was concentrated under reduced pressure

and the crude product was purified by chromatography (1:50 methanol-chloroform) to

give a diastereomeric mixture of **24a** and **24b** (0.23 g, 0.77 mmol) in 77% yield as an

equal population of diastereomers, 50:50.

^{1}H NMR (CDCl₃): δ 1.50 (d, _J_ = 6.7 Hz, 1.5 H), 1.52 (d, _J_ = 6.7 Hz, 1.5 H), 1.75

(m, 2 H), 1.89 (m, 2 H), 2.15 (d, _J_ = 12.6 Hz, 3 H), 3.20 (t, _J_ = 9.1 Hz, 1 H), 3.32 (t, _J_ =

6.5 Hz, 2 H), 4.46-4.56 (m, 1 H), 7.23-7.33 (m, 5 H).

^{31}P NMR (CDCl₃): δ 49.5 (s), 50.9 (s).

(A)

(B)
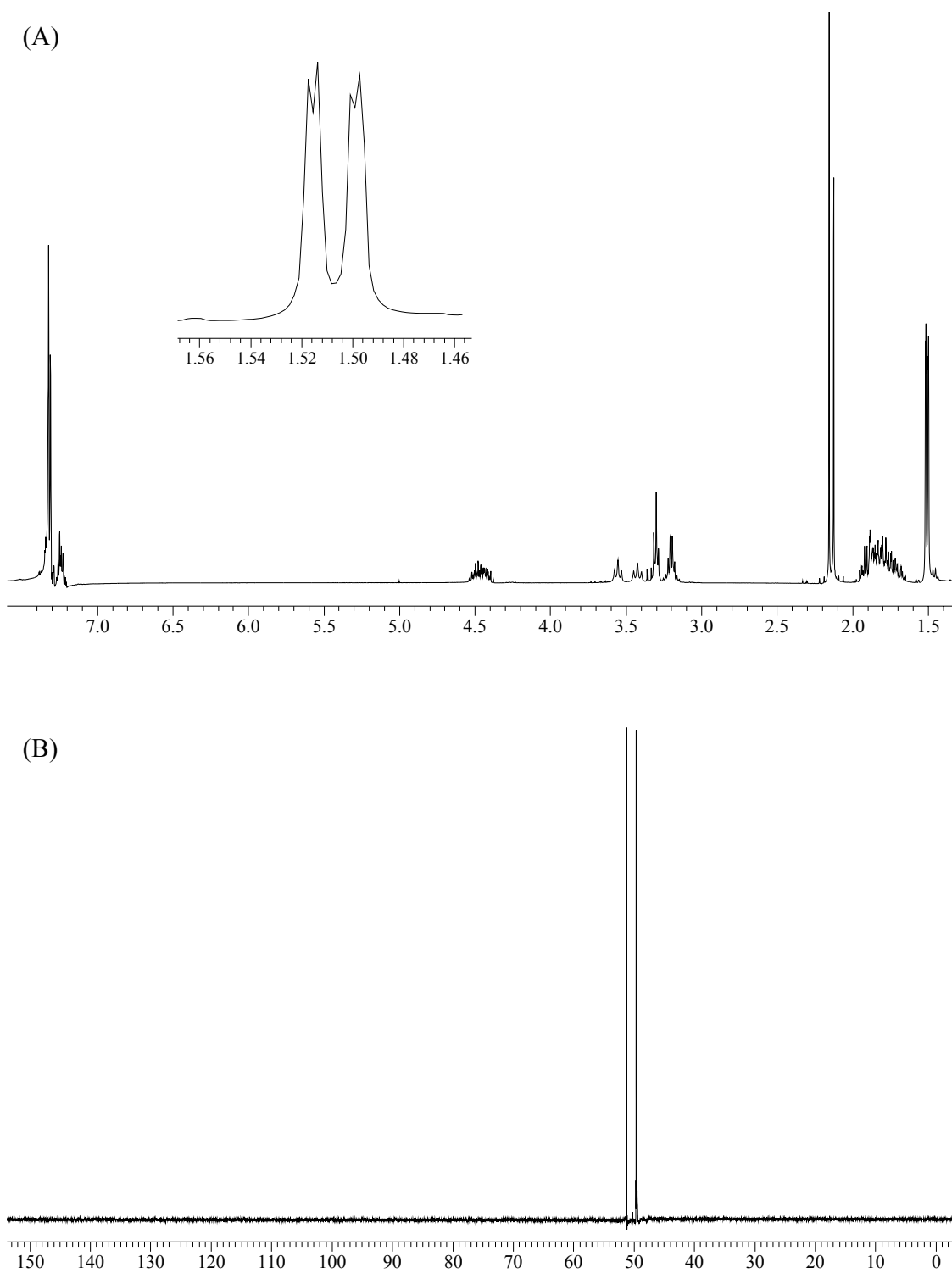
Figure 7.26. (A) ^{1}H and (B) ^{31}P NMR spectra of phosphonamidothiolate (**24**).
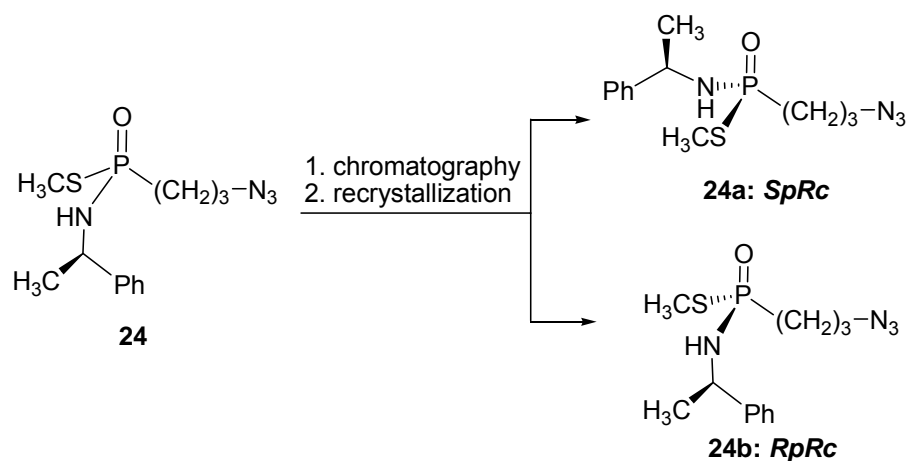
Diastereomers of phosphonamidothiolate 24: *SpRc* (24a) and *RpRc* (24b).

The diastereomeric mixture of **24a** and **24b** was separated by a gradient chromatography (from 1:100 to 1:40 methanol-chloroform) and pure fractions of the two diastereomers were collected and concentrated. The first diastereomer after chromatography (**24a**) was dissolved in warm ethyl ether and crystallized as needle-like crystals. The second diastereomer after chromatography (**24b**) was dissolved in methanol-ethyl ether (1:20) and crystallized as a colorless needle-like crystals. Both crystals were subsequently recrystallized prior to diffraction analysis.

High resolution MS (ESI-TOF): Calcd for $C_{12}H_{20}N_4OPS$ (M+H) 299.1095; found 299.1093.

Anal. Calcd for $C_{12}H_{19}N_4OPS$: C 48.31, H 6.42, N 18.78; found: C 48.30, H 6.44, N 18.68.

SpRc (24a):

mp: 95.5 - 95.8 ºC.

$[\alpha]_D^{20}$ = +23.6º (c = 1.40 g/100 mL, CHCl$_3$).

^{1}H NMR (CDCl$_3$): δ 1.53 (d, J = 6.7 Hz, 3 H), 1.85 (m, 2 H), 1.94 (m, 2 H), 2.17 (d, J = 12.6 Hz, 3 H), 3.22 (t, J = 9.1 Hz, 1 H), 3.32 (t, J = 6.5 Hz, 2 H), 4.46-4.56 (m, 1 H), 7.23-7.33 (m, 5 H).

^{13}C NMR (CDCl$_3$): δ 11.2 (d, $^2J_{CP}$ = 3.1 Hz), 22.5 (d, $^2J_{CP}$ = 4.6 Hz), 25.2 (d, $^2J_{CP}$ = 4.6 Hz), 30.3 (d, $^1J_{CP}$ = 96.1 Hz), 50.6, 51.4 (d, $^3J_{CP}$ = 18.4 Hz), 126.0, 127.3, 128.6, 144.6 (d, $^3J_{CP}$ = 4.6 Hz).

^{31}P NMR (CDCl$_3$): δ 49.5 (s).

(A)
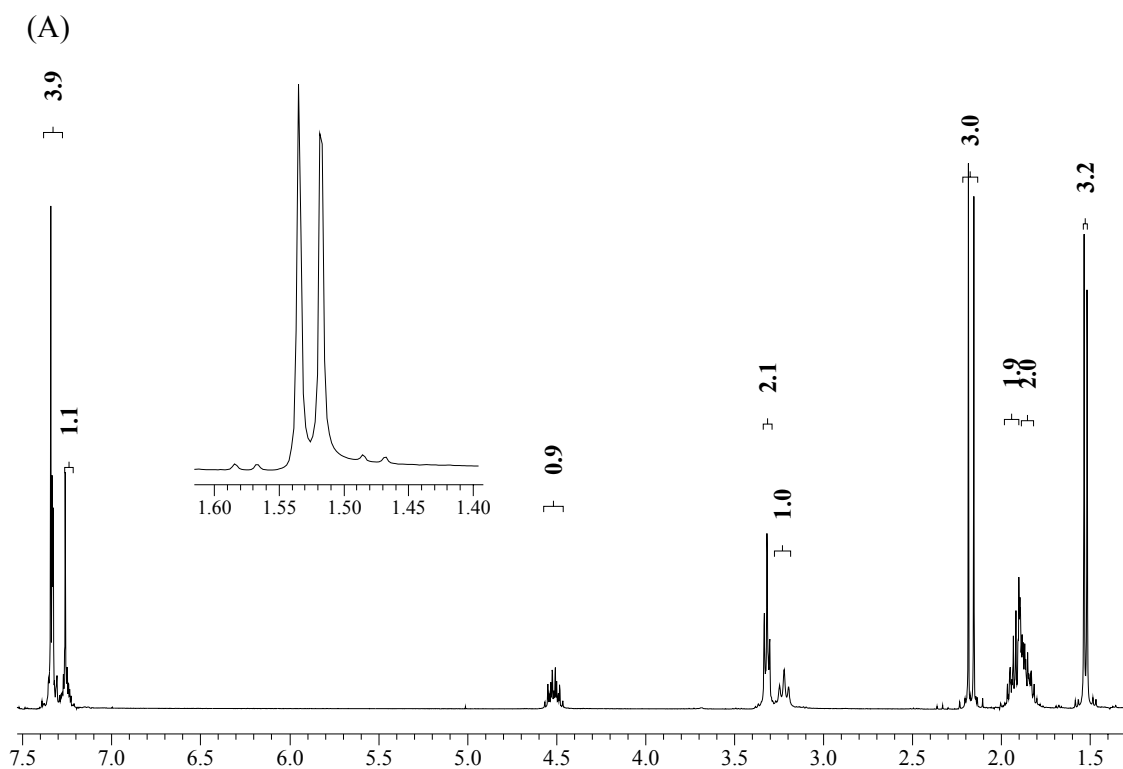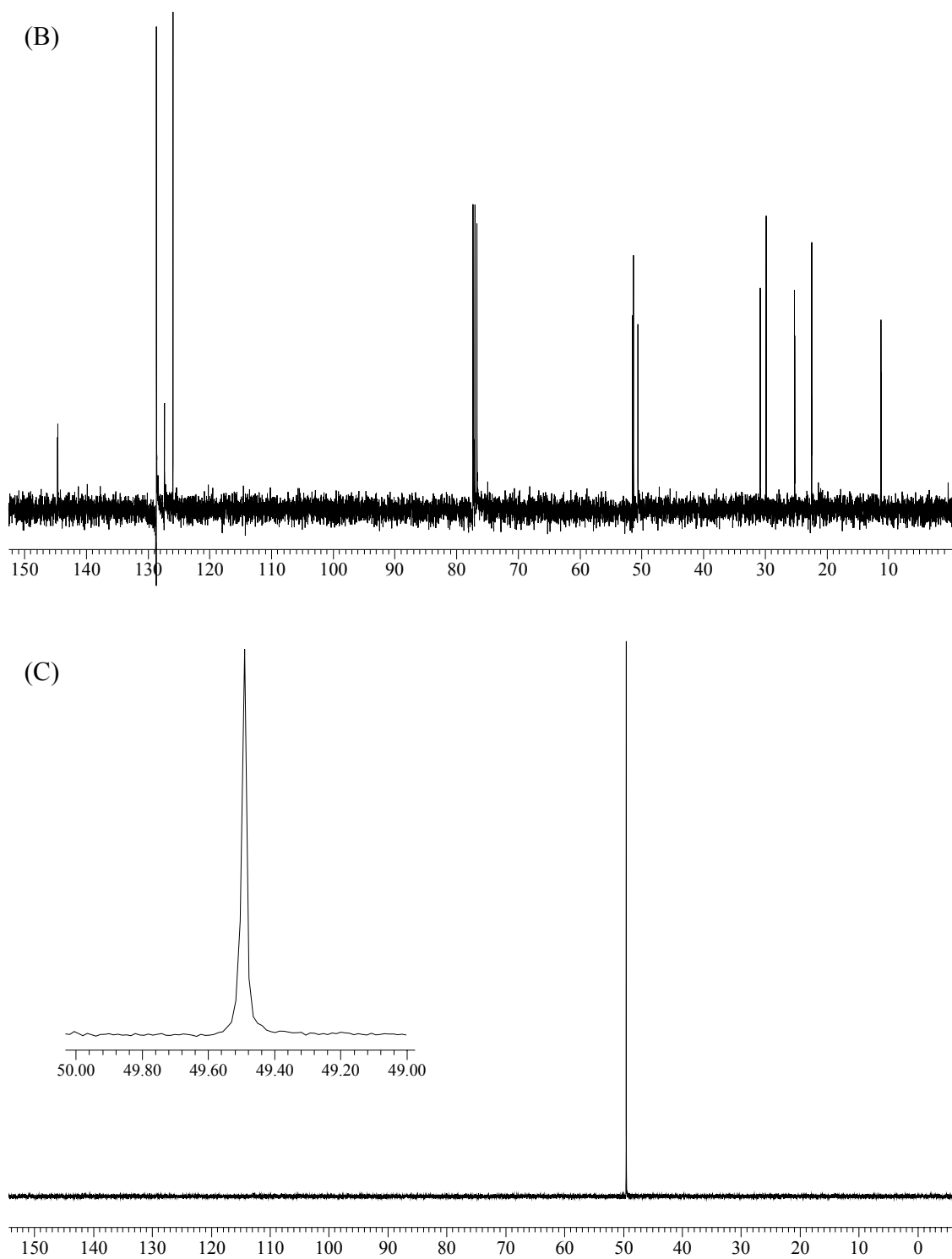
Figure 7.27. (A) ^{1}H, (B) ^{13}C and (C) ^{31}P NMR spectra of phosphonamidothiolate **24a**.

_Rp_R_c (24b):

mp 88.5 - 88.8 ºC.

$[\alpha]_D^{20}$ = +60.1º (c = 1.04 g/100 mL, CHCl$_3$).

^{1}H NMR (CDCl$_3$): δ 1.54 (d, J = 6.7 Hz, 3 H), 1.75 (m, 2 H), 1.86 (m, 2 H), 2.18 (d, J = 12.6 Hz, 3 H), 3.25 (t, J = 9.1 Hz, 1 H), 3.33 (t, J = 6.5 Hz, 2 H), 4.48-4.58 (m, 1 H), 7.24-7.35 (m, 5 H).

^{13}C NMR (CDCl$_3$): δ 11.0 (d, $^2J_{CP}$ = 3.0 Hz), 22.1 (d, $^2J_{CP}$ = 4.6 Hz), 25.8 (d, $^2J_{CP}$ = 6.1 Hz), 30.2 (d, $^1J_{CP}$ = 94.6 Hz), 51.2, 51.4 (d, $^3J_{CP}$ = 16.8 Hz), 126.0, 127.5, 128.7, 144.5 (d, $^3J_{CP}$ = 4.6 Hz).

^{31}P NMR (CDCl$_3$): δ 50.9 (s).

(A)
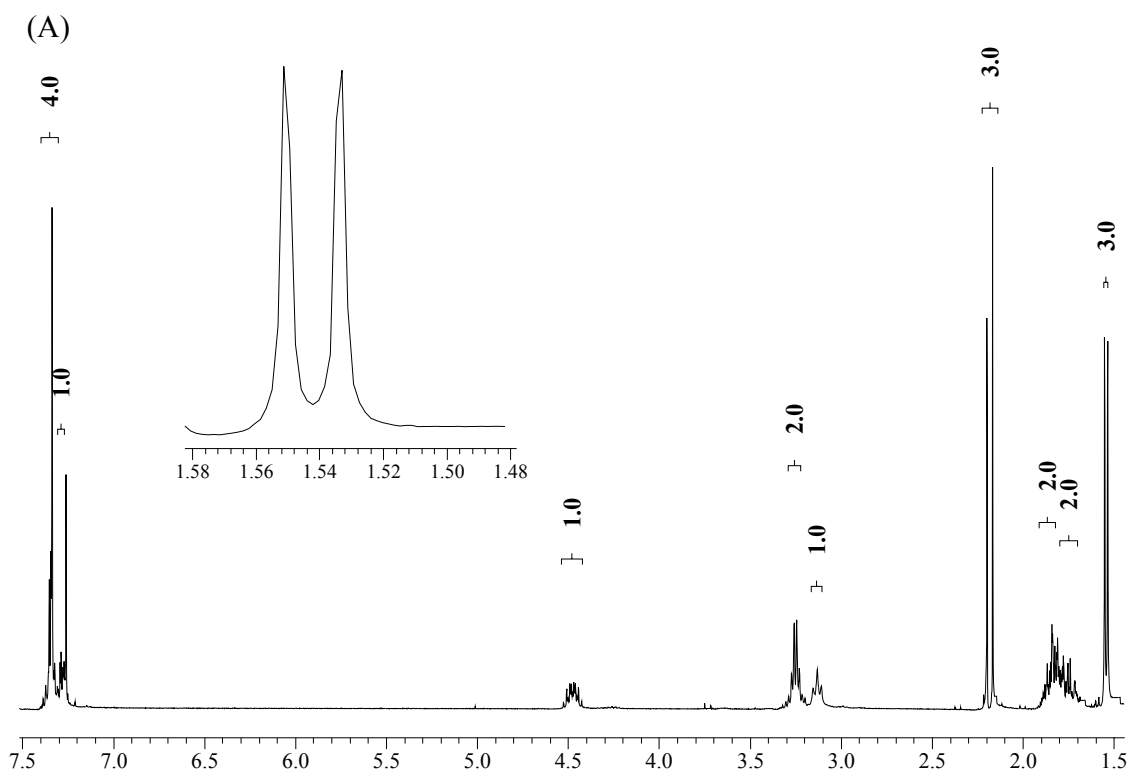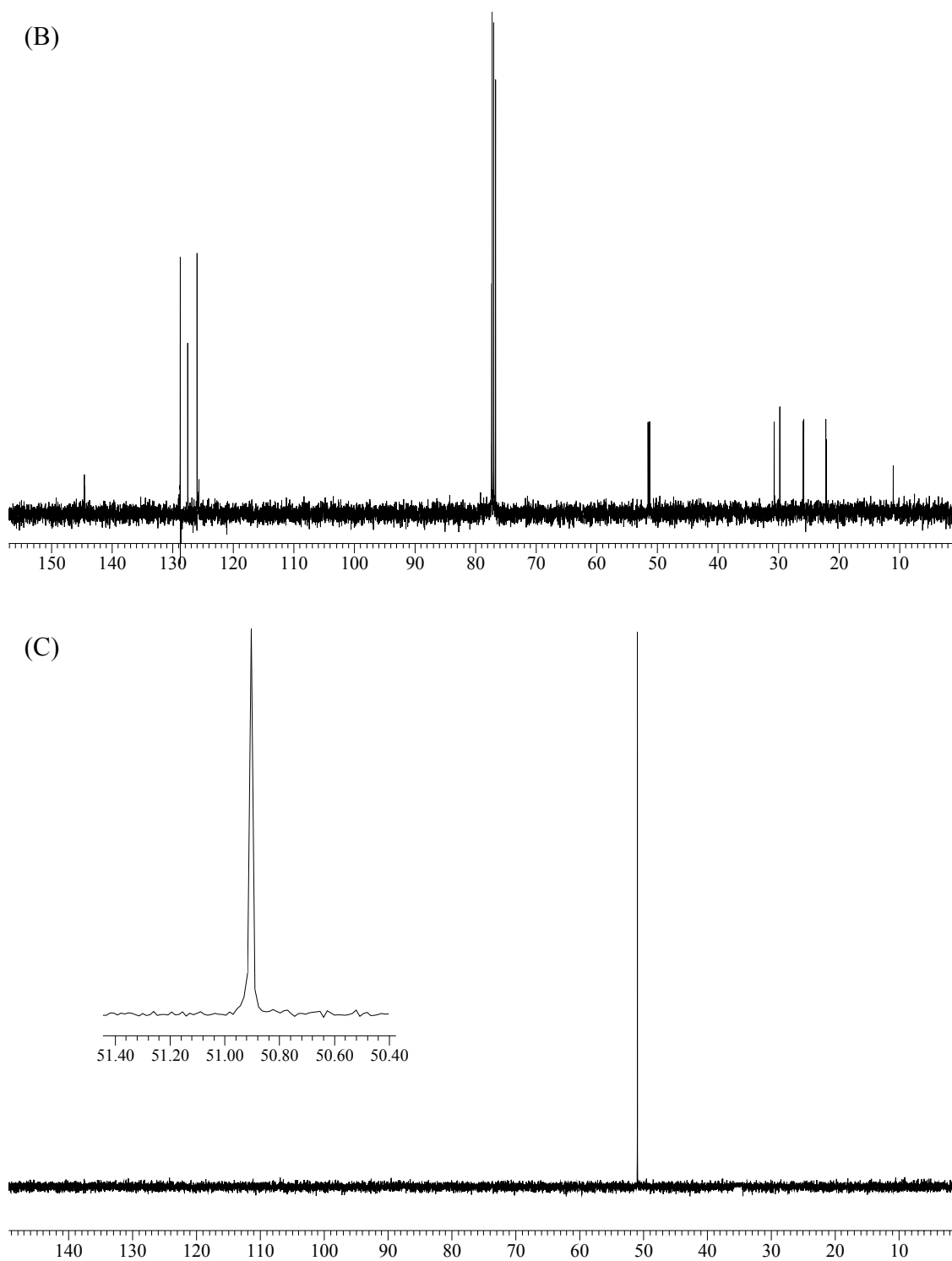
Figure 7.28. (A) ^{1}H, (B) ^{13}C and (C) ^{31}P NMR spectra of phosphonamidothiolate **24b**.

24a: *SpRc*

25a: *Sp*

24b: *RpRc*

25b: *Rp*
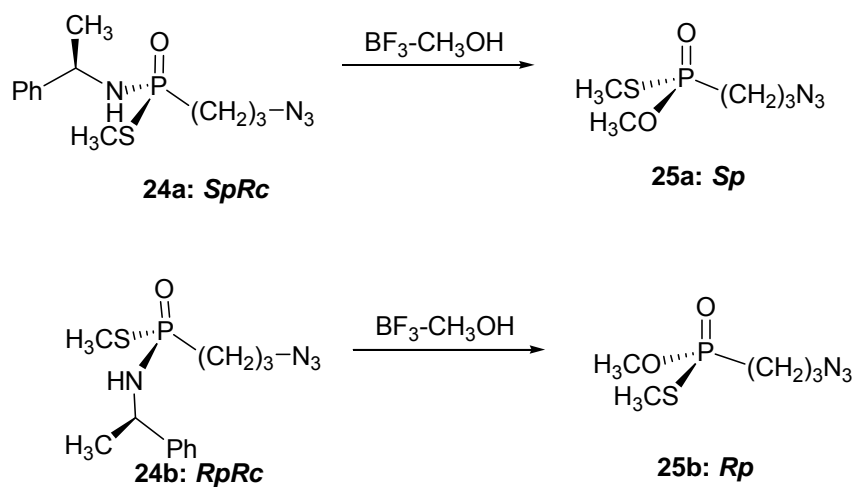
***O,S*-Dimethyl (3-azopropyl) phosphonothiolate (25a/25b).**

Methanolysis of phosphonamidothiolates **24a/24b** was achieved by boron

trifluoride-methanol complex (Ryu, 1991). To an oven-dried flask under an argon

atmosphere was added 0.50 mmol of phosphonamidothioate (**24a** or **24b**, 0.15 g) in 1 mL

of anhydrous methanol. The solution was stirred at 0 ºC for 20 min, at which point BF_3-

MeOH complex (5.00 mmol) was added dropwise over 5 min. The temperature was

maintained for 1 h and then stirred at rt overnight. The reaction mixture was added

dropwise to a saturated solution of sodium bicarbonate (10 mL) and extracted twice with

ethyl ether (2 x 10 mL). The ethyl ether extracts were combined, washed with saturated

sodium bicarbonate and brine, and dried over sodium sulfate. Filtration, evaporation, and

chromatography (1:40 methanol-chloroform) afforded the product (0.052 g, 0.25 mmol).

25a: $[\alpha]_D^{20}$ = -48.4º (c = 0.95 g/100 mL, $CHCl_3$).

25b: $[\alpha]_D^{20}$ = +48.4º (c = 0.62 g/100 mL, $CHCl_3$).

^{1}H NMR (CDCl$_3$): δ 1.92 (m, 2 H), 2.02 (m, 2 H), 2.26 (d, $^3J_{PH}$ = 12.5 Hz, 3 H), 3.38 (t, J = 6.5 Hz, 2 H), 3.73 (d, $^3J_{PH}$ = 12.5 Hz, 3 H).

^{13}C NMR (CDCl$_3$): δ 12.0 (d, $^2J_{CP}$ = 3.1 Hz), 22.0 (d, $^2J_{CP}$ = 4.7 Hz), 28.9 (d, $^1J_{CP}$ = 110.1 Hz), 51.2 (d, $^3J_{CP}$ = 7.8 Hz), 51.4 (d, $^2J_{CP}$ = 6.4 Hz).

^{31}P NMR (CDCl$_3$): δ 59.5 (s).

(A)
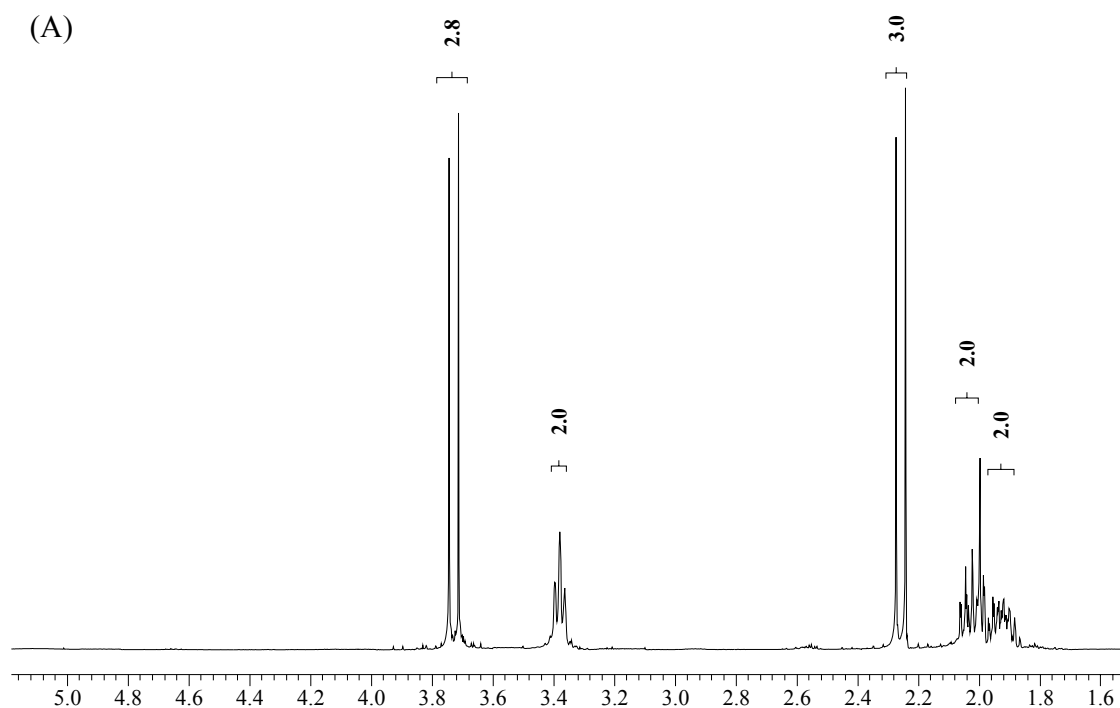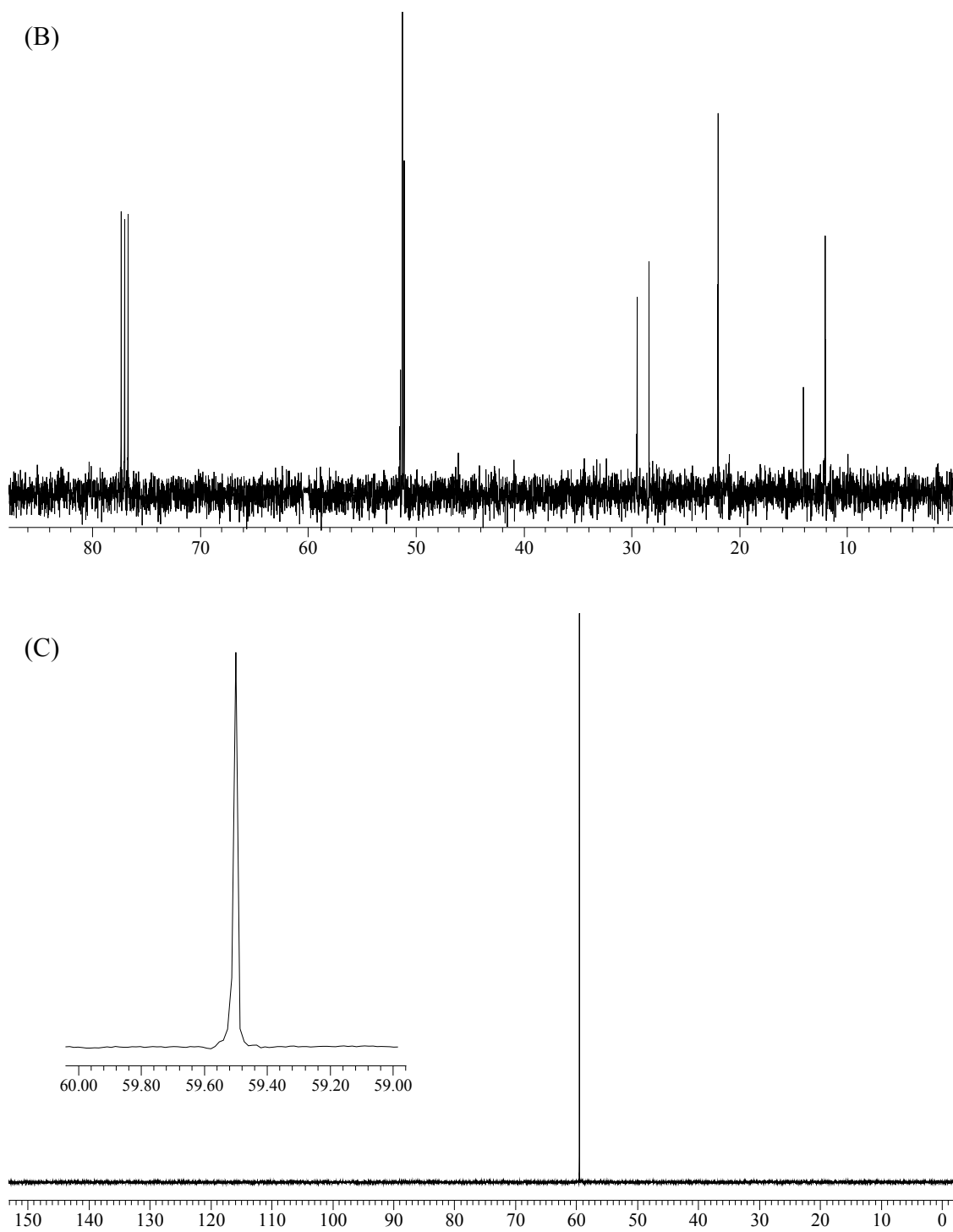
Figure 7.29. (A) ^{1}H, (B) ^{13}C and (C) ^{31}P NMR spectra of *O,S*-dimethyl (3-azopropyl) phosphonothiolate (**25**).
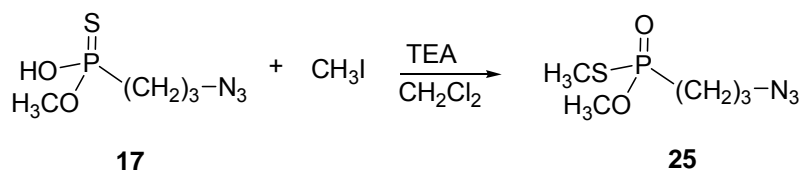
The racemate of *O,S*-dimethyl (3-azopropyl) phosphonothiolate (25) from *O*-methyl (3-azopropyl) phosphonothioic acid (17).

To a solution of compound **17** (0.19 g, 1.00 mmol) in dichloromethane (2 mL), triethylamine (TEA, 0.20 mL) was added, followed with methyl iodide (0.10 mL). The reaction mixture was stirred at rt under argon for 1 h until the ^{31}P NMR spectrum did not contain the peak of the starting material. After evaporation under vacuum, compound **25** was obtained as a yellow oil (quantitative yield).

The spectral data of compound **25** is same as enantiopure isomers, **25a** and **25b**.
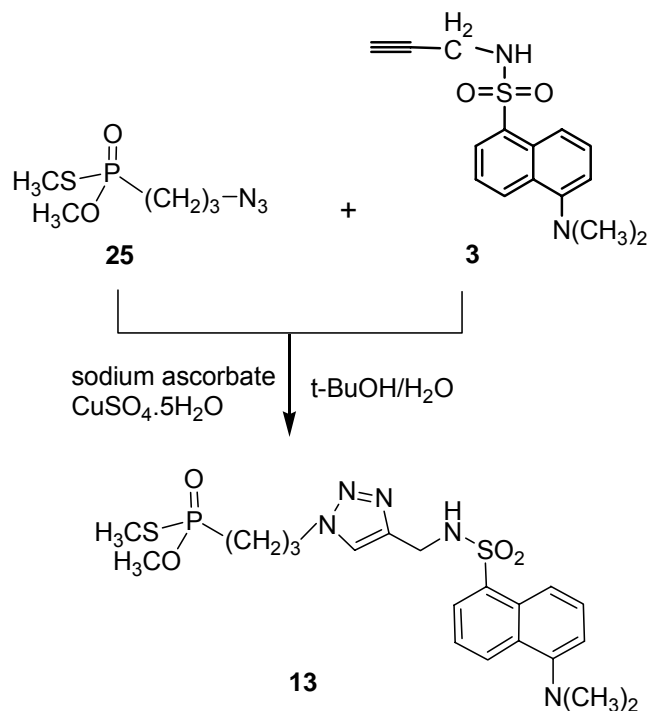
The racemate of dansyl-linked *O*, *S*-dimethyl phosphonate (13) synthesized by click chemistry from the racemate of *O,S*-dimethyl (3-azopropyl) phosphonothiolate (25).

Phosphonothiolate **25** (0.14 g, 0.67 mmol) and dansyl sulfonamide **3** (0.20 g, 0.67 mmol) were suspended in a 1:1 mixture of water and *tert*-butyl alcohol (5 mL total) under argon. Sodium ascorbate (0.067 mmol, 0.67 mL of freshly prepared 0.1 M solution in water) was added, followed by copper (II) sulfate pentahydrate solution (0.0067 mmol, 0.67 mL of 0.01 M solution in water). The heterogeneous mixture was stirred vigorously for 4 h, at which point it cleared and TLC analysis indicated complete consumption of the reactants. Water (3 mL) and ethyl acetate (6 mL) were added and the organic layer was washed with water, collected and dried over anhydrous $MgSO_4$. Evaporation under

reduced pressure and purification by flash chromatography using silica (1:40 methanol-chloroform) gave 0.22 g (0.44 mmol, 66%) of pure product as a yellow oil.

For NMR spectral, see the synthesis of compound **13** from compound **12**.

7.3 X-ray Crystallography Analysis

In an effort to assign the absolute configuration of the carbon and phosphorus stereocenters of the resolved diastereomers **24a/24b**, x-ray crystallographic analysis was desired.

X-ray analysis of **24a**: The suitable crystal was selected, attached to a glass fiber and data were collected at 90(2) K using a Bruker/Siemens SMART APEX instrument (Mo Kα radiation, λ = 0.71073 Å) equipped with a Cryocool NeverIce low temperature device (performed by Prof. Twamley in the University of Idaho). Data were measured using omega scans 0.3 ° per frame for 5 seconds, and a full sphere of data was collected. A total of 2400 frames were collected with a final resolution of 0.77 Å. Cell parameters were retrieved using SMART (v. 5.632, Bruker AXS, Madison, WI, 2005**)** software and refined using SAINTPlus (v. 7.23a, Data Reduction and Correction Program, Bruker AXS, Madison, WI, 2004) on all observed reflections. Data reduction and correction for Lp and decay were performed using the SAINTPlus software. Absorption corrections were applied using SADABS (v.2007/4, an empirical absorption correction program, Bruker AXS Inc., Madison, WI, 2007). The structure was solved by direct methods and refined by least squares method on F^2 using the SHELXTL program package (v. 6.14, Structure Determination Software Suite, Sheldrick, G.M., Bruker AXS Inc., Madison, WI, 2004). The structure was solved in the space group P2(1)2(1)2(1) (# 19) by analysis of systematic absences. All non-hydrogen atoms were refined anisotropically. Stereochemistry assignment: C9, R; P1, S. No decomposition was observed during data collection.

X-ray analysis of **24b**: Similar experimental procedures for **24b** showed stereochemistry assignment: C9, R; P1, R.

7.4 Kinetic Analysis

Each organophosphorus compound synthesized as irreversible inhibitor of the active site of acetylcholinesterases was studied and the kinetic parameter was determined. As previously described (Section 2.5), a concentration-dependent method was primarily used for measuring the bimolecular inhibition constant k_i, K_D and k_p:

$$\frac{1}{[i]} = \left(\frac{\Delta t}{\Delta \ln v}\right)k_i - \frac{1}{K_D} \qquad (7.1)$$

in which v represents the relative velocity. In the concentration-dependent method, v is the relative activity of AChE with no inhibitor to AChE with an inhibitor under same conditions.

The potency of chromophores prepared as potential reversible inhibitors of AChEs was also determined. By measuring the inactivation percentage with a concentration-dependent method, IC_{50} of each chromophore was determined by plotting with Kaleidagraph 3.6 (Synergy Software, Reading, PA) and the inhibition constant K_i was deduced from Lineweaver-Burk plot.

In order to measure the activity of AChE (A), a colorimetric assay originally developed by Ellman et al. (Ellman, 1961) was utilized. In this method, acetylthiocholine iodide (ATCh-I) is used as the substrate for AChE instead of ACh. The determination of AChE activity is dependent upon the enzyme-catalyzed hydrolysis of ATCh-I and the subsequent thiocholine-mediated reaction with 5,5'-dithiobis-2-nitrobenzoic acid (DTNB), a chromogen, to yield a chromophore whose absorbance is measured spectrophotometrically at 412 nm. The rate at which the absorbance is generated is proportional to the enzyme's rate of hydrolysis.

7.4.1 Materials

Chemicals in the enzyme assay were commercially obtained as follows: Acetylthiocholine iodide (ATCh-I), 5,5'-dithio(2-nitrobenzoic acid) (DTNB), paraoxon, pyridine-2-aldoxime methiodide (2-PAM), EEAChE type V-S, and recombinant human AChE, Aldrich and Sigma Chemical Company (Milwaukee, WI). Soluble recombinant mouse AChE was expressed in HEK 293 cells and purified by affinity chromatography as described in Section 7.2 (Marchot, 1996).

Phosphate buffer solution (0.1 M, pH7.6) was prepared in distilled deionized water.

A Beckman DU-7500 diode-array spectrophotometer was used to measure rates, which is the changes in absorbance against real time.

7.4.2 Enzyme and Tissue Preparation

Recombinant Mouse AChE. rMAChE was truncated at its carboxyl-terminal end by the insertion of an early stop codon at position 549. This modification allowed the enzyme to be expressed into the extra-cellular medium as the deleted residues undergo post-translational modifications, including glycosylation, which dictated their association with the cell membrane. Soluble recombinant mouse AChE was expressed in HEK 293 cells and purified by a meta-inhibitor resin chromatography (Marchot, 1996; Bourne, 1999).

The modifications on the enzyme have been demonstrated to have a negligible effect on the enzymes activity and specificity relative to the native enzyme. It has been shown that this lack of glycosylation decreases the stability of the expressed AChE

(Velan, 1993). Our experiments with rMAChE verified these observations of thermal and organic solvent stability.

Consequently, prior to use of rMAChE was stored at -20 ºC with concentration of 1 mg/mL and data collecting time of all kinetic analysis was controlled within less than 30 min. Studies that required an incubation period greater than 30 min were conducted at 0-4 ºC. The highest final concentration of organic solvent used to dissolve inhibitors present in all experiments was less than 0.5%, and the control experiment in each assay contained the same amount of solvent as was present in the inhibited samples.

Stock solutions of rMAChE were prepared by diluting 0.1 mL of the purified enzyme (1 mg/mL) to a final volume of 10 mL in 0.1 M Phosphate Buffer Solution (PBS, pH = 7.6) and were stored at 4 ºC. Working solutions were prepared as needed by diluting the necessary amount of stock solution in 0.1 M PBS (pH = 7.6) to achieve desired activity. In most cases in our study, the working concentration of rMAChE is approximately 0.25 μg/mL. Activity of the working solution might be attenuated from time to time such that the optical density of the experiment is suitable for the detection of the spectroscopic device used to monitor the inhibition course.

Electric Eel AChE. EEAChE (type V-S, lyophilized powder) was obtained from Sigma-Aldrich without any further purification. Gel electrophoresis and Western blotting experiments demonstrated the presence of contaminants in the commercially available preparations of EEAChE. Despite these observations, it was found that this enzyme is relatively robust to both thermal extremes and solvent effects and consistently provides

reproducible results. These factors combined with the availability of this source have made it the enzyme of choice for conducting most preliminary studies.

Stock solutions of EEAChE were prepared by dissolving 5 mg (5000 units) in 10 mL of 0.1 M PBS with pH 7.6 and kept on ice. Working solutions of EEAChE were prepared by diluting a certain amount of stock solution to about 1 unit/mL in most cases. All studies were conducted in 0.1 M PBS with pH 7.6 at 20 ºC. These pH and temperature conditions were chosen for all assays to facilitate comparisons with work on various types of AChEs.

Human Recombinant AChE. rHAChE was obtained from Aldrich without any further purification. Stock solutions of rHAChE were prepared by dissolving 1 mg (2000 units) in 1 mL of 0.1 M PBS with pH 7.6 and kept on ice. Working solutions of rHAChE were prepared by diluting a certain amount of stock solution to about 1 unit/mL in most cases. All studies were conducted in 0.1 M PBS with pH 7.6 at 20 ºC.

7.4.3   Methods for Irreversible OP Inhibitors

As discussed in section 2.5, the inhibition potency of organophosphorus compounds is generally evaluated by kinetic parameters, k_i, K_D, and k_p, in which k_i is the bimolecular reaction constant, K_D is dissociation constant, and k_p is phosphorylation constant.

Method 1: Concentration-dependent determination of k_i, K_D, and k_p.

Since the concentration-dependent method (Ellman, 1961) affords k_i, K_D, and k_p all together, this more rigorous method was primarily used and reported.

Six cuvettes containing 480 μL of DTNB solution (1.32 mM DTNB, 59 mM

NaHCO$_3$, PBS pH 7.6) 150 μL of working solution of AChE, and 1340 μL of PBS (pH

7.6) were placed in a Beckman DU-7500 diode-array spectrophotometer and maintained

at 20 ºC. The first cuvette treated with 10 μL of the solvent to dilute the inhibitors served

as the control (A_{no}); the other 5 cuvettes were treated with 10 μL of five gradient inhibitor

concentrations (A_i). All six experiments were incubated for same period of time, 6 mins.

The remaining enzyme activity (v) was determined by adding 20 μL aliquots of the

ATCh-I solutions to the cuvette and the rate of ATCh-I hydrolysis was monitored at 412

nm over a period of 10 min (22 sec intervals). The final concentrations of the reactants

during enzyme assay were: 0.33 mM DTNB, 0.59 mM ATCh-I, and 0.58 mM NaHCO$_3$.

The bimolecular reaction constant (k_i), dissociation constant (K_D), and phosphorylation

constant (k_p) were determined using equation 7.1:

$$\frac{1}{[i]} = \left(\frac{\Delta t}{\Delta \ln v} \right) k_i - \frac{1}{K_D} \qquad (7.1)$$

Where: t = the time of inhibition (6 min),

$\ln v = \ln(A_{no}/A_i)$,

$k_p = k_i \times K_D$.

Method 2: Time-dependent determination of k_i.

Where appropriate, a time-dependent method of analysis was also applied:

$$\frac{1}{[i]} = \left(\frac{\Delta t}{\Delta \ln v}\right) k_i \qquad (7.2)$$

$$\Delta \ln v = k_i[i]\Delta t \qquad (7.3)$$

The time-dependent analysis was performed to verify the accuracy of the kinetic parameters obtained from the concentration-dependent method.

Ten cuvettes containing 480 μL of DTNB solution (1.32 mM DTNB, 59 mM NaHCO$_3$, PBS 7.6), 150 μL of working solution of AChE, and 1340 μL of PBS 7.6 were prepared and maintained at 20 °C. The first five cuvettes treated with 10 μL of the solvent used to dilute the inhibitors served as the control (A_0). At $t = 0$, 10 μL of the inhibitor solution was added to the other five cuvettes and stirred gently. At select time points (t), a control solution and an inhibited solution were placed in a Beckman DU-7500 diode-array spectrophotometer and the residual activity of each solution was determined by adding 20 μL of ATCh-I and the hydrolysis was monitored at 412 nm (10 sec intervals) for 3 min. The bimolecular rate constant (k_i) was determined as the average of 5 runs by plotting ln(A_0/A_t) versus the incubation time. The resulting slopes were determined by linear regression based on the equation:

$$\ln\frac{A_0}{A_t} = k_i[i]\Delta t \qquad (7.4)$$

where:

A_0 is the activity of the uninhibited enzyme at time = t without adding the inhibitor,

A_t is the activity of the uninhibited enzyme at time = t following addition of a specific concentration of the inhibitor ([i]).

Method 3: Determination of k_3, the rate constant of spontaneous reactivation.

0.2 mL of working enzyme solutions containing inhibitor that had caused 90% loss of enzyme activity after 20 min incubation were isolated. The inhibition reaction was stopped by diluting the mixture 100 fold with 0.1 M PBS 7.6. Immediately following dilution ($t = 0$), and at discrete time points thereafter (t), 1 mL aliquots of diluted solution were added to cuvettes containing DTNB solution and the residual enzyme activity (A_0 and A_t, respectively) was determined using Beckman DU-7500 as detailed in Method 2. In parallel, a second set of aliquots from working enzyme solution that had been exposed to the same amount of solvent as used to dilute the inhibitor in the first sample were diluted with PBS 7.6 100 fold and their residual enzyme activity and served as a control for the reaction (A).

The rate constant for spontaneous reactivation, k_{3spon}, was calculated from the linear portion of the graph using the following equation (Clothier 1981; Berkman 1993):

$$\ln(100\ /\ \%\text{inhibition}) = k_3 t \qquad (7.5)$$

where:

% inhibition = $(A - A_t)/(A - A_0)$ x 100.

Enzyme activity was assayed periodically to determine the total percentage of reactivation of enzyme activity after 60 min. Total percentage of reactivation was calculated by using the following equation:

$$\% \text{ reactivation} = 100 - (\% \text{ inhibition at 60 min}).$$

Method 4: Determination of k_3 (2-PAM), the rate constant of oxime-mediated reactivation.

This procedure is identical to that described in Method 3 except that the buffer solution used to dilute the samples also contains 2-PAM (final concentration of 50 mM). The rate constant for oxime-mediated reactivation k_3 (2-PAM) and the amount of total percentage of reactivation was calculated using the procedures detailed in method 3.

7.4.4 Methods for Reversible Inhibitors

Reversible inhibitors bind to the enzyme by different mechanisms, so it is difficult to use a single kinetic parameter as a measure of inhibition potency for all types of reversible inhibitors. Here, a general estimation by using IC_{50} and a detailed method to calculate K_i were utilized.

Method 1: Concentration-dependent screening to determine IC_{50}.

This procedure is identical to that described in concentration-dependent method for irreversible OP inhibitors (Method 1 in 7.4.3). Six cuvettes containing 480 μL of DTNB solution (1.32 mM DTNB, 59 mM $NaHCO_3$, PBS pH 7.6) 150 μL of working solution of AChE, and 1340 μL of PBS (pH 7.6) were placed in a Beckman DU-7500

diode-array spectrophotometer and maintained at 20 ºC. The first cuvette treated with 10

µL of the solvent to dilute the inhibitors served as the control (A_{no}); the other 5 cuvettes

were treated with 10 µL of five gradient inhibitor concentrations (A_i). All six

experiments were incubated for same period of time, 6 mins. The remaining enzyme

activity (v) was determined by adding 20 µL aliquots of the ATCh-I solutions to the

cuvette and the rate of ATCh-I hydrolysis was monitored at 412 nm over a period of 10

min (22 sec intervals). The final concentrations of the reactants during enzyme assay

were: 0.33 mM DTNB, 0.59 mM ATCh-I, and 0.58 mM NaHCO$_3$. In order to get a good

estimation of IC$_{50}$, the inhibitor concentration range was chosen to ensure the AChE

inactivation from 20% to 80%.

The remaining enzyme activity (v) was determined for five solutions containing

different inhibitor concentrations.

$$v = \frac{A_i}{A_{no}} \times 100\% \qquad (7.6)$$

where:

A_{no} is the activity of the uninhibited enzyme without adding the inhibitor,

A_i is the activity of the uninhibited enzyme following addition of a specific

concentration of the inhibitor ($[i]$).

Plotting remaining activity v vs. log[i] in Kaleidagraph 3.6 (Synergy Software,

Reading, PA), IC$_{50}$ can be determined by curve fitting using the following equation:

$$Y = F\ (M0;\ 1 - M1 * (M0/(M2 + M0));\ M1 = 1;\ M2 = 50)\quad (7.7)$$

228

in which IC_{50} is determined as the M2 value.

Method 2: Concentration-dependent pharmacological analysis of K_i.

Six cuvettes containing 480 µL of DTNB solution (1.32 mM DTNB, 59 mM NaHCO$_3$, PBS pH 7.6) 150 µL of working solution of AChE, 10 µL inhibitor, and 1340 µL of PBS (pH 7.6) were placed in a Beckman DU-7500 diode-array spectrophotometer and maintained at 20 ºC. After 10 mins incubation, 20 µL of six gradient concentrations of the ATCh-I solutions ([S]) was added and the substrate hydrolysis (A) was monitored at 412 nm over a period of 10 min (22 sec intervals).

According to Michaelis–Menten equation (Henri, 1903):

$$\frac{1}{v} = \frac{\alpha K_m}{V_{max}} \times \frac{1}{[S]} + \frac{\alpha'}{V_{max}} \qquad (7.8)$$

A linear relationship was observed by plotting $1/A$ vs. $1/[S]$ (Lineweaver, 1934). All other parameters are constants when inhibitor concentration is specified.

The above experiment was repeated five times with five inhibitor concentrations, including one with no inhibitor ([i] = 0). All five equations were plotted on the same graph to determine the mechanism of inhibitor's inactivation.

The competitive inhibition constant K_i is determined by secondary plot of the slope versus the inhibitor concentration and the resulting x axis intercept represents -K_i of the inhibitor. The noncompetitive inhibition constant -K_i' is determined by secondary plot of the intercept versus the inhibitor concentration and the resulting x axis intercept represents K_i'.

$$\frac{1}{v} = \left(\frac{K_m}{V_{max}} + \frac{K_m[I]}{V_{max}K_i} \right) \times \frac{1}{[S]} + \left(\frac{1}{V_{max}} + \frac{[I]}{V_{max}K_i'} \right) \quad (7.9)$$

7.4.5 **Data Analysis**

Experiments were repeated at least 3 times for every single inhibitor to acquire duplicate data sets, and only plots with $R^2 > 0.95$ were accepted to ensure the accuracy of the data.

7.5 Molecular Modeling

In order to elucidate the configuration of protein-ligand complex and explain the kinetic analysis data, the OP compounds synthesized as inhibitors have been docked into the active gorge of rMAChE, followed by the comparison of the results.

Organophosphorus inhibitors can chemically react with Ser203 of AChE. There are three main steps in this binding process: 1) The ligand (OP inhibitor) gets into the gorge of AChE and the phosphorus on the ligand is placed close to Ser203 so that the distance between phosphorus and Ser203 allows a chemical reaction to happen. 2) The chemical reaction takes place. The conformation of the ligand and protein change at the same time to assist the reaction. 3) The ligand-protein complex is stabilized by conformational changes, followed by aging, reactivation or any other post-inhibitory processes. The second and third steps are too complicated to simulate in modeling program, thus the first step is the focus of this study. How close the ligand can reach the active site or how well the chemical bond can be formed is visualized by docking the ligand into the protein.

FlexX was chosen as the docking program because it offers specification of the active site and customization of any kind of constraint between the ligand and protein, which satisfied the requirement of OP-AChE interaction.

7.5.1 Structure Preparation

According to the FlexX requirement, structures of reference ligand, ligand, and protein were prepared before docking.

<u>1) Protein file preparation</u>

Crystal structures of various sources of AChE are available in the RCSB Protein Data Bank (PDB) (http://www.rcsb.org). Recombinant mouse AChE (1maa, resolution 2.90 Å) (Fig 7.30) (Bourne, 1999), used in kinetic analysis, was chosen for simulation.
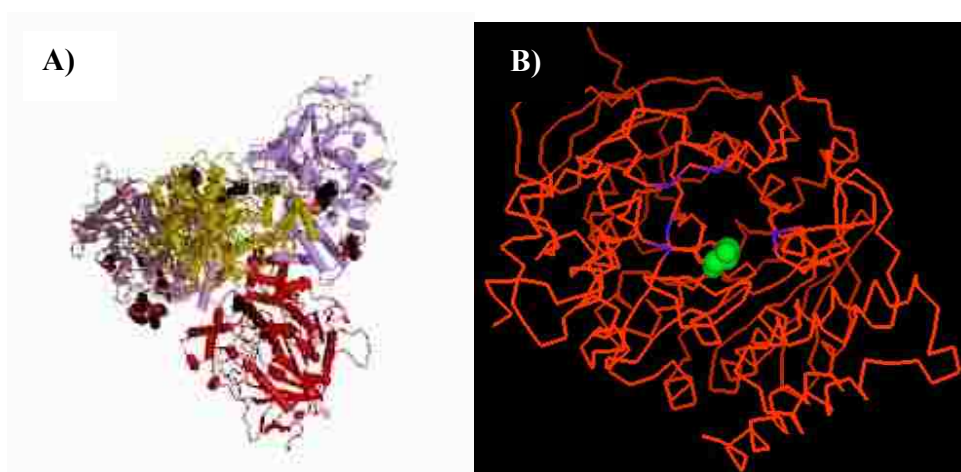
Figure 7.30. Structure of 1maa A) tetramer and B) monomer (ser203 colored in green).

Monomer AChE structure file (Fig 7.28.B) was created by extracting one chain from 1maa as the original 1maa PDB file contains a tetramer. Serine 203, the reaction site of the gorge, was colored in green and shown as spheres.

<u>2) Ligand file preparation</u>

The structure of ligand inhibitor, for example, dansyl-linked fluorophosphonate (**6a**), was first constructed in SYBYL 7.0 (Fig 7.31). Then atom and bond types were carefully checked, and formal charges were properly assigned (FlexX only reads formal charges) to the ligand.
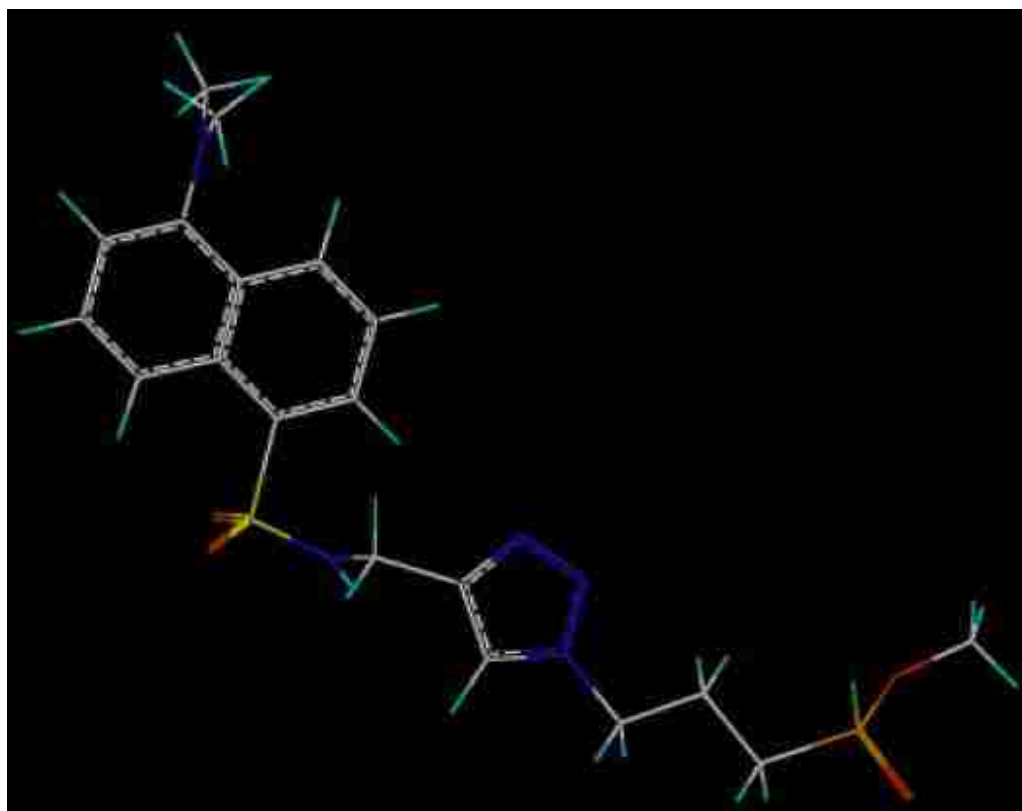
Figure 7.31. Structure of dansyl-linked fluorophosphonate (**6a**) in SYBYL.

After making sure that the ligand was defined appropriately, hydrogen atoms were added to the ligand and the whole structure was minimized energy-wise. After 1000 minimizations, the structure of ligand was optimized (Fig 7.32) and saved as a ligand file (.mol2 file). In this optimized structure, the distance between phosphorus and carbon (attached with dimethylamino group) is 14.4 Å.
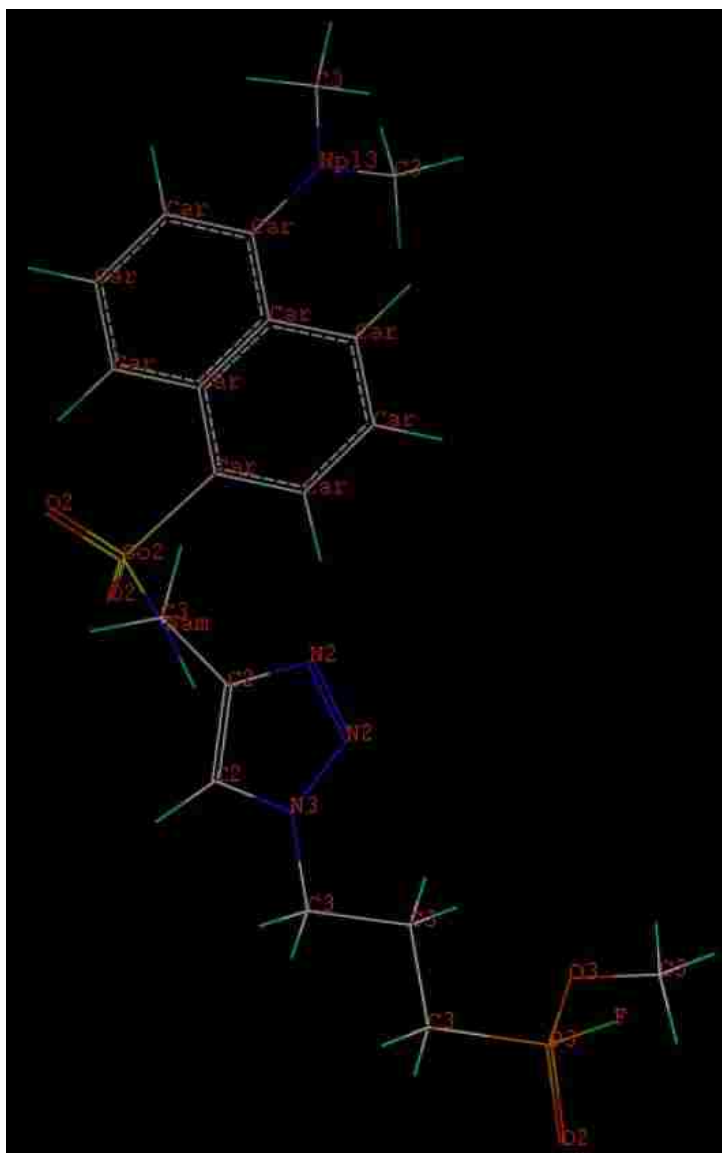
Figure 7.32. Structure of dansyl-linked fluorophosphonate (**6a**) after energy minimization**.**

3) Reference ligand file

Inserting the ligand file into protein space can be achieved by either "JOINing" the ligand file into the protein file, or "MERGEing" the ligand file and protein file together. "JOINing" was used in this study by creating a bond between the phosphorus

on the ligand and the hydroxyl oxygen on Ser203 of the active site. By this way, the

ligand molecule was dragged into the active site of the protein.

Torsion angles of the ligand structure were adjusted to make the ligand fit for the

gorge best. Also, minimizing the residues in the sphere centered at the ligand with a

certain radius (including the ligand) provided a most favorable conformation of ligand-

protein complex without significantly changing the protein. After adjustments of torsions

and minimization of substructure, new PDB file containing both reference ligand and

protein was saved as a reference file (pdb file) (Fig 7.33).
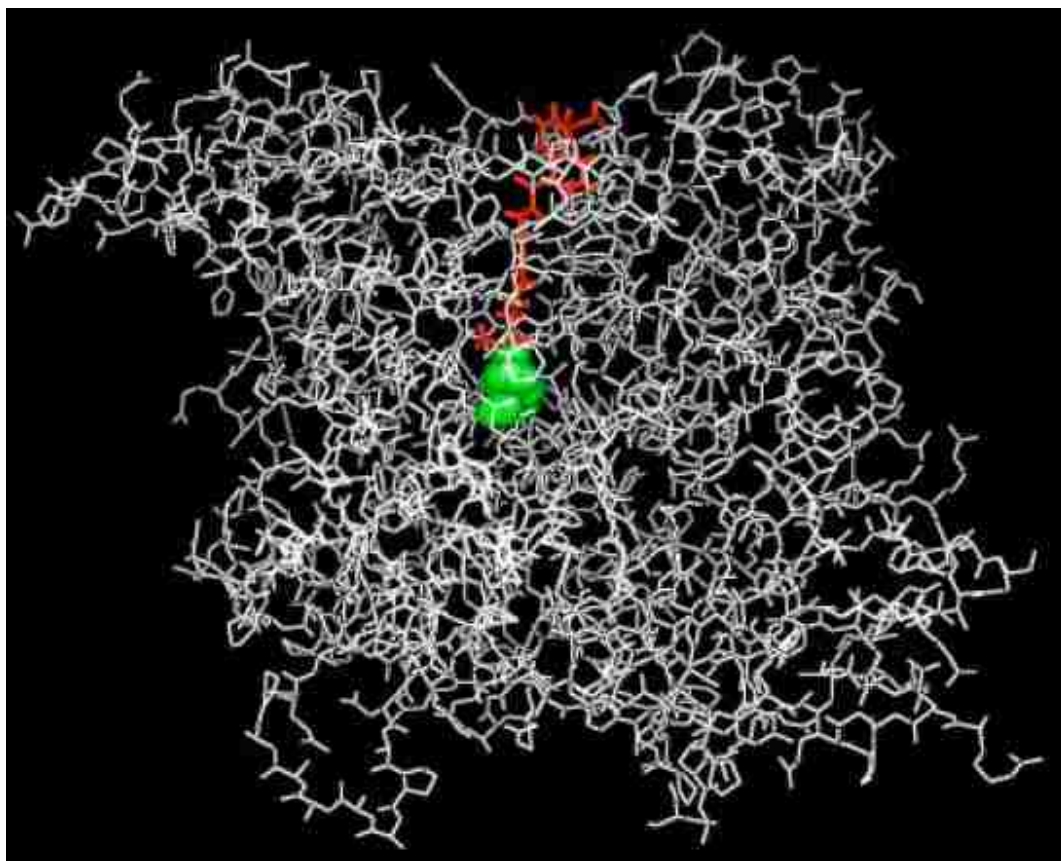
Figure 7.33. Reference file of dansyl-linked fluorophosphonate (compound **6a**): The
reference ligand lying along the gorge colored in red, and Ser203 colored in green
spheres. The distance between phosphorus on the ligand and hydroxyl oxygen on Ser203
is 1.6 Å.

After extracting the reference ligand file from the reference file, the ligand structure was checked again by "FIXing SYBYL atom types in ligand" because the molecule information might be misrepresented when it was transferred from a pdb file. The reference file was used to define the active site and compare with the docking results.

7.5.2 Docking with FlexX

Docking a single ligand with FlexX and optional FlexX-Pharm requires finishing following steps:

<u>1) Creating FlexX Receptor Definition File (RDF)</u>

The RDF contains the information about the protein, its amino acids, the definition of the active site, and the specific torsion angles.

First, the protein structure was loaded. By default, FlexX ignores all HETATM records in the PDB file. The included HETATM (reference ligand) was only for defining the active site. The active site was defined as a sphere containing all residues of protein within 8.5 Å around HETATM (ligand), including Ser203. It has been shown that all residues along the gorge have been selected as the active site with this radius. The RDF was also customized by changing the torsion angle of Ser203 on AChE from 180° to 0.0°, thus the nucleophilic oxygen on Ser203 was exposed to the ligand.

<u>2) Creating Constraint Description File (CDF)</u>

The CDF consists of the FlexX-Pharm interaction, spatial and partial pharmacophore constraints. In this study of docking OP inhibitors, a spatial constraint is preferred to define the distance between Ser203-OH to OP-phosphorus where a chemical

reaction can occur. For dansyl-linked fluorophosphonate (**6a**), the distance between the

hydroxyl group on Ser203 and the phosphorus atom of OP was constrained at less than

2.5 Å and this constraint was set to be "required" (Fig 7.34).
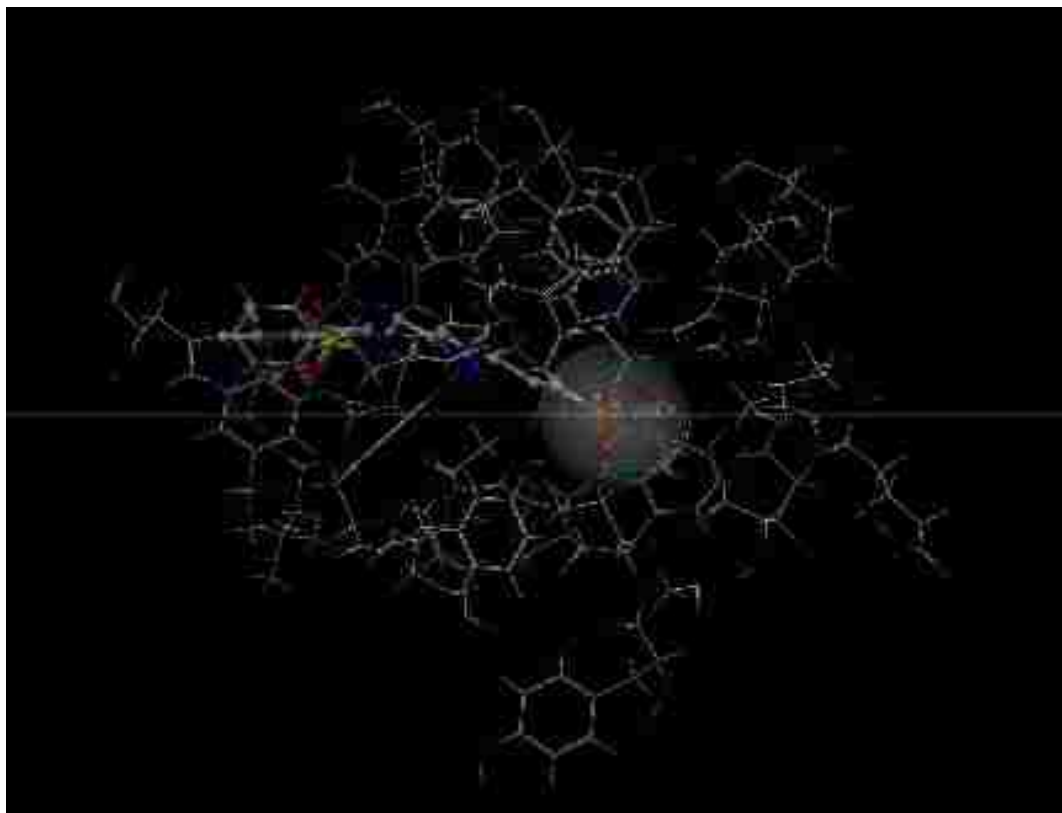
Figure 7.34. CDF of dansyl-linked fluorophosphonate (**6a**).

3) Reading in ligand file and reference ligand file

The ligand file and reference ligand file previously created were opened.

4) Other options

CSscore calculation was used, so that we would have additional scoring functions

to evaluate the interaction between the ligand and the receptor.

FlexX works with formal charges rather than partial atomic charges, thus
"Formal charges" was set to be "Assign".

5) Running FlexX

After running FlexX, only solutions with RMS < 1.5 were generated. Each
solution contains various scoring information and some important factors used to
evaluate the solutions are listed below (Tripos Inc., 2004):

- Rank = ranking of the conformation by decreasing FlexX total score

- Total Score = the total FlexX docking score

- Match Score = contribution of the matched interacting groups

- Lipo Score = contribution of the lipophilic contact area

- Ambig Score = contribution of the lipophilic-hydrophilic contact area

- Clash Score = contribution of the clash penalty (a bump check)

- Rot Score = ligand rotational entropy score

- RMS = the RMS difference of coordinates against the reference

  structure or against the highest ranking structure if the reference is

  omitted

- Similarity = a measure of similarity between solution coordinates and

  reference coordinates. If there are no reference coordinates, all entries of

  this column are -1.0.

- CSCORE = the consensus score computed from these additional and the FlexX

  scoring functions.

For dansyl-linked fluorophosphonate (**6a**), the docking solution with highest score is illustrated in Figure 7.35.
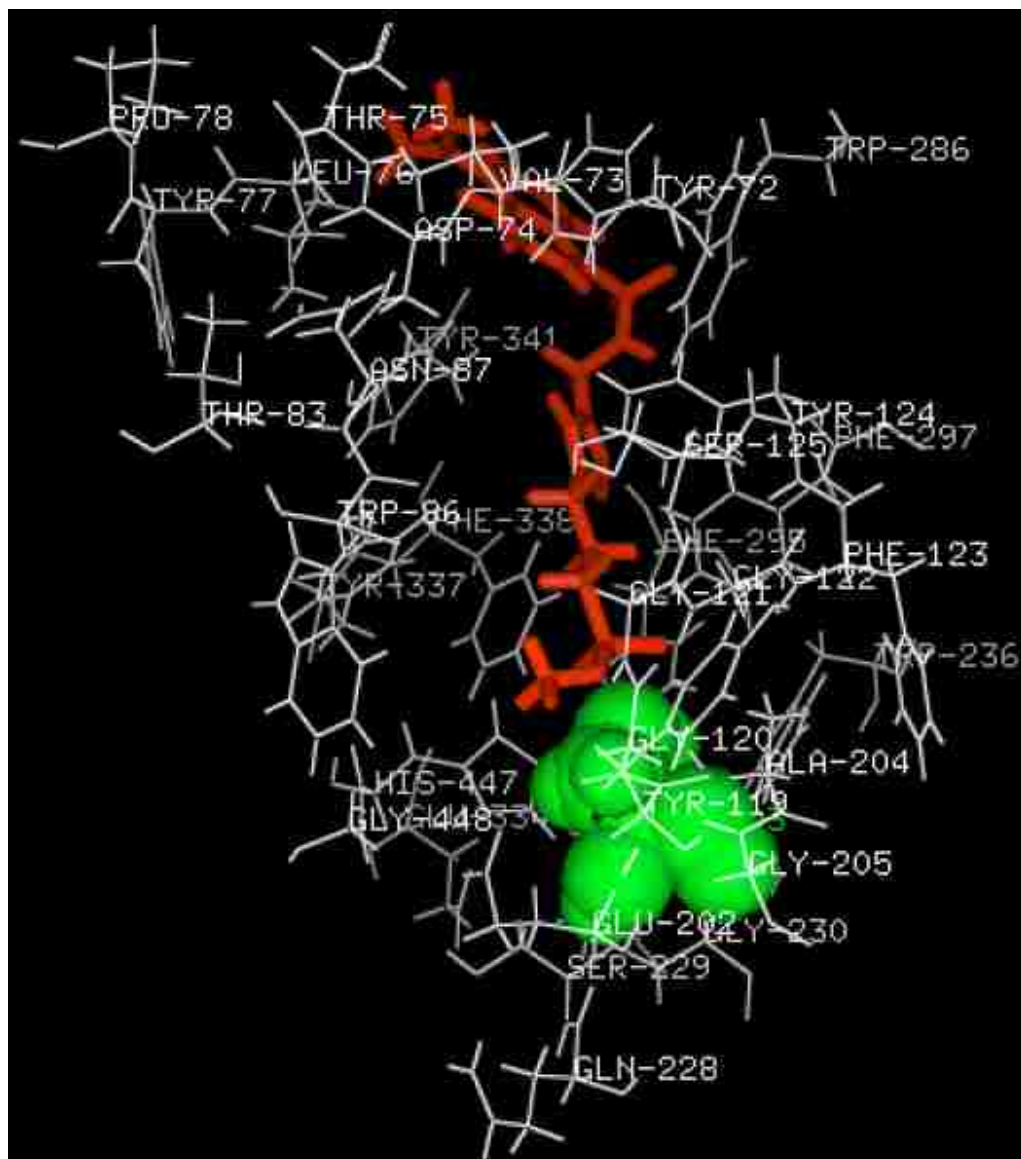
Figure 7.35. Best docking solution of dansyl-linked fluorophosphonate (**6a**).

7.6 Preparation of Meta-inhibitor Coupled Resin
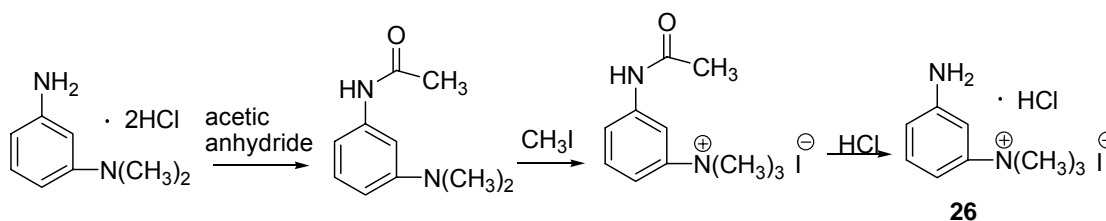
Meta-trimethylaminophenyl amine (meta-inhibitor, 26) (Bourne, 1999). *N,N-*Dimethyl-1,3-phenylenediamine dihydrochloride (10.00 g, 47.80 mmol) was dissolved in acetic anhydride (45 mL). Seven drops of sulfuric acid (H_2SO_4) was added and the solution mixture was brought to reflux with stirring (around 75 ºC). After 30 min refluxing, the reaction was cooled to rt and water (184 mL) was added very slowly. The entire solution was treated with 5N NaOH (1380 mL) and cooled overnight at 4 ºC to afford brownish crystals (7.90 g, 93%). The crystals were collected and dissolved in acetone (40 mL), methyl iodide (3.30 mL) was added with stirring. The reaction was refluxed for 30 min and a precipitate was formed and collected. The filtrate was refluxed for one more hour with adding more methyl iodide (2.20 mL). Precipitates were combined and rinsed with cold acetone (40 mL) to afford a beige powder. The beige powder was dissolved in ethanol (35 mL) and hydrochloric acid (35 mL, 12 N) was added. The reaction was stirred and refluxed for 2 h until the deprotection process was complete. Acetone (600 mL) was added after the solution was cooled to rt to form a precipitate (4.82 g, 20% yield). This meta-inhibitor was shielded from light.

^{1}H NMR (CDCl$_3$): δ 3.67 (s, 9 H), 7.60 (dd, J = 8.0, 2.3 Hz, 1 H), 7.77 (t, J = 8.5 Hz, 1 H), 7.85 (t, J = 2.3 Hz, 1 H), 7.93 (dd, J = 8.8, 3.0 Hz, 1 H).
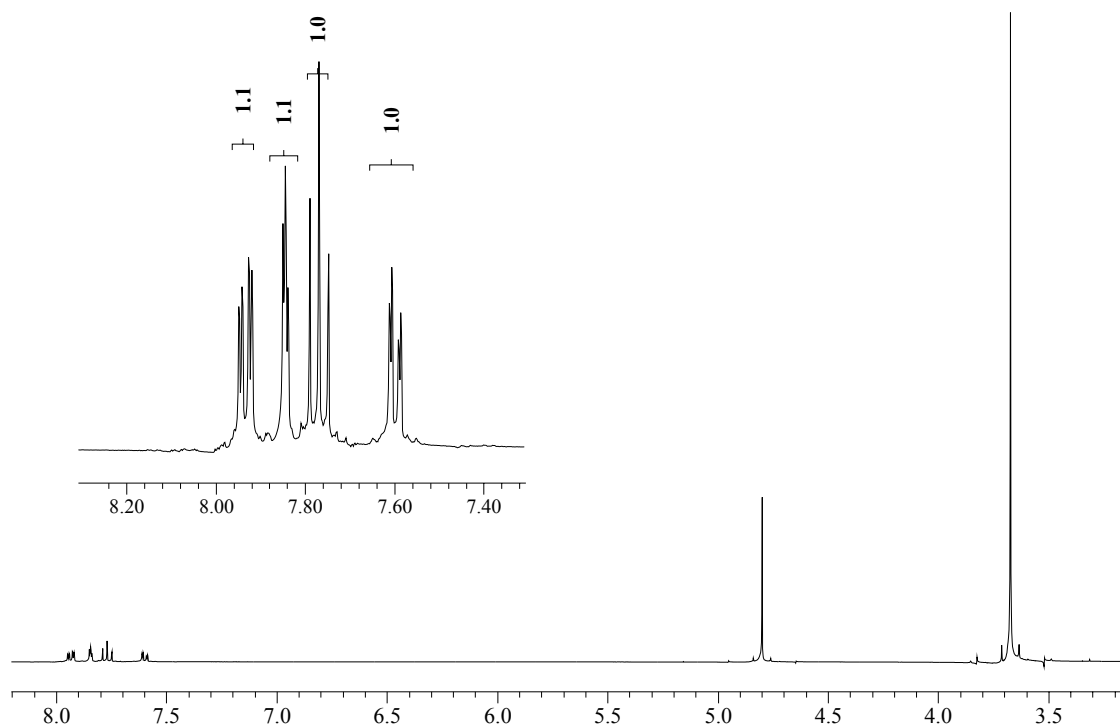
Figure 7.36. ^{1}H NMR spectrum (D$_2$O) of meta-trimethylaminophenyl amine (meta-inhibitor, **26**).
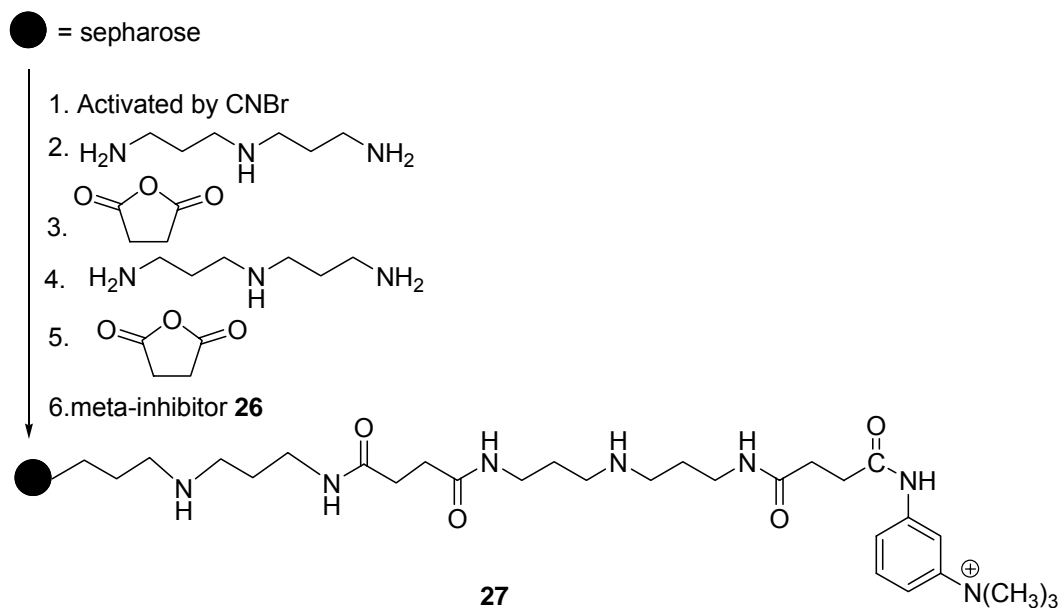
Meta-inhibitor coupled resin (27) (Bourne, 1999). Sepharose resin (CL-4B, 100 mL) was activated by cyanogen bromide (13.00 g) and NaOH (5 N) was used to maintain pH11. 3,3'-Iminobispropylamine (4.30 mL) was added to the activated resin and the mixture was stirred at 0 ºC overnight. Succinic anhydride (10.00 g) was added and NaOH (5 N) was used to maintain pH at 6. The coupling reaction was complete after stirring overnight at 0 ºC. Another portion of 3,3'-iminobispropylamine (18.00 mL) was added to the resin, followed by the slow addition of 1-cyclohexyl-3-(2-morpholino-ethyl)carbodiimide metho-p-toluene sulfonate (7.00 g). The pH was maintained at 5 using HCl (12 N) and the resin solution was kept at 0 ºC overnight. One more portion of succinic anhydride (8.00 g) was added to the resin while maintaining the pH at 6 and the solution was stirred overnight. Meta-inhibitor (compound **26**, 2.00 g) was added, followed with 1-cyclohexyl-3-(2-morpholino-ethyl)carbodiimide metho-p-toluene sulfonate (7.00 g). The pH was maintained at 5 before stirring overnight at 0 ºC. The

resin coupled with the meta-inhibitor was assayed with wild type AChE to ensure the

activity.

REFERENCES

Aaron, H. S.; Braun, J.; Shryne, T. M.; Frack, H. F.; Smith, G. E.; Uyeda, R. T.; Miller, J. I., The stereochemistry of asymmetric phosphorus compounds. III. The resolution of a series of O-alkyl alkylphosphonothioic acids. *J Am Chem Soc* **1960,** 82, 596-598.

Aldridge, W. N.; Davison, A. N., The inhibition of erythrocyte cholinesterase by tri-esters of phosphoric acid. I. Diethyl p nitrophenyl phosphate (E600) and analogues. *Biochem J* **1952,** 51, (1), 62-70.

Aldridge, W. N.; Reiner, E., *Enzyme inhibitors as substrates.* Elsevier Publishing Co.: New York, 1975.

Amitai, G.; Ashani, Y.; Gafni, A.; Silman, I., Novel pyrene-containing organophosphates as fluorescent probes for studying aging-induced conformational changes in organophosphate-inhibited acetylcholinesterase. *Biochemistry* **1982,** 21, (9), 2060-9.

Amitai, G.; Moorad, D.; Adani, R.; Doctor, B. P., Inhibition of acetylcholinesterase and butyrylcholinesterase by chlorpyrifos-oxon. *Biochem Pharmacol* **1998,** 56, (3), 293-9.

Aschner, M., Interactions between pesticides and glia: an unexplored experimental field. *Neurotoxicology* **2000,** 21, (1-2), 175-80.

Axelsen, P. H.; Harel, M.; Silman, I.; Sussman, J. L., Structure and dynamics of the active site gorge of acetylcholinesterase: synergistic use of molecular dynamics simulation and X-ray crystallography. *Protein Sci* **1994,** 3, (2), 188-97.

Barak, D.; Kronman, C.; Ordentlich, A.; Ariel, N.; Bromberg, A.; Marcus, D.; Lazar, A.; Velan, B.; Shafferman, A., Acetylcholinesterase peripheral anionic site degeneracy conferred by amino acid arrays sharing a common core. *J Biol Chem* **1994,** 269, (9), 6296-305.

Bartolucci, C.; Perola, E.; Cellai, L.; Brufani, M.; Lamba, D., "Back door" opening implied by the crystal structure of a carbamoylated acetylcholinesterase. *Biochemistry* **1999,** 38, (18), 5714-9.

Berg, J. M.; Tymoczko, J. L.; Stryer, L., *Biochemistry*, Fifth ed.; **2002**.

Berkman, C. E.; Ryu, S.; Quinn, D. A.; Thompson, C. M., Kinetics of the postinhibitory reactions of acetylcholinesterase poisoned by chiral isomalathion: a surprising nonreactivation induced by the RP stereoisomers. *Chem Res Toxicol* **1993,** 6, (1), 28-32.

Berkman, C. E.; Thompson, C. M.; Perrin, S. R., Synthesis, absolute configuration, and analysis of malathion, malaoxon, and isomalathion enantiomers. *Chem Res Toxicol* **1993,** 6, (5), 718-23.

Berman, H. A.; Taylor, P., Fluorescent phosphonate label for serine hydrolases, pyrenebutyl methylphosphonofluoridate: reaction with acetylcholinesterase. *Biochemistry* **1978,** 17, (9), 1704-13.

Bolletta, F.; Fabbri, D.; Lombardo, M.; Prodi, L.; Trombini, C.; Zaccheroni, N., Synthesis and Photophysical Properties of Fluorescent Derivatives of Methylmercury. *Organometallics* **1996,** 15, (9), 2415-17.

Bourne, Y.; Taylor, P.; Bougis, P. E.; Marchot, P., Crystal structure of mouse acetylcholinesterase. A peripheral site-occluding loop in a tetrameric assembly. *J Biol Chem* **1999,** 274, (5), 2963-70.

Bourne, Y.; Taylor, P.; Radić, Z.; Marchot, P., Structural insights into ligand interactions at the acetylcholinesterase peripheral anionic site. *Embo J* **2003,** 22, (1), 1-12.

Briggs, G. E.; Haldane, J. B., A Note on the Kinetics of Enzyme Action. *Biochem J* **1925,** 19, (2), 338-9.

Burk, D.; Lineweaver, H.; Horner, C. K., The Specific Influence of Acidity on the Mechanism of Nitrogen Fixation by Azotobacter. *J Bacteriol* **1934,** 27, (4), 325-40.

Clothier, B.; Johnson, M. K.; Reiner, E., Interaction of some trialkyl phosphorothiolates with acetylcholinesterase. Characterization of inhibition, aging and reactivation. *Biochim Biophys Acta* **1981,** 660, (2), 306-16.

Coats, S. J.; Link, J. S.; Gauthier, D.; Hlasta, D. J., Trimethylsilyl-directed 1,3-dipolar cycloaddition reactions in the solid-phase synthesis of 1,2,3-triazoles. *Org Lett* **2005,** 7, (8), 1469-72.

Cohen, R. S., Therapeutic Education and Day Treatment: A New Professional Liaison. *Except Child* **1965,** 32, 23-8.

Colletier, J. P.; Fournier, D.; Greenblatt, H. M.; Stojan, J.; Sussman, J. L.; Zaccai, G.; Silman, I.; Weik, M., Structural insights into substrate traffic and inhibition in acetylcholinesterase. *Embo J* **2006,** 25, (12), 2746-56.

Cravatt, B. F.; Sorensen, E. J., Chemical strategies for the global analysis of protein function. *Curr Opin Chem Biol* **2000,** 4, (6), 663-8.

245

Doorn, J. A.; Gage, D. A.; Schall, M.; Talley, T. T.; Thompson, C. M.; Richardson, R. J., Inhibition of acetylcholinesterase by (1S,3S)-isomalathion proceeds with loss of thiomethyl: kinetic and mass spectral evidence for an unexpected primary leaving group. *Chem Res Toxicol* **2000,** 13, (12), 1313-20.

Drabowicz, J.; Legedz, S.; Mikolajczyk, M., Organosulfur compounds. XLIX. Optically active sulfinates. A new type of enantioselective asymmetric synthesis and kinetic resolution. *Tetrahedron* **1988,** 44, (16), 5243-51.

Eglen, R. M., Muscarinic receptor subtypes in neuronal and non-neuronal cholinergic function. *Auton Autacoid Pharmacol* **2006,** 26, (3), 219-33.

Ellman, G. L.; Courtney, K. D.; Andres, V., Jr.; Feather-Stone, R. M., A new and rapid colorimetric determination of acetylcholinesterase activity. *Biochem Pharmacol* **1961,** 7, 88-95.

Eto, M., *Organophosphorus Pesticides: Organic and Biological Chemistry.* CRC Press: Cleveland. OH, 1974.

Evans, D. A.; Funkenstein, H. H.; Albert, M. S.; Scherr, P. A.; Cook, N. R.; Chown, M. J.; Hebert, L. E.; Hennekens, C. H.; Taylor, J. O., Prevalence of Alzheimer's disease in a community population of older persons. Higher than previously reported. *Jama* **1989,** 262, (18), 2551-6.

Feldman, R. S.; Quenzer L. F., *Fundamentals of Neuropsychopharmacology.* Sunderland, MA: Sinauer, 1984.

Fisher, T. C.; Crane, M.; Callaghan, A., An optimized microtiterplate assay to detect acetylcholinesterase activity in individual Chironomus Riparius meigen. *Environ Toxical and Chem* **2000,** 19, (7), 1749-1752.

Friesner, R. A.; Banks, J. L.; Murphy, R. B.; Halgren, T. A.; Klicic, J. J.; Mainz, D. T.; Repasky, M. P.; Knoll, E. H.; Shelley, M.; Perry, J. K.; Shaw, D. E.; Francis, P.; Shenkin, P. S., Glide: a new approach for rapid, accurate docking and scoring. 1. Method and assessment of docking accuracy. *J Med Chem* **2004,** 47, (7), 1739-49.

Froede, H. C.; Wilson, I. B., *The enzymes.* Academic Press: New York, 1971.

Fukuto, T. R., Mechanism of action of organophosphorus and carbamate insecticides. *Environ Health Perspect* **1990,** 87, 245-54.

Gabb, H. A.; Jackson, R. M.; Sternberg, M. J. E., Modelling Protein Docking using Shape Complimentarity, Electrostatics and Biochemical Information. *J Mol Biol* **1997**, 272, (1), 106-120.

Goodsell, D. S.; Olson, A. J., Automated docking of substrates to proteins by simulated annealing. *Proteins* **1990,** 8, (3), 195-202.

Gray, W. R., End-group analysis using dansyl chloride. *Meth Enzymol* **1972,** 25, 121-138.

Growdon, J. H.; Cohen, E. L.; Wurtman, R. J., Huntington's disease: clinical and chemical effects of choline administration. *Ann Neurol* **1977,** 1, (5), 418-22.

Halgren, T. A.; Murphy, R. B.; Friesner, R. A.; Beard, H. S.; Frye, L. L.; Pollard, W. T.; Banks, J. L., Glide: a new approach for rapid, accurate docking and scoring. 2. Enrichment factors in database screening. *J Med Chem* **2004,** 47, (7), 1750-9.

Harel, M.; Kleywegt, G. J.; Ravelli, R. B.; Silman, I.; Sussman, J. L., Crystal structure of an acetylcholinesterase-fasciculin complex: interaction of a three-fingered toxin from snake venom with its target. *Structure* **1995,** 3, (12), 1355-66.

Harel, M.; Quinn, D. M.; Nair, H. K.; Silman, I.; Sussman, J. L., The X-ray structure of a transition state analog complex reveals the molecular origins of the catalytic power and substrate specificity of acetylcholinesterase. *J Am Chem Soc* **1996,** 118, 2340-46.

Harel, M.; Schalk, I.; Ehret-Sabatier, L.; Bouet, F.; Goeldner, M.; Hirth, C.; Axelsen, P. H.; Silman, I.; Sussman, J. L., Quaternary ligand binding to aromatic residues in the active-site gorge of acetylcholinesterase. *Proc Natl Acad Sci U S A* **1993,** 90, (19), 9031-5.

Haugland, R. P., *Molecular Probes Handbook for Fluorescent Probes and Research Chemicals*. 6th ed.; 1996.

He, Z.-J.; Liu, J.-X.; Tang, C.-C., A new convenient synthesis of phosphoro(-no)chloridothionates. *Synth Commun* **1998,** 28, (15), 2769-2772.

Herzsprung, P.; Weil, L.; Quentin, K. E., Determination of organophosphorus compounds and carbamates by their inhibition of cholinesterase. Part 1: Inhibition values on immobilized cholinesterase. *Z Wass Abwass Forsch* **1989,** 22, 67-72.

Horner, L.; Lindel, H., Organophosphorus compounds. 100. Thiophosphyl compounds by P:O/P:S exchange. *Phosphorus Sulfur Silicon Relat Elem* **1982,** 12, (2), 259-261.

Hosea, N. A.; Berman, H. A.; Taylor, P., Specificity and orientation of trigonal carboxyl esters and tetrahedral alkylphosphonyl esters in cholinesterases. *Biochemistry* **1995,** 34, (36), 11528-36.

Howell, S. J.; Spencer, N.; Philp, D., Recognition-mediated regiocontrol of a dipolar cycloaddition reaction. *Tetrahedron* **2001,** 57, (23), 4945-54.

Itier, V.; Bertrand, D., Neuronal nicotinic receptors: from protein structure to function. *FEBS Lett* **2001,** 504, (3), 118-25.

Jarv, J., Stereochemical aspects of cholinesterase catalysis. *Bioorg Chem* **1984,** 2, 259-278.

Johnson, G.; Moore, S. W., The peripheral anionic site of acetylcholinesterase: structure, functions and potential role in rational drug design. *Curr Pharm Des* **2006,** 12, (2), 217-25.

Johnson, J. L.; Cusack, B.; Davies, M. P.; Fauq, A.; Rosenberry, T. L., Unmasking tandem site interaction in human acetylcholinesterase. Substrate activation with a cationic acetanilide substrate. *Biochemistry* **2003,** 42, (18), 5438-52.

Jones, G.; Willett, P.; Glen, R. C., Molecular recognition of receptor sites using a genetic algorithm with a description of desolvation. *J Mol Biol* **1995,** 254, (1), 43-53.

Joseph-McCarthy, D., Computational approaches to structure-based ligand design. *Pharmacol Ther* **1999,** 84, (2), 179-91.

Kalyanaraman, C.; Bernacki, K.; Jacobson, M. P., Virtual screening against highly charged active sites: identifying substrates of alpha-beta barrel enzymes. *Biochemistry* **2005,** 44, (6), 2059-71.

Kardos, S. A.; Sultatos, L. G., Interactions of the organophosphates paraoxon and methyl paraoxon with mouse brain acetylcholinesterase. *Toxicol Sci* **2000,** 58, (1), 118-26.

Katz, B.; Miledi, R., Release of acetylcholine from a nerve terminal by electric pulses of variable strength and duration. *Nature* **1965,** 207, (1), 1097-8.

Kellogg, G. E.; Semus, S. F.; Abraham, D. J., HINT: a new method of empirical hydrophobic field calculation for CoMFA. *J Comput Aided Mol Des* **1991,** 5, (6), 545-52.

Kihara, T.; Shimohama, S., Alzheimer's disease and acetylcholine receptors. *Acta Neurobiol Exp (Wars)* **2004,** 64, (1), 99-105.

Koellner, G.; Kryger, G.; Millard, C. B.; Silman, I.; Sussman, J. L.; Steiner, T., Active-site gorge and buried water molecules in crystal structures of acetylcholinesterase from Torpedo californica. *J Mol Biol* **2000,** 296, (2), 713-35.

Koizumi, T.; Amitani, H.; Yoshii, E., A new method of preparing optically active alkyl phenyl phosphonates. *Tetrahedron Lett* **1978,** 19, (39), 3741-42.

Kokotos, G.; Noula, C., Selective One-Pot Conversion of Carboxylic Acids into Alcohols. *J Org Chem* **1996,** 61, (20), 6994-6996.

Kolb, H. C.; Finn, M. G.; Sharpless, K. B., Click Chemistry: Diverse Chemical Function from a Few Good Reactions. *Angew Chem Int Ed Engl* **2001,** 40, (11), 2004-2021.

Kramer, B.; Rarey, M.; Lengauer, T., Evaluation of the FLEXX incremental construction algorithm for protein-ligand docking. *Proteins* **1999,** 37, (2), 228-41.

Krasinski, A.; Radić, Z.; Manetsch, R.; Raushel, J.; Taylor, P.; Sharpless, K. B.; Kolb, H. C., In situ selection of lead compounds by click chemistry: target-guided optimization of acetylcholinesterase inhibitors. *J Am Chem Soc* **2005,** 127, (18), 6686-92.

Kua, J.; Zhang, Y.; Eslami, A. C.; Butler, J. R.; McCammon, J. A., Studying the roles of W86, E202, and Y337 in binding of acetylcholine to acetylcholinesterase using a combined molecular dynamics and multiple docking approach. *Protein Sci* **2003,** 12, (12), 2675-84.

Kuntz, I. D., *DOCK 5.3 User Manual*. 2005.

Lanks, K. W.; Seleznick, M. J., Spontaneously reactivation of acetylcholinesterase inhibited by diisopropylfluorophosphate. *Biochim Biophys Acta* **1981,** 660, (1), 91-5.

Law, D. S.; Ten Eyck, L. F.; Katzenelson, O.; Tsigelny, I.; Roberts, V. A.; Pique, M. E.; Mitchell, J. C., Finding needles in haystacks: Reranking DOT results by using shape complementarity, cluster analysis, and biological information. *Proteins* **2003,** 52, (1), 33-40.

Lecher, H. Z.; Greenwood, R. A.; Whitehouse, K. C.; Chao, T. H., The phosphonation of aromatic compounds with phosphorus pentasulfide. *J Am Chem Soc* **1956,** 78, (19), 5018-22.

Lee, S. L.; Hepburn, T. W.; Swartz, W. H.; Ammon, H. L.; Mariano, P. S.; Dunaway-Mariano, D., Stereochemical probe for the mechanism of phosphorus-carbon bond cleavage catalyzed by the Bacillus cereus phosphonoacetaldehyde hydrolase. *J Am Chem Soc* **1992,** 114, (19), 7346-54.

Lewis, W. G.; Green, L. G.; Grynszpan, F.; Radić, Z.; Carlier, P. R.; Taylor, P.; Finn, M. G.; Sharpless, K. B., Click chemistry in situ: acetylcholinesterase as a reaction vessel for the selective assembly of a femtomolar inhibitor from an array of building blocks. *Angew Chem Int Ed Engl* **2002,** 41, (6), 1053-7.

Lieske, C. N.; CLark, J. H.; Meyer, H. G.; Lowe, J. R., Spontaneous and induced reactivation of Eel Acetylcholinesterase inhibited by three organophophinates. *Pestic Biochem Physiol* **1980,** 13, 205-212.

Lieske, C. N.; Gessner, C. E.; Gepp, R. T.; Clark, J. H.; Meyer, H. G.; Broomfield, C. A., pH effects in the spontaneous reactivation of phosphinylated acetylcholinesterase. *Life Sci* **1990,** 46, (17), 1189-96.

Liu, Y.; Patricelli, M. P.; Cravatt, B. F., Activity-based protein profiling: the serine hydrolases. *Proc Natl Acad Sci U S A* **1999,** 96, (26), 14694-9.

Lu, H.; Berkman, C. E., Stereoselective inhibition of glutamate carboxypeptidase by chiral phosphonothioic acids. *Bioorg Med Chem* **2001,** 9, (2), 395-402.

Luo, C.; Saxena, A.; Smith, M.; Garcia, G.; Radić, Z.; Taylor, P.; Doctor, B. P., Phosphoryl oxime inhibition of acetylcholinesterase during oxime reactivation is prevented by edrophonium. *Biochemistry* **1999,** 38, (31), 9937-47.

Maguire, A. R.; Plunkett, S. J.; Papot, S.; Clynes, M.; O'Connor, R.; Touhey, S., Synthesis of indomethacin analogues for evaluation as modulators of MRP activity. *Bioorg Med Chem* **2001,** 9, (3), 745-62.

Main, A. R., Affinity and Phosphorylation Constants for the Inhibition of Esterases by Organophosphates. *Science* **1964,** 144, 992-3.

Malany, S.; Sawai, M.; Sikorski, R. S.; Seravalli, J.; Quinn, D. M.; Radić, Z.; Taylor, P.; Kronman, C.; Velan, B.; Shafferman, A., Transition State Structure and Rate Determination for the Acylation Stage of Acetylcholinesterase Catalyzed Hydrolysis of (Acetylthio)choline. *J Am Chem Soc* **2000,** 122, (13), 2981-2987.

Manetsch, R.; Krasinski, A.; Radić, Z.; Raushel, J.; Taylor, P.; Sharpless, K. B.; Kolb, H. C., In situ click chemistry: enzyme inhibitors made to their own specifications. *J Am Chem Soc* **2004,** 126, (40), 12809-18.

Marcel, V.; Palacios, L. G.; Pertuy, C.; Masson, P.; Fournier, D., Two invertebrate acetylcholinesterases show activation followed by inhibition with substrate concentration. *Biochem J* **1998,** 329 (Pt 2), 329-34.

Marchot, P.; Ravelli, R. B.; Raves, M. L.; Bourne, Y.; Vellom, D. C.; Kanter, J.; Camp, S.; Sussman, J. L.; Taylor, P., Soluble monomeric acetylcholinesterase from mouse: expression, purification, and crystallization in complex with fasciculin. *Protein Sci* **1996,** 5, (4), 672-9.

Metcalf, R. L.; March, R. B., The isomerization of organic thionophosphate insecticides. *J. Econ. Entomol.* **1953,** 46, 288-94.

Michalski, J.; Ratajczak, A.; Tulimowski, Z., Resolution of asymmetric dialkylphosphorothioic acids. *Bull Acad Pol Sci Chim* **1963,** 11, (5), 237-40.

Mikolajczyk, M.; Omelanczuk, J.; Perlikowska, W.; Markovskii, L. N.; Romanenko, V. D.; Ruban, A. V.; Drapailo, A. B., A new enantioselective asymmetric synthesis of tricoordinate phosphorus compounds from dicoordinate l3-aryl(alkyl)iminophosphines. *Phosphorus Sulfur Silicon Relat Elem* **1988,** 36, (3-4), 267-70.

Millard, C. B.; Kryger, G.; Ordentlich, A.; Greenblatt, H. M.; Harel, M.; Raves, M. L.; Segall, Y.; Barak, D.; Shafferman, A.; Silman, I.; Sussman, J. L., Crystal structures of aged phosphonylated acetylcholinesterase: nerve agent reaction products at the atomic level. *Biochemistry* **1999,** 38, (22), 7032-9.

Miller, M. D.; Kearsley, S. K.; Underwood, D. J.; Sheridan, R. P., FLOG: a system to select 'quasi-flexible' ligands complementary to a receptor of known three-dimensional structure. *J Comput Aided Mol Des* **1994,** 8, (2), 153-74.

Mionetto, N.; Morel, N.; Massoulié, J.; Schmid, R. D., Biochemical determination of insecticides via cholinesterases. 1. Acetylcholinesterase from rat brain: functional expression using a baculovirus system, and biochemical characterization. *Biotechnol Techn* **1997,** 11, (11), 805-812.

Mitchell, J. C.; Kerr, R.; Ten Eyck, L. F., Rapid atomic density methods for molecular shape characterization. *J Mol Graph Model* **2001,** 19, (3-4), 325-30, 388-90.

Morris, G. M.; Goodsell, D. S.; Huey, R.; Olson, A. J., Distributed automated docking of flexible ligands to proteins: parallel applications of AutoDock 2.4. *J Comput Aided Mol Des* **1996,** 10, (4), 293-304.

Olson, A. J.; Goodsell, D. S., Automated docking and the search for HIV protease inhibitors. *SAR QSAR Environ Res* **1998,** 8, (3-4), 273-85.

Ordentlich, A.; Barak, D.; Kronman, C.; Flashner, Y.; Leitner, M.; Segall, Y.; Ariel, N.; Cohen, S.; Velan, B.; Shafferman, A., Dissection of the human acetylcholinesterase active center determinants of substrate specificity. Identification of residues constituting the anionic site, the hydrophobic site, and the acyl pocket. *J Biol Chem* **1993,** 268, (23), 17083-95.

Parsons, S. M.; Prior, C.; Marshall, I. G., Acetylcholine transport, storage, and release. *Int Rev Neurobiol* **1993,** 35, 279-390.

Pei, J.; Wang, Q.; Zhou, J.; Lai, L., Estimating protein-ligand binding free energy: atomic solvation parameters for partition coefficient and solvation free energy calculation. *Proteins* **2004,** 57, (4), 651-64.

Pisani, A.; Bonsi, P.; Picconi, B.; Tolu, M.; Giacomini, P.; Scarnati, E., Role of tonically-active neurons in the control of striatal function: cellular mechanisms and behavioral correlates. *Prog Neuropsychopharmacol Biol Psychiatry* **2001,** 25, (1), 211-30.

Purnanand; Batra, B. S.; Lal, G., A simple route to chiral phosphonothionates from diastereomeric phosphonamidothionates. *Tetrahedron Lett* **1994,** 35, (26), 4641-4.

Radić, Z.; Reiner, E.; Taylor, P., Role of the peripheral anionic site on acetylcholinesterase: inhibition by substrates and coumarin derivatives. *Mol Pharmacol* **1991,** 39, (1), 98-104.

Reddy, P. M.; Kovach, I. M., Synthesis of chiral 4-nitrophenyl alkyl methylphosphonothioates: BF3×Et2O-catalyzed alcoholysis of phosphonamidothioates. *Tetrahedron Lett* **2002,** 43, (22), 4063-4066.

Reznik, V. S.; Akamsin, V. D.; Galyametdinova, I. V., Two-fragment a-adrenolytics 4. Synthesis of phosphorylated derivatives of 2-aryloxyethylamines and N-phenylpiperazine. *Russ Chem Bull* **2001,** 50, (1), 125-129.

Rosenberry, T. L.; Mallender, W. D.; Thomas, P. J.; Szegletes, T., A steric blockade model for inhibition of acetylcholinesterase by peripheral site ligands and substrate. *Chem Biol Interact* **1999,** 119-120, 85-97.

Rostovtsev, V. V.; Green, L. G.; Fokin, V. V.; Sharpless, K. B., A stepwise huisgen cycloaddition process: copper(I)-catalyzed regioselective "ligation" of azides and terminal alkynes. *Angew Chem Int Ed Engl* **2002,** 41, (14), 2596-9.

Ryu, S.; Jackson, J. A.; Thompson, C. M., Methanolysis of phosphoramidates with boron trifluoride-methanol complex. *J Org Chem* **1991,** 56, 4999-5002.

Ryu, S. M.; Lin, J.; Thompson, C. M., Comparative anticholinesterase potency of chiral isoparathion methyl. *Chem Res Toxicol* **1991,** 4, (5), 517-20.

Saltmarsh, J. R.; Boyd, A. E.; Rodriguez, O. P.; Radić, Z.; Taylor, P.; Thompson, C. M., Synthesis of fluorescent probes directed to the active site gorge of acetylcholinesterase. *Bioorg Med Chem Lett* **2000,** 10, (14), 1523-6.

Schumacher, M.; Camp, S.; Maulet, Y.; Newton, M.; MacPhee-Quigley, K.; Taylor, S. S.; Friedmann, T.; Taylor, P., Primary structure of Torpedo californica acetylcholinesterase deduced from its cDNA sequence. *Nature* **1986,** 319, (6052), 407-9.

Silman, I.; Sussman, J. L., Acetylcholinesterase: 'classical' and 'non-classical' functions and pharmacology. *Curr Opin Pharmacol* **2005,** 5, (3), 293-302.

Singer, V. L.; Johnson, I. D., *Molecular Probes Handbook for Fluorescent Probes and Research Chemicals*. 6th ed.; 1996.

Steinberg, N.; Grunwald, J.; Roth, E.; August, R.; Haas, E.; Ashani, Y.; Silman, I., Conformational differences between aged and non-aged organophosphoryl conjugates of chymotrypsin. *Prog Clin Biol Res* **1989,** 289, 293-304.

Stojan, J.; Brochier, L.; Alies, C.; Colletier, J. P.; Fournier, D., Inhibition of Drosophila melanogaster acetylcholinesterase by high concentrations of substrate. *Eur J Biochem* **2004,** 271, (7), 1364-71.

Sussman, J. L.; Harel, M.; Frolow, F.; Oefner, C.; Goldman, A.; Toker, L.; Silman, I., Atomic structure of acetylcholinesterase from Torpedo californica: a prototypic acetylcholine-binding protein. *Science* **1991,** 253, (5022), 872-9.

Sussman, J. L.; Millard, C. B.; Kryger, G.; Ordentlich, A.; Greenblatt, H. M.; Harel, M.; Raves, M. L.; Segall, Y.; Barak, D.; Shafferman, A.; Silman, I., Crystal Structures of Aged Phosphnylated Acetylcholinesterase: Nerve Agent Reaction Products at the Atomic Level. *Biochemistry* **1999,** 38, (22), 7032-9.

Tam, A.; Arnold, U.; Soellner, M. B.; Raines, R. T., Protein prosthesis: 1,5-disubstituted[1,2,3]triazoles as cis-peptide bond surrogates. *J Am Chem Soc* **2007,** 129, (42), 12670-1.

Tao, P.; Lai, L., Protein ligand docking based on empirical method for binding affinity estimation. *J Comput Aided Mol Des* **2001,** 15, (5), 429-46.

Taylor, P.; Lappi, S., Interaction of fluorescence probes with acetylcholinesterase. The site and specificity of propidium binding. *Biochemistry* **1975,** 14, (9), 1989-97.

Taylor, P.; Radić, Z.; Hosea, N. A.; Camp, S.; Marchot, P.; Berman, H. A., Structural bases for the specificity of cholinesterase catalysis and inhibition. *Toxicol Lett* **1995,** 82-83, 453-8.

Thompson, C. M.; Suarez, A. I.; Rodriguez, O. P., Synthesis and 31P chemical shift identification of tripeptide active site models that represent human serum acetylcholinesterase covalently modified at serine by certain organophosphates. *Chem Res Toxicol* **1996,** 9, (8), 1325-32.

Tongcharoensirikul, P.; Suarez, A. I.; Voelker, T.; Thompson, C. M., Stereoselective addition of dimethyl thiophosphite to imines. *J Org Chem* **2004,** 69, (7), 2322-6.

Tornoe, C. W.; Christensen, C.; Meldal, M., Peptidotriazoles on solid phase: [1,2,3]-triazoles by regiospecific copper(i)-catalyzed 1,3-dipolar cycloadditions of terminal alkynes to azides. *J Org Chem* **2002,** 67, (9), 3057-64.

Tripos Inc, *SYBYL Interface to the FlexX™ Suite*. SYBYL® 7.0 ed.; St. Louis, 2004.

Valentine, D., Preparation of the enantiomers of compounds containing chiral phosphorus centers. *Asymmetric Synth* **1984,** 4, 263-312.

Verdonk, M. L.; Cole, J. C.; Taylor, R., SuperStar: a knowledge-based approach for identifying interaction sites in proteins. *J Mol Biol* **1999,** 289, (4), 1093-108.

Wallace, A. C.; Laskowski, R. A.; Thornton, J. M., LIGPLOT: a program to generate schematic diagrams of protein-ligand interactions. *Protein Eng* **1995,** 8, (2), 127-34.

Westheimer, F. H., Why nature chose phosphates. *Science* **1987,** 235, (4793), 1173-8.

Wilson, B. W.; Hooper, M. J.; Hansen, M. E.; Nieberg, P. S., Reactivation of organophosphorus inhibited AChE with oximes. In *Organophosphates: chemistry, fate, and effects*, Academic Press: San Diego, 1992; 107-137.

Wilson, I. B.; Ginsburg, B., A powerful reactivator of alkylphosphate-inhibited acetylcholinesterase. *Biochim Biophys Acta* **1955,** 18, (1), 168-70.

Wilson, I. B.; Ginsburg, S.; Quan, C., Molecular complementariness as basis for reactivation of alkyl phosphate-inhibited enzyme. *Arch Biochem Biophys* **1958,** 77, (2), 286-96.

Wlodek, S. T.; Antosiewicz, J.; McCammon, J. A.; Straatsma, T. P.; Gilson, M. K.; Briggs, J. M.; Humblet, C.; Sussman, J. L., Binding of tacrine and 6-chlorotacrine by acetylcholinesterase. *Biopolymers* **1996,** 38, (1), 109-17.

Wong, L.; Radić, Z.; Bruggemann, R. J.; Hosea, N.; Berman, H. A.; Taylor, P., Mechanism of oxime reactivation of acetylcholinesterase analyzed by chirality and mutagenesis. *Biochemistry* **2000,** 39, (19), 5750-7.

Wriggers, W.; Milligan, R. A.; McCammon, J. A., Situs: A package for docking crystal structures into low-resolution maps from electron microscopy. *J Struct Biol* **1999,** 125, (2-3), 185-95.

Wu, P.; Feldman, A. K.; Nugent, A. K.; Hawker, C. J.; Scheel, A.; Voit, B.; Pyun, J.; Frechet, J. M.; Sharpless, K. B.; Fokin, V. V., Efficiency and fidelity in a click-chemistry route to triazole dendrimers by the copper(i)-catalyzed ligation of azides and alkynes. *Angew Chem Int Ed Engl* **2004,** 43, (30), 3928-32.

Wu, S.-Y.; Casida, J. E., Asymmetric synthesis of (Rp)- and (Sp)-2-ethyl-, (Rp)-2-pentyloxy-, (Sp)-2-pentylthio- and (Sp)-2-pentylamino-4H-1,3,2-benzodioxaphosphorin 2-oxides. *Phosphorus Sulfur Silicon Relat Elem* **1994,** 88, (1-4), 129-37.

Zhou, H. X.; Wlodek, S. T.; McCammon, J. A., Conformation gating as a mechanism for enzyme specificity. *Proc Natl Acad Sci U S A* **1998,** 95, (16), 9280-3.